University of Padua

Department of Industrial Engineering

Master Degree in Mechanical Engineering

Development of local approaches for fatigue life prediction of Austempered Ductile Iron-to-Steel dissimilar joints

Master's thesis

Supervisor
Prof. Giovanni Meneghetti

Co-supervisors
Alberto Campagnolo, Stefano Masaggia

Author
Elena Pullin

December 2019

Elena Pullin:
Development of local approaches for fatigue life prediction of Austempered Ductile Iron-to-Steel dissimilar joints
,
Master Degree in Mechanical Engineering, © December 2019

Dedicated to my family,
for their love and endless support

Abstract

Nowadays, the use of different classes of materials in the same structure is increased to keep pace with innovation and high-performance requirements for products. In this context, structural components made of different materials need to be joined together and a possible solution for metals is given by arc-welding technologies. As dissimilar welded joints must be able to withstand high cyclic loads under service conditions, the present contribution aims to compare the fatigue behaviour of Austempered Ductile Iron-to-S355J2 steel dissimilar joints to the categories of the corresponding homogeneous steel welded joints, suggested in International Standards and Recommendations. First, metallographic analyses, micro-hardness measurements and residual stresses profiles were obtained on a selection of joints. Angular and linear misalignments were quantified for all specimens. Then, experimental fatigue tests were carried out on the dissimilar welded details. Finally, experimental data were re-analysed in terms of local approaches to explicitly take into consideration stress concentrations and provide the best level of accuracy for the fatigue assessment of the welded structures.

Begin challenging your own assumptions.
Your assumptions are your windows on the world.
Scrub them off every once in a while, or the light won't come in.

Alan Alda

Acknowledgments

It's not easy to express my gratitude to who gave me the strength and the courage to reach this important achievement. The first people I want to thank are my parents, who always believed in me and made this possible. Both of you taught me that determination and passion are the keys to reach my goals. To my dad, who passed me on his passion for mechanics. To my mum, who taught me to be strong and to stand for what I believe: Mum, you will always be my heroine and my greatest inspiration.
Thanks to my beloved Matteo. You have been my rock in the most difficult moments, you have always encouraged me to achieve my dreams and I owe you the confidence I have in myself. You stood by my side all over these years, even when you were thousand miles away. You are a great man and I will forever be grateful to have you in my life.
I would like to thank my friends for supporting me, for all the days spent together on the books, for sharing successes and fails with me. To my fellow students for their feedback, cooperation and of course friendship.
I would like to express my sincere gratitude to my supervisor Prof. G. Meneghetti for the continuous support of my Master's thesis, for his motivation and immense knowledge. Nevertheless, I am also grateful to Alberto Campagnolo, my co-supervisor, for his patience and for sharing his precious advises. Their guidance helped me in all the time of research and writing of this thesis.

Elena Pullin

Inizia a sfidare le tue stesse convinzioni.
Le tue convinzioni sono le tue finestre sul mondo.
Puliscile di tanto in tanto, o la luce non entrerà..

Alan Alda

Ringraziamenti

Non è mai facile esprimere gratitudine verso coloro che ci hanno sostenuto: com'è possibile racchiudere in poche righe tutta la forza che, anche inconsapevolmente, ci hanno trasmesso?
Le prime persone che vorrei ringraziare sono i miei genitori, che hanno sempre creduto nelle mie capacità e che hanno reso possibile questo traguardo. Entrambi mi avete insegnato che passione e determinazione sono fondamentali per raggiungere i miei obiettivi. A mio papà, che mi ha trasmesso il suo senso pratico e la sua passione per la meccanica. A mia mamma, che mi ha insegnato ad essere forte e indipendente, a non abbassare mai la testa di fronte alle difficoltà: sarai sempre il mio modello e la mia più grande fonte di ispirazione.
A Matteo, per essere stato al mio fianco per tutti questi anni. Sei stato la mia roccia nei momenti più difficili e a te devo la sicurezza che ora ho in me stessa. Grazie per avermi sempre incoraggiato ad essere me stessa e per essermi sempre stato vicino, anche a migliaia di kilometri di distanza. Sei un uomo straordinario e sarò per sempre grata di averti nella mia vita.
Un grazie a tutti i miei amici, con cui ho condiviso le giornate sui libri, le ansie pre-esame, le delusioni e i successi di questo percorso di studio. Un riconoscimento va anche ai miei compagni di corso, con cui ho condiviso opinioni e idee.
Ringrazio il Professor G. Meneghetti che ha reso possibile la realizzazione di questa tesi e che, con passione e professionalità, mi ha guidata durante questi mesi. Un grazie Alberto Campagnolo che mi ha sempre aiutato a trovare risposta ai dubbi più spinosi e i cui preziosi consigli sono stati fondamentali per la buona riuscita di questa tesi.

Elena Pullin

Contents

List of Figures

List of Tables

Chapter 1

Introduction

Due to functional needs and technological limitations, it is usually not possible to manufacture a product without joining of some sort. The improvement of material properties and traditional processes for monolithic structures can reduce the need for joining and the number of joints in a product. Nevertheless, the use of different classes of materials makes a “joint-free” concept unrealistic in most cases.
The main challenge of joining together different materials is to choose the proper technology, which should not modify the mechanical properties of the components. In the case of metals, thermal fusion processes are usually adopted, and the most common one is electric arc welding. The latter usually leads to a larger size of the Heat Affected Zone and to the formation of a brittle layer at the interface between metals. Being a recently available joining technology, the literature lacks experimental data on arc-welded dissimilar joints and therefore, dedicated investigations are necessary.
The choice of joining Austempered Ductile Iron (ADI) to steel is due to the high performance properties of the ADI itself: the latter is obtained from a low-alloyed Pearlitic-Ferritic Ductile Iron by means of an isothermal heat-treatment, called "austempering". This process provides mechanical properties comparable with those of structural steel, together with additional qualities such as:

- higher wear resistance;
- the ability of hardening under service conditions;
- higher toughness;
- lower weight;
- good both static and fatigue resistance;

As a consequence, the use of steel can be limited where necessary or mandatory and thus, economical advantages can be gained. Furthermore, thanks to the good castability of ADI, the components can be designed with more complex shape and lower thickness.

When considering a new structural detail, the first step is to analyse the material and its microstructure. A bibliographic research has to be carried out

to understand the mechanical properties of the employed materials, i.e. austempered ductile iron (EN-JS-1050) and construction steel (S355J2). The second step is the set-up of the welding process: the main issue is to prevent the formation of brittle material within the heat-affected zone, especially on the ADI side. After that, metallographic analysis and micro-hardness profile are needed to identify phase transitions. Residual stress profiles complete the specimens' characterisation.
Dissimilar welded joints have to be designed considering high cyclic loads under service conditions, but International Standards and Recommendations [2],[3]and [5] provide fatigue strength categories only for homogeneous welded joints made of structural steels or aluminium alloys. Thus, experimental fatigue tests have to be performed to define new design curves suitable for dissimilar joints.
Concerning the design of welded joints against fatigue loading, different approaches are available, namely the nominal stress, the hot-spot stress, the notch stress and the Linear Elastic Fracture Mechanics (LEFM).
Whereas fracture mechanics procedures are now well established for normal stress fields and homogeneous materials, there is a lack of experimental data for current approaches applied in more complex situations. Thus, even though local approaches give a higher grade of accuracy, the nominal stress approach is still the easiest and the most widely adopted. For these reasons, the present work will define S-N curves in the first place, basing the stress calculations on Solid Mechanics as suggested in the International Standards. The fatigue strength categories will be compared to those of the corresponding homogeneous steel welded joints.
Successively, innovative approaches will be applied to take local stress raising effects into account and to reduce the scatter of the experimental data. The methods employed will be the Notch Stress Intensity Factor Approach (N-SIF), the Strain Energy Density (SED) approach and the Peak Stress Method (PSM).

In conclusion, the present thesis aims to point out the mechanical properties and the fatigue behaviour of austempered ductile iron-to-steel dissimilar joints, starting from the material characterisation and experimental fatigue tests, going up to the application of latest local approaches based on fracture mechanics.

1.1 Organization of the document

The document is organised as follows:

- Chapter 2 gives an overview on the state of the art on welding dissimilar joint, focusing on Austempered Ductile Iron properties and arc-welding technologies.
- Chapter 3 providse a survey on related works.
- Chapter 4 describes the procedure for misalignments measurement and reports the results obtained for all the specimens.
- Chapter 5 reports the specimens' characterisation from a metallurgic point of view.
- Chapter 6 reports the results of the experimental fatigue tests and defines the S-N design curves for ADI-to-steel joints.

- Chapter 7 gives an overview of the local approaches, based on non-conventional extension of Linear Elastic Fracture Mechanics.
- Chapter 8 proposes the application of local approaches to dissimilar arc-welded joint and defines the new design curves.

Chapter 2

Background

2.1 Trends in dissimilar joints

In several industries the trend for more optimal, lightweight and high performance structures leads to the adoption of hybrid components. The combination of various materials allows to take advantage of their different properties for integrating an increased number of function in each part. This approach is mainly adopted in the field of Aeronautics, Automotive, Tooling, Power Generation and Marine application. These components made of dissimilar materials are to be joined together,but the joining processes can, on the other hand, be challenging when materials present different chemical, mechanical, thermal, or electrical properties. The potential incompatibility can create problems not only for the joining process itself, but also for the structural integrity of the joints during the life-cycle of the product. Moreover, dissimilar materials can present more vulnerable microstructures, in addition to the mismatch between tensile and plasticity properties of the different materials: this may affect crack nucleation and its tendency to propagate. Martinsen et al. [13] have recently reviewed advantages and challenges of joining dissimilar materials.
Structural components made of dissimilar materials can be joined together by welding. In the relevant literature, several contributions have been devoted to investigate the possibility of joining dissimilar materials by different welding techniques: the most widely adopted is the friction-welding [19],[18], but also arc-welding [21],[7], [20], laser-welding [6],[17] and other techniques are employed. In the context of arc-welding, Austempered Ductile Iron (ADI) to structural steel dissimilar joints offer the possibility to improve mechanical response of structural components, combining weight reduction and net-to-shape geometry at the same time. Indeed, ADI offers very good static, impact, fatigue performances and moderate wear resistance together with the possibility for iron castings to be designed with complex shape and low thickness. This leads to the optimization of mass distribution based on both actual stiffness and required load levels and the use of steel can be limited where needed or mandatory.
Several contributions in the recent literature have addressed the analysis of the fatigue behaviour of dissimilar joints made of different grades of structural steels [19],[21],[7], [20], different series of aluminium alloys , a steel and an aluminium alloy [18] or other metallic materials welded together. However, there is no contribution which has investigated the fatigue behaviour of dissimilar arc-welded

joints made of ADI and structural steel. Due to the lack of information in the technical literature and in all International Standards and Recommendations [2],[5], the fatigue behaviour of austempered ductile iron (EN-JS-1050)-to-steel (S355J2) dissimilar arc-welded joints has been experimentally investigated to determine the fatigue strength categories of some typical welded details and to compare them with the categories provided by standards and recommendations for homogeneous steel welded joints. S355J2 EN10025-2 hot rolled construction steel (S355J2) is commonly used in structural applications such as freight cars, trucks, cranes, excavators, etch, while ISO 17804 JS/1050-6 Austempered Ductile Iron (ADI 1050) typical applications are for earth movement undercarriage components, passenger vehicles and freight cars suspension parts, axles, power transmission components, crankshafts, etc.The application of ADI in heavy machinery and transportation equipment has many advantages due to the low cost and design flexibility.

2.2 Austempered Ductile Iron: recent research and development

Zanardi Fonderie currently produces 10000 tons/year of ADI (Austempered Ductile Iron) castings, about 90 % machined after heat treatment. ADI is produced by heat-treating a low alloyed Pearlitic-Ferritic Ductile Iron, cast after special preconditioning of the metal bath. The cast material is iron where carbon is mainly present in the form of spheroid graphite particles.The isothermal treatment, called "austempering",of spheroidal graphite cast iron consists in to phases:

- heating the cast at $900°C$
- cooling in salt bath having constant temperature of 350°C,at a cooling rate that promote the formation of ausferrite.

Figure 2.1 shows the CCT diagram for ductile iron.

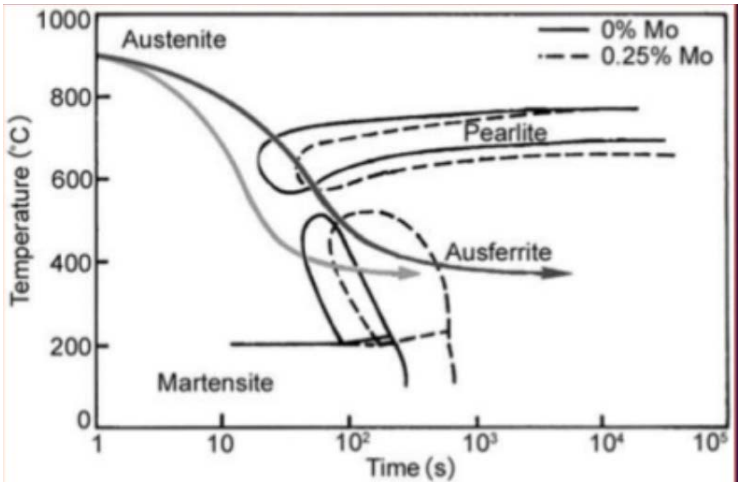

Figure 2.1: CCT diagrams for 3.3% C, 2.6% Si, 0.3% Mn ductile iron with superimposed cooling curves.

2.2.1 Mechanical and fatigue properties of ADI

Austempered ductile iron (ADI) has attracted considerable interest in recent years because of its excellent mechanical properties such as high strength together with good ductility, good wear resistance, and good fatigue properties, comparable and in some cases, superior to those of structural steel. These properties of ADI are attributed to its microstructure consisting of retained austenite and acicular ferrite. This structure is known as "ausferritic", shown in Figure 2.2.

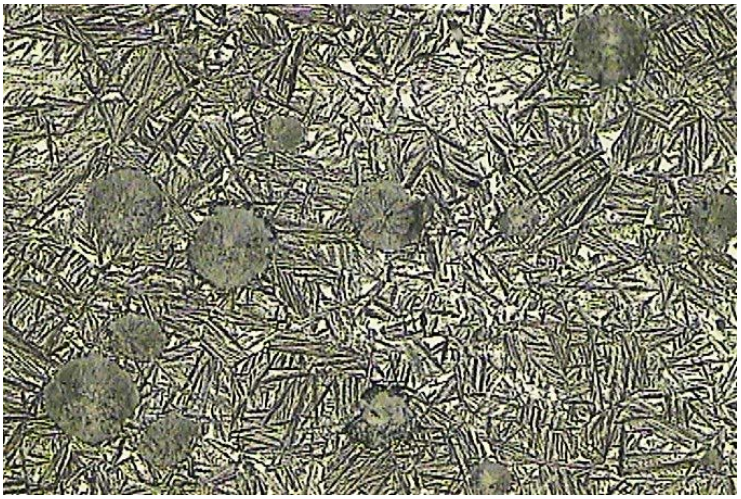

Figure 2.2: ADI 1050 microstructure after austempering

Thank to the presence of graphite nodes, ADI has a lighter specific weight than the one of homogenous metallic structure. This, together with a optimum castability, enables to obtain complex geometries with great lightweight characteristics at lower price. Due to the previously reported treatment, ADI presents an ultimate tensile strength in a range between 800 and 1600MPa depending on the composition, while the hardness can reach a value of 500HB both on the surface and at the heart. On top of that, the metastable structure of ADI tends naturally towards martensitic transformation on the surface when highly stressed. Thus, the material can be easily machined after the heat-treatment, while hardening under operating conditions. Looking at the standards ISO17804 (Figure 2.3), replacing steel with iron seems a quite good and alternative solution.

Material designation	0,12 % proof stress $R_{p0,2}$ N/mm² min.	Tensile strength R_m N/mm² min.			Elongation A % min.		
		Relevant wall thickness t (mm)					
		$t \leq 30$	$30 < t \leq 60$	$60 < t \leq 100$	$t \leq 30$	$30 < t \leq 60$	$60 < t \leq 100$
ISO 17804/JS/800-10-C	500	790	740	710	8	5	4
ISO 17804/JS/900-8-C	600	880	830	800	7	4	3
ISO 17804/JS/1050-6-C	700	1 020	970	940	5	3	2
ISO 17804/JS/1200-3-C	850	1 170	1 140	1 110	2	1	1
ISO 17804/JS/1400-1-C	1 100	1 360	To be agreed upon between the manufacturer and purchaser				

Figure 2.3: Standard grades for ADI according to ISO

While tensile strengths are well known and comparable with those of structural steels, very limited information is available for fatigue behaviour of ADI. Zanardi s.p.a. has carried out a large number of tests on both smooth and notched specimens in order to plot Kitigawa's diagram (Figure 2.4 and 2.5)

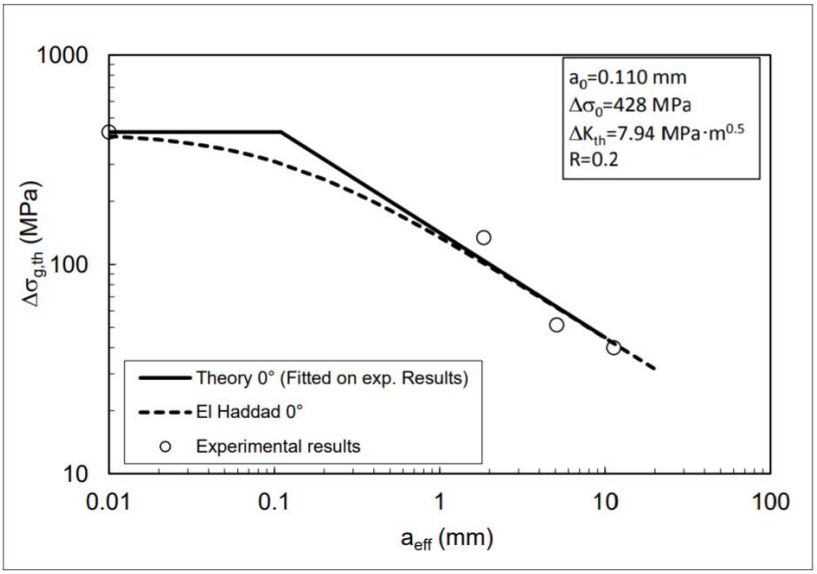

Figure 2.4: Kitagawa-Takahashi's diagram for ADI-1050

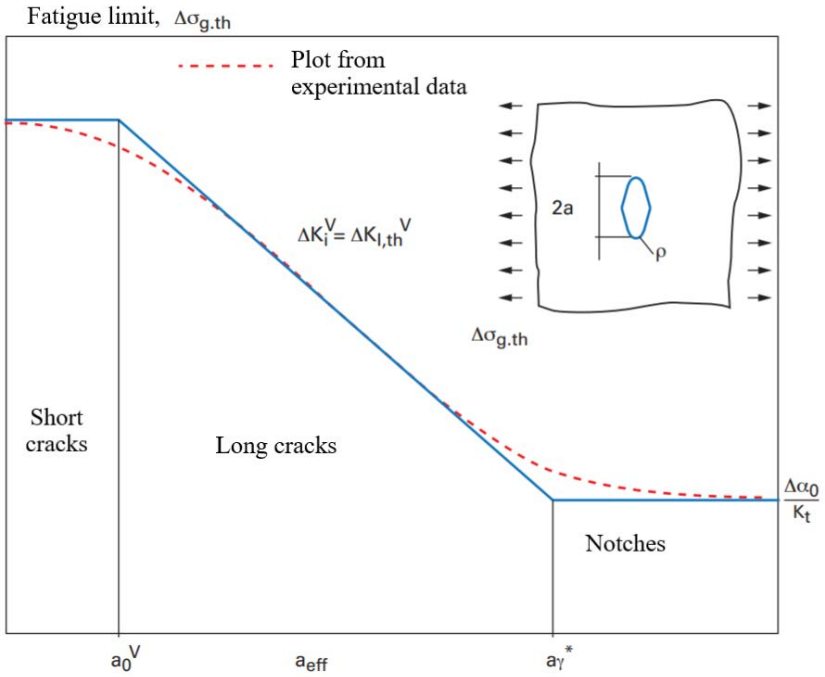

Figure 2.5: Kitigawa's diagram extended to U-notch

The Kitigawa's diagram synthesise Linear Elastic Fracture Mechanics (LEFM) and Classical Mechanics in one representation and it is useful to estimate the fatigue limit for U- and V- notched mechanical components. The endurance limit $\Delta\sigma_0$ (also typically quoted as fatigue strength or fatigue limit) was found equal to 428 MPa, while the fracture toughness ΔK_{th} is 7.94MPa$m^{0.5}$, calculated with El Haddad's equation. It is worth noting that the value of exponent for opening angle $2\alpha = 45°$ is near to the one for cracks ($2\alpha = 0°$) and the length a_0 is supposed equal to zero as the notch is more than 10 times longer than a_0.

2.3 The welding process

Nowadays, welding is one of the most used process in manufacturing for joining structural components. The main characteristic of this process is the transformation of the base material from a metallurgic and physical point of view: the resulting material can show different mechanical properties from the base material depending on welding parameters, temperature reached during the process and heat treatments eventually applied after welding. There are three main zones (Figure 2.6) that can be recognised in welds:

- the Fuse Zone (FZ), which builds the weld bead
- the base material
- the Heat Affected Zone (HAZ)

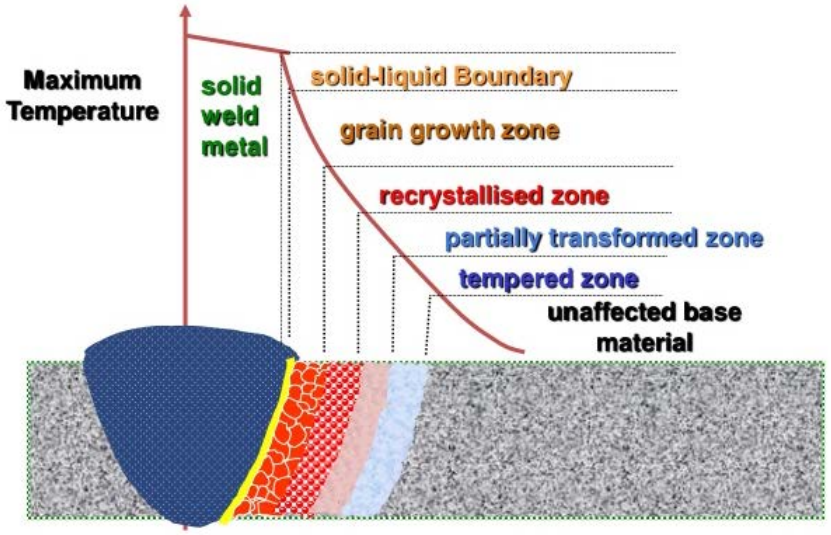

Figure 2.6: Typical zones in welded joints

The structure and the properties of the FZ and HAZ strongly depend on:

- the metals to be joined and their characteristics
- the welding process
- the filler material
- the process' setting

More specifically, heating rate and heat properties of metals have great influence in hybrid joints: melting point, coefficient of thermal expansion, thermal conductivity and resistance to corrosion could differ among metals and, thus, choosing a wrong control temperature for the process may lead to microstructure degeneration. Besides these difficulties, dissimilar joints show also typical defects of welds, such as residuals stresses, inclusions, porosities and cracks. For all these reasons, the choice of the welding process must be careful. Various joining technologies are available nowadays. The most common are friction welding, arc-welding, laser-welding and other techniques such as resistance spot welding and magnetic pulse welding. Referring to our ADI-to-steel joints, arc-welding was adopted.

All specimens were obtained from plates having dimensions 300x150x12mm. Ductile Iron plates were produced by Zanardi Foderie S.p.a. in horizontal greensand moulds; they were sand cleaned, austempered to material grade ADI 1050 and milled to the final thickness of 10 mm.Steel plates, having same initial dimensions, were prepared from commercial hot rolled plates and then reduced to 10 mm thickness by milling.All plates were grinded, brushed and properly clamped by means of tack welded fixture bracket in order to minimize welding distortions. Final specimen's dimensions were obtained by cutting after welding. All welding operations were done by 'Istituto Italiano della Saldatura' (IIS).

Preliminary dummy tests were carried out on 20-mm-thick ADI 1050 plates, in order to set up welding parameters. First of all, beads on plate (BoP) were created using fully mechanized TIG-welding process without filler material for tuning HI (heat input) and Tp (preheat temperature): HI range was increased up to 2.2 kJ/mm, whereas Tp up to 300°C. In particular, ADI 1050 exhibits two heat affected zones: HAZ1 microstructural response is fully influenced by HI and Tp whereas HAZ2 undergoes light softening for any combination of HI and Tp. Different behaviour of HAZ1 and HAZ2 is shown in Figures 2.7 and 2.8; during the preliminary tests, it has been found that the microstructure remains the same for HI and Tp above 1.8 kJ/mm and 250°C, respectively.

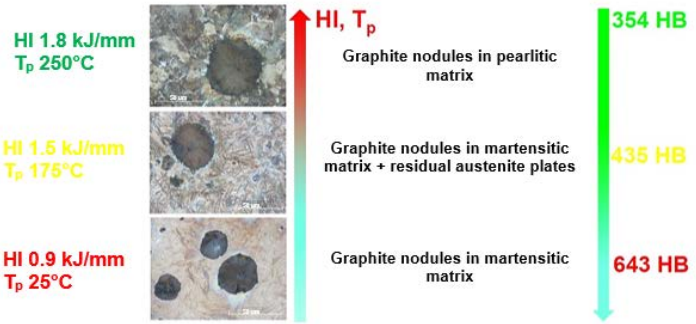

Figure 2.7: ADI 1050 BiP HAZ1, trend according to HI and Tp

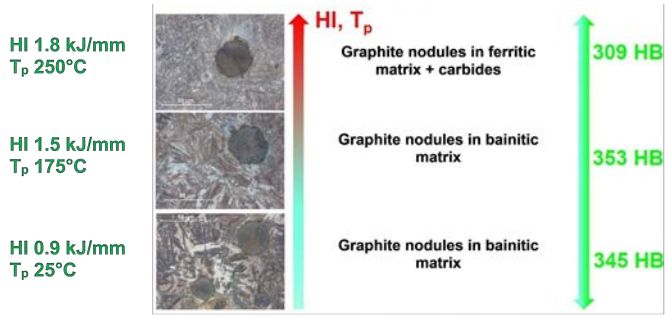

Figure 6: ADI 1050 BoP HAZ2, trend according to HI and Tp.

Figure 2.8: ADI 1050 BoP HAZ2, trend according to HI and Tp

Due to the isothermal heat treatment at 350°C required for ADI 1050, proper HI and Tp were selected in order to avoid martensite formation within HAZ1, thus requirement was to obtain HBW values similar to base material, and secondly to avoid extended softening.

It is worth noting that remelted metal microstructure, because of metastable solidification after welding, consists in ledeburite at room temperature: cooling rate after welding is always too fast to allow carbon in molten metal to precipitate in the form nodules once again. Therefore, carbon remains in the matrix as iron carbides which forms the ledeburite.

The next step required HI and Tp to be adjusted for creating BoP with filler material in order to evaluate different mode of metal transfer and the tendency to crack formation. Fully mechanized GMAW-welding process with S C NiFe-2 EN ISO 1071 ϕ 1.2 mm filler material and MCAW-welding process with T C NiFe T3-CI EN ISO 1071 ϕ 1.2 mm filler material (by Voestalpine Bohler Welding) were adopted; Ar-CO2 80-20 ISO14175 M21 gas shielding was used. Based on the evidence coming from Macrographic test (UNI EN ISO 17639), Visual testing VT (UNI EN ISO 17637), Penetrating testing PT (UNI EN ISO 3452-1), Brinell Hardness HBW test (UNI EN ISO 6506-1) and Micrographic test (EN ISO 945-1), pulsed arc and short arc GMAW-welding processes gave the best results. The relevant welding process parameters are reported in Table 2.1.

Mode of metal transfer	Current [A]	Voltage [V]	Travel Speed [mm/min]	Heat Input [kJ/mm]
PULSED ARC(P)	180-200	29.7-30.3	260	1.2-1.3
SHORT AR (D)	175-180	22.8-23.0	260	0.8-0.9
Preheat temperature 300°C				

Table 2.1: ADI 1050 BoP with fiiler material, GMAW welding parameters

.

Afterwards, parameters were tuned to consider the actual specimen's thickness of 10mm, weld bead dimensions, misalignments, runs number and all the different types of dissimilar joint investigated. The main issue was to prevent martensite formation and cracks nucleation within HAZ of ADI 1050. The proper set of welding parameters was identified in such a way that the resulting hardness was as close as possible to the base ADI material. Regarding the formation of ledeburite layer close to the weld metal, it cannot be avoided because in this area ductile iron always undergoes metastable solidification after remelting.
The complete set of welding parameters is reported in Table 2.2. In particular, pulsed arc fully mechanized GMAW-welding process was adopted. Macrographic/micrographic analyses as well as HBW test were carried out on all specimens. Quality level for imperfections was according to ISO 5817-B.

Mode of metal transfer	Torche angle direction	Filler Material	Current &Polarity [A]	Voltage [V]	Travel Speed [mm/min]	Heat Input [kJ/mm]
P	15° forehand	C NiFe-2 EN-ISO 1071 $\phi 1.2mm$	CCPI 120-130	24-25	230-340	0.41-0.71

Preheat temperature	EN 13916-TC 200°C
Interpass temperature	EN 13916-TC 250°C
Shielding	ISO 14175 M21 (Ar-CO2 80-20), flow rate 16-18 lt/min

Table 2.2: GMAW welding parameters adopted for specimens, following UNI EN ISO 6947 PA

.

Chapter 3

Related works

This chapter aims to give a comprehensive overview of the research project, together with the related works and papers that refer to dissimilar joints made of Austempered Ductile Iron and steel. A brief introduction to actual Standards and Recommendations [2],[5] for welded joints is given , even though a deeper examination will be done while reviewing experimental results in Chapter 6.

3.1 Project overview

The research project began in October 2018 thank to an agreement [15] between Zanardi Fonderie S.p.a. and the Department of Industrial Engineering (University of Padua). The main goal is to define design methods for the structural durability of ADI1050-to-steelS355 welded joints. The methodology is based on the Fracture Mechanics and its non-conventional extensions to V-notched specimens. The project consists in two main parts:

- the experimental test campaign
- the theoretical and numerical evaluation of the results

Experimental campaign The specimens, manufactured as explained in Chapter 2, include 9 series of welded plates:

- 15 partial-penetration butt-welded joints (Series A)
- 15 full-penetration butt-welded joints (Series B1)
- 15 full-penetration ground butt joints (Series B2)
- 30 cruciform non-load-carrying fillet-welded joints (Series C)
- 5 stress-relieved cruciform non-load-carrying fillet-welded joints (Series C)
- 15, T non-load-carrying fillet-welded joints (Series D)
- 15 cruciform load-carrying fillet-welded joints (Series E)
- 15 cruciform full penetration K-butt-welded joints (Series F)
- 15 plain specimens for material characterization

Some parameters are to be measured for specimens characterization:

- both angular and linear misalignments for each specimens
- micro-hardness profiles for one specimen of each series in the neighbourhood of the weld bead (ZF,ZTA, base metal) on both ADI and steel side
- metallographic analysis for each series
- residual stresses by x-ray diffraction for each series

All fatigue tests (about 9 specimens for each geometry) are carried out at stress ratio both $R \approx 0$ and 0.5, except for Series B. The load condition is either axial or bending depending on the actual misalignment of the specimens. The data are given by the mean of the nominal stress approach. The PS curves (the probability statistical distribution of fatigue strength) at $50\%, 97.7\%$ and 2.3% has to be determined and the slope k has to be compared with respect to the one reported in the actual standards. A brief overview of the the schematized geometry and corresponding load condition of each joint series are reported in Figs. 3.1-3.8.

Numerical analysis Starting from the experimental data available, numerical analyses should be carried out on the structural details in order to :

- define a design method to forecast the influence of misalignments on specimens' load conditions.
- define the structural/control volume by an accurate analysis of the geometry and failure modes
- calculate NSIFs (Notch- Stress Intensity Factors) at weld toe and weld root by definition
- determine NSIFs by using the Peak Stress Method (PSM) and compare them with the ones of previous item
- synthesise the experimental results through plain strain models

Finally, the design curves will be defined and local approaches will be compared with the nominal approach.

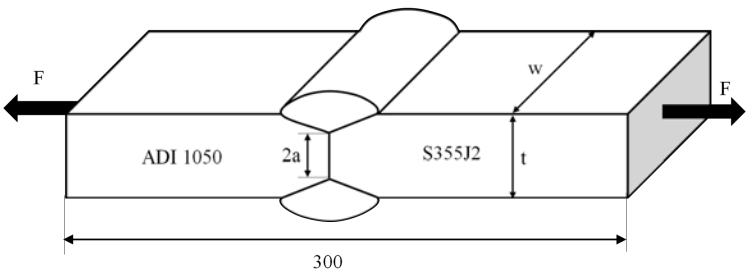

Figure 3.1: Geometry of the partial-penetration butt joint

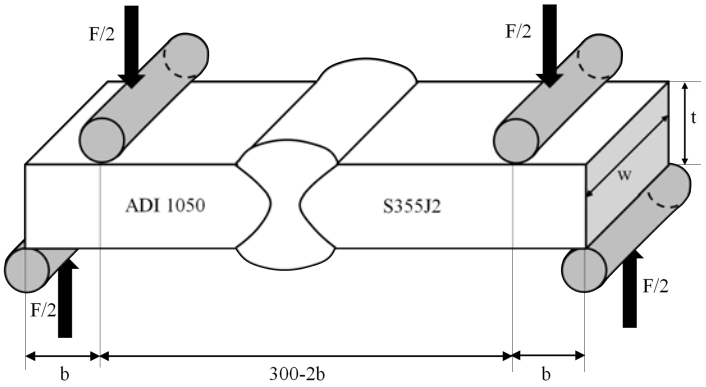

Figure 3.2: Geometry of the full-penetration butt joint under bending load

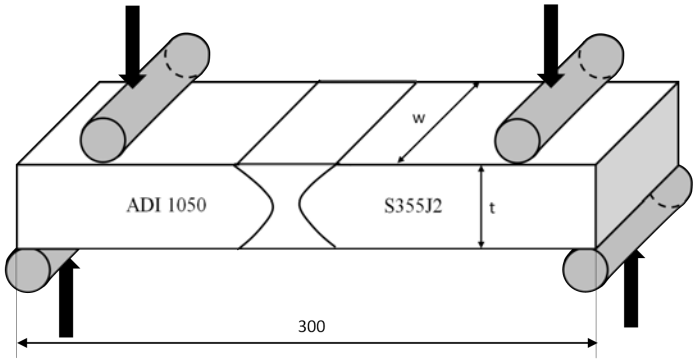

Figure 3.3: Geometry of the full-penetration ground butt joint under bending load

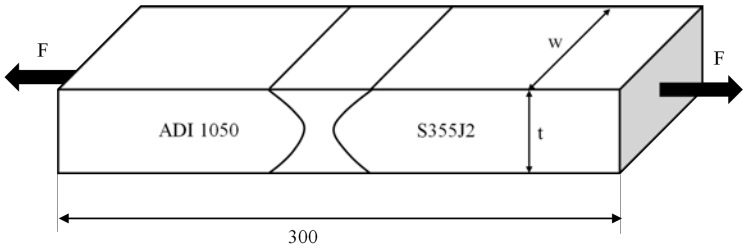

Figure 3.4: Geometry of the full-penetration ground butt joint under axial load

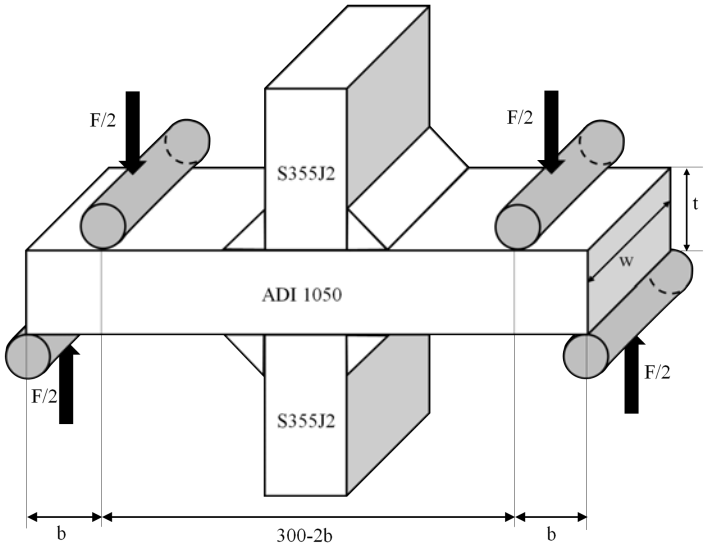

Figure 3.5: Geometry of the cruciform nlc fillet-welded joints under bending load

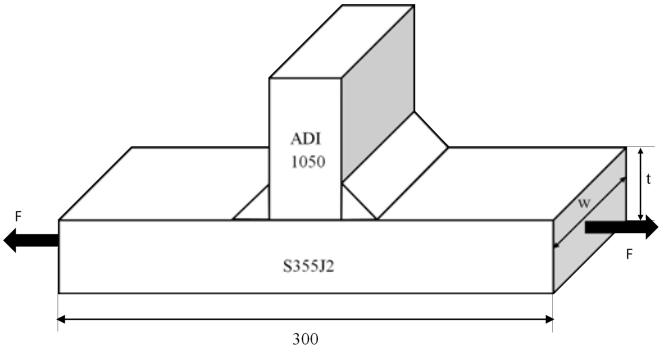

Figure 3.6: Geometry of the T nlc fillet-welded joints under axial load

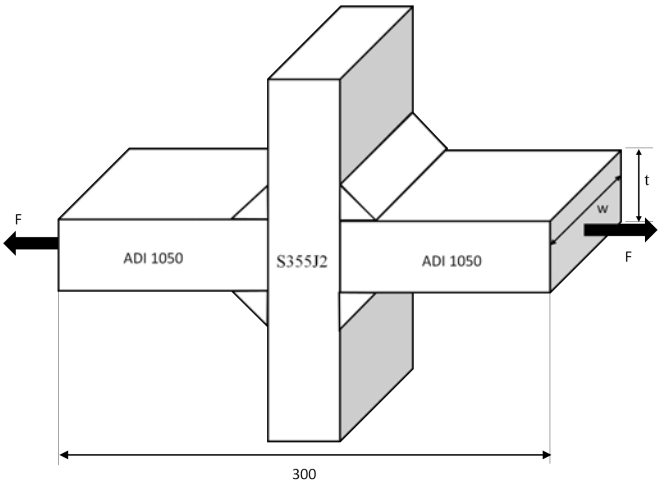

Figure 3.7: Geometry of the cruciform load-carrying fillet welded joints under axial load

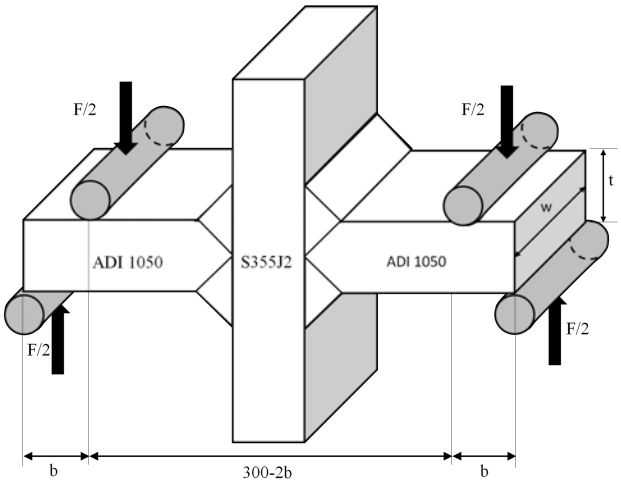

Figure 3.8: Geometry of the cruciform full-penetration K-butt-welded joints under bending load

3.2 The starting point

The starting point of this contribution is D. Berto's Master Thesis [1]. As part of the reported-above work was already done, some results from specimens characterization and fatigue tests are briefly reported in the following paragraphs for the sake of completeness.

Angular and linear misalignment D. Berto [1] measured the misalignments for some specimens of the series A, B, C, E and F. The procedure used for this purpose is described in the following Chapter 4, whereas Table 3.1 - 3.5, reported in this chapter, summarize the misalignments obtained in the previous work.

Material Characterization Some micro-hardness and metallographic profiles were already obtained in [1], for some specimens of series A, B1 and B2. However, while the results of the full-penetration butt joint (B1) and the full-penetration ground butt joint (B2) can be considered correct, the measures on the partial-penetration butt joint (A) deviated significantly from the values in the literature. Thus, the hardness had to be checked and re-measured on another specimen. The incompatibilities were caused by a unproper procedure, but the details about the procedure and the results obtained for all the series are reported in Chapter 5.

Fatigue tests and experimental results In the previous work, fatigue tests were performed on series A, B1, B2 and C at nominal load ratio R= 0.05. Some preliminary tests at nominal load ratio R=0.5 were carried out on series C. Design curves were derived from the experimental results in terms of the applied nominal stress range $\Delta\sigma_{nom}$ versus the number of cycles to failure, as required by Standards and Reccomendations [2], [5]. All the details about the performed tests and the failure mode of these specimens can be found in the data sheets in Appendix A of Berto's Thesis [1]. In order to give the most complete and comprehensive overview of the experimental results, the old design curves will be updated with new data and reported in Chapter 6 , where also the latest fatigue tests on other series will be described in detail.

Specimen code	e [mm]	ΔZ [mm]	e1 [mm]	α [rad]	α [deg]
A1-1	0.765	2.706	1.941	0.015	0.876
A1-2	0.725	2.901	2.176	0.017	0.974
A1-3	0.810	2.975	2.165	0.017	0.984
A1-4	0.513	2.710	2.197	0.017	0.999
A1-5	0.523	2.711	2.189	0.017	0.995
A1-6	0.593	1.901	1.308	0.010	0.595
A11-1	0.290	1.239	0.949	0.009	0.518
A11-2	0.283	1.155	0.872	0.008	0.467
A11-3	0.363	1.315	0.953	0.009	0.520
A11-4	0.200	1.272	1.072	0.010	0.574
A11-5	0.200	0.892	0.692	0.007	0.374
A11-6	0.128	1.171	1.044	0.010	0.570
A2-1	0.165	0.238	0.073	0.001	0.033
A2-2	0.250	0.556	0.306	0.002	0.139
A2-3	0.163	0.896	0.733	0.006	0.333
A2-4	0.061	1.071	1.011	0.008	0.460
A2-5	0.670	1.770	1.100	0.009	0.500
A2-6	0.715	1.956	1.241	0.010	0.564

Table 3.1: Misaligment of partial-penetration ground butt joints from previous work

.

Specimen code	e [mm]	ΔZ [mm]	e1 [mm]	α [rad]	α [deg]
B1-1	0.095	0.351	0.256	0.002	0.117
B1-2	0.060	0.120	0.060	0.000	0.027
B1-3	0.140	0.470	0.330	0.003	0.150
B1-4	0.080	0.503	0.423	0.003	0.191
B1-5	0.290	0.308	0.018	0.000	0.008
B1-6	0.217	0.116	-0.100	-0.001	-0.046
B2-1	0.578	0.708	0.130	0.001	0.062
B2-2	0.678	0.504	-0.174	-0.001	-0.083
B2-3	0.808	0.369	-0.438	-0.004	-0.211
B2-4	0.763	0.342	-0.420	-0.004	-0.204
B2-5	0.670	0.394	-0.276	-0.002	-0.134
B2-6	0.603	0.382	-0.220	-0.002	-0.108
B4-1	0.423	2.944	2.522	0.018	1.040
B4-3	0.125	2.122	1.997	0.016	0.901
B4-5	0.188	2.226	2.039	0.016	0.934

Table 3.2: Misaligment of full-penetration butt joints from previous work

.

Specimen code	e [mm]	ΔZ [mm]	e1 [mm]	α [rad]	α [deg]
C1-1	0.223	1.075	0.853	0.008	0.444
C1-2	0.078	0.318	0.241	0.002	0.126
C1-3	0.398	1.175	0.778	0.007	0.398
C4-1	-0.730	0.903	1.633	0.014	0.780
C5-1	0.575	3.124	2.549	0.023	1.304
C5-2	0.200	0.860	0.660	0.006	0.357
C5-3	0.575	3.119	2.544	0.023	1.302
C6-2	0.638	3.542	2.905	0.026	1.513
C6-3	0.655	3.505	2.850	0.025	1.458
C7-1	0.200	0.849	0.649	0.006	0.351
C7-3	0.200	1.296	1.096	0.010	0.587
C8-1	0.638	3.569	2.932	0.027	1.527
C8-3	0.655	3.508	2.853	0.025	1.460

Table 3.3: Misaligment of cruciform nlc fillet-welded joints from previous work
.

Specimen code	e [mm]	ΔZ [mm]	e1 [mm]	α [rad]	α [deg]
E1-2	0.678	0.209	-0.469	-0.004	-0.217
E1-3	0.915	2.547	1.632	0.013	0.767
E1-4	0.075	2.132	2.057	0.016	0.935
E1-5	0.245	2.326	2.081	0.016	0.939
E1-6	0.208	2.147	1.940	0.015	0.875

Table 3.4: Misaligment of cruciform joints with load-carrying fillet-welds from previuos work
.

Specimen code	e [mm]	ΔZ [mm]	e1 [mm]	α [rad]	α [deg]
F1-1	0.823	3.492	2.670	0.024	1.404
F1-2	0.638	3.563	2.925	0.027	1.524
F1-3	0.773	3.758	2.986	0.027	1.570
F1-4	0.655	3.523	2.868	0.026	1.467
F1-5	0.575	3.138	2.563	0.023	1.312
F1-6	0.670	3.176	2.506	0.023	1.318

Table 3.5: Misaligment of cruciform full-penetration joints
.

3.3 Actual Standards and Recommendations for fatigue design of welded details

Standards and Recommendations provide general guidelines for the assessment of fatigue life in welded components. Eurocode 3 [2] and Hobbacher IIW Recommendations [5] are the most widespread. The aim of these contributions is to give methods for the design and the analysis of welded components loaded by variable forces in order to avoid failure by fatigue. In general, they report strength categories for homogeneous joints made of aluminium and structural steel, but design curves for dissimilar joints haven't been derived yet. The fatigue data are mainly in the form of S-N curves or fatigue crack growth curves, based on constant amplitude test results, and different approaches can be employed for fatigue assessment of welded joints, namely nominal stress, structural hot-spot stress, effective notch stress and fracture mechanics. Even though all these methods are well-established, the approaches based on fracture mechanics require an adequate level of knowledge and experience; thus, the nominal stress approach remain the easiest and the most largely employed in fatigue design.

3.3.1 Basic Principles

In the standards, the fatigue resistance data are expressed in terms of the same type of stress, derived from constant amplitude tests. The failure in fatigue endurance test can be defined in two main ways:

- in small welded specimens, complete rupture is set very close to through-thickness cracking
- in large components or vessels, larger or through-wall crack is taken as failure.

Fatigue failure in S-N curves in following paragraphs correspond to through-section cracking. The form of the S-N curve is:

$$N = \frac{C}{\Delta\sigma^m} \; or \; N = \frac{C}{\Delta\tau^m}$$

where the slope **m** may have different values depending on the range of fatigue lives.

In fracture mechanics approach, the fatigue resistance refers to the relationships between the Stress Intensity Factor range ΔK and the crack growth rate da/dN. All fatigue resistance data are assumed to represent a survival probability at least 95%, but other existing definition corresponding to a survival probability of 97.7% are practically equal for engineering application. The nominal stress range should be within the limits of the elastic properties of the material.

3.3.2 Fatigue Resistance of Classified Structural Details

The fatigue assessment of classified welded joints is based on the nominal stress approach. Separate S-N curve are provided for both normal and shear stress ranges. For each classified structural details, the stress, which has to be used for fatigue assessment, is reported in tables. Figs. 3.9 and 3.10 show the S-N curves for standard applications and very high cycles application respectively,

taken from IIW Reccomendations [5], while the S-N curve poposed by Eurocode 3 [2] is reported in Figure 3.11

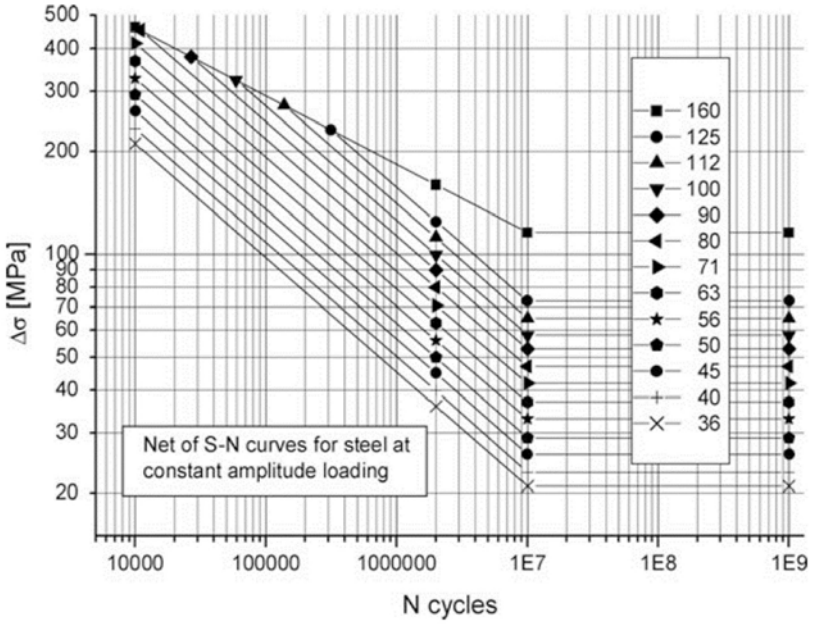

Figure 3.9: Fatigue resistance S-N curves for steel, normal stress, standard applications from IIW Recommendation

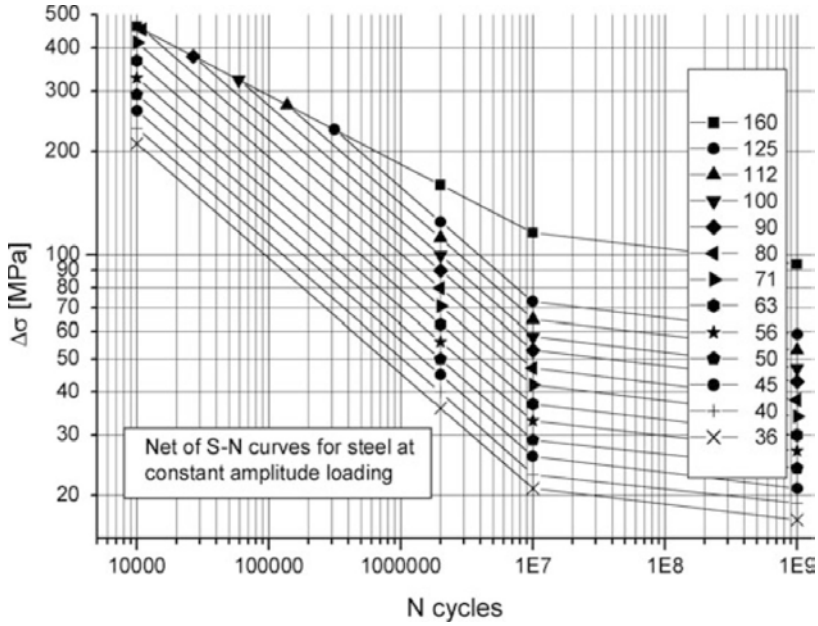

Figure 3.10: Fatigue resistance S-N curves for steel, normal stress, for very high cycles applications from IIW Recommendation

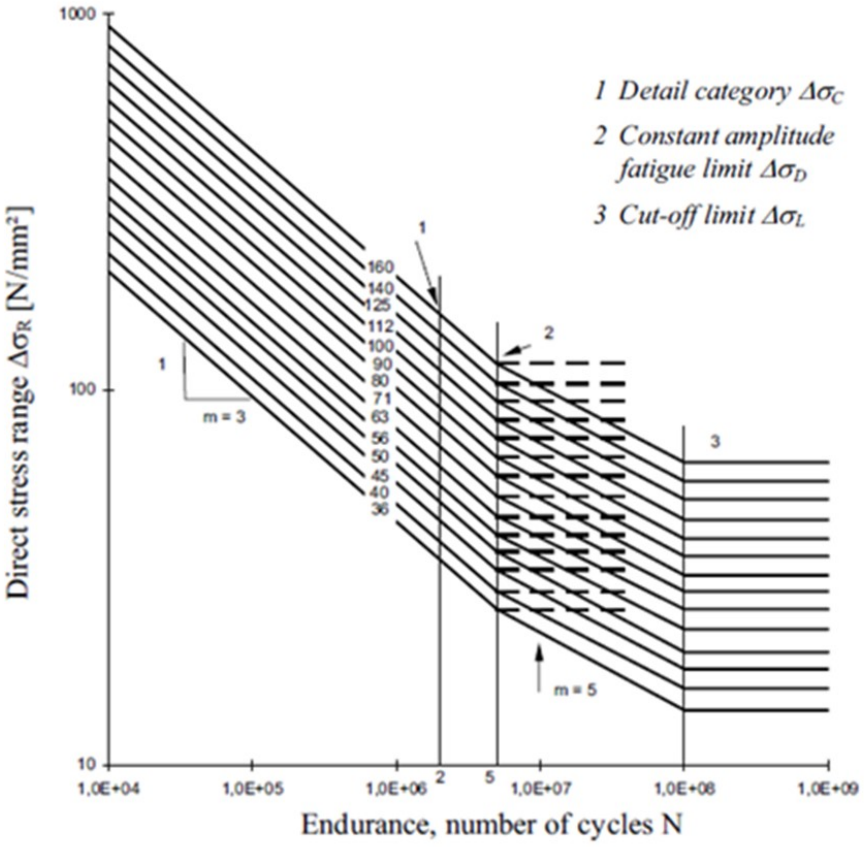

Figure 3.11: Fatigue resistance S-N curves for direct stress ranges, from Eurocode 3.

The structural details corresponding to the strength categories in the curves are tabulated in the Normative references.

Based on experimental investigations, the fatigue curves include the effect of:

- structural hot spot stress concentrations due to the geometry of the detail
- local stress concentration due to the weld bead
- imperfections according to normal fabrication standards
- applied load
- residual stresses
- metallurgical conditions
- welding process
- post weld treatment, where specified

On top of that, the fatigue curves are independent of the material tensile strength within the limits imposed by static considerations. Each S-N curve is identified by the characteristic fatigue strength of the classified detail in MPa at 2 million cycles. This value correspond to the fatigue class FAT. The slope of the S-N curves is equal to **m=3** for details assessed on the basis of the normal stressess. At 10^7 cycles, the curve becomes a horizontal line as there is the conventional assumption that failure will not occur below this point. This constant amplitude fatigue limit (CAFL) is also referred as 'knee point'. Even though the latter assumption is admissible for standard applications, new experimental data proved that CAFL does not exist and thus, the S-N curves should continue with a slope of **m=22** for very high cycles application (Figure 3.10).

Chapter 4

Linear and angular misalignment of specimens

In this chapter I will explain the method used for the measure of the specimens' misalignment. Misalignment can influence the fatigue life of a specimens; the experimental fatigue tests are carried out by adopting a MFL axial servo-hydraulic machine. When the specimens are gripped by the machine, they tends to straighten as the MFL's clamps are perfectly aligned. This leads to undesired displacements of the specimens' extremes and consequently, an secondary shell bending moment may be introduced. Thus, in order to predict the real stress acting near the weld bead, it is essential to be aware of the entity of the misalignment. Misalignment can be both linear and angular. The first consists in a eccentricity between the axes of the two plates, considered as perfectly parallel (Figure 4.1a). The second one corresponds to the angle between the axes, when they origin from the same point (Figure 4.1b). Usually the specimens present both of them simultaneously as shown in Figure 4.1.

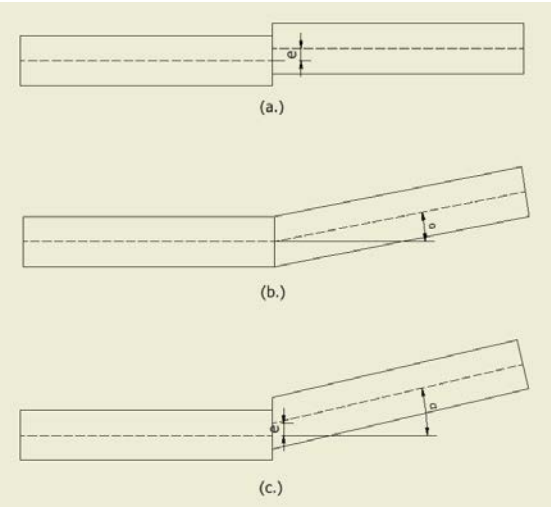

Figure 4.1: Typical misalignment of the welded specimens. a) linear misalignment, b) angular misalignment, c) combined misalignment

.

4.1 Measurement method

In order to measure both of the misalignment, a numerical-controlled milling machine was used with a touch probe. The procedure is reported step-to-step in the following lines.
1. First, the specimen has to be clamped on the work-plane of the machine. It is preferable to constrain the weld on the steel side, which presents a more regular surface than the one on the ADI side. (Figure 4.2).

Figure 4.2: Specimen clamped on the work-plane

.

2. The touch probe has to be positioned at the middle-point of the joint width in order to measure all the point on the longitudinal plane.
3. Now, the touch probe is on the edge of the specimen and the X axis is set to zero. (Figure 4.3)

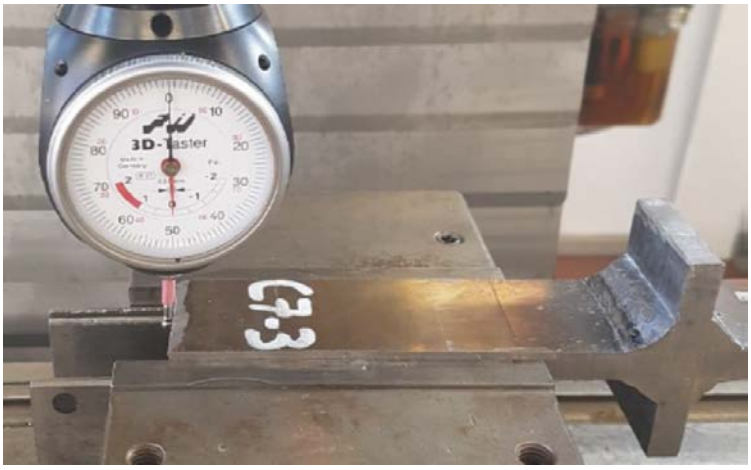

Figure 4.3: reset of the X axis at the edge of the specimen

.

4. Move the probe to x=2mm and reset all the coordinates : X, Z axis will change, while Y is kept constant at the middle-point. (Figure 4.4)

Figure 4.4: Set of the reference point O for the measurement

.

5. Measure the x and z coordinates at the point A just before the weld toe on S355 side. If the joint is cruciform, one should be carefull to avoid hurting the fillet with the head of the probe. (Figure 4.5)

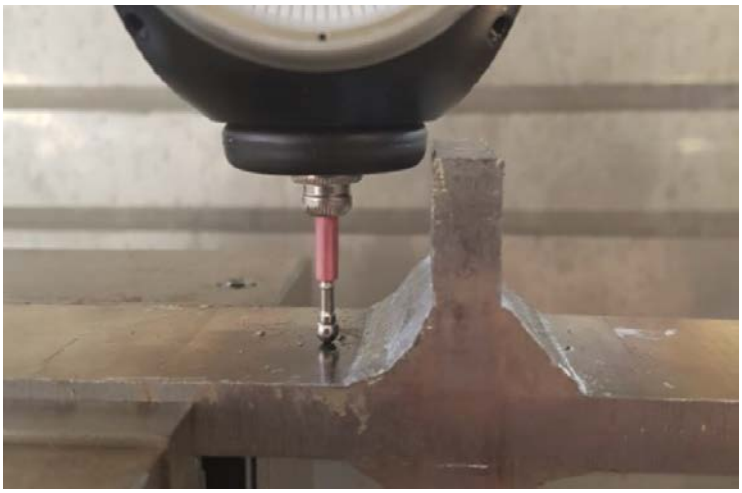

Figure 4.5: The measurement point A before the weld toe

.

6. Measure the x and z coordinates at the point A' just beyond the weld toe on ADI side. (Figure 4.6)

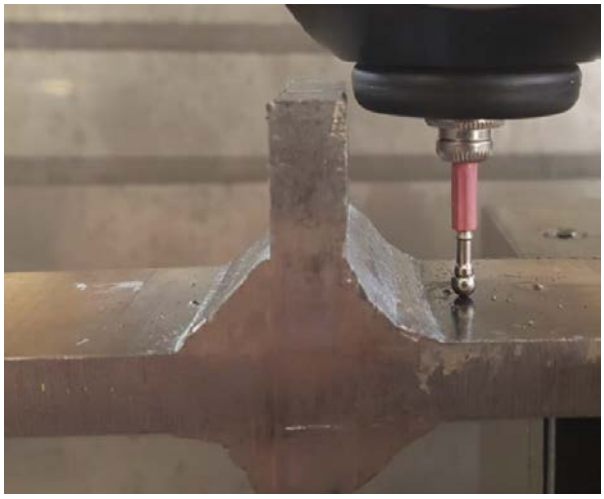

Figure 4.6: The measurement point A' beyond the weld toe on ADI side

.

7. Measure the x and z coordinates at the end point O' of the specimen on ADI side. (Figure 4.7)

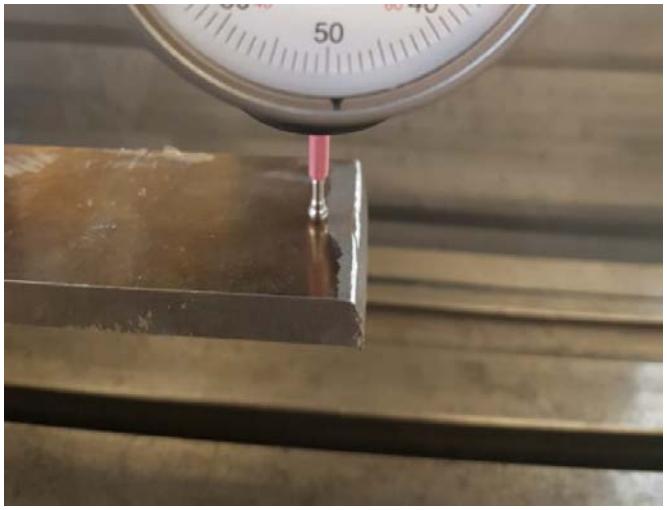

Figure 4.7: The measurement point at the end point of the specimen on ADI side

.

8. Rotate the specimen of 180° and measure the same points on the lower surface.
9. Calculate the misalignment with the following equations (see also Figure 4.8).

The linear misalignment is calculated as the difference between the z-coordinates at the point before and beyond the weld toe. For a greater accuracy, the average value is obtained from the ones obtained on the upper and lower surface of the

specimen:

$$e = Z_A - Z_{A'} \tag{4.1}$$

Having the coordinates of the four points on the surface, the total misalignment ΔZ is obtained from:

$$\Delta Z = Z_{O'} + l \cdot \beta_{S355} \tag{4.2}$$

where:

- l is the total length of the specimen
- L_{S355} is the length of the steel plate
- β_{S355} is the angle between the specimen and the work-plane calculated as:

$$\beta_{S355} = \arctan \frac{Z_A - Z_O}{L_{S355}} \tag{4.3}$$

Subtracting e from ΔZ, we obtain *e1* which represents the misalignment due to the angular component α:

$$e_1 = \Delta Z - e \tag{4.4}$$

Finally, the angular misalignment is:

$$\alpha = tan \frac{e_1}{l_{ADI}} [rad] \tag{4.5}$$

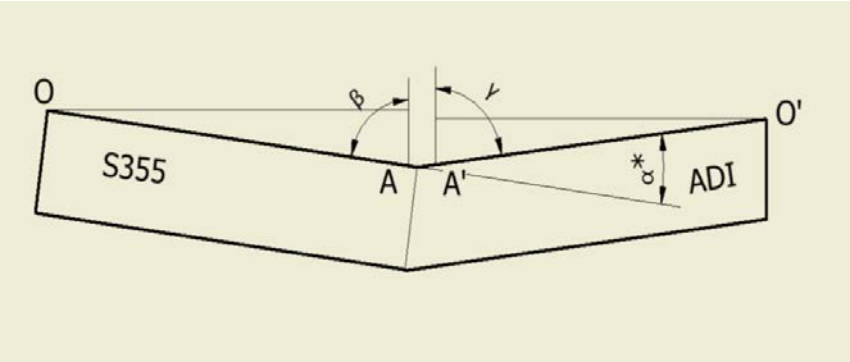

Figure 4.8: Parameters for the misalignment calculation

.

4.2 Resulting misalignment for all joint series

The misalignment for each specimen are reported in Tables 4.1 - 4.8.

Specimen code	e [mm]	ΔZ [mm]	e1 [mm]	α [rad]	α [deg]
A2-1	0.033	1.412	1.380	0.010	0.596
A2-2	0.165	1.774	1.609	0.012	0.694
A2-3	0.073	1.538	1.465	0.011	0.637
A3-1	0.863	1.560	0.698	0.005	1.035
A3-2	0.068	0.869	0.802	0.006	0.352
A3-3	0.033	1.174	1.142	0.009	0.516
A3-4	0.213	1.334	1.122	0.010	0.513
A3-5	-0.090	1.498	1.406	0.011	0.630
A3-6	0.040	1.603	1.563	0.012	0.662

Table 4.1: Misaligment of partial-penetration ground butt joints

.

Specimen code	e [mm]	ΔZ [mm]	e1 [mm]	α [rad]	α [deg]
B6-1	0.158	0.850	0.692	-0.006	0.507
B6-2	0.210	0.993	0.783	-0.007	0.598
B6-3	0.085	1.527	1.442	-0.012	0.695

Table 4.2: Misaligment of full-penetration butt joints

.

Specimen code	e [mm]	ΔZ [mm]	e1 [mm]	α [rad]	α [deg]
B7-1	0.030	0.963	0.933	0.008	0.399
B7-2	0.040	0.958	0.918	0.008	0.407
B7-3	0.053	0.611	0.559	0.005	0.288
B8-1	0.048	0.549	0.502	0.004	0.235
B8-2	0.055	0.795	0.740	0.006	0.355
B8-3	0.048	0.241	0.194	0.002	0.111
B8-4	0.038	0.166	0.128	0.001	0.074
B8-5	0.048	0.141	0.094	0.001	0.062
B8-6	0.130	0.555	0.425	0.004	0.305

Table 4.3: Misaligment of full-penetration ground butt joints

.

Specimen code	ΔZ [mm]	e1 [mm]	α [rad]	α [deg]
C13-3	3.609	3.609	0.030	1.695
C15-1	3.552	3.552	0.030	1.696
C15-2	3.584	3.584	0.029	1.684
C17-4	3.515	3.515	0.029	1.665
C16-1	2.770	2.770	0.023	1.301
C16-2	3.198	3.198	0.026	1.515
C16-3	4.044	4.044	0.034	1.932
C17-1	3.933	3.933	0.032	1.848
C17-2	3.881	3.881	0.032	1.823
C18-1	3.068	3.068	0.026	1.465
C18-2	3.032	3.032	0.025	1.448

Table 4.4: Misaligment of cruciform nlc fillet-welded joints

.

Specimen code	ΔZ [mm]	e1 [mm]	α [rad]	α [deg]
C13-1	3.837	3.837	0.032	1.833
C13-2	3.563	3.563	0.030	1.702
C14-1	2.492	2.492	0.020	1.161
C14-2	3.033	3.033	0.025	1.413
C14-3	2.600	2.600	0.021	1.211

Table 4.5: Misaligment of stress-relieved cruciform nlc fillet-welded joints

.

Specimen code	ΔZ [mm]	e1 [mm]	α [rad]	α [deg]
D2-4	0.385	0.385	0.004	0.245
D3-1	3.800	3.800	0.034	0.524
D3-2	1.119	1.119	0.011	0.346
D1-1	0.586	0.586	0.004	0.182
D1-4	2.153	2.153	0.020	0.604
D1-3	2.347	2.347	0.022	0.960
D1-2	0.307	0.307	0.003	0.311
D1-5	1.082	1.082	0.011	0.384
D1-6	0.823	0.823	0.008	0.322
D2-6	0.948	0.948	0.009	0.213
D2-5	0.581	0.581	0.004	0.233

Table 4.6: Misaligment of T nlc fillet welded joints

.

Specimen code	e [mm]	ΔZ [mm]	e1 [mm]	α [rad]	α [deg]
E2-1	0.438	0.890	0.452	0.004	0.230
E2-2	0.178	0.428	0.250	0.002	0.207
E2-3	0.378	0.346	-0.031	0.000	0.083
E2-4	0.345	0.585	0.240	0.002	0.237
E2-5	0.380	0.690	0.310	0.002	0.243
E2-6	0.370	0.640	0.270	0.002	0.245
E3-1	0.813	0.748	-0.064	-0.001	0.184
E3-2	1.323	1.418	0.096	0.001	0.243
E3-3	1.738	2.024	0.286	0.002	0.300
E3-4	1.850	1.100	-0.750	-0.006	0.322
E3-5	2.015	2.775	0.760	0.006	0.364
E3-6	1.355	0.666	-0.689	-0.006	0.327
E4-1	0.160	0.351	0.191	0.002	0.148
E4-2	0.155	0.244	0.089	0.001	0.177
E4-3	0.175	0.423	0.248	0.002	0.138

Table 4.7: Misaligment of cruciform joints with load-carrying fillet-welds

.

Specimen code	e [mm]	ΔZ [mm]	e1 [mm]	α [rad]	α [deg]
F2-1	0.145	4.966	4.821	0.044	1.032
F2-2	0.440	1.475	1.035	0.009	0.514
F3-1	0.360	1.899	1.539	0.013	0.775
F3-2	0.798	3.044	2.246	0.019	1.057
F3-3	0.218	2.493	2.275	0.019	1.085
F3-4	0.238	2.369	2.131	0.018	1.027
F3-5	0.490	2.263	1.775	0.015	0.868
F3-6	0.263	2.445	2.183	0.018	1.099
F4-1	1.08	4.47	3.39	0.03	1.59
F4-2	0.09	3.86	3.77	0.03	1.76
F4-3	1.62	3.86	2.25	0.02	2.49
F4-4	1.33	4.99	3.67	0.03	1.77
F4-5	1.30	19.07	17.76	0.15	0.80

Table 4.8: Misaligment of cruciform full-penetration joints

.

Chapter 5

Specimens characterization: metallographic analysis, hardness measurement and residual stresses

The aim of this chapter is to describe the methods used for the material characterization. In order to study the main properties of the specimens, three analyses have been performed:

- Microstructure characterization
- Determination of micro-hardness profiles
- Determination of the amount of residual stresses

5.1 Metallographic analysis

Metallography is the study of physical structure and components of metals, by using microscopy. The surface of a metallographic specimen is prepared by various methods of grinding, polishing, and etching. Mechanical preparation is the most common method. Finer abrasive particles are successively used to remove material from the sample surface until the desired quality is achieved. Many different machines are available for doing this, which are able to meet different demands for quality and reproducibility. The microstructural constituents of the specimen are revealed by using a suitable chemical etchant. After preparation, it is often analysed using optical or electron microscopy.
To understand how the material is transformed by the welding process, a metallographic analysis was performed on a selection of joints. The ADI presents the ausferritic microstructure, consisting of retained austenite and acicular ferrite, while on the steel S355J2 side, the base material presents the typical microstructure with parallel grains due to the lamination process (Figures 5.1 and 5.2).

At the ADI side, because of the metastable solidification after re-melting, graphite precipitates out of the melt and produces an austenite-cementite eutectic. The latter, known as ledeburite, cannot be avoided at the HAZ-FZ

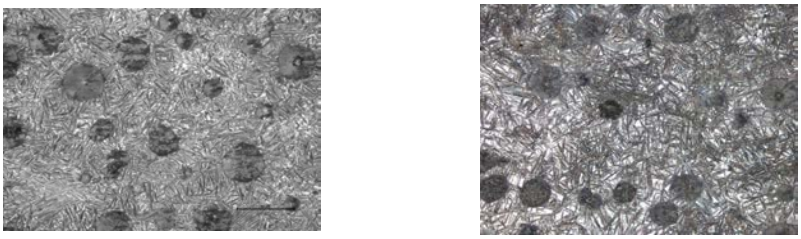

Figure 5.1: On the left, the base material of ADI with ausferritic matrix, while on the right, the HAZ of ADI with graphite nodules in pearlitic matrix

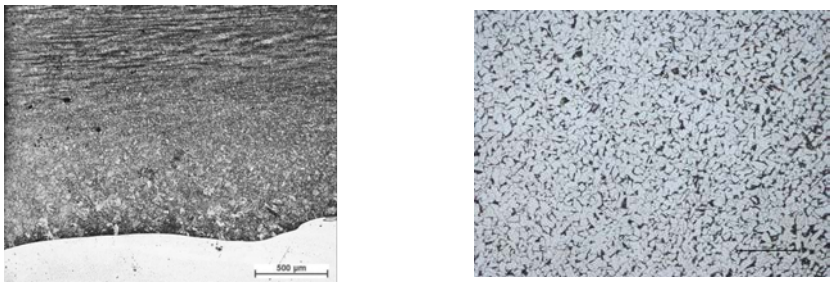

Figure 5.2: On the left, it can be noticed the laminate microstructure of the base material above the pearlite in HAZ due to the tempering. On the rigth, a zoom-in at 100x of the steel microstructure.

interface, but it is essential to prevent the formation of martensite in this area. In all series, the results confirm that heat-affected zone of ADI 1050 mainly consists in graphite nodules in pearlitic matrix and thin ledeburite layer close to weld metal (Figure 5.3). On the other hand, HAZ of S355J2 consists in ferritic-pearlitic matrix (Figure 5.2).

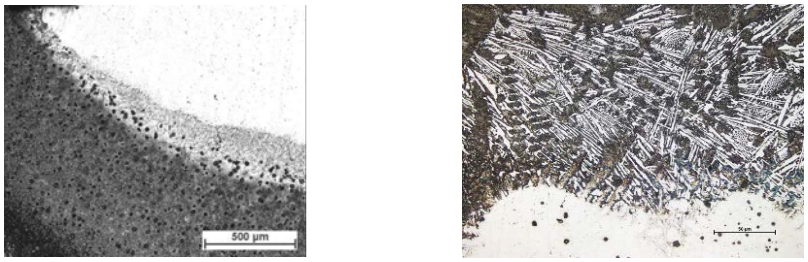

Figure 5.3: On the left, an view of the HAZ of ADI with ledeburite layer. On the right, a zoom-in at 500x of the ledeburite microstructure.

5.2 Micro-hardness measurement

The hardness of a material can be defined by different concepts, depending on the field of application. From a technological point of view, hardness is the resistance of a material to deformation, indentation, or penetration by means such as abrasion, drilling, impact, scratching, and/or wear. Hardness tests such as Brinell, Knoop, Rockwell, or Vickers are usually static, performed by specific devices. The term Micro Hardness Testing usually refers to static indentations made by loads of 1kgf. or less. The Brinell Hardness Test uses a 1mm carbide ball, while the Vickers Hardness Test employs a diamond with an apical angle of 136°, and the Knoop Hardness Test uses a narrow rhombus shaped diamond indenter. The test surface usually must be highly polished. The smaller the force applied, the higher the metallographic finish required. Traditional micro-hardness test methods optically analyse the indented impression, convoluting data with operator bias and thus, microscopes with a magnification of around 500x are required to accurately measure the indentations produced.

5.2.1 Vickers hardness test

During Vickers test, the indenter is pushed onto the component surface. The time interval for penetration is set at 30 seconds by standards. The Vickers Hardness (HV) is defined as the ratio between the applied load (kg) and the area (mm^2) of the indented impression. The penetrator is a pyramidal diamond with square base and an apical angle of 136° (Figure 5.4).

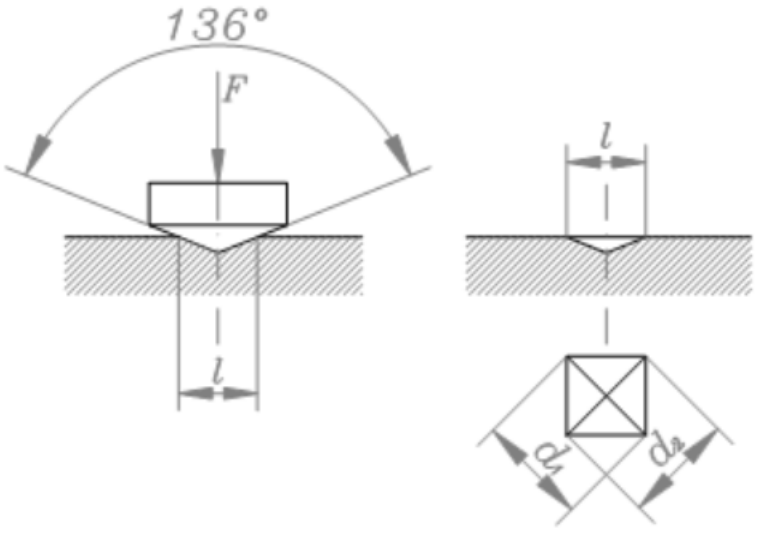

Figure 5.4: The penetrator for Vickers hardness test and the indented impression

The equation employed for HV calculation is:

$$HV = \frac{F}{A} = \frac{2 \cdot F \sin\frac{\theta}{2}}{d^2} = 1.854\frac{F}{d^2} \tag{5.1}$$

where the force F is in kg and the diagonal d in mm. The applied load should reach the maximum within 10-15 seconds and the dwell time is 15 seconds. For

any given load, the hardness increases rapidly at low diagonal lengths, with the effect becoming more pronounced as the load decreases. Thus at low loads, small measurement errors will produce large hardness deviations and one should always use the highest possible load in any test. The main advantages of this test are:

- the unlimited field of application for both hardness value and specimen's dimension
- the hardness is independent from the applied load

The cons are the need of great accuracy in specimen preparation and the limited area of the material involved by the indenter.

5.2.2 Microhardness tests on dissimilar joints: procedure and specimens preparation

The hardness measurement on dissimilar ADI-to-steel welded joints were carried out with an applied load of 500g. The tester employed was a Leitz MINILOAD Microhardness Tester, with two lenses at low and high grade of magnification: observation and measurement of the indentation can be done directly on the eyepiece at 500x total magnification.

Procedure One ought to follow the steps reported below for carrying out the hardness test:

1. Applying the load on the proper support;
2. Finding a suitable area on the surface with the stage spindles and the 10x objective. The surface must be clean and free from scratches and impurities;
3. Turning in the 50x (high magnification) for focusing on the surface;
4. Turning in the diamond;
5. Release the diamond movement;
6. The diamond descends (10 secs) and makes an indentation (20 secs)
7. Lifting the diamond with the apposite knob.
8. The 50x objective is turned in and the indentation measured. If the centre lines of the eyepiece are set on the diagonals, their point of intersection serves as sighting point for further indentations, which can be made with a high degree of spotting accuracy.

Specimens preparation As already introduced, the samples need to be accurately prepared for the hardness test. In particular, the metal specimens have to be ground and polished with different grades of abrasive paper until the surface finish is satisfactory. The abrasive paper are placed on a smooth, flat surface and it is necessary to follow a sequence of P120, P240, P320, P500, P1200, P2500 and P4000 grits. In between each paper, the surface has to be

polished with alcohol to keep away the rebound that may affect the success of the surface preparation. After each grinding step, the sample must be rotated 90° and all scratches from the previous paper removed before proceeding to a smaller grit paper. After the final grinding step, the base of the mount must be ground parallel with the surface to be indented. The latter step is fundamental in order to have reliable results from the hardness test. The Leitz Tester, employed for the measurement reported here, is not equipped with a paralleling device, thus it is operator's responsibility to guarantee a good parallelism between surfaces. Two methods were employed for grinding and polishing:

- Initially, trying to keep the specimen intact for further fatigue test, a surface plate was employed. The abrasive paper were attached on the plate and the sample was ground pushing and moving it against the flat surface, as show in Figure 5.5

- The second procedure involves metallographic polishing machine. In this case, the specimen needs to be cut to a smaller size, so it can fit into the abrasive disk diameter(Figure 5.6). However,the joints cannot be used for further fatigue tests.

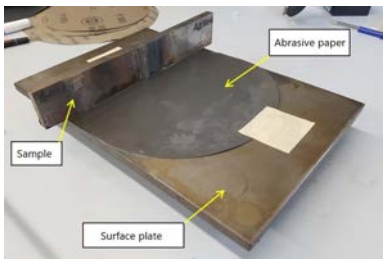

Figure 5.5: Equipment initially employed for grinding the samples

Figure 5.6: Metallographic polishing machine employed for samples preparation

The second method was prove to give better and more reliable results as it ensures a good surface finish and the parallelism between the work-plane and the surface to be indented. If the latter is not planar enough, the hardness measurement can be highly biased as it is shown in Figure 5.7. The indentations were realized on the same specimen (cruciform non-load-carrying fillet-welded joints, code C17_1): the sample was ground by the mean of abrasive papers in the case of the blue plot, while the red plot was obtained with the second method, i.e. the specimen was cut and then ground on the metallographic polishing machine. The red plot is in line with the hardness values in literature for the same microstructure, whereas the blue plot reports uneven and incorrect results.

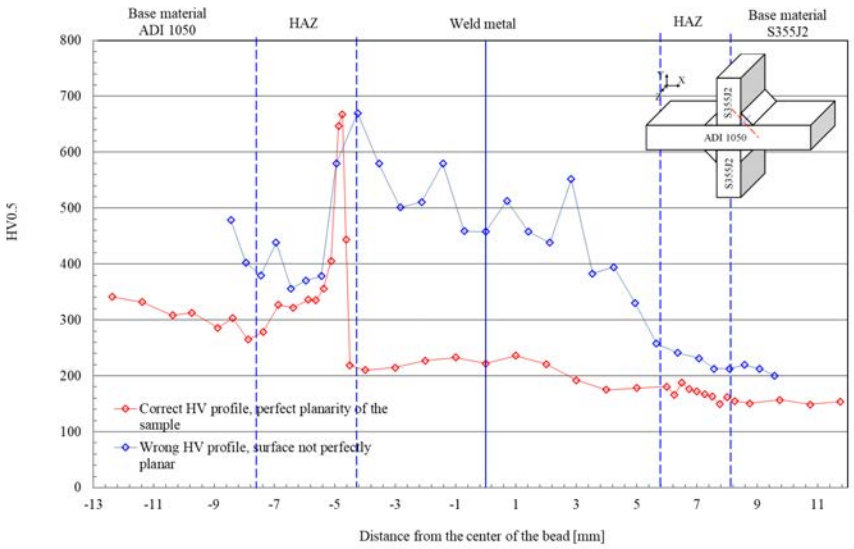

Figure 5.7: Comparison between hardness measurement on specimen of joint series C. A non-proper surface finish leads to biased results (blue plot). The red plot refers to the same sample with a finest surface finish.

5.2.3 Micro-hardness profiles

For structural welded components, it is important to investigate material properties in the neighbourhood of the weld bead, where the microstructure is altered by the welding process. The hardness, coupled with metallographic analysis, can give a comprehensive overview of this matter. The micro-hardness profile must include the 3 typical zones of a weld (Fuse Zone, Heat Affected Zone and Base Material) both on the ADI and steel side (Figure 5.8)

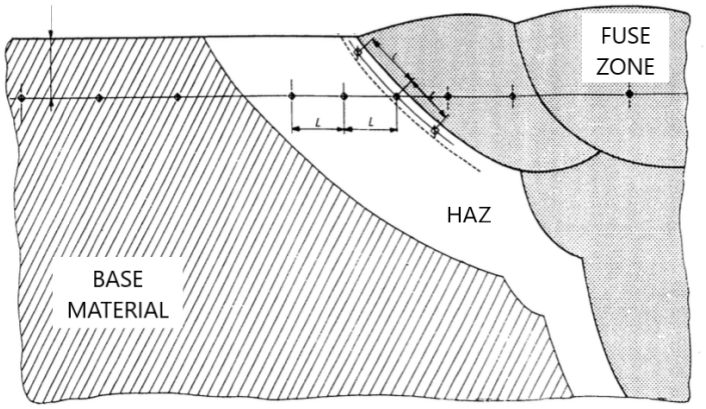

Figure 5.8: Micro-hardness measurements on the Base Metal, HAZ and Fuse Zone

The micro-hardness profiles were obtained for:

- partial-penetration butt-welded joints (specimen code A1_6)
- full-penetration butt-welded joints (specimen code B2_6)
- full-penetration ground butt joints (specimen code B4_2)
- cruciform non-load-carrying fillet-welded joints (specimen code C17_1)
- stress-relieved cruciform non-load-carrying fillet-welded joints (specimen code C14_3)
- T non-load-carrying fillet-welded joints (D)
- cruciform load-carrying fillet-welded joints (specimen code E1-3)
- cruciform full penetration K-butt-welded joints (F)

Micro-hardness: partial penetration butt joint

Table 5.1 reports the hardness values for the partial penetration butt joint, while Figure 5.9 reports the micro-hardness profile. In the latter, the attached pictures show the corresponding microstructure in the indentation point. On the ADI side, hardness is around 300-400HV in the base material and it increases up to 500HV in the HAZ. At the interface between ADI and the weld metal, there is the high peak due to the ledeburite layer, which may reach the value of 700HV. On the S355J2 side, the hardness starts from a value of 200HV and decreases to 150HV in the base material, where the steel was not affected by the welding process.

d	Hardness	d	Hardness	d	Hardness	d	Hardness
[mm]	HV	[mm]	HV	[mm]	HV	[mm]	HV
7.25	158	0.75	208	-1.5	538	-5	349
6.25	160	0.5	205	-1.75	508	-5.25	310
5.25	150	0.25	211	-2	520	-5.5	365
4.25	176	0	202	-2.25	470	-5.75	294
3.75	178	-0.125	208	-2.5	438	-6.25	292
3.25	172	-0.25	329	-2.75	446	-6.75	295
2.75	184	-0.375	333	-3	503	-7.25	321
2.5	195	-0.5	692	-3.25	472	-7.75	312
2.25	190	-0.625	595	-3.5	431	-8.25	319
2	180	-0.75	519	-3.75	390	-8.75	319
1.75	160	-0.875	486	-4	503	-9.25	322
1.5	180	-1	510	-4.25	519	-9.75	330
1.25	203	-1.125	534	-4.5	488	-10.75	350
1	204	-1.25	517	-4.75	438	-11.75	339

Table 5.1: Hardness values for the Partial Penetration butt joint

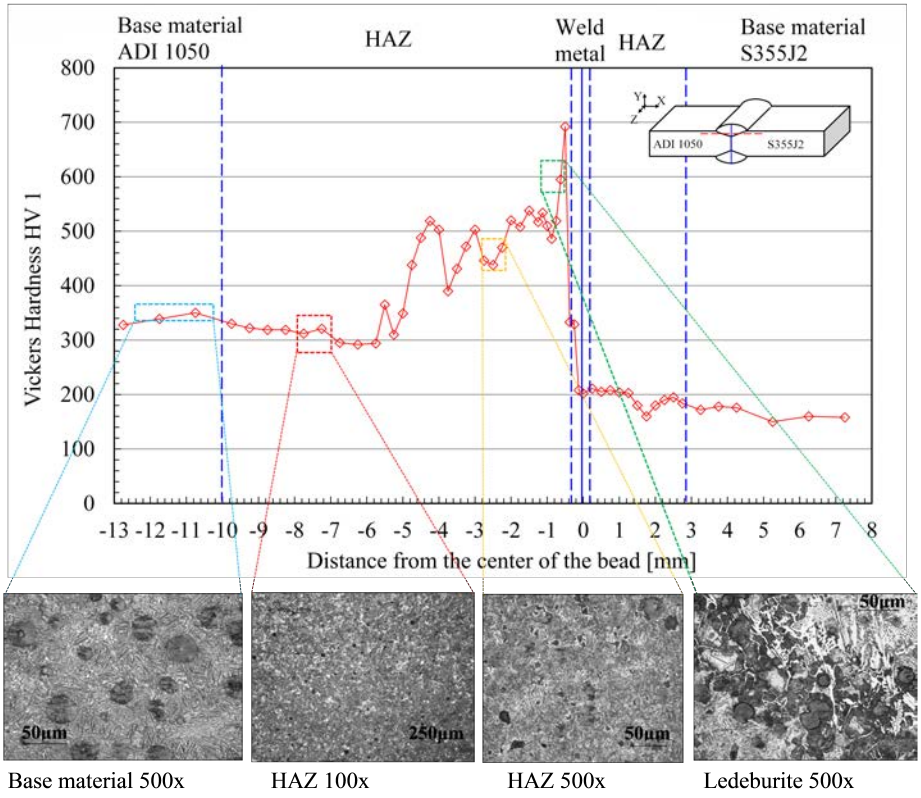

Figure 5.9: HV1 measurement on cross-section of a joint type A (partial-penetration butt-joint)

Micro-hardness: full penetration butt joint

Table 5.2 reports the hardness values for the full penetration butt joint, while Figure 5.10 reports the micro-hardness profile. As reported above, the attached pictures show the corresponding microstructure in the indentation point. On the ADI side, hardness is around 350-400HV in the base material and at the beginning of the HAZ. At the interface between ADI and the weld metal, there is the high peak due to the ledeburite layer, which reaches the value of 526HV. On the S355J2 side, the hardness starts from a value of 200HV and decreases to 180HV in the base material, where the steel was not affected by the welding process. Figure 5.11 shows the line along which the indentations were performed.

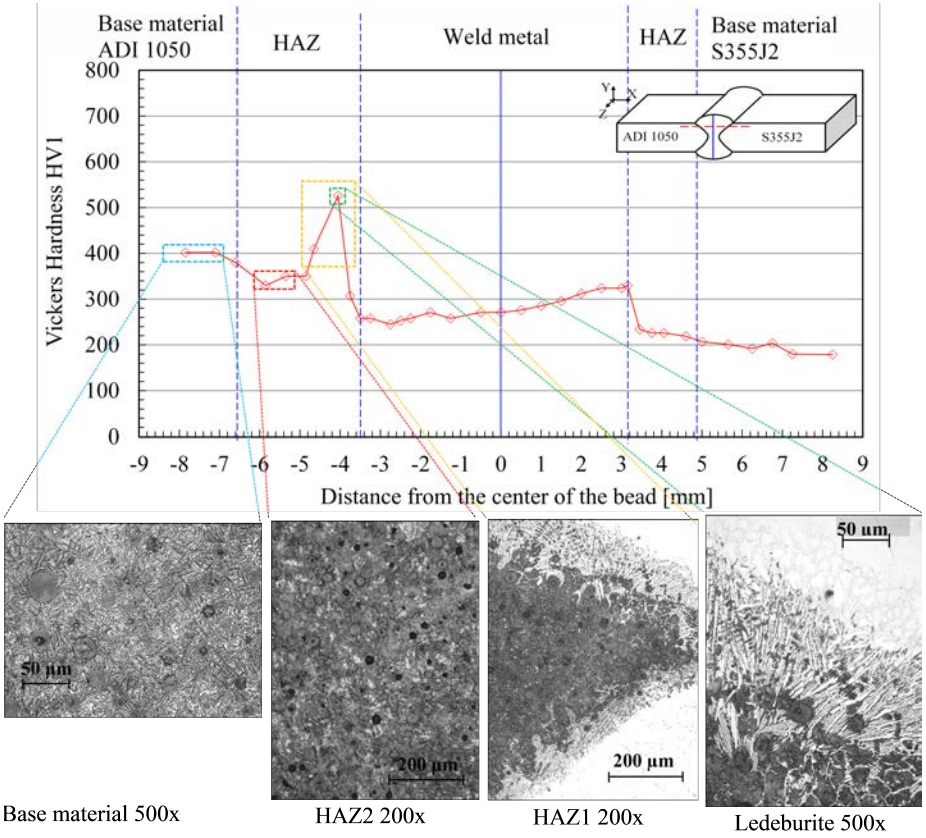

Figure 5.10: HV1 measurement on cross-section of a joint type B1 (full-penetration butt joint)

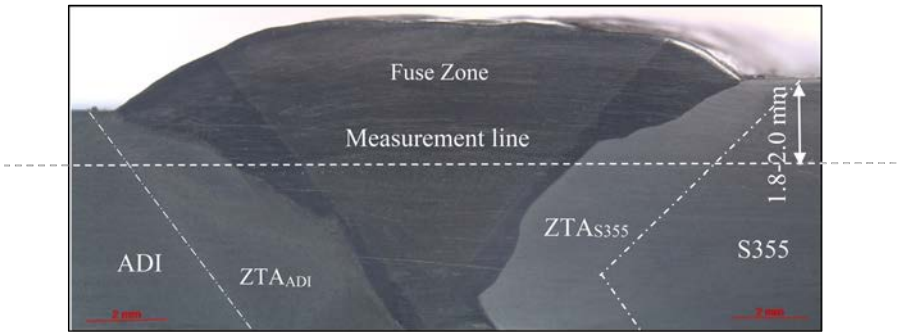

Figure 5.11: HV1 measurement line on on cross-section of a joint type B1 (full-penetration butt joint)

d [mm]	Hardness HV	d [mm]	Hardness HV
-7.85	402	0.5	276
-7.1	402	1	285
-6.6	380	1.5	296
-5.85	330	2	312
-5.35	350	2.5	324
-4.85	350	3	324
-4.65	410	3.15	330
-4.05	526	3.45	234
-3.75	307	3.75	226
-3.5	258	4.05	226
-3.25	258	4.6	219
-2.75	245	5	207
-2.5	253	5.65	201
-2.25	258	6.25	192
-1.75	271	6.75	204

Table 5.2: Hardness values for the full-penetration butt joint

Micro-hardness: full penetration ground butt joint

Table 5.3 reports the hardness values for the full penetration ground butt joint, while Figure 5.12 reports the micro-hardness profile. As reported above, the attached pictures show the corresponding microstructure in the indentation point. On the ADI side, hardness is around 307-330HV in the base material and 550-560HV at the beginning of the HAZ. At the interface between ADI and the weld metal, there is the high peak due to the ledeburite layer, which reaches the value of 715HV. On the S355J2 side, the hardness starts from a value of 250HV and decreases to 180HV in the base material, where the steel was not affected by the welding process.

d [mm]	Hardness HV	d [mm]	Hardness HV
-9	371	1.5	241
-8	330	2	258
-7.5	307	2.5	253
-7	336	3	280
-6.5	330	3.5	249
-6	330	4	285
-5.5	566	4.5	226
-5	552	5	210
-4.5	715	5.5	192
-4	490	6	198
-3.5	234	6.5	189
-3	230	7	182
-2.5	223	7.5	176
-2	249	8	179
-1.5	226	9	184
-1	249		
-0.5	226		
0	241		
0.5	234		
1	234		

Table 5.3: Hardness values for the full-penetration ground butt joint

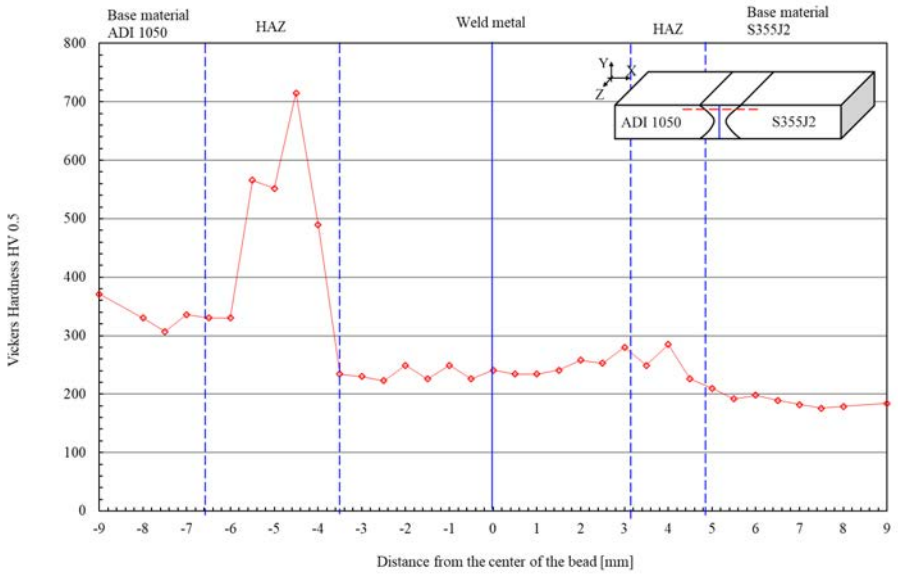

Figure 5.12: HV1 measurement on cross-section of a joint type B1 (full-penetration ground butt joint)

Micro-hardness: cruciform non-load-carrying fillet-welded joint

The hardness values for cruciform non-load-carrying fillet-welded joint are reported in Table 5.4, while the corresponding micro-hardness profile is plotted in Figure 5.14. The measurement line with the indentation points is shown in Figure 5.13. On the ADI side, hardness is around 250-350HV in the base material and at the beginning of the HAZ. At the interface between ADI and the weld metal, there is the high peak due to the ledeburite layer, which reaches the value of 668HV. On the S355J2 side, the hardness starts from a value of 236HV and decreases to 150HV in the base material, where the steel was not affected by the welding process.

d [mm]	Hardness HV	d [mm]	Hardness HV
-12.375	341	1	236
-11.375	332	2	221
-10.375	308	3	192
-9.735	313	4	175
-8.875	286	5	178
-8.375	303	6	181
-7.875	265	6.25	166
-7.375	278	6.5	188
-6.875	327	6.75	176
-6.375	322	7	172
-5.875	336	7.25	167
-5.625	335	7.5	163
-5.375	356	7.75	150
-5.125	405	8	162
-4.875	647	8.25	155
-4.75	668	8.75	151
-4.625	444	9.75	157
-4.5	219	10.75	149

Table 5.4: Hardness values for the cruciform non-load-carrying fillet-welded joint

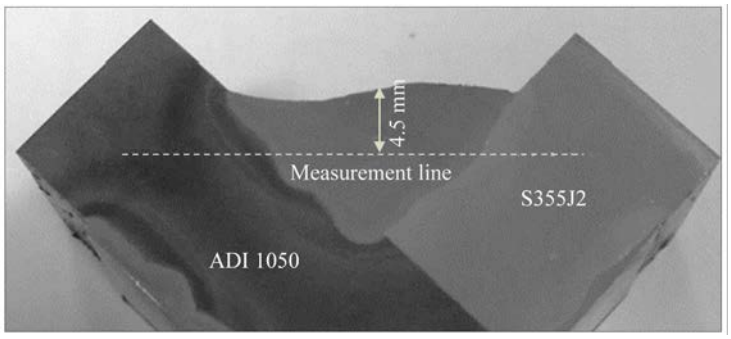

Figure 5.13: HV1 measurement line on cross-section of a joint type C (cruciform non-load-carrying fillet-welded joint)

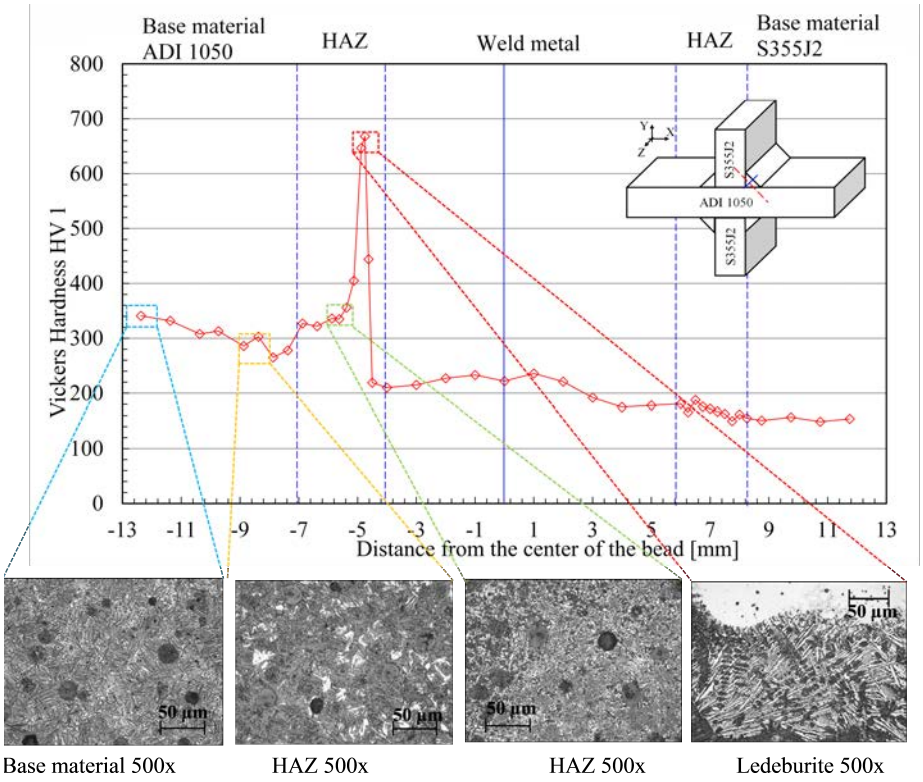

Figure 5.14: HV1 measurement on cross-section of a joint type C (cruciform non-load-carrying fillet-welded joint)

Micro-hardness: stress-relieved cruciform non-load-carrying fillet-welded joint

The hardness values for stress-relieved cruciform non-load-carrying fillet-welded joint are reported in Table 5.5, while the corresponding micro-hardness profile is plotted in Figure 5.15 with the pictures of the corresponding microstructure. The measurement line with the indentation points is shown in Figure 5.16. On the ADI side, hardness is around 300-320HV in the base material and at the beginning of the HAZ. At the interface between ADI and the weld metal, there is the high peak due to the ledeburite layer, which reaches the value of 576HV. In the weld metal the hardness maintains a value around 200HV and it decreases to 150HV in the S35J2 steel.

d [mm]	Hardness HV	d [mm]	Hardness HV	d [mm]	Hardness HV
10	147	1.5	175	-5	296
9	148	1	198	-5.25	304
8	143	0.5	196	-5.5	319
7	143	0	194	-5.75	299
6	145	-0.5	192	-6	303
5.5	145	-1	179	-6.5	275
5	162	-1.5	208	-7	285
4.5	160	-2	203	-7.5	298
4.25	158	-2.5	196	-8	327
4	165	-3	212	-9	299
3.75	152	-3.5	206	-10	307
3.5	209	-4	180	-6	303
3	191	-4.125	177	-6.5	275
2.5	215	-4.25	449		
2	216	-4.375	576		

Table 5.5: Hardness values for the cruciform non-load-carrying fillet-welded joint

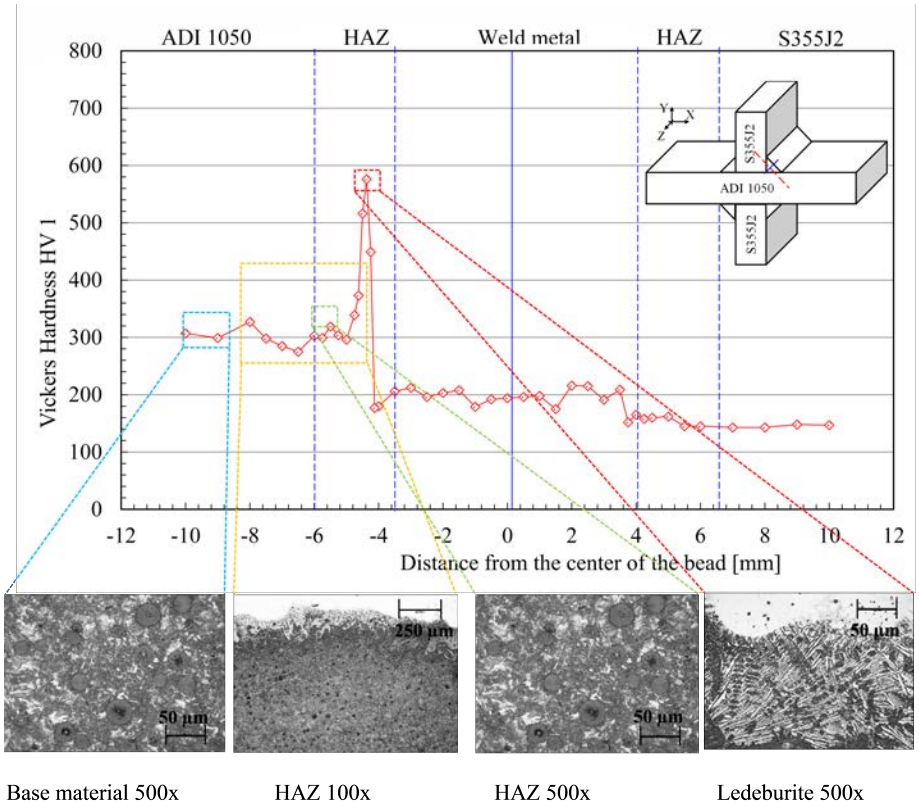

Figure 5.15: HV1 measurement on cross-section of a stress-relieved joint type C (cruciform non-load-carrying fillet-welded joint)

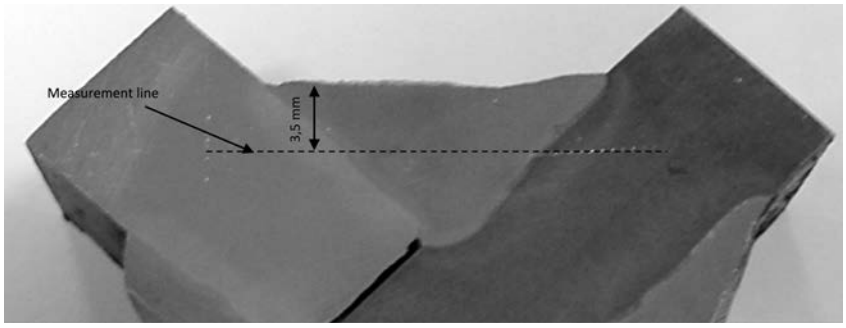

Figure 5.16: HV1 measurement line on cross-section of a stress-relieved joint type C (cruciform non-load-carrying fillet-welded joint)

Micro-hardness: T non-load-carrying fillet-welded joint

The hardness values for T non-load-carrying fillet-welded joint are reported in Table 5.6, while the corresponding micro-hardness profile is plotted in Figure 5.17. On the ADI side, hardness is around 330-420HV in the base material and at the beginning of the HAZ. At the interface between ADI and the weld metal, the peak due to the ledeburite layer reaches the value of 851HV. In the weld metal, the hardness drops down to 312HV and then to 245HV going towards the steel side. The base material at steel side presents 180HV hardness.

d [mm]	Hardness HV	d [mm]	Hardness HV
-12.5	386.09	-3.5	266.30
-12	363.49	-2.5	312.09
-11.5	370.80	-1.5	306.45
-11	330.01	0	295.60
-10	386.09	3	280.38
-9	419.65	4.5	266.30
-8.5	370.80	6	275.56
-8	356.40	7.5	245.09
-7.5	402.34	8.5	285.32
-7	306.45	9.5	212.81
-6.5	735.57	10.5	189.18
-6	457.78	12	178.82
-5.5	851.24	13	189.18
-5	715.28		
-4.5	801.90		

Table 5.6: Hardness values for T non-load-carrying fillet-welded joint

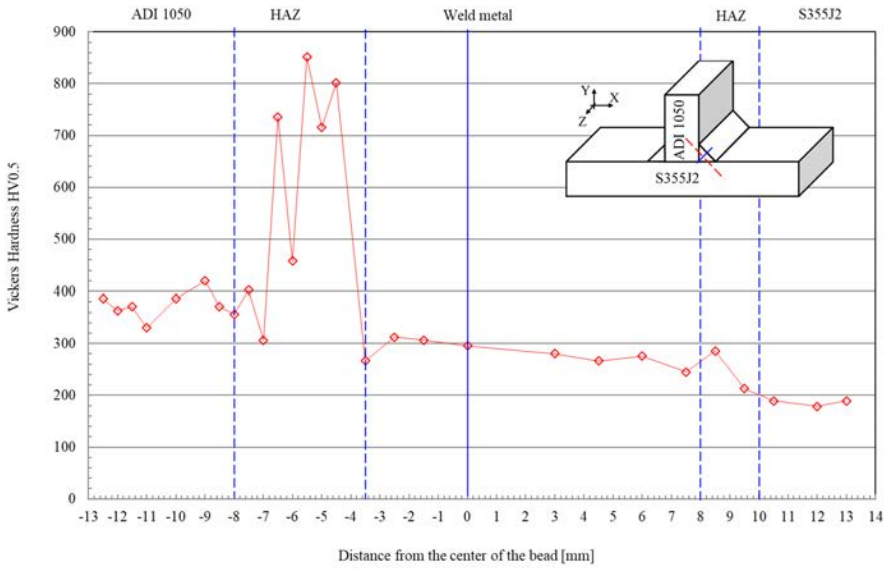

Figure 5.17: HV1 profile on cross-section of a joint type D (T non-load-carrying fillet-welded joint)

Micro-hardness: cruciform load-carrying fillet-welded joints

The hardness values for cruciform full penetration K-butt-welded joint are reported in Table 5.7, while the corresponding micro-hardness profile is plotted in Figure 5.18. On the ADI side, hardness is in a range from 360 up to 500HV in the base material and at the beginning of the HAZ. At the interface between ADI and the weld metal, the peak due to the ledeburite layer reaches the value of 700HV. In the weld metal, the hardness exhibits values around 400HV near the ADI side, while it drops down to 257HV going towards the steel side. The base material at steel side presents 160HV hardness.

d [mm]	Hardness HV	d [mm]	Hardness HV
12	370.8	-3	394.0908
-11.5	478.8223	-2	342.8254
-11	468.1227	0	386.0891
-10.5	386.0891	2	257.5
-10	419.6469	4	257.5
-9.5	428.7201	5	275.5648
-9	363.4938	6	285.3186
-8.5	363.4938	7	206.5048
-8	363.4938	7.5	183.8921
-7.5	419.6469	8	164.8
-7	609.4675	8.5	160.4917
-6.5	513.218	9.5	169.2841
-6	579.375	10.5	169.2841
-5.75	695.8153		
-5	438.0907		
-4	402.3438		

Table 5.7: Hardness values for the cruciform load-carrying fillet-welded joints

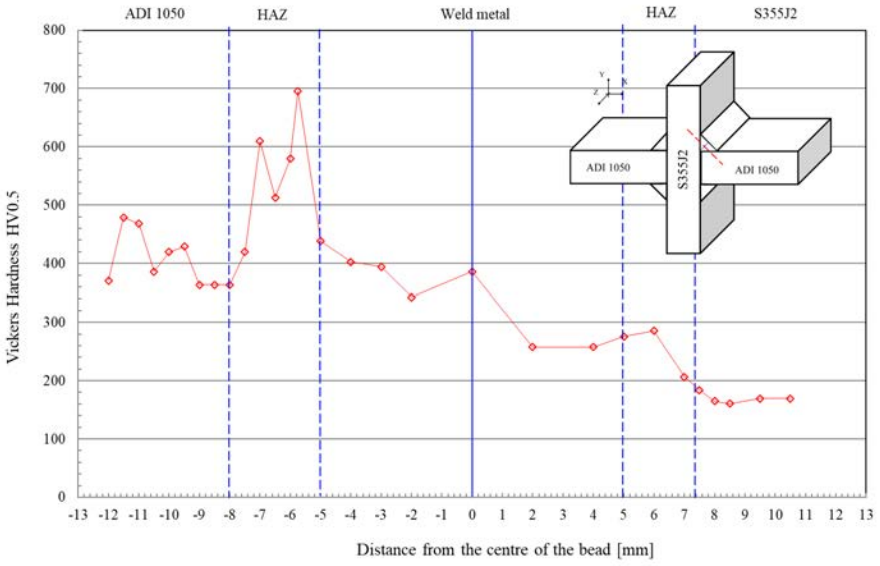

Figure 5.18: HV1 profile on cross-section of a joint type E (cruciform load-carrying fillet-welded joint)

Micro-hardness: cruciform full penetration K-butt-welded joint

The hardness values for cruciform full penetration K-butt-welded joint are reported in Table 5.8, while the corresponding micro-hardness profile is plotted in Figure 5.19. On the ADI side, hardness is around 340-370HV in the base material and at the beginning of the HAZ. At the interface between ADI and the weld metal, the peak due to the ledeburite layer reaches the value of 964HV. In the weld metal, the hardness exhibits values around 430-490HV near the ADI side, while it drops down to 261HV going towards the steel side. The base material at steel side presents 190HV hardness.

d [mm]	Hardness HV	d [mm]	Hardness HV
-12	370.8	-1	438.0907
-11.5	342.8254	0	419.6469
-11.25	356.4014	1	323.8711
-11	489.893	2	261.8459
-10.5	457.7778	3	306.4463
-9.5	428.7201	4	300.9496
-8.5	501.3521	5	270.8744
-7.5	801.9031	6	241.155
-7	695.8153	6.5	229.8965
-6.5	801.9031	7	226.3184
-6	964.6202	7.5	229.8965
-5.5	428.7201	8	212.8099
-5	438.0907	9	209.6218
-4	478.8223	10	194.707
-3	489.893	11	206.5048
-2	438.0907		
-1	438.0907		
0	419.6469		

Table 5.8: Hardness values for the cruciform full penetration K-butt-welded joint

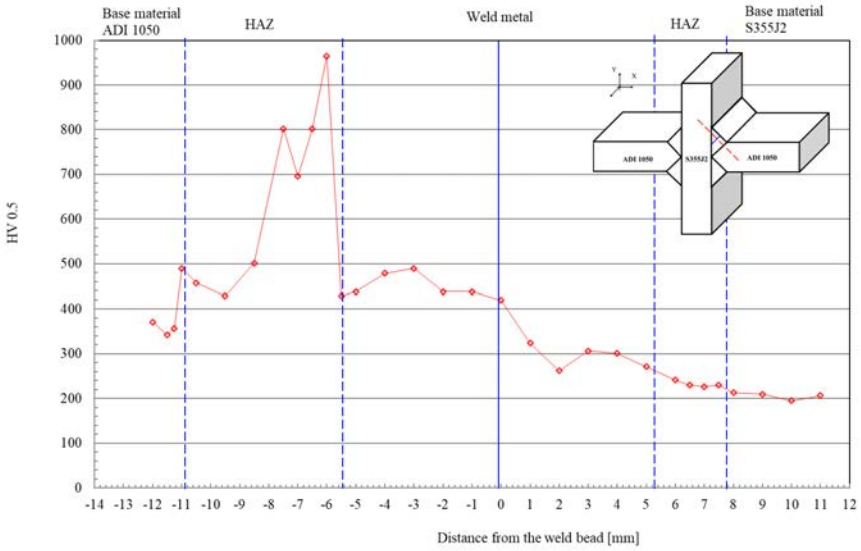

Figure 5.19: HV1 measurement on cross-section of a welded joint type F (cruciform full penetration K-butt-welded joint)

Chapter 6

Testing program and fatigue results:comparison with actual standards

The experimental results are reported in this chapter. First, an introduction on the tests and loading condition will be given. Then, the failure mode and fracture surfaces will be analysed in detail. The design curves for the hybrid joints will be reported in terms of the applied load versus the number of cycles to failure and compared to the design curves for welded joints made of structural steel.

6.1 Introduction to experimental fatigue tests

Experimental fatigue tests have been performed on welded joints presented previously in Chapter 3. On the base of the measured misalignments, the fatigue loads were applied to each test series as follows:

- partial-penetration butt joints (A) and cruciform load-carrying fillet welded joints (E) were fatigue tested under axial loading to assess weld root as well as weld toe failure, after having milled the clamping surfaces to minimize the misalignments and reduce secondary bending effects;
- full-penetration ground butt-joints (B2),T nlc fillet-welded joints (D) and plain specimens (L) were fatigue tested under axial loading without milling the clamping surfaces due to the limited misalignments;
- full-penetration ground butt-joints (B2) were also fatigue tested under four-point bending loading;
- full-penetration butt joints (B1), as-welded cruciform nlc fillet-welded joints (C), stress-relieved cruciform nlc fillet-welded joints and cruciform full-penetration K-butt-welded joints (F) were fatigue tested under four-point bending loading, in order to avoid secondary bending effects.
- a couple of cruciform load-carrying fillet welded joints (E) were fatigue tested under four-point bending loading to compare them with the cruci-

form nlc fillet-welded joints, as the failure mode was always at the weld toe for the both of them

All structural details were tested in standard laboratory environment, using an MFL axial servo-hydraulic machine, which has a maximum load capacity of 250 kN and it is equipped with an MTS TestStar IIm digital controller. The experimental tests were carried-out under closed-loop load control by applying sinusoidal cyclic load with constant amplitude and nominal load ratio R. The load frequency was set ranging from 10 up to 30 Hz depending on the applied load level. The number of loading cycles Nf at complete separation has been defined as the fatigue life to failure of each specimen, while run-out was fixed at $2 \cdot 10^6$ cycles, when no failure occurred. Figure 6.1 shows the MFL machine with a butt joint under axial loading and a cruciform joint under four-point bending loading. A brief overview of the experimental tests and load condition applied on the tested series is reported in Table 6.1.

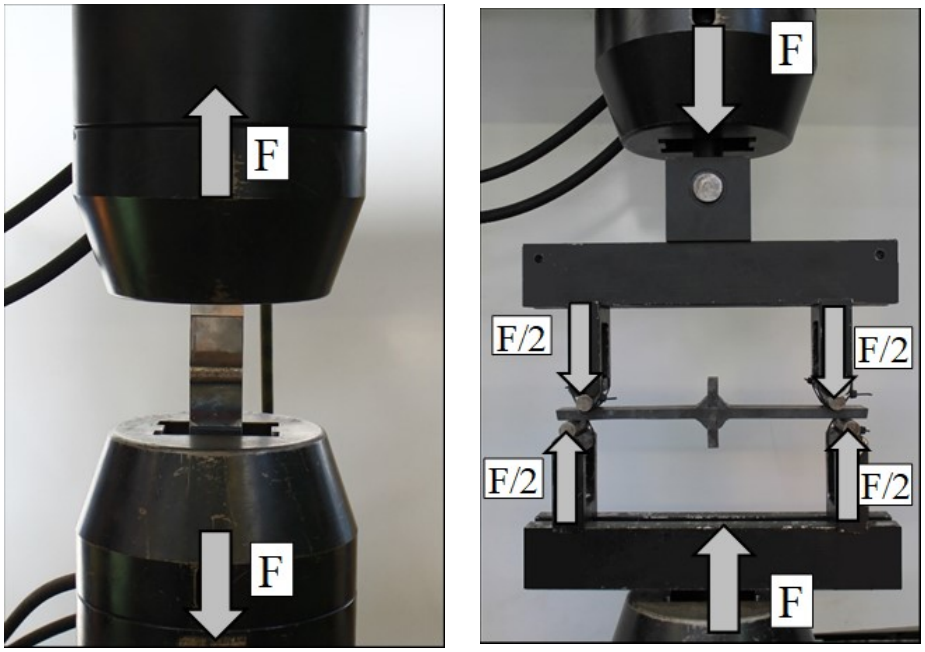

Figure 6.1: The MFL machine employed for the fatigue tests. On the right, a partial-penetration butt-joint tested in the axial fatigue test machine under axial loading. On the right, a cruciform nlc fillet-welded joints tested in the fatigue test machine under four-point bending loading by means of a dedicated loading fixture.

Series	Geometry	Test conditions	Load	Number of tested specimens	Load ratio R
A	Partial-penetration butt joints	AW*	AX	12	0.05
				4	0.5
B1	Full-penetration butt joints	AW	4PB	14	0.05
B2	Full-penetration ground butt-joints	AW	Ax	8	0.05
			4PB	5	0.05
C	Cruciform nlc fillet-welded joints	AW	4PB	17	0.05
			4PB	11	0.5
		SR**	4PB	3	0.05
D	T nlc fillet-welded joints	AW	AX	9	0.05
				2	0.5
E	Cruciform load-carrying fillet welded joints	AW	Ax	7	0.05
				4	0.5
F	Cruciform full-penetration K-butt-welded joints	AW	4PB	8	0.05
				2	0.5

*As Welded **Stress Relieved

Table 6.1: Synthesis of fatigue tests carried out in the research project

.

6.2 Damage analysis

This section reports some examples of fracture surfaces, obtained after fatigue testing each series. Failures mostly occurred at weld toe on the ADI side, with the only exception of joints from series A, where mixed failure modes were observed, as explained in the following lines. For the sake of brevity, I reported here only a number of fracture surfaces, but all the specimens' sheets with the respective fracture surfaces are reported in Appendix [ref]. In particular, it has been observed that:

- Partial-penetration butt-joints show multiple crack initiation locations (see Figure 6.2 and 6.3). In most cases crack initiated at the root side, then propagated through the weld throat. Propagating cracks were observed also at the interface between the ADI plate and the weld bead and, in few cases, at the weld toe at the ADI side, too.

- Dealing with full-penetration butt-joints, the fatigue crack initiation always occurred at the weld toe at the ADI side, then the crack propagated through the thickness of the joint, as shown in Figure 6.4. Only in one specimen, the fatigue crack initiation was observed at the weld toe at the steel side.

- Concerning full-penetration ground butt-joints, crack initiation always occurred in the ledeburite region. Then, cracks propagated mainly at the interface between the ADI plate and the weld bead (see Figure 6.5) and, in some cases, across the thickness of the joint.

- In the case of cruciform non-load-carrying fillet-welded joints (Series C), cruciform load-carrying fillet-welded joints (Series E) and cruciform full penetration K-butt-welded joints (Series F) the fatigue crack initiation always occurred at the weld toe at the ADI side and then propagated through the thickness of the joint. Some example of fracture surfaces at the weld toe are reported in Figures 6.6- 6.8.

- On the contrary, the stress relieved specimens from series C presented always failure far away from the weld bead: the absence of residual stresses on the joint seems to make ADI's defects more critical than the notch tip at the weld toe.

- Dealing with T non-load-carrying fillet-welded joints (Series D), the fatigue crack initiation always occurred at the weld toe and then propagated through the thickness of the steel plate. Figure 6.9 shows an example of fracture surfaces.

From a macroscopic point of view, it is well known that cracks nucleate preferably where stress raises due to the presence of a root or a notch tip. On the other hand, the crack nucleation in plain specimens is driven by the ledeburite layer at the interface; the latter is the only case where failures occur in this specific way, even if the ledeburite layer is always present in all the tested details. As already explained in previous Chapter 2, the ledeburite is a brittle material with very poor mechanical properties.

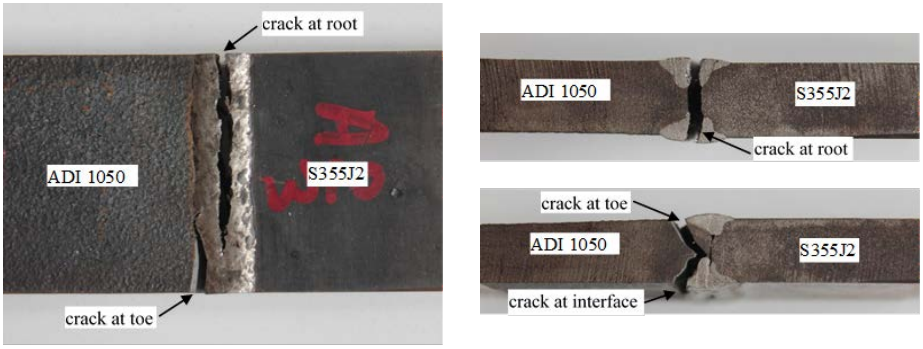

Figure 6.2: Crack initiation locations of partial-penetration butt-joints: specimen A2-3,as welded, axial loading, R=0.05, $\Delta\sigma = 105.5MPa$, $N_f = 1926134cycles$

Figure 6.3: Fracture surfaces of partial-penetration butt-joints: specimen A3-4,as welded, axial loading, R=0.05, $\Delta\sigma = 270MPa$, $N_f = 67315cycles$

Figure 6.4: Fracture surfaces of full-penetration butt-joints : specimen B2-6,as welded, 4PB loading, R=0.05, $\Delta\sigma = 293.6MPa$, $N_f = 331582cycles$

Figure 6.5: Fracture surfaces of full-penetration ground butt-joints : specimen B2-4,as welded, axial loading, R=0.05, $\Delta\sigma = 320MPa$, $N_f = 109630cycles$

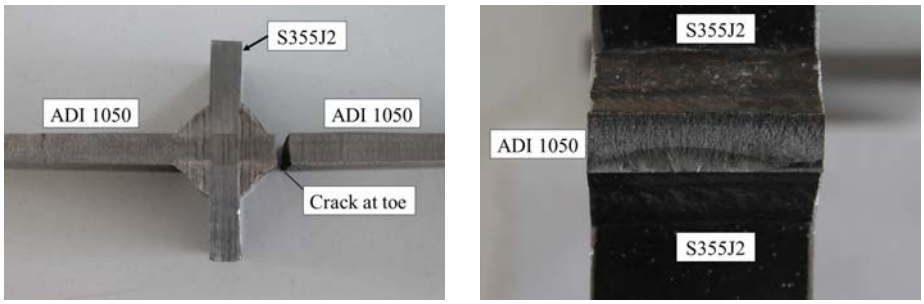

Figure 6.6: Fracture surfaces of cruciform non-load-carrying fillet-welded joints: specimen C18-2,as welded, 4PB loading, R=0.5, $\Delta\sigma = 190MPa$, $N_f = 179361cycles$

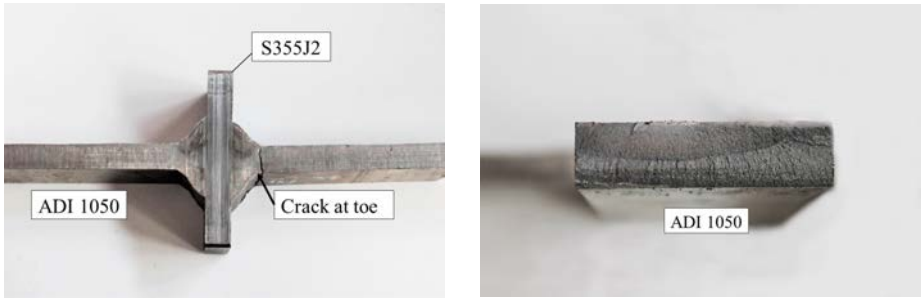

Figure 6.7: Fracture surfaces of cruciform load-carrying fillet-welded joints: specimen E3-1,as welded, axial loading $\Delta\sigma = 208MPa$, $N_f = 118526cycles$

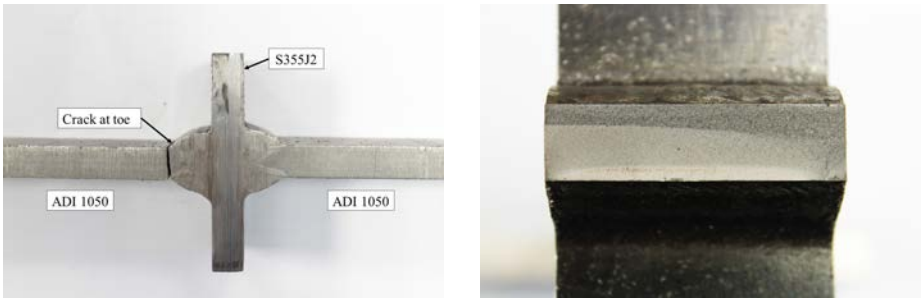

Figure 6.8: Fracture surfaces of cruciform full penetration K-butt-welded joints: specimen F4-3,as welded, 4PB loading, R=0.05, $\Delta\sigma = 191MPa$, $N_f = 1222986cycles$

Figure 6.9: Fracture surfaces of T non-load-carrying fillet-welded joints: specimen D1-1,as welded, axial loading, R=0.05, $\Delta\sigma = 234MPa$, $N_f = 353034cycles$

For the reasons reported above, some metallographic analyses were carried out in order to investigate the presence of ledeburite near the crack nucleation site and to analyse the microstructure crossed by the crack during its propagation. In particular, two specimens from each series were selected on the base of the failure mode, i.e. only specimens with failures at the weld toe were chosen. They were cut and polished in the neighbourhood of the fracture surface, then microstructure was made visible by the mean of Nital etching. It was observed that the nucleation sites are mainly located in the ledeburite matrix near the weld toe. The crack usually follows this path for a short length (about $\approx 250\mu m$), until the stress raising effect of the weld toe wins over the brittle layer. At this point, the crack leaves the ledeburite to enter in the HAZ, characterized by unstable ausferrite, and it propagates across the thickness of the joint. Figures 6.10-6.11 show some examples of the nucleation site and the propagation zone. There were only few cases where the nucleation site was not characterized by the ledeburite and cracks initiated in the HAZ (see Figure 6.12).

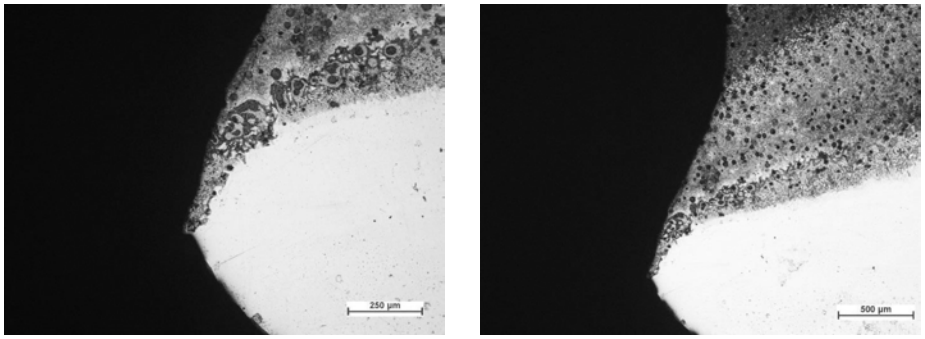

Figure 6.10: On the left, a magnification (100x) of the nucleation site, characterized by the ledeburite matrix. On the right, the path of the crack, crossing the ledeburite layer and the Heat Altered Zone (50x). Specimen B5-4, 4PB loading, R=0.05, $\Delta\sigma = 233MPa$, $N_f = 590166cycles$

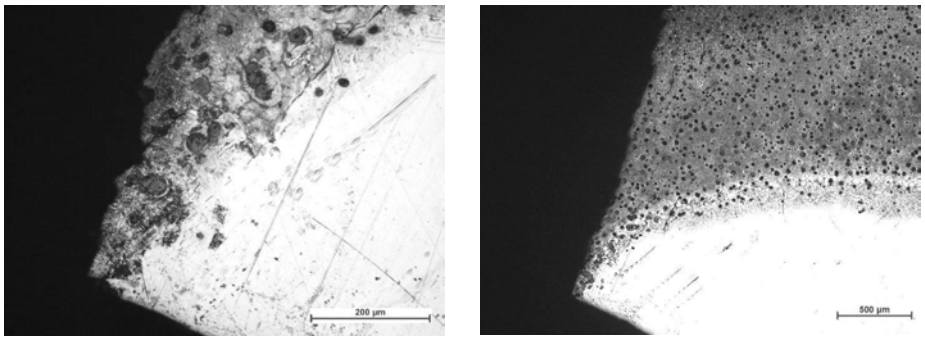

Figure 6.11: On the left, a magnification (200x) of the nucleation site, characterized by the ledeburite matrix. On the right, the path of the crack, crossing the ledeburite layer and the Heat Altered Zone (50x). Specimen C16-3, 4PB loading, R=0.5, $\Delta\sigma = 266MPa$, $N_f = 110198cycles$

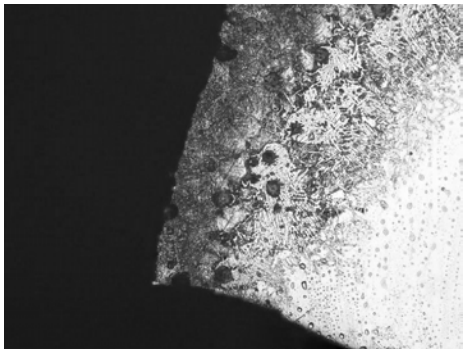

Figure 6.12: Example of crack nucleation and propagation in the HAZ (200x). Failure was not influenced by the ledeburite layer. Specimen F4-3, 4PB loading, R=0.05,$\Delta\sigma = 191MPa$, $N_f = 1222986cycles$

6.3 Results of fatigue tests

The detailed experimental results are reported in Tables 6.2-6.12, where the applied load, the obtained fatigue life and the crack initiation location are listed for each tested joint. In the case of partial-penetration butt-joints under axial loading, the nominal stress range (defined as the difference between the maximum and the minimum value) is evaluated with respect to the weld throat area according to the following expression (see Figure 3.1):

$$\Delta\sigma = \frac{\Delta F}{A_{throat}} = \frac{\Delta F}{w(t-2a)} \tag{6.1}$$

In all other joints under axial loading, the nominal stress range is calculated in the gross section area according to Equation 6.2

$$\Delta\sigma = \frac{\Delta F}{A_g} = \frac{\Delta F}{w \cdot t} \tag{6.2}$$

In the case of the joints under four-point bending loading, the Equation 6.3 yields the nominal stress.

$$\Delta\sigma = \frac{\Delta M_f}{W_f} = \frac{\Delta M_f}{\frac{1}{6}wt^2} \tag{6.3}$$

Specimen code	w	t	2a	A	R	ΔF	$\Delta\sigma$	N	Failure mode
	$[mm]$	$[mm]$	$[mm]$	$[mm^2]$		$[kN]$	$[MPa]$		
A3-4	40.0	10.0	4.0	240.0	0.05	65.0	270.8	67315	R
A1-5	45.2	12.0	4.3	350.3	0.05	38.0	108.5	965951	R+T_{ADI}
A1-6	45.2	11.9	4.4	339.0	0.05	64.2	189.4	38752	T_{ADI}+I_{ADI}
A2-1	45.1	12.1	4.0	363.1	0.05	47.4	130.6	516620	R+T_{ADI}
A2-3	45.2	12.1	4.1	358.9	0.05	37.9	105.6	1926134	R+T_{ADI}
A2-4	45.1	12.1	4.0	365.3	0.05	52.0	142.3	275454	R+T_{ADI}
A2-2	45.4	11.9	4.0	358.3	0.05	58.3	162.7	163970	R+T_{ADI}+I_{ADI}
A11-1	40.2	10.1	3.9	246.9	0.05	40.3	163.2	340012	R
A11-2	40.4	10.1	3.7	260.6	0.05	35.0	134.3	666819	R+T_{ADI}
A11-3	40.5	10.1	3.8	255.2	0.05	45.0	176.4	228734	R+T_{ADI}
A11-5	40.4	10.1	3.2	280.4	0.05	31.5	112.3	894146	R
A11-4	40.3	10.1	3.9	249.9	0.05	31.0	124.1	867608	R
A3-2	40.5	10.0	4.0	243.0	0.5	35.0	144.0	333653	R
A3-3	40.4	10.0	4.0	242.4	0.5	45.0	185.6	158137	R
A3-1	40.5	10.0	4.0	243.0	0.5	65.0	267.5	27731	R+T_{ADI}
A3-5	40.5	10.0	4.0	243.0	0.5	62.0	255.1	41461	R+T_{ADI}

R=root, T_{ADI}=toe at ADI 1050 side, I_{ADI}=interface between ADI 1050 and weld bead

Table 6.2: Fatigue test results obtained from partial-penetration butt-joints under axial loading with nominal load ratio R=0.05 and R=0.5

Specimen code	w	t	W_f	R	ΔF	b	ΔM_f	$\Delta\sigma$	N	Failure mode
	$[mm]$	$[mm]$	$[mm^3]$		$[kN]$	$[mm]$	$[Nm]$	$[MPa]$		
B2-4	40.6	10.3	718	0.05	25	17.0	212.5	296	228112	T_{ADI}
B5-2	40.4	10.0	667	0.05	24	16.3	195.6	293	358504	T_{ADI}
B2-3	40.2	10.4	718	0.05	23	15.0	172.5	240	455291	T_{ADI}
B5-4	40.5	10.0	675	0.05	21	17.2	180.6	268	590166	T_{ADI}
B5-6	40.6	10.0	677	0.05	21.5	16.1	172.5	255	625883	T_{ADI}
B5-5	40.5	10.1	682	0.05	21	15.2	159.1	233	627827	T_{ADI}
B5-3	40.3	9.9	657	0.05	21	16.4	171.7	261	974888	T_{ADI}
B5-1	40.5	9.9	662	0.05	20	15.0	150.0	227	2000000	Run-out
B2-6	40.2	10.1	677	0.05	20.5	16.0	163.5	242	2000000	Run-out
B5-1#	40.5	9.9	662	0.05	25	15.0	187.5	283	261184	T_{ADI}
B2-6#	40.2	10.1	677	0.05	29	16.0	231.3	342	103560	T_{ADI}
B6-1	40.1	10.1	682	0.05	27	14.7	198.5	291	590273	T_{ADI}
B6-2	40	10	667	0.05	29	13.5	195.8	294	331582	T_{ADI}
B6-3	40.45	10.1	688	0.05	26	17.5	227.5	331	826913	T_{S355J2}

T_{ADI}=toe at ADI 1050 side, #=specimen retested after run-out

Table 6.3: Fatigue test results obtained from full-penetration butt-joints under four-point-bending loading with nominal load ratio R=0.05

Specimen code	w	t	A	R	ΔF	$\Delta\sigma$	N	Failure mode
	$[mm]$	$[mm]$	$[mm^2]$		$[kN]$	$[Mpa]$		
B8-5	40.0	8.1	324.0	0.05	97.0	299.4	1764636	I_{ADI}
B4-5	40.3	8.1	324.4	0.05	110.3	340.0	12950	I_{ADI}
B4-6	40.9	8.1	329.2	0.05	105.4	320.0	184873	I_{ADI}
B4-2	40.0	8.0	318.0	0.05	101.8	320.0	109630	I_{ADI}
B4-4	30.1	8.1	243.8	0.05	73.1	299.8	157445	I_{ADI}
B4-1	40.6	7.3	296.4	0.05	124.5	420.0	212	I_{ADI}

T_{ADI}=toe at ADI 1050 side, I_{ADI}=interface between ADI 1050 and weld bead

Table 6.4: Fatigue test results obtained from full-penetration ground butt-joints under pure axial loading with nominal load ratio R=0.05

Specimen code	w	t	W_f	R	ΔF	b	ΔM_f	$\Delta\sigma$	N	Failure mode
	$[mm]$	$[mm]$	$[mm^3]$		$[kN]$	$[mm]$	$[Nm]$	$[MPa]$		
B8-1	40.2	8.3	461.6	0.05	22	15	315	341.2	1024018	I_{ADI}
B7-3	40.1	8.7	505.9	0.05	22	15	330	326.2	2000000	Run-out
B7-3#	40.1	8.7	505.9	0.05	24	15	360	355.8	1281889	I_{ADI}
B8-6	40.2	8.3	461.6	0.05	26	15	390	422.5	505197	T_{ADI}
B8 -2	40.2	8.3	461.6	0.05	31	15	465	503.7	45029	T_{ADI}

T_{ADI}=toe at ADI 1050 side, I_{ADI}=interface between ADI 1050 and weld bead, #=specimen retested after run-out

Table 6.5: Fatigue test results obtained from full-penetration ground butt-joints under four-point bending loading with nominal load ratio R=0.05

Specimen code	w	t	W_f	R	ΔF	b	ΔM_f	$\Delta\sigma$	N	Failure mode
	$[mm]$	$[mm]$	$[mm^3]$		$[kN]$	$[mm]$	$[Nm]$	$[MPa]$		
C6-3	39.3	10.0	654.2	0.05	30.5	15.0	457.5	349.7	42931	T_{ADI}
C11-1	40.7	10.1	691.1	0.05	29.7	15.0	445.5	322.3	782127	T_{ADI}
C12-1	40.3	10.1	678.4	0.05	39.0	15.0	585.0	431.2	153004	T_{ADI}
C7-1	40.2	10.5	731.7	0.05	32.0	15.0	480.0	328.0	175019	T_{ADI}
C8-3	39.9	10.0	665.0	0.05	36.0	15.0	540.0	406.0	175437	T_{ADI}
C7-3	40.2	10.2	690.3	0.05	30.0	15.0	450.0	326.0	226568	T_{ADI}
C5-1	40.0	10.6	749.1	0.05	36.0	15.0	540.0	360.4	327322	T_{ADI}
C9-3	40.7	10.0	677.5	0.05	29.5	15.0	442.5	326.6	104687	T_{ADI}
C10-2	40.1	10.2	688.5	0.05	42.0	15.0	630.0	457.5	104527	T_{ADI}
C8-2	40.2	10.1	676.7	0.05	44.0	15.0	660.0	487.6	54270	T_{ADI}
C11-2	40.1	10.3	709.0	0.05	44.0	15.0	660.0	465.4	90293	T_{ADI}
C12-3	40.5	10.2	702.3	0.05	29.0	15.0	435.0	309.7	3375268	T_{ADI}
C10-1	40.0	10.1	680.1	0.05	29.0	15.0	435.0	319.8	2000000	Run-out
C8-1	40.3	10.1	678.4	0.05	26.0	15.0	390.0	287.4	2000000	Run-out
C5-2	39.7	10.3	695.2	0.05	29.5	15.0	442.5	318.3	2000000	Run-out
C8-1#	40.3	10.1	678.4	0.05	36.0	15.0	540.0	398.0	82159	T_{ADI}
C5-2#	39.7	10.3	695.2	0.05	38.0	15.0	570.0	410.0	299261	T_{ADI}

T_{ADI}=toe at ADI 1050 side, #=specimen retested after run-out

Table 6.6: Fatigue test results obtained from cruciform nlc fillet-welded joint under four-point-bending loading with nominal load ratio R=0.05

Specimen code	w	t	W_f	R	ΔF	b	ΔM_f	$\Delta\sigma$	N	Failure mode
	$[mm]$	$[mm]$	$[mm^3]$		$[kN]$	$[mm]$	$[Nm]$	$[MPa]$		
C9-1	40.2	10.0	669	0.5	35	13.9	243.3	364	52884	T_{ADI}
C12-2	40.2	10.1	683	0.5	28	14.0	196.0	287	587809	T_{ADI}
C9-2	40.2	10.1	683	0.5	29.5	14.4	212.4	311	212312	T_{ADI}
C18-2	40	10	667	0.5	26	14.9	193.7	291	179361	T_{ADI}
C18-3	39.9	10	665	0.5	26	16.2	210.6	317	109229	T_{ADI}
C16-3	40	10	667	0.5	22	16.2	177.7	266	110198	T_{ADI}
C17-1	40	10	667	0.5	20	14.9	148.5	223	1691834	Run-out
C13-3	39.9	10	665	0.5	24	14.8	177.6	267	107812	T_{ADI}
C16-2	39.5	10	658	0.5	27	13.8	186.3	283	242797	T_{ADI}

T_{ADI}=toe at ADI 1050 side

Table 6.7: Fatigue test results obtained from cruciform nlc fillet-welded joint under four-point-bending loading with nominal load ratio R=0.5

Specimen code	w	t	A	R	ΔF	$\Delta\sigma$	N	Failure mode
	$[mm]$	$[mm]$	$[mm^2]$		$[kN]$	$[Mpa]$		
D2-2	40.1	10.1	405.0	0.05	44.6	110.1	2000000	Run-out
D2-1	40.6	10.1	410.1	0.05	61.5	150.0	2000000	Run-out
D2-1	40.6	10.1	410.1	0.05	123.0	300.0	271405	T_{S355J2}
D2-3	40.4	10.1	407.5	0.05	71.3	175.0	2000000	Run-out
D1-1	40.5	10.0	405.0	0.05	95.0	234.6	353034	T_{S355J2}
D1-6	40.3	10.0	403.0	0.05	81.0	201.0	1990000	Run-out
D1-6#	40.3	10.0	403.0	0.05	97.0	240.7	2000000	Run-out
D1-6#	40.3	10.0	403.0	0.05	115.0	285.4	350104	T_{S355J2}
D2-6	40.4	10.0	404.0	0.05	124.0	306.9	174533	T_{S355J2}
D2-4	40.8	10.0	408.0	0.05	133.0	326.0	73446	T_{S355J2}
D1-2	40.7	10.0	407.0	0.05	137.0	336.6	42005	T_{S355J2}
D1-5	40.5	10.0	405.0	0.05	139.0	343.2	60781	T_{S355J2}
D3-1	40.2	10.0	402.0	0.5	95.0	236.3	512356	T_{S355J2}
D3-2	41.0	10.0	410.0	0.5	93.0	226.8	209569	T_{S355J2}

T_{S355J2}=toe at S355J2 side, #=specimen retested after run-out

Table 6.8: Fatigue test results obtained from T non-load-carrying fillet-welded joints under pure axial loading with nominal load ratio R=0.05 and R=0.5

Specimen code	w	t	A	R	ΔF	$\Delta\sigma$	N	Failure mode
	$[mm]$	$[mm]$	$[mm^2]$		$[kN]$	$[Mpa]$		
E3-1	40.0	10.2	408.0	0.05	85	208.3	118526	T_{ADI}
E2-1	40.1	10.0	401.0	0.05	70	174.6	2000000	Run-out
E2-1#	40.1	10.0	401.0	0.05	77	192.0	256157	T_{ADI}
E4-3	39.9	10.0	399.0	0.05	74	185.5	548082	T_{ADI}
E4-1	39.9	9.9	395.0	0.05	90	227.8	140969	T_{ADI}
E4-2	39.7	9.8	389.1	0.05	72	185.1	248030	T_{ADI}
E3-3	40.3	10.2	411.1	0.05	97	236.0	82736	T_{ADI}
E2-4	40.2	10.0	402.0	0.5	75	186.6	60672	T_{ADI}
E2-2	40.0	10.0	400.0	0.5	75	187.5	89887	T_{ADI}
E2-6	40.3	10.0	403.0	0.5	70	173.7	80167	T_{ADI}
E3-4	40.2	10.1	406.0	0.5	65	160.1	94490	T_{ADI}

T_{ADI}=toe at ADI 1050 side, #=specimen retested after run-out

Table 6.9: Fatigue test results obtained from cruciform load-carrying fillet-welded joints under pure axial loading with nominal load ratio R=0.05 and R=0.5

Specimen code	w $[mm]$	t $[mm]$	W_f $[mm^3]$	R	ΔF $[kN]$	b $[mm]$	ΔM_f $[Nm]$	$\Delta\sigma$ $[MPa]$	N	Failure mode
E3-5	40.2	10.0	670	0.05	28	15.0	420.0	313.4	344181	T_{ADI}
E3-6	40.2	10.0	670	0.05	26	16.8	435.5	325.0	630368	T_{ADI}

T_{ADI}=toe at ADI 1050 side

Table 6.10: Fatigue test results obtained from ruciform load-carrying fillet-welded joints under four-point-bending loading with nominal load ratio R=0.05

Specimen code	w $[mm]$	t $[mm]$	W_f $[mm^3]$	R	ΔF $[kN]$	b $[mm]$	ΔM_f $[Nm]$	$\Delta\sigma$ $[MPa]$	N	Failure mode
F1-4	45.0	12.0	1080	0.05	22	15.0	330	152.8	544633	T_{ADI}
F1-5	43.0	11.7	981.0	0.05	30	15.9	477	243.1	122085	T_{ADI}
F1-6	44.7	11.6	1003	0.05	20	16.5	330	164.6	300768	T_{ADI}
F4-1	39.8	10.0	663.3	0.05	24	14.8	355	267.7	186215	T_{ADI}
F4-2	40.0	10.2	693.6	0.05	30	15.0	450	324.4	111413	T_{ADI}
F4-3	40.0	10.0	666.7	0.05	15	15.0	225	168.8	2000000	T_{ADI}
F4-3#	40.0	10.0	666.7	0.05	17	15.0	255	191.3	1222986	T_{ADI}
F4-5	40.0	10.4	721.1	0.05	38	15.0	570	395.2	39973	T_{ADI}
F3-2	40.0	10.2	693.6	0.5	22	15.0	330	237.9	266386	T_{ADI}
F2-2	40.0	10.3	707.3	0.5	31	15.0	465	328.7	49658	T_{ADI}
F4-6	40.1	10.0	668.3	0.5	30	15.0	450	336.7	6085	T_{ADI}

T_{ADI}=toe at ADI 1050 side, #=specimen retested after run-out

Table 6.11: Fatigue test results obtained from cruciform full-penetration joints under four-point-bending loading with nominal load ratio R=0.5

Specimen code	w $[mm]$	t $[mm]$	A $[mm^2]$	R	ΔF $[kN]$	$\Delta\sigma$ $[Mpa]$	N
L1	14.8	8.9	131.7	0.05	45	341.6	2000000
L1#	14.8	8.9	131.7	0.05	57	432.7	706530
L2	15.0	8.7	129.8	0.05	66	508.7	255318
L3	15.0	9.0	135.0	0.05	76	563.0	20505
L4	15.0	9.0	135.0	0.05	72	533.3	76723
L5	15.0	8.8	132.0	0.05	55	416.7	101859
L6	15.0	8.8	132.0	0.05	50	378.8	2000000
L6#	15.0	8.8	132.0	0.05	54	409.1	362387
L7	14.9	8.9	132.6	0.05	74	558.0	127830
L8	15.0	8.9	133.5	0.05	54	404.5	1115066

#=specimen retested after run-out

Table 6.12: Fatigue test results obtained from ADI plain specimens under pure axial loading with nominal load ratio R=0.05

6.3.1 S-N curves for dissimilar ADI-to-steel welded joints

Figures 6.13- 6.22 show the fatigue results in terms of the applied nominal stress range versus the number of cycles to failure. The scatter bands refer to survival probabilities of 2.3 and 97.7% and to a 95% confidence level.

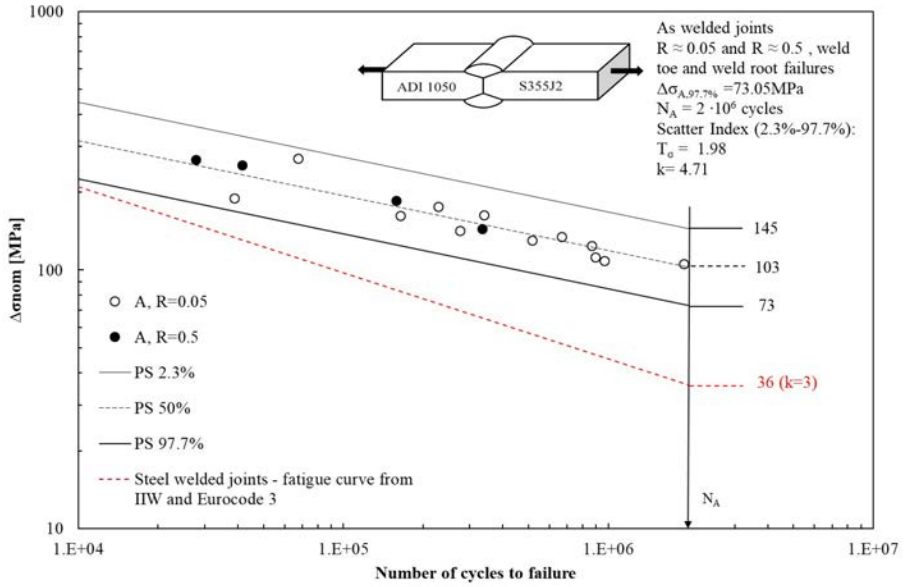

Figure 6.13: Experimental results of axial fatigue tests performed on partial-penetration butt-joints; nominal axial stress range evaluated in the weld throat area.

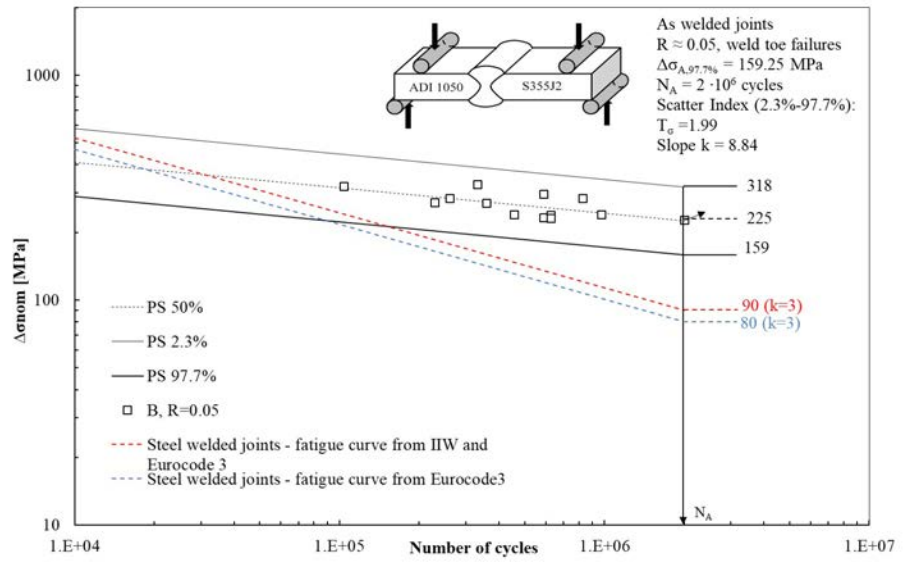

Figure 6.14: Experimental results of four-point-bending fatigue tests performed on full-penetration butt-joints; nominal four-point bending stress range evaluated in the cross-section area.

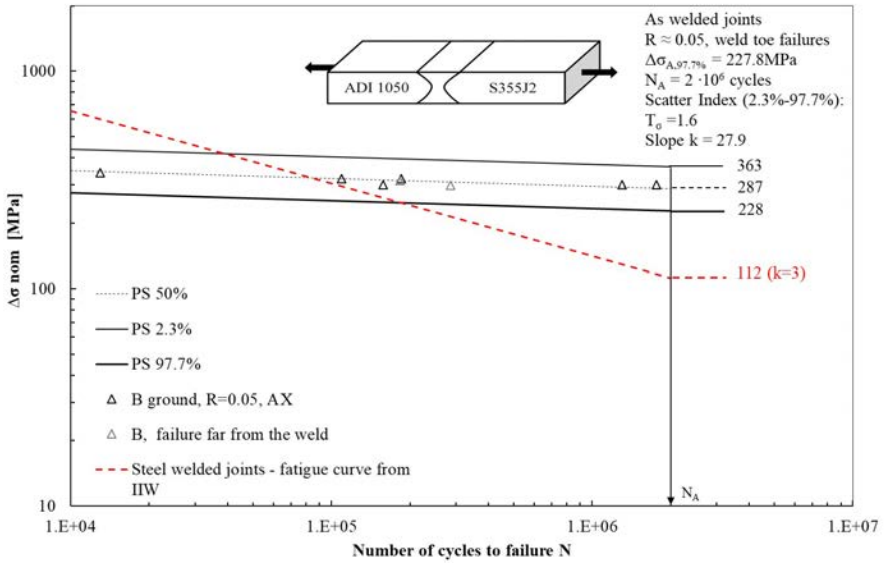

Figure 6.15: Experimental results of axial fatigue tests performed on full-penetration ground butt-joints; nominal axial stress range evaluated in the cross-section area.

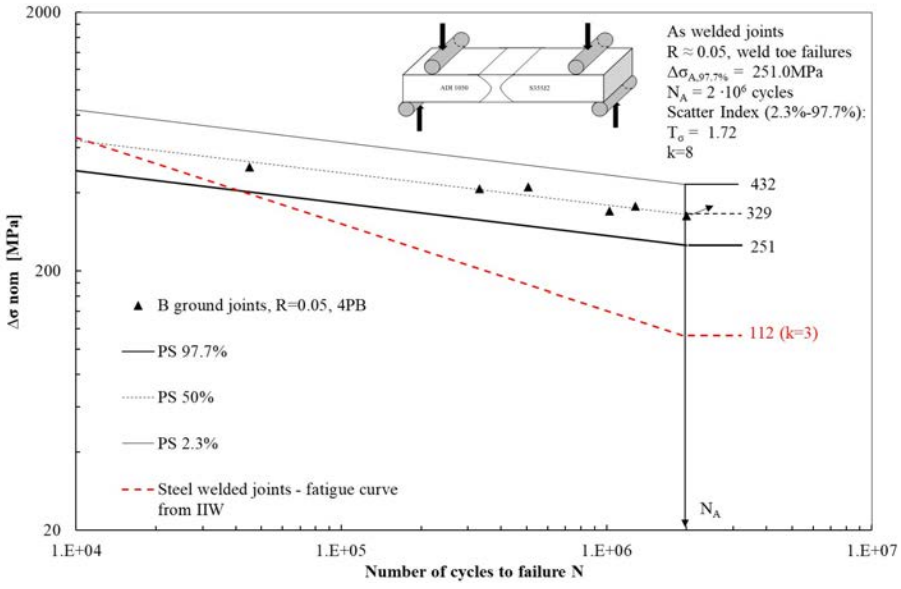

Figure 6.16: Experimental results of four-point-bending fatigue tests performed on full-penetration ground butt-joints; nominal bending stress range evaluated in the cross-section area.

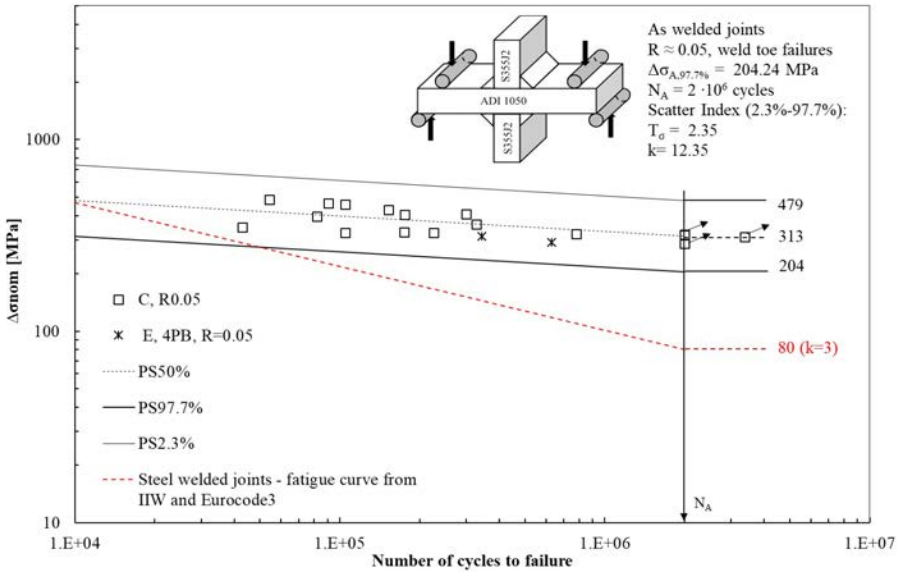

Figure 6.17: Experimental results of four-point-bending fatigue tests at nominal load ratio R=0.05, performed on cruciform nlc fillet-welded joints. In the plot, cruciform load-carrying fillet-welded joints tested under four-point bending loanding are reported for comparison; nominal four-point bending stress range evaluated in the cross-section area.

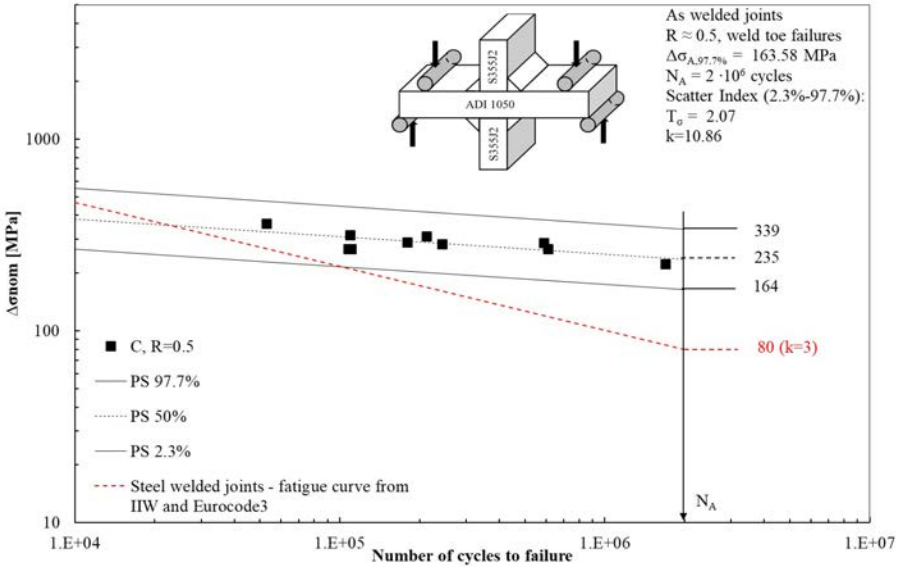

Figure 6.18: Experimental results of four-point-bending fatigue tests at nominal load ratio R=0.5, performed on cruciform nlc fillet-welded joints; nominal four-point bending stress range evaluated in the cross-section area.

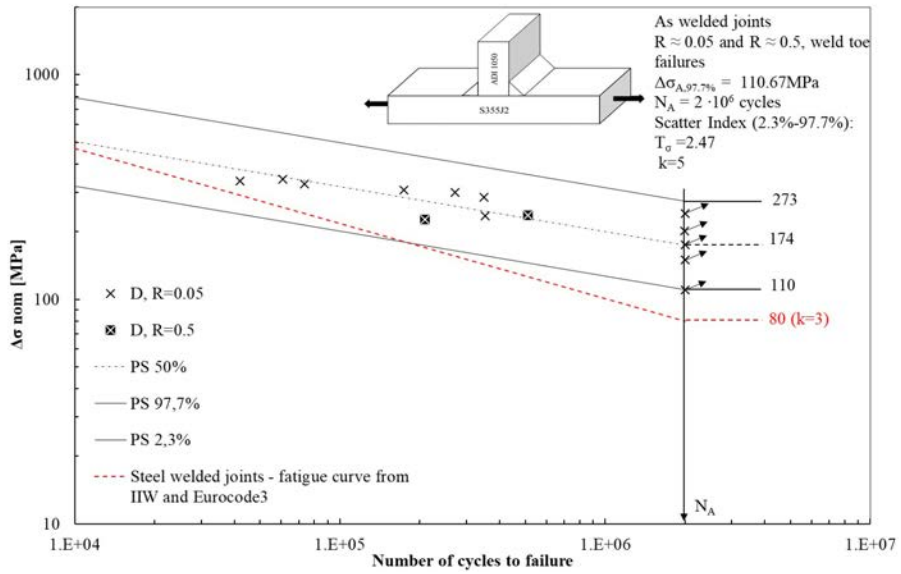

Figure 6.19: Experimental results of axial fatigue tests performed on T non-load-carrying fillet-welded joints; nominal axial stress range evaluated in the weld throat area.

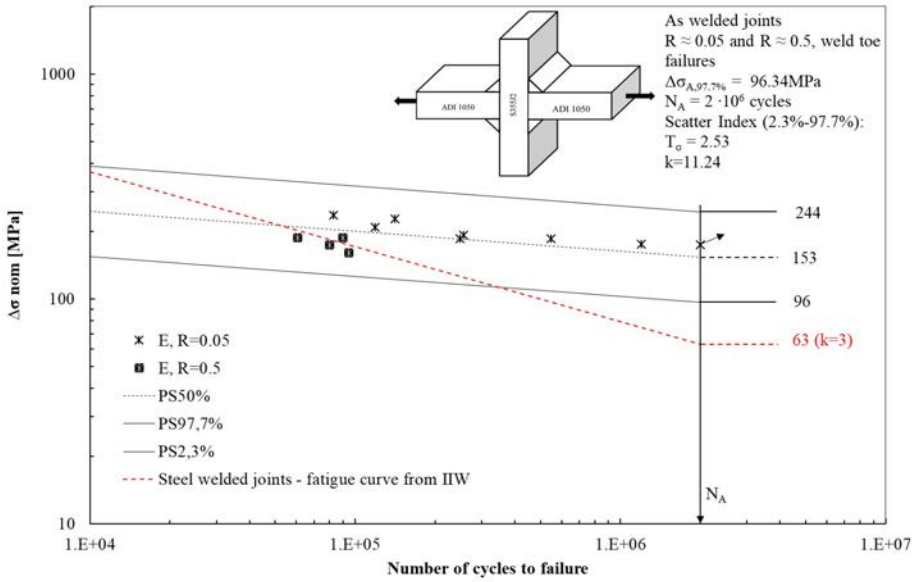

Figure 6.20: Experimental results of axial fatigue tests performed on cruciform load-carrying fillet-welded joints; nominal axial stress range evaluated in the weld throat area.

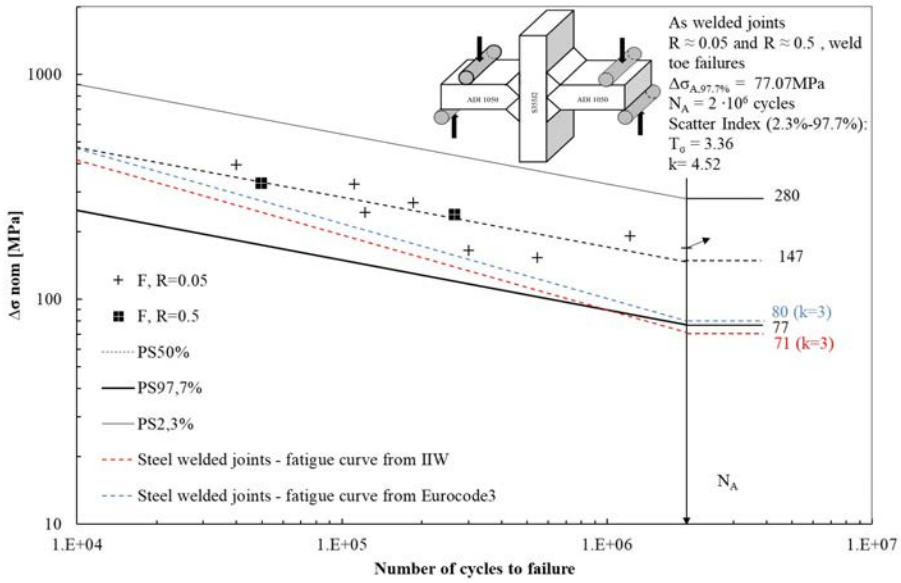

Figure 6.21: Experimental results of four-point-bending fatigue tests performed on cruciform full-penetration joints; nominal four-point bending stress range evaluated in the cross-section area.

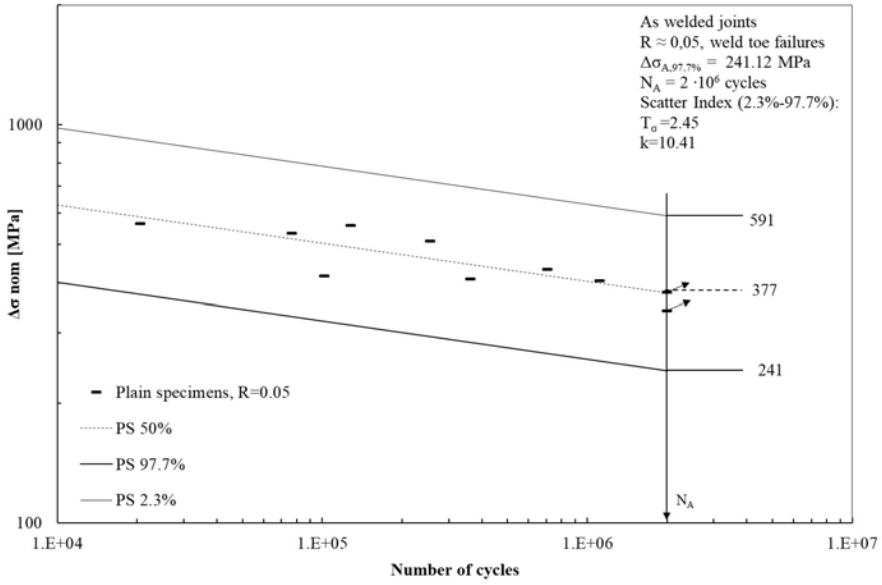

Figure 6.22: Experimental results of axial fatigue tests performed on plain specimens; nominal axial stress range evaluated in the cross-section area.

6.3.2 Discussion and comparison with current standards

According to the experimental results and referring to a survival probability of 97.7% at 2 million loading cycles, it can be observed that the tested details exhibit an endurable stress range higher than the FAT values suggested by Eurocode 3 and IIW Recommendations for the corresponding homogeneous steel joints. Consequently, austempered ductile iron-to-steel arc-welded joints have higher fatigue performances than those for the corresponding homogeneous steel joints at the medium-high cycle fatigue regime. In particular,regarding partial-penetration butt joints, full-penetration butt joints, cruciform nlc fillet-welded joints and T non-load-carrying fillet-welded joints, the fatigue assessment could be performed on the safe side by applying the nominal stress approach proposed by International Standards and Recommendations for the corresponding steel welded joints. On the other hand, current standards cannot be applied on the safe side for full-penetration ground butt joints, cruciform load-carrying fillet-welded joints and cruciform full-penetration k-butt-welded joints. On top of that,care must be taken when considering fatigue assessment at the low cycle regime: the fatigue strength of dissimilar joints tends to become lower than the one of steel joints especially below 100000 cycles. The lack of experimental data in this range of fatigue life requires further investigations to understand the actual behaviour of austempered ductile iron-to-steel joints under very high loads. Table 6.13 summarises the endurable stress ranges at 2 million loading cycles for a survival probability of 97.7%, the inverse slope k, and the scatter index T for each tested series.

Test series	Joint geometry	Load	Nominal load ratio R	$\Delta\sigma*$ [MPa]	k	T_σ
A	partial-penetration butt-joints	Ax	0.05+0.5	73	4.71	1.98
B1	full-penetration butt-joints	4PB	0.05+0.5	159	8.84	1.99
B2	full-penetration ground butt-joints	Ax	0.05	228	27.9	1.6
		4PB	0.05	251	8	1.72
C	cruciform nlc fillet-welded joints	4PB	0.05	204	12.35	2.35
			0.5	164	10.86	2.07
D	T nlc fillet-welded joints	Ax	0.05+0.5	111	5	2.47
E	cruciform load-carrying fillet-welded joints	Ax	0.05+0.5	96	11.24	2.54
F	cruciform full-penetration k-butt-welded joints	4PB	0.05+0.5	77.0	4.52	3.36

$*$ endurable stress range referred to a survival probability 97.7% and N_A=2 million loading cycles
Ax=axial load, 4PB=four-pont bendin load

Table 6.13: Summary of experimental fatigue results: dissimilar ADI-to-steel joints in as-welded condition

Chapter 7

Introduction to local approaches for stress analysis of welds

In welded joints subjected to cyclic loading, the weld toes and roots are usually the highly stressed zones where cracks initiate and propagate. The investigation of the stress and strain in the neighbourhood of cracks is an interesting and complex problem when the main goal is to establish the relation between stress levels and the fatigue strength of structural welded components. In the standards in force (Eurocode 3 [2]), a nominal approach is proposed. This method evaluates the fatigue strength of the weld through the range of the nominal tension $\Delta\sigma$: the S-N curves relate a design stress S to the number of cycles N to failure and the fatigue strength is related to the nominal stress distribution, defined disregarding stress raising effect due to the geometry or the weld itself. Essentially, the fatigue strength assessment of a welded structure is performed by comparing the calculated nominal stress with the proper design category of the joint, which primarily depends on the considered geometry and loading condition. As the fatigue is a local phenomenon due the stress concentrations, the nominal approach leads to high scatter in the statistical analysis of experimental data: each geometry has a different ratio between the applied nominal stress and the intensity of the local stress field at the weld toe/root. Thus, in the standards, different design curves referring to precise probabilities of survival are reported for a number of selected welded details. In order to explicitly take into consideration stress concentrations and singularities, local approaches have been developed. In this work, we shall consider the following approaches:

- N-SIFs (Notch Stress Intensity Factors) Approach;
- Peak Stress Method (PSM);
- Local Strain-Energy Density (SED) approach.

7.1 Notch-Stress intensity factors approach

In order to quantify the influence of stress distribution on fatigue behaviour close to weld toes, the Notch Intensity Approach follows a stress field criterion.

This method is based on Williams' theory of Linear Elastic Fracture Mechanics (LEFM), where the whole stress distribution is given by a reduced number of stress field parameters: the Stress Intensity Factors (SIF). Verreman and Nie proposed a field parameter for welded joints, called Notch-Stress Intensity Factor (N-SIF) and Finite Elements Analyses confirmed the possibility of using Williams analytical solution, already obtained for open V-shaped cracks. Indeed, one can associate the weld toe geometry to a lateral open V-shaped notch, with an opening angle of 135°.

William's approach The basic analysis of linear elastic stress-strain fields at sharp open notches was given by Williams. He stated that in cracks, as well as in open notches, the stress field is singular and the its intensity is given by the so-called singularity exponent. The latter is related to the notch opening angle (2α). The exponent values for the stress distribution are the eigenvalues defined by the expressions:

$$\sin(\lambda_1 q)\pi + \lambda_1 \sin(q\pi) = 0 \tag{7.1}$$

$$\sin(\lambda_2 q\pi) + \lambda_2 \sin(q\pi) = 0 \tag{7.2}$$

Where q is related to the opening angle 2α through the expression $2\alpha = \pi(2-q)$.

Definition of Notch Stress Intensity Factors In order to give a physical meaning to the constant values present in Williams' formulae, Gross and Meldenson [4] proposed to extend the definition of the Stress Intensity Factor, commonly used to describe crack stress fields, to open notches. They assumed the direction with $\theta = 0$ to be the most useful, since the symmetric and skew-symmetric components are uncoupled along this direction. Based on the stress field components, the definitions for N-SIFs are:

$$K_1 = \sqrt{2\pi} \lim_{r\to 0} (\sigma_\theta) r^{1-\lambda_1} \tag{7.3}$$

$$K_2 = \sqrt{2\pi} \lim_{r\to 0} (\tau_{r\theta}) r^{1-\lambda_2} \tag{7.4}$$

The intensity of the stress field at the weld toe can be evaluated considering only the stress terms depending on K_1 , while the $\tau_{r\theta}$ is not singular and thus it can be neglected.

Limitations of N-SIFs approach The main limitations of this method are two:

- In a welded joint, cracks can initiate and propagate either at the weld root or the weld toe. In this case the opening angle 2α of the notch is different (0° and 135° respectively). As the unite of measure of the NSIF depends directly on the eigenvalues λ_i, the resulting NSIFs are not comparable to each other.

- This method is very expensive in terms of calculation time as one needs a very high number of elements in the neighbourhood of the notch; indeed, to calculate the gradient of the local stress field, the mesh should have a minimum element dimension of 10^{-5}mm at the point of singularity.

7.2 Peak Stress method

The evaluation of the notch stress intensity factors from a numerical analysis of the local stress field requires very refined meshes and large computational effort. The advantages of the Peak Stress Method is that only the elastic peak stress evaluated at the V-notch tip is needed and the adopted meshes are rather coarse if compered to those necessary for the whole stress field evaluation. The PSM allows the evaluation of the NSIFs K_1 and K_2 through the linear elastic stresses of opening mode ($\sigma_{\theta\theta,\theta=0peak}$) and sliding mode ($\tau_{r\theta,\theta=0peak}$) which are referred to the bisector of the opening angle of the V-notch. The following expressions have been verified:

$$K_1 = K_{fe}^{*} \cdot \sigma_{\theta\theta,\theta=0peak} \cdot d^{1-\lambda_1} \tag{7.5}$$

$$K_2 = K_{fe}^{**} \cdot \tau_{r\theta,\theta=0peak} \cdot d^{1-\lambda_2} \tag{7.6}$$

where

- d is the average dimension of the finite elements, i.e. the so called "*Global Element Size*"
- K_{fe}^{*} and K_{fe}^{**} are constants depending on the software, the element type and the FE mesh pattern

The PSM has been calibrated for the software Ansys with the following conditions:

- *Element type*: linear quadrilateral plane element with 4 nodes (PLANE 182 or PLANE 42) and Keyoption "*simple enhanced strain*" activated
- *Mesh pattern*: automatically generated by the free-mesh generation algorithm.
- *Global Element Size*: chosen so that the ratio a/d is either greater than 3 for Mode I or greater than 14 for Mode II (a is the reference dimension of the component)
- *Number of elements at notch tip*: 2 for $2\alpha = 135°$, 4 for $2\alpha = 0°$
- *Opening angle*:$0° \leq 2\alpha \leq 135°$ for Mode I and $0°$ for Mode II

The calibration leads to $K_{FE1} = 1.38$ and $K_{FE2} = 3.38$.

Despite the reduction of the calculation time, the Peak Stress Method does not solve all the problems of the Notch-Stress Intensity Factors approach, as the NSIFs are still not comparable. In order to find a solution to this, Lazzarin and Zambardi developed an energy-based criterion that allows the comparison between welded joints with different opening angles. This method is based on the strain-energy density measured into a structural volume which circumscribes the points of stress singularity.

7.3 Local Strain-Energy Density Approach

The non-comparability of the results has been overcome in some recent papers [12] by using the mean value of the strain energy density range, calculated in a control-volume of radius R_c surrounding the weld toe or the weld root, asshown in Figure 7.1. This energy approach is based of the idea of structural volume proposed by Nueber: the critical parameter for the structural strength is the average strain energy density into the circular sector and the radius R_c is a characteristic of the material (f.i. $R_c = 0.28mm$ for welded steel).

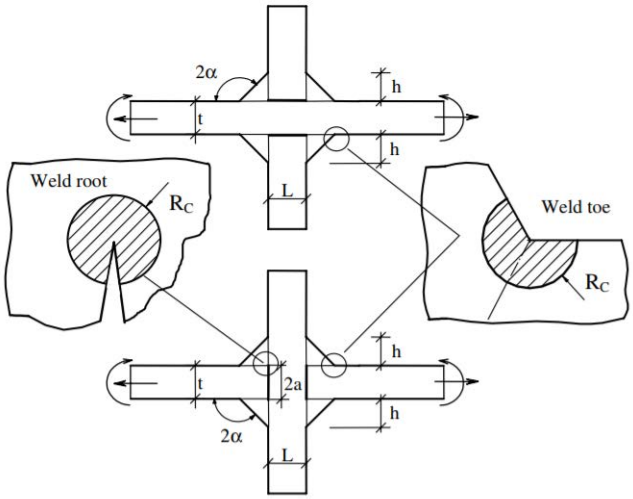

Figure 7.1: Examples of control volume at both weld toe and weld root

In plane problems, all stress and strain components in the highly stressed region are correlated to mode I and mode II NSIFs. Under a plane strain hypothesis, the strain energy density for an elastic and isotropic material is:

$$W(r,\theta) = \frac{1}{2}\sigma_{rr} \cdot \epsilon_{rr} + \frac{1}{2}\sigma_{\theta\theta} \cdot \epsilon_{\theta\theta} + \frac{1}{2}\sigma_{zz} \cdot \epsilon_{zz} + \frac{\tau_{r\theta}^2}{2G} \tag{7.7}$$

Substituing in 7.7, the equation of the stress field derived from 7.3 and 7.4 , it yields:

$$W_1(r,\theta) = \frac{1}{2E} \cdot \frac{K_1^2}{r^{2(1-\lambda_1)}} \cdot f_1 \tag{7.8}$$

$$W_2(r,\theta) = \frac{1}{2E} \cdot \frac{K_2^2}{r^{2(1-\lambda_2)}} \cdot f_2 \tag{7.9}$$

where f_1 and f_2 represent the terms dependent by the angular coordinate θ.

It is possible evaluate the total elastic strain energy contained in a semicircular sector of radius R_c:

$$E(R) = \int_A W\, dA = \int_0^{R_c} \int_{-\gamma}^{+\gamma} [W_1(r,\theta) + W_2(r,\theta)] r\, dr\, d\theta = \\ = \frac{1}{E} \cdot \left(\frac{I_1(\gamma)}{4\lambda_1} \cdot K_1^2 \cdot R_c^{2\lambda_1} + \frac{I_2(\gamma)}{4\lambda_2} \cdot K_2^2 \cdot R_c^{2\lambda_2} \right) \tag{7.10}$$

where I_1 and I_2 are the integrals of the angular function $f_1(\theta)$ and $f_2(\theta)$, depending on γ and the Poisson ratio ν.

The area of the circular sector with radius R_c is:

$$A(R) = \int_0^{R_c} \int_{+\gamma}^{-\gamma} r\, dr\, d\theta = R_c^2 \gamma \tag{7.11}$$

The average strain energy on the area A results:

$$W = \frac{E(R)}{A(R)} = \frac{1}{E} \left(\frac{I_1(\gamma)}{4\lambda_1 \gamma} \cdot \frac{K_1^2}{R_c^{2(1-\lambda_1)}} + \frac{I_2(\gamma)}{4\lambda_2 \gamma} \cdot \frac{K_2^2}{R_c^{2(1-\lambda_1)}} \right) = \\ = \frac{1}{E} \left(e_1 \cdot \frac{K_1^2}{R_c^{2(1-\lambda_1)}} + e_2 \cdot \frac{K_2^2}{R_c^{2(1-\lambda_1)}} \right) \tag{7.12}$$

where e_1 and e_2 are two parameters which synthesise the dependence on the opening angle. Finally, dealing with multiaxial fatigue loading condition (mixed mode I+II+III loading), the SED averaged over the control volume can be expressed as follows:

$$\Delta W = c_{w1} \cdot \frac{e_1}{E} \cdot \frac{K_1^2}{R_c^{2(1-\lambda_1)}} + c_{w2} \cdot \frac{e_2}{E} \cdot \frac{K_2^2}{R_c^{2(1-\lambda_2)}} + c_{w3} \cdot \frac{e_3}{E} \cdot \frac{K_3^2}{R_c^{2(1-\lambda_3)}} \tag{7.13}$$

where the coefficients c_{wi} (i=1,2,3 indicates the loading mode) depend on the nominal load ratio R according to the following expressions:

$$c_w(R) = \begin{cases} \frac{1+R^2}{(1-R)^2} \; if \; -1 \leq R \leq 0 \\ \frac{1-R^2}{(1-R)^2} \; if \; 0 \leq R \leq 1 \end{cases}$$

In particular c_w equals 1 for R=0. It should be noted that welded joints loaded in the as-welded conditions are almost not senstive to mean stresses, according to design standards [2], therefore Eq.7.13 with c_w1 should be applied.

7.3.1 Fatigue strength of steel welded joints based on local energy approach

Having introduced the general formulation of the SED approach, we need to estimate the radius of the control volume R_c. As it is thought as being dependent on the properties of the welded material, the radius can be estimated by using the fatigue strength $\Delta\sigma_D$ of the butt ground welded joints (in order to quantify the influence of the welding process, in the absence of any stress concentration effect) and the NSIF-based fatigue strength of welded joints having a constant V-notch angle at the weld toe and large enough to ensure the non-singularity of mode II stress distributions. A convenient expression is (Lazzarin and Zambardi [11]):

$$R_C = \left(\frac{\sqrt{2e_1}\Delta K_{1D}^N}{\Delta\sigma_D} \right)^{\frac{1}{1-\lambda_1}} \tag{7.14}$$

Referring to a fatigue life of $N_D = 5 \cdot 10^6$ cycles and R=0, it yields to $R_C \simeq 0.28mm$.

Knowing R_c, it is now possible to apply the SED method to every possible trigger point for the crack in a steel welded joint.

It is worth noting that the SED approach allows to collect and compare data obtained from joints with different values of the opening angle, as well as cases of failures from weld root and weld toe. In Figure 7.2, a synthesis of about 900 data of fatigue failures of welded joints is shown in terms of strain energy density.

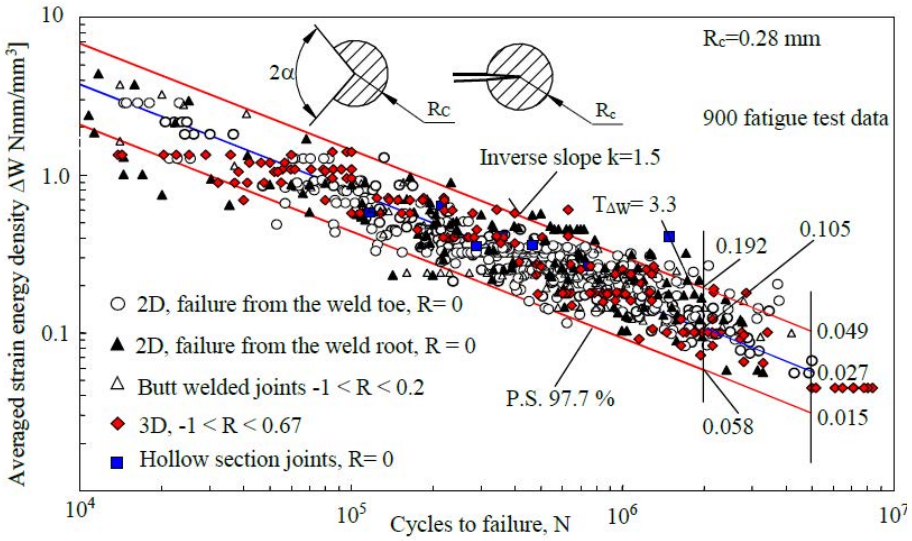

Figure 7.2: *Strain energy-based scatter band summarising fatigue strength data of steel welded joints subjected to tension and bending loads; main plate thickness ranging from 3 to 100 mm, weld flank angle from* 0° *to* 135°.

7.3.2 The latest formulation of the Peak Stress Method based on SED approach

Even thought the SED approach gave gave excellent results in terms of statistical synthesis of the experimental data, the computational effort is still high as there should be at least 20 elements into the structural volume. Furthermore, a geometrical construction has to be build at the notch tip. For these reasons, the PSM is the most promising method for industrial application for the ease of use and the coarseness needed for the mesh. On the averaged Strain Energy Density criterion, a so-called *equivalent peak stress* has been defined to assess either weld toe or weld root failures in conjunction with a properly calibrated design curve.

By using the PSM-based relationships (Eqs. 7.5-7.6), the closed-form expression of the averaged SED, Eq 7.13 can be rewritten as a function of the

singular, linear elastic FE peak stresses $\sigma_{\theta\theta,\theta=0peak}$.$\tau_{r\theta,\theta=0peak}$ and $\tau_{\theta z,\theta=0peak}$. Then, the strain energy equality $W = (1-\nu^2)\cdot\sigma^2_{eq,peak}/2E$ valid under plain strain conditions yields the following equivalent peak stress $\sigma_{eq,peak}$:

$$\begin{aligned}\Delta W =& c_{w1}\frac{e_1}{E}\left[K^{*}_{fe}\cdot\sigma_{\theta\theta,\theta=0peak}\cdot d^{1-\lambda_1}\right]^2 + c_{w2}\frac{e_2}{E}\left[K^{**}_{fe}\cdot\tau_{r\theta,\theta=0peak}\cdot d^{1-\lambda_2}\right]^2 + \\ & c_{w3}\frac{e_3}{E}\left[K^{***}_{fe}\cdot\tau_{\theta z,\theta=0peak}\cdot d^{1-\lambda_3}\right]^2 \longrightarrow = (1-\nu^2)\cdot\frac{\Delta\sigma^2_{eq,peak}}{2E}\end{aligned} \tag{7.15}$$

Afterward, the following expression is obtained for a general multiaxial loading condition:

$$\begin{aligned}\Delta\sigma_{eq,peak} =& \sqrt{c_{w1}\cdot f^2_{w1}\cdot\Delta\sigma^2_{\theta\theta,\theta=0peak} + c_{w2}\cdot f^2_{w2}\cdot\Delta\tau^2_{r\theta,\theta=0peak} + \\ & + c_{w3}\cdot f^2_{w3}\cdot\Delta\tau^2_{\theta z,\theta=0peak}}\end{aligned} \tag{7.16}$$

The correction parameters f_{w1},f_{w2} and f_{w3} weight the peak stresses both around the notch tip and along the radial direction, i.e. θ and r, respectively. These coefficients are defined as follows:

$$f_{wi} = K_{FE}\cdot\sqrt{\frac{2e_i}{1-\nu^2}}\cdot\left(\frac{d}{R_o}\right)^{1-\lambda_1} \qquad where \quad i = 1,2,3 \tag{7.17}$$

It is worth noting that while the parameters both the parameters f_{wi} and the peak stresses of Eq. 7.16 depend on the adopted FE side d, the equivalent peak stress does not.

7.4 Practical application of the local approaches for the stress analysis of welded joints

In this section, one can find the analysis of fatigue strength of steel welds by the means of the nominal and the local approaches. Thank to the latter, it will be shown that a single design scatter band can be calibrated for different geometries and failure typologies. Original data were taken from Maddox (1987) and Gurney (1991). In those series the main plate thickness ranged from 6 mm to 100 mm and the variation of the transverse stiffeners was even more pronounced (from 3 mm to 220 mm). All fatigue failures originated from the weld toes and the mean value of the weld angle did not vary ($2\alpha = 135°$) The first joint analysed (Figure 7.3) has cruciform shape and it was tested with axial loading in as-welded condition and nominal stress ratio equal to or slightly greater than zero. More information about the welded joints are reported in Figure 7.4.

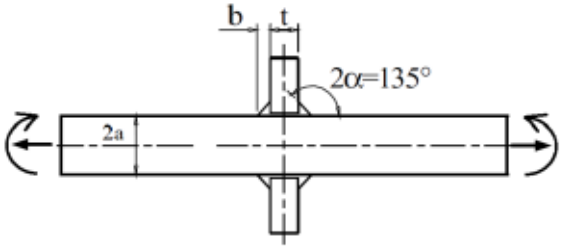

Figure 7.3: Geometry if the steel crucifurm joint

Serie	Geometria del giunto	Tipo di carico	Eventuali trattamenti	Materiale	E [MPa]	ν	2a [mm]	t [mm]	b [mm]
1	Cruciforme-NLC	T	*as-welded*	acciaio	206000	0.3	13	10	8
2	Cruciforme-NLC	T	*as-welded*	acciaio	206000	0.3	100	220	15
3	Cruciforme-NLC	B	*as-welded*	acciaio	206000	0.3	100	13	8
4	T-NLC	B	*as-welded*	acciaio	206000	0.3	6	6	6

Figure 7.4: Main characteristics of the steel welded joints

The applied methods are:

- Nominal Stress Approach
- The NSIFs approach
- Strain Energy Density (SED) approach
- Peak Stress Method (PSM) approach

All experimental data are reported in the following Table 7.1.

Series	Geometry, load	Thickness a [mm]	N [n of cycles]	$\Delta\sigma_{nominal}$ [MPa]
1/Maddox	cruciform/ bending	13	192000	200
(1987)		13	507000	140
		13	2937000	100
		13	4297000	80
12/Gurney	cruciform/ bending	100	109000	150
(1991)		100	224000	120
		100	322000	100
		100	1153000	65
		100	2147000	55
16/Gurney	cruciform/ bending	100	120000	260
(1991)		100	200000	220
		100	302000	180
		100	744000	140
		100	1180000	120
		100	2158000	110
23/Gurney	T/bending	6	135000	300
(1997)		6	237000	260
		6	407000	200
		6	573000	190
		6	665000	180
		6	1525000	160
		6	1534000	150
		6	2601000	140

Table 7.1: Experimental data of steel welded joint

7.4.1 Application of the Nominal stress approach

As already told, due to large variations in the geometrical parameters, the scatter of the experimental data is obviously very pronounced in terms of nominal stress range. Figure 7.5 shows the graph of the nominal tension range versus the number of cycles to failure (reported in logarithmic scale). In fact, the value of the scatter band is 6.59 as this method does not take into consideration that different geometries leads to different stress intensity factors at the weld toes and roots.

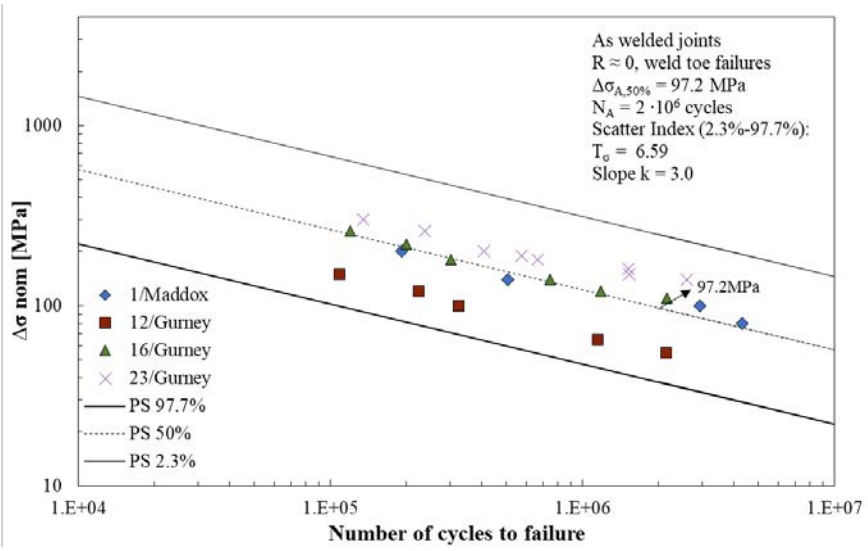

Figure 7.5: Fatigue data for as-welded joints in terms of nominal stress

7.4.2 Application of the N-SIF Approach

The scatter greatly decreases as soon as the mode I NSIF K_1 is used as a meaningful parameter for summarising fatigue life data. In the following paragraphs, the method used for the determination of k_1 is described.

The first step of this approach is to calculate the values of the parameter N-SIF K_1 at the weld toe for each joint through FEM analysis.

Geometry of the weld modeled on Ansys Mechanical APDL First I generated the 2D geometrical model of the weld on Ansys Mechanical. Thank to the symmetric shape of the weld, it was possible to consider only a quarter of the joint. In order to tighten the mesh near the point of singularity, two circumferences were created with a radius of 0.28mm and 0.0001mm respectively and with the center located at the weld toe. These arcs were divided by the V-notch opening angle's bisector for evaluating the s orthogonal components of the nodal stress. The described construction is shown in Figure 7.6 and Figure 7.7.

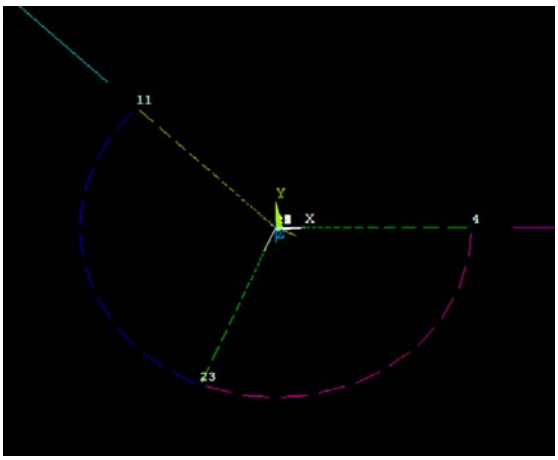

Figure 7.6: Circumference with radius equal to 0.28mm at the weld toe

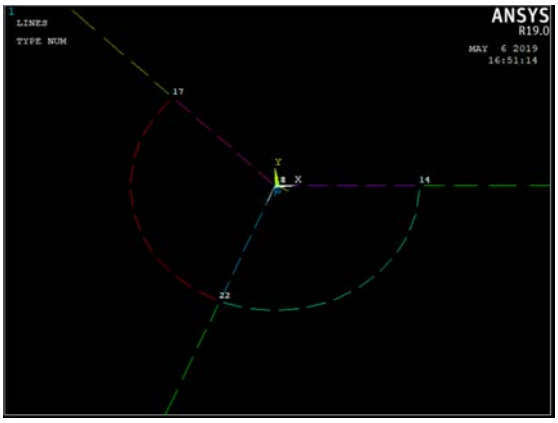

Figure 7.7: Circumference with radius equal to 0.0001mm at the weld toe

Generation of the mesh As we need a regular mesh which become thicker as it gets closer to the weld toe, the lines of the previous geometric construction and the bisector are divided into segments For the inner circle (radius 0.0001mm, see Figure 7.7), the following options were set through the ANSYS' commands SIZE CONTROL→ MANUAL SIZE→ LINES :

- For arc lengths of 1/8 of circumference: 4 subdivisions, spacing ratio 1
- For arc lengths of 1/4 of circumference: 8 subdivisions, spacing ratio 1
- For radial segments: 5 subdivisions, spacing ratio 1

For the inner circle (radius 0.0001mm, see Figure 7.6), the following options were set through the ANSYS' commands SIZE CONTROL, MANUAL SIZE and LINES :

- For arc lengths of 1/8 of circumference: 4 subdivisions, spacing ratio 1
- For arc lengths of 1/4 of circumference: 8 subdivisions, spacing ratio 1
- For radial segments: 50 subdivisions, spacing ratio 2000

Plane Elements 182 were used with the following key-options activated:

- K1=3 (*Simple Enhanced Strain*)
- K3=1 (*Plane Strain*)

The generate mesh was:

- **Free** in the circular sector of radius 0.0001mm and on the ouside of the circles
- **Mapped** in the circular sector of radius 0.28

The meshed geometry is shown in Figg. 7.8, 7.9 and 7.10.

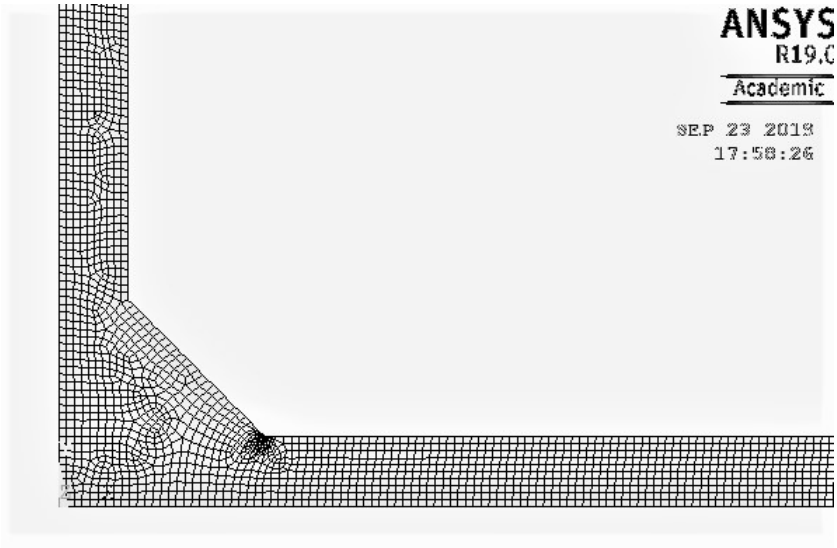

Figure 7.8: Free mesh outside the geometric construction

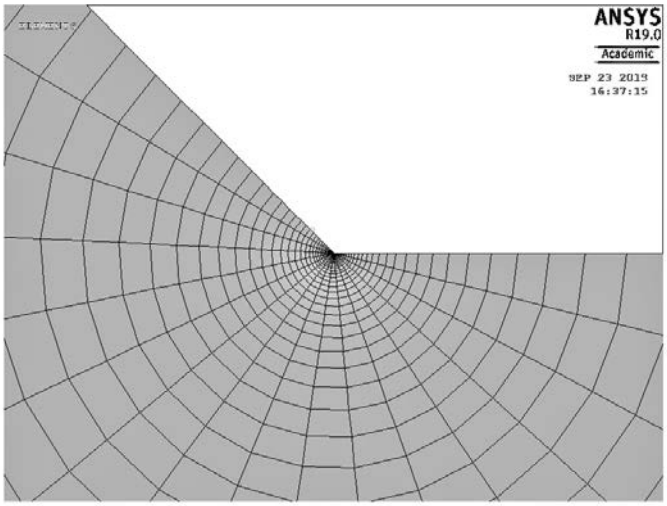

Figure 7.9: Mapped mesh in circular sector of radius 0.28mm

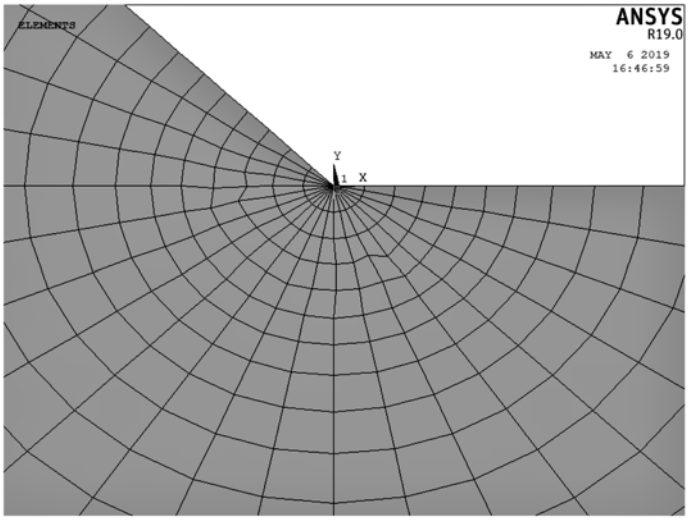

Figure 7.10: Free mesh in circular sector of radius 0.0001mm

Application of the loads and post-processing After applying 1MPa traction load and symmetry condition, the solution is launched. At this point a new local reference system is needed and it has to be located at the weld toe: the X-axis has the direction of the bisector of the opening angle 2α and the new-built reference system is selected as output reference system in "OPTIONS FOR OUTPUT". Then, one has to create a *path*, selecting all the nodes from the edge of the V-notch to the border of the control area.and the value of the stress component σ_{yy} is associated to each node. Now the values of the coordinates of the nodes, along with the corresponding stress components are exported to Excel. The data of the stresses are plotted as function of the radial coordinates,

except for the ones referring to the inner circle of 0.0001mm: this is to avoid the overestimation of the stresses. By the definition of N-SIF for an opening angle of 135°, the exponent of the interpolating curve should be equal to 0.326. Figure 7.11 shows the plot.

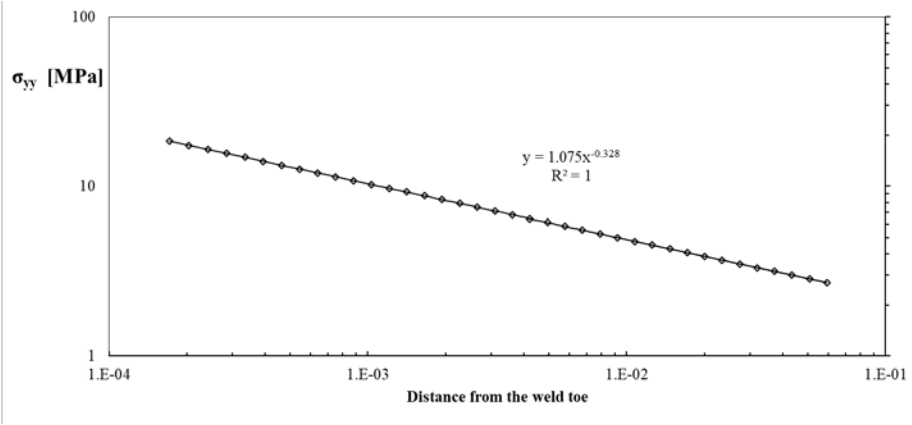

Figure 7.11: Plot of the stresses versus distance from the weld toe along the bisector of the opening angle

Given the N-SIF ΔK_1 by the Eq. 7.18

$$\Delta K_1 = \sqrt{2\pi}\Delta\sigma_{yy} r^{1-\lambda_1} \tag{7.18}$$

ΔK_1 can be plotted versus the distance from the notch's edge (Figure 7.12)

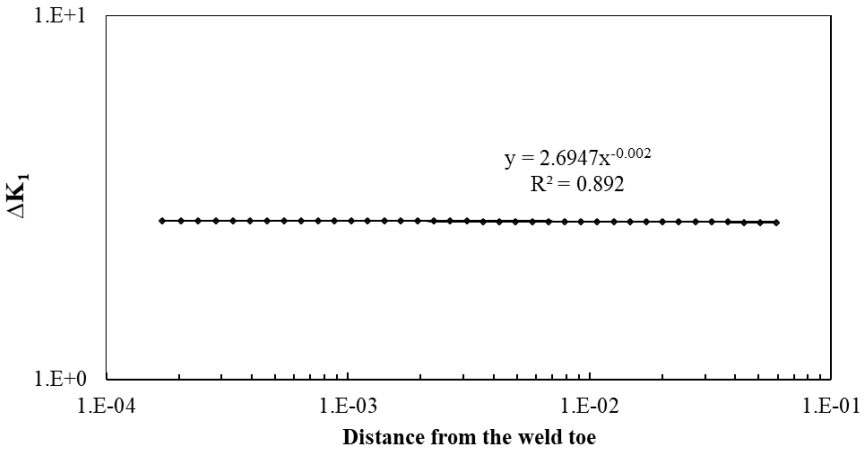

Figure 7.12: Plot of the N-SIF ΔK_1 as function of the distance from the weld toe

As the Δk is a linear elastic parameter, it is enough to multiply the obtained value by the corresponding nominal tension applied to the joint in order to

obtain a new plot of the N-SIf as function of the number of cycles to failure. In the following Tables 7.2 and 7.3, one can find the values of ΔK for unit loads and the effective ΔK versus the fatigue life for each serie of the analyzed joints.

Series	ΔK_1 for unit load $[MPa * mm^{0.326}]$
1/Maddox (1987)	2.7253
12/Gurney (1991)	5.5348
16/Gurney (1991)	3.0862
23/Gurney (1997)	1.91

Table 7.2: Values of ΔK_1 for unit load for each tested series

Series	Geometry, Load condition	N [n of cycles]	ΔK_1 $[MPa \cdot mm^{0.326}]$
1/Maddox (1987)	cruciform/tension	192000	538.94
		507000	377.26
		2937000	269.47
		4297000	215.58
12/Gurney (1991)	cruciform/tension	109000	150
		224000	830.22
		322000	664.18
		1153000	359.76
		2147000	304.4
16/Gurney (1991)	cruciform/bending	120000	802.41
		200000	678.964
		302000	555.516
		744000	432.07
		1180000	370.344
		2158000	339.48
23/Gurney (1997)	T/bending	135000	573
		237000	496.6
		407000	382
		573000	362.9
		665000	343.8
		1525000	305.6
		1534000	286.5
		2601000	367.4

Table 7.3: The effective ΔK and number of cycles for each serie of the analyzed joints

Figure 7.13 shows the design curve in terms of N-SIF. It is worth noting that by the use of the local parameter K_1, the scatter band obtained is much smaller than the one related to the nominal stress approach and the value of T_σ is 2.13.

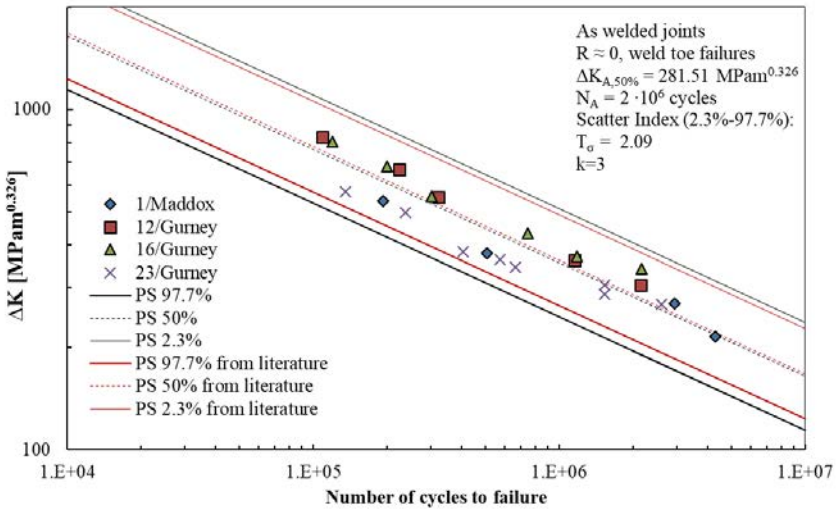

Figure 7.13: Design curve in terms of Stress Intensity Factors approach. The values of the N-SIF of mode I ΔK_1 in reported as function of the number of cycles

.

The Stress Intensity Factor approach allows a better condensation of the experimental data and leads to an improved accuracy in the prediction of joint fatigue life.

7.4.3 Application of the Strain Energy Density Approach

In order to apply this method, one can simply evaluate the average energy density in the structural control volume of radius 0.28mm. As we have already build this geometric construction in the previous model, it is possible to directly obtain the volume and its corresponding energy density for the selected elements into the outer circle. The sum of these values correspond to the total volume and the total average energy density respectively of the control volume, as reported in Table 7.4. The ratio between these two values is the SED for unit load; Table 7.5 reports the SED for each series. Finally, these parameters have to be multiplied by the squared nominal stress applied to the welded components. Table 7.6 shows results for all the specimens analyzed.

SENE	1.44e-06 [Nmm]
Volume	0.152951 $[mm^3]$
SED	9.44e-06 [Nmm/mm^3]

Table 7.4: SED parameters pulled out from FEM analisys

Series	SED for unit load
1	9.44e-06
12	3.91e-05
16	1.12e-05
23	4.62e-06

Table 7.5: SED for unit load

Series	Geometry, Load condition	N [n of cycles]	SED [Nmm/mm^3]
1/Maddox (1987)	cruciform/tension	192000	0.377
		507000	0.185
		2937000	0.094
		4297000	0.0604
12/Gurney (1991)	cruciform/tension	109000	0.879
		224000	0.563
		322000	0.391
		1153000	0.165
		2147000	0.118
16/Gurney (1991)	cruciform/bending	120000	0.8247
		200000	0.5905
		302000	0.395
		744000	0.239
		1180000	0.175
		2158000	0.147
23/Gurney (1997)	T/bending	135000	0.416
		237000	0.312
		407000	0.1848
		573000	0.167
		665000	0.149
		1525000	0.118
		1534000	0.104.5
		2601000	0.905

Table 7.6: The effective SED and number of cycles for each serie of the analyzed joints

The data are sintentyzed in Figure 7.14, where the plot of δW versus N is reported into a log-log scale. The scatter band index is 4.37; as the SED value depends on the nominal stress squared, the deviation is double. Also in this case, the scatter band obtained is much smaller than the one related to the nominal stress approach.

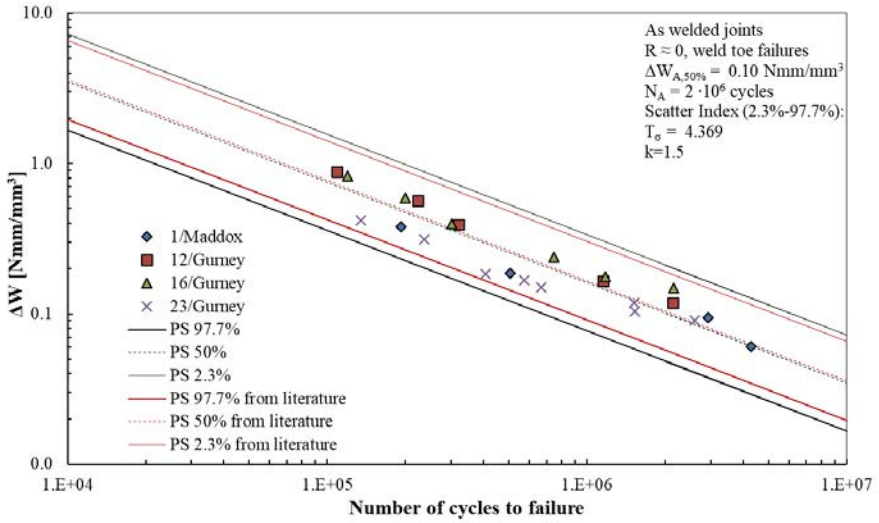

Figure 7.14: Design curve in terms of SED approach. The values of the Strain Energy Density are reported as function of the number of cycles

.

7.4.4 Application of the Peak Stress Method

For the application of the Peak Stress Method, a new mesh was generated in the previous models following these items:

- Plane Element 182 with active Key Option K1=3 and K3=1
- Ratio t/d greater than 3 (t= thickness, d=global element size)
- only two element at the edge of the notch
- Type *Free* Mesh

Figure 7.15 shows an example of mesh obtained for the Maddox Joint (Serie 1) with a Global Element Size of 2mm.

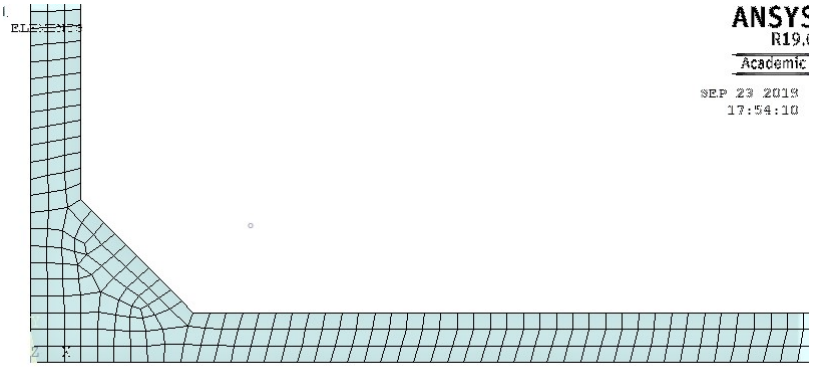

Figure 7.15: Free mesh for the application of Peak Stress Method with a Global Element Size of 2mm and two elements at the notch

.

Launched the solution with 1MPa tension load and symmetric condition applied, the first principal peak stress is plotted thank to the command: GENERAL POSTPROC→ PLOT RESULTS→CONTOUR PLOT→ NODAL SOLUTION → STRESS → 1st principal stress. The maximum stress in the screen is the sought peak stress. Figure 7.16 shows an example.

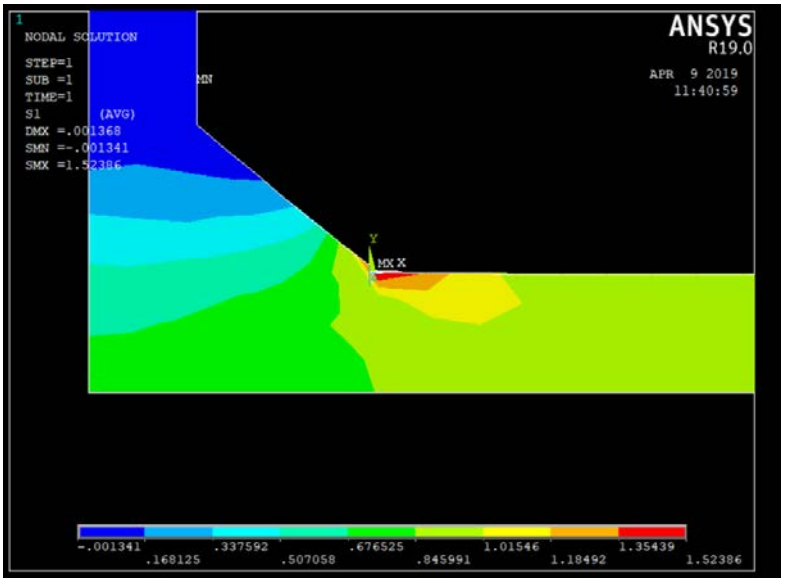

Figure 7.16: Contour plot of the first principal stress in Ansys Mechanical. The maximum value in the bar at the bottom of the screen corresponds to the Peak Stress

.

Table 7.7 reports the chosen global element size and the Peak Stress obtained for each series of joints.

Series	d[mm]	$\Delta\sigma_{11,peak}$ [MPa]
1	2	1.524
12	14	1.658
16	6	1.253
23	1	1.363

Table 7.7: Values of global Element Size and Peak stress for each series

From the values of the Peak Stress, the equivalent peak stress is calculeted using Equation 7.19.

$$\Delta\sigma_{eq,peak} = f_{w1}\Delta\sigma_{peak} \tag{7.19}$$

where the coefficient f_{w1} is given by the following relation :

$$f_{w1} = K^*_{FE} \cdot \sqrt{\frac{2e_1}{1-\nu^2}} \cdot \left(\frac{d}{R_c}\right)^{1-\lambda_1}$$

One can find the values for the coefficients of the previous formulas according to Figure 7.17 . These values have been calibrated as function of the opening angle of the V-notch in Ansys.

2α (deg)	λ_1	e_1	$R_c = 0.28$ mm	
			$f_{w1,d=0.5mm}$ [(a)]	$f_{w1,d=1mm}$ [(a)]
0	0.500	0.133	0.997	1.410
90	0.544	0.146	1.015	1.392
120	0.616	0.129	0.918	1.198
135	0.674	0.118	0.849	1.064

(a): valori calcolati con $\nu = 0.3$, $K^*_{FE} = 1.38$

Figure 7.17: Scalar coefficients for the calculation of f_{w1} as function pf th opening angle 2α

.

Considering an opening angle 2α of 135° and the global element size reported previously in 7.7, f_{w1} can be obtained for all the series. The calculation leads to the results reported in following Table 7.8.

Series	Geometry/ Load condition	Loaded thickness [mm]	N [cycles to failure]	$\Delta\sigma_{eq,peak}$ [MPa]
1/Maddox (1987)	Cruciform/ Tension	13	192000	406.6
		13	507000	284.6
		13	2937000	203.3
		13	4297000	162.6
12/Gurney (1991)	Cruciform/ Tension	100	109000	625.7
		100	224000	500.6
		100	322000	417.2
		100	1153000	271.2
		100	2147000	229.4
16/Gurney (1991)	Cruciform/ Bending	100	120000	622.0
		100	200000	526.3
		100	302000	430.6
		100	744000	334.9
		100	1180000	287.1
		100	2158000	263.2
23/Gurney (1997)	T/ Bending	6	135000	435.0
		6	237000	377.0
		6	407000	290.0
		6	573000	275.5
		6	665000	261.0
		6	1525000	232.0
		6	1534000	217.5
		6	2601000	203.0

Table 7.8: Number of cycles to failure and corresponding peak stress of all the analyzed specimens

Finally, in Figure 7.18 the design curve is reported for the Peak Stress Method. The scatter band is greatly decreased with respect ot the nominal load and the scatter index is 2.13.

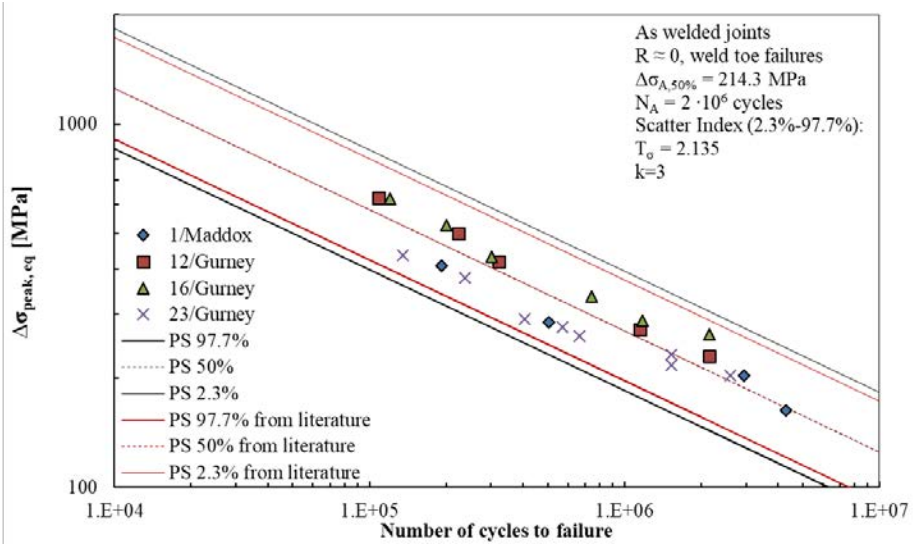

Figure 7.18: Design curve is reported for the Peak Stress Method. The fatigue life of the specimens is reported as function of the equivalent peak stress versus the number of cycles to failure.

Chapter 8

Finite Element Analysis of dissimilar ADI-to-steel welded joints

Finite Element Analyses have been performed in order to define the design curves based on the local approaches. As introduced in previous Chapter 7 for steel joints, the scatter of the experimental data is very high in terms of nominal stress approach. The same issue came up in the tested dissimilar joints: due to the high variety of geometries, the local stress field and its intensity have to be taken into consideration in order to decrease the scatter bands. The first step of the FEM analysis was to define a simplified geometrical model to describe each structural detail. Successively, a proper set of constrains and loads was applied to replicate the testing conditions. Then, the mesh was generated depending on the applied local approach. In the following paragraph will be described the procedure to adequately perform the simulations on Ansys Mechanical. Due to the large number of experimental data, it became necessary to parametrise and automate the FE analyses: Appendix C reports all the APDL (Ansys Parametric Design Language) scripts employed for the simulations. The local approaches applied are:

- Notch Stress Intensity Factors approach
- Strain Energy Density approach
- Peak Stress Method

As the theory behind these approaches has been already presented, the reader is referred to the previous Chapter 7 for more information and Chapter 8 will focus on their practical application on ADI-to-steel dissimilar joints.

8.1 Nominal stress approach: synthesis of the experimental results

In order to understand the advantages of numerically analyse the joints, it is useful to plot all the experimental results in one S-N curve. As expected, the data do not syntetize in terms of the nominal stress approach, as shown in Figure 8.1. The scatter index T_σ is equal to 5, considering all the joint with failure at both the weld toe and the weld root. Considering only the failure at the weld toe on the ADI side (see following Figure 8.2), the scatter slightly decrease to T_σ=3.64. It is worth noting that only joints with failure at toe on the ADI side will be considered in the following paragraph. The main reason for this choice is that the present work aims to analyse the influence of ADI on the fatigue properties of welded joints: the series A (partial penetration butt-joint) and the series D (T nlc fillet-welds joints) present failure on the filler material and weld toe at steel side, respectively. Thus, they shall be regarded as homogeneous steel welded joints.
Even thought the tested series present quite different geometries, one could notice that the scatter is less pronounced with respect to the case of corresponding homogenous steel welded joints (see Figure7.5). The reason can be found looking at the actual dimensions of joints' plates and stiffeners: considering the steel joints of the previous Chapter 7, the variation of thickness was very pronounced from series to series, while it was kept constant at 10mm for all the dissimilar joints. Thus, the scatter is less influenced by the scale effect in ADI-to-steel dissimilar welded details.

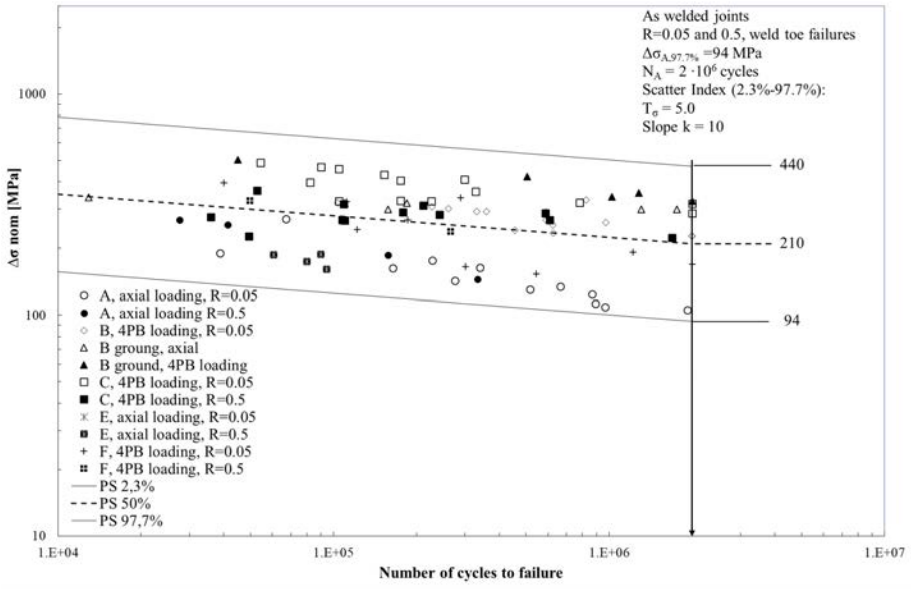

Figure 8.1: Synthesis of all experimental results in terms of Nominal Stress approach

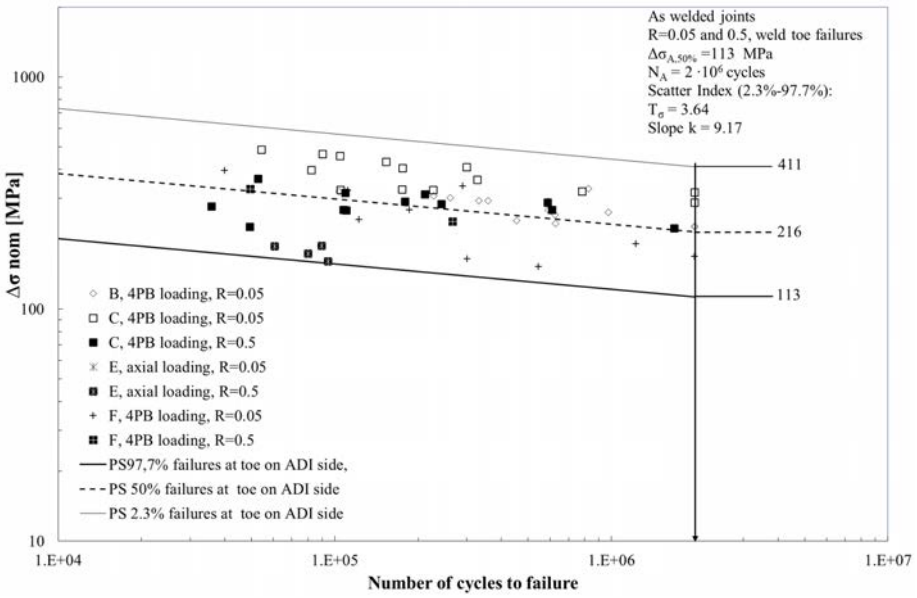

Figure 8.2: Synthesis of experimental data,considering failure at weld toe on ADI side

8.2 FE modelling of dissimilar welded details

Welded joints are often modelled as 2D objects and FEM analyses are carried out with Plane conditions, i.e. Plane Stress or Plane Strain depending on the geometrical parameters of the real tested specimens. The notch of the weld bead is a stress raiser and a point of singularity, i.e. the stress field goes towards infinity. Thus, in all the simulations reported in the present work, the weld toe/root is modelled as a sharp edge with tip radius equal to 0. The latter assumption is on the safe-side as a tip radius greater than 0 results into a lower-grade singularity of the stress-field.

8.2.1 Geometry and material properties

Figure 8.3 reports the comparison between the real and the simplified model of a **partial-penetration butt-joint**. The parametric values used in the APDL code correspond to:

- **l_root** is the half-length of the weld root;
- **ltot** is the total length of the joint;
- **t** is the half-thickness of the joint;
- **b** is the width of the weld bead;
- **h** is the height of the weld bead;
- **alfa_ADI** corresponds to the opening angle 2α at the weld toe on the ADI side;

- **alfa_S355** corresponds to the opening angle 2α at the weld toe on the S355 side;

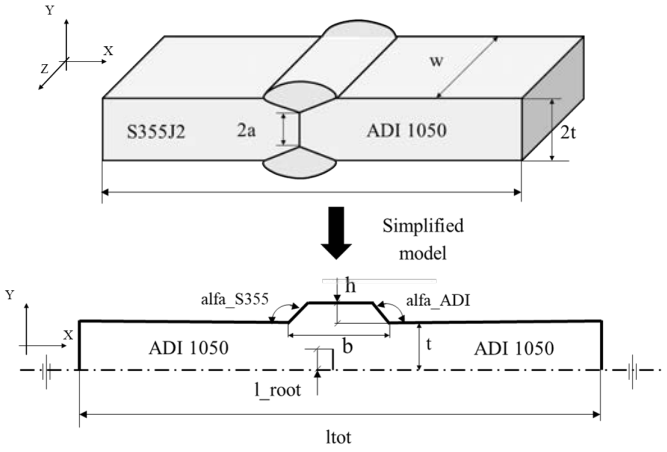

Figure 8.3: Simplification of the partial-penetration butt-joint into a FE model.

Full-penetration butt-joint was modelled as reported in Figure 8.4.The nomenclature for the geometric parameters is equal to the one of the partial-penetration butt-joint. For both of them, only half of the joint is modelled thanks to the symmetry along the longitudinal plane x-z.

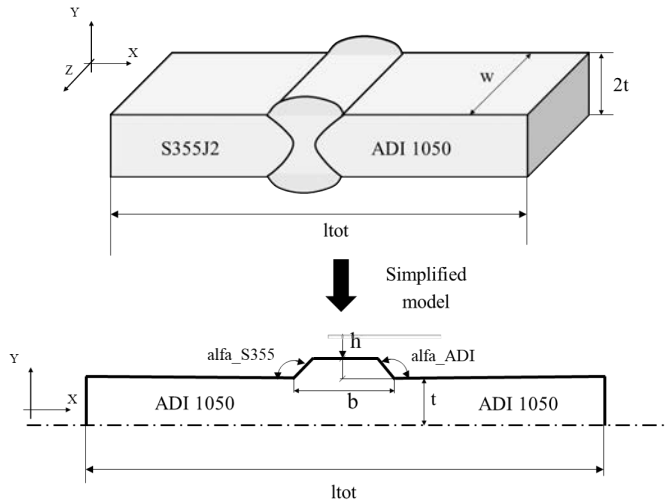

Figure 8.4: Simplification of the full-penetration butt-joint into a FE model.

For all the cruciform joints, the symmetry along both the x- and y-axis allows only a quarter of the specimen to be modelled, as shown in Figure 8.5. The parametric values used in the APDL code for cruciform joints correspond to:

- **ltot** is the total length of the joint;
- **t** is the half-thickness of the joint;
- **h** is the height of the weld bead;
- **alfa_ADI** corresponds to the opening angle 2α at the weld toe on the ADI side;

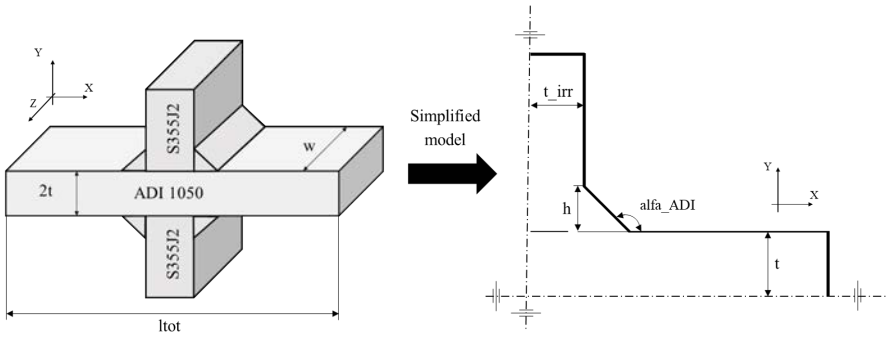

Figure 8.5: Example of a cruciform joint into a simplified FE model

For all the welded details, the material is the same for the whole model, even if the joint has both ADI plates and steel plates. In particular, it is set on ADI or structural steel, depending on the main plate's material where the load is applied and where the nominal stress is consequently calculated. It is supposed isotropic and linear elastic, while the Young's Modulus E is set at either 168000 or 206000 MPa and Poisson's ratio ν at either 0.27 or 0.3 for ADI and steel respectively.

8.2.2 The applied load and boundary conditions

For each structural detail, the load condition can be chosen between both Axial loanding and four-point-bending loading. Regarding joints under axial loading, boundary conditions have been set as reported in Figure 8.6:

- in the case that half joint is modelled, symmetry condition (S in the figure) is applied along the x-axis. The displacement along x-direction is fixed on one extreme, while the uniform unit pressure is applied on the opposite side.
- in the case that only a quarter of the joint is considered, symmetry boundary conditions on both x- and y- axis are sufficient to constrain the model. The unit pressure is applied as in the previous point.

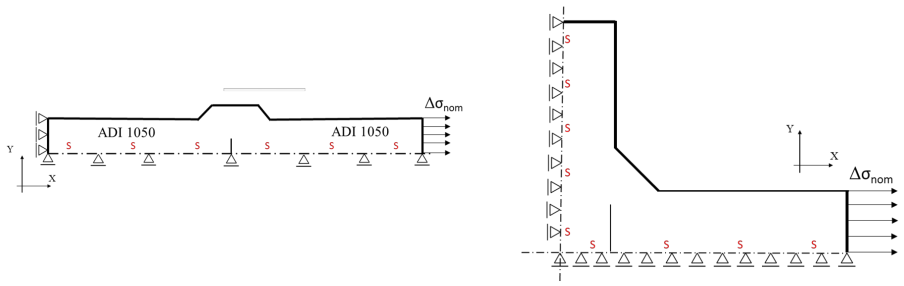

Figure 8.6: Examples of applied boundary conditions for butt- and cruciform-joint under axial loading

On the other hand, considering four-point bending loading, the boundary conditions were applied as follows (see also Figure 8.7):

- in the case that half joint is modelled, anti-symmetry condition (A in the figure) is applied along the x-axis. All DOFs (degrees of freedom) are fixed on one extreme, while the pressure is applied on the opposite side: in order to simulate bending, the maximum tensile stress is located at the uppermost edge of the beam, while it is set to 0 at the lower edge.
- in the case that only a quarter of the joint is considered, the model is constrained applying symmetry condition along y-axis and anti-symmetry condition along x-axis. At the lower left edge, the displacement is set to 0 along the y-direction. The pressure is applied as in the previous point.

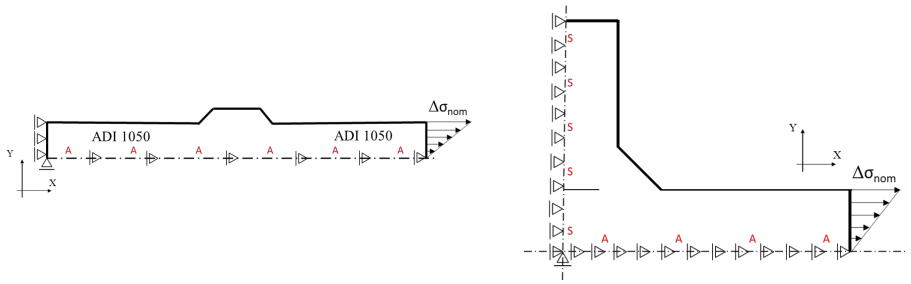

Figure 8.7: Examples of applied boundary conditions for butt- and cruciform-joint under four-point-bending loading

8.3 Local approaches applied on dissimilar ADI-to-steel joints

As procedure is the same for both homogeneous steel joints and dissimilar joints, for the sake of brevity the reader is referred to previous Chapter 7 for setting up the simulations and exporting data to Excel spreadsheets. Before proceeding with the application of the NSIFs, SED and PSM approaches, a consideration on failure mode has to be done. In most cases, cracks nucleated at the weld toe on the ADI side where the material is mainly composed by ledeburite and

unstable ausferrite. As both the Strain Energy Density and the PSM approaches have been calibrated only for homogeneous steel joints, a new control radius R_c is needed to consider the material properties of the weld bead in the case of dissimilar ADI-to -steel joints.

8.3.1 Calibration of the control radius R_c for Austemperd Dictile Iron

In order to calibrate the control volume at the weld toe, one has to match the strain energy density ΔW of the notched and plain specimens at a reference number of cycles N_A. Referring to the V-notched specimens with opening angle 2α , the range of the strain energy density can be calculated as :

$$\Delta W_{V-notch} = \frac{e_1}{E} \cdot \left[\frac{\Delta K_{1,N_A}}{R_c^{1-\lambda_1}} \right]^2 \tag{8.1}$$

where

- ΔK_1 is the N-SIF-based fatigue strength of welded joints having constant V-notch angle 2α ;
- λ_1 is the William's exponent depending on the opening angle 2α;
- Young's Modulus E and the parameter e_1 depend on the material
- R_c is the unknown control radius to be found

Referring to the plain specimens and according to the Beltrami's hypothesis, the range of the strain energy density can be calculated as:

$$\Delta W_{ground} := \begin{cases} \frac{\Delta\sigma_A^2}{2E} \textit{ under Plain Stress conditon or} \\ \frac{\Delta\sigma_A^2}{2E} \cdot (1-\nu^2) \textit{ under Plain Strain conditon} \end{cases} \tag{8.2}$$

where $\Delta\sigma_A$ is the nominal stress range at the reference number of cycles N_A, E is the Young's Modulus and ν is the Poisson's ratio.
In particular, the strain energy density for ground specimens were calculated under the Plane Stress hypothesis. In order to choose between Plane Strain and Plain Stress, one has to check whether the stress σ_z or the strain ϵ_z is equal to 0 (see Figure 8.8). If the first condition is satisfied, pure Plane Stress condition should be applied. Otherwise, if $\epsilon_z = 0$, pure Plain Strain condition shall be set.

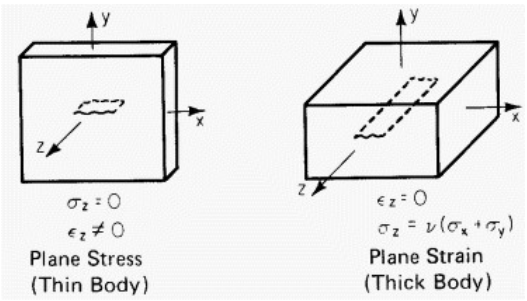

Figure 8.8: Examples of Plane Strain and Plane Stress condition.

The following coefficient can be helpful to check which hypothesis is the most realistic:

$$\begin{aligned} C_z &= \frac{\sigma_z}{\nu(\sigma_x + \sigma_y)} \\ &\longrightarrow \begin{cases} Plane\ Strain\ if\ C_z = 1 \\ Plane\ Stress\ if\ C_z = 0 \end{cases} \end{aligned} \tag{8.3}$$

where σ_x is the applied nominal load. By the mean of a simple 3D FE model of a ground joint under axial loading, it easy to extract the values of σ_x, σ_y and σ_z in the main reference system. As σ_x is equal to the applied load and $\sigma_x \gg \sigma_y, \sigma_z$, the index $C_z \to 0$. Thus, the strain energy density is calculated under Plane Stress condition for plain and ground specimens.

The combination of Eq. 8.1 with Eq. 8.2 yields the control radius R_c:

$$\begin{aligned} &\Delta W_{V-notch} = \Delta W_{ground} \\ &\longrightarrow \frac{e_1}{E} \cdot \left[\frac{\Delta K_{1,N_A}}{R_c^{1-\lambda_1}} \right]^2 = \frac{\Delta \sigma_A^2}{2E} \\ &\longrightarrow R_c = \left(\sqrt{2e_1} \cdot \frac{\Delta K_{1,N_A}}{\Delta \sigma_A} \right)^{\frac{1}{1-\lambda_1}} \end{aligned} \tag{8.4}$$

Eq 8.4 allows to calculate the control radius if the parameters $\Delta K_{1,N_A}$ and $\Delta \sigma_A$ are known. With reference to fatigue life of $N_A = 2 \cdot 10^6$ cycles and a nominal load ratio R=0.05, it was considered:

- the value of $\Delta \sigma_A$ at $N_A = 2 \cdot 10^6$ cycles referred to a survival probability of 50% of full-penetration ground butt joints tested under axial loading (hypothesis of uniform stress field). Indeed, the fatigue strength of ground specimens is influenced only by the material alterations induced by the welding process, as there are no stress concentrations due to the weld bead.

- the value of $\Delta K_{1,N_A=2\cdot 10^6}$ referred to a survival probability of 50%, considering only as-welded joints having opening angle $2\alpha \approx 135°$, tested under either axial or four-point-bending loading and characterized by failures at the weld toe on the ADI side.

In order to have the most accurate value for the NSIF-based fatigue strength ΔK_1 at 2 millions cycles, the joints were accurately analysed and selected. Only the joints with opening angle $133° \leq 2\alpha \leq 138°$ were taken into account, as the William's exponent λ_1 depends on the V-nocth geometry and so does the stress field. Furthermore, only joints tested at nominal load ratio R=0.05 were considered in the first place.
The N-SIF K_1 was calculated for the full-penetration butt-joints (series B), nlc fillet-welds cruciform joints (series C), cruciform joints with load carrying fillet-welds (serie E) and cruciform full-penetration k-butt welded joints (series F). Table 8.1 reports the results of the FE analyses, while the N-SIF ΔK_1 is plotted versus the corresponding number of cycles to failure in Figure 8.9.

Specimen code	K_1 $[MPamm^{0.236}]$	$\Delta\sigma_{nom}$ [MPa]	N [cycles]	ΔK_1 $[MPamm^{0.236}]$
C7-1	1.85	328.02	175019	605.40
C8-3	1.85	406.02	175437	749.34
C5-2	1.85	318.27	2000000	587.40
C5-2restest	1.85	410.00	299261	756.70
C5-1	1.85	360.45	327322	665.24
C9-3	1.86	326.57	104687	606.63
C10-2	1.90	457.49	104527	867.04
C11-2	1.83	465.42	90293	851.44
B5-5	1.80	233.33	590166	420.76
B5-1retest	1.81	301.37	627827	546.47
B5-1	1.81	226.73	2000000	411.14
B2-6retest	1.82	321.40	974888	586.21
B2-6	1.82	227.20	2000000	414.39
F1-5	1.93	243.11	122085	469.78
F1-6	1.93	164.59	300768	318.06
E4-2	3.06	185.06	248030	565.47
E3-3	3.06	235.98	82736	721.05
E3-5	1.92	313.43	344181	602.51
E3-6	1.92	325.00	630368	624.23

Table 8.1: Values of ΔK_1 employed in the calibration of the control volume.

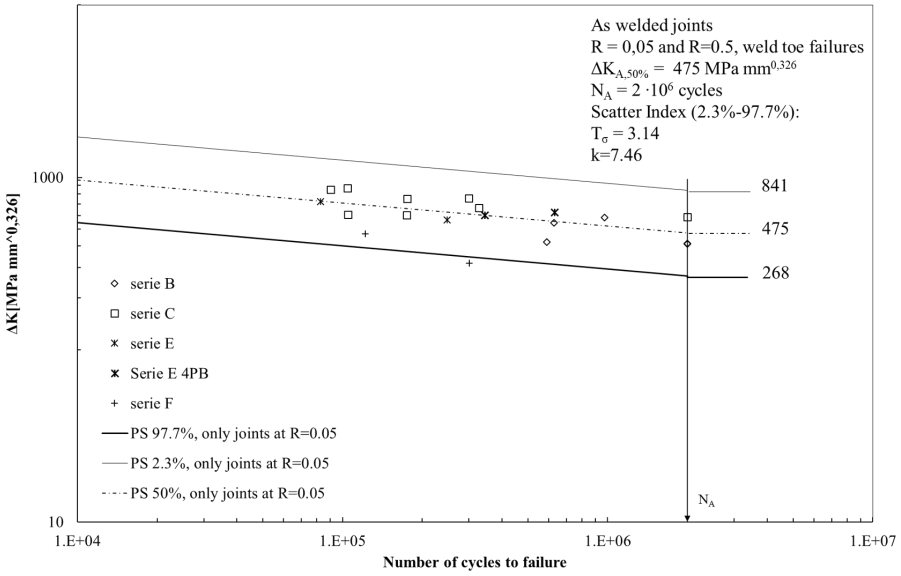

Figure 8.9: Plot of the N-SIF ΔK_1 versus the corresponding number of cycles to failure. Only joints with opening angle $133° \leq 2\alpha \leq 138°$ and nominal load ratio R=0.05

Applying the parameters:

- $e_1 = 0.1214$
- λ_1=0.674
- ΔK_1= 475 $MPa\,mm^{0.236}$
- $\Delta\sigma$= 287 MPa

Eq. 8.4 yields a control radius R_C = 0.534mm.

In order to confirm the value obtained for R_c, the curve in terms of the N-SIF ΔK_1 was re-calculated including the latest experimental results at nominal load ratio R=0.5. As before, the specimens were selected considering only joints with V-notch opening angles $2\alpha \approx 135°$. The additional data are reported in Table 8.2 and Figure 8.10 shows the new curve.

Specimen code	K_1 $[MPamm^{0.236}]$	$\Delta\sigma_nom$ [MPa]	N [cycles]	ΔK_1 $[MPamm^{0.236}]$
C16-3	1.85	266.48	110198	493.35
C13-3	1.87	267.30	107812	500.87
C9-1	1.88	363.51	52884	683.26
C9-2	1.86	311.16	212312	578.13
F2-2	1.93	328.73	49658	635.24
E2-4	3.06	186.57	60672	570.07
E2-6	3.06	187.50	80167	572.93
E3-4	3.06	160.09	94490	489.17

Table 8.2: Values of ΔK_1 for the calibration of the new control volume (nominal load ratio 0.05 and 0.5)

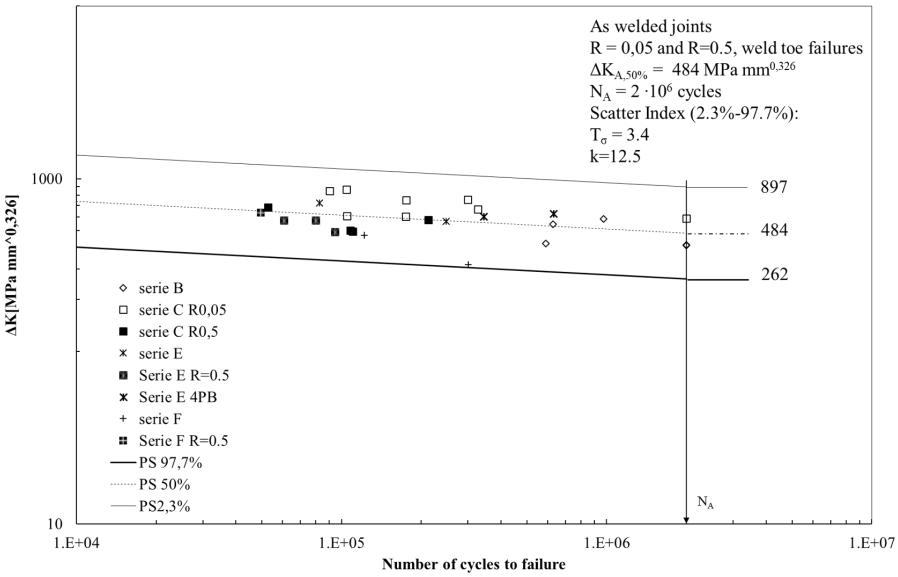

Figure 8.10: Plot of the N-SIF ΔK_1 versus the corresponding number of cycles to failure. Only joints with opening angle $133° \leq 2\alpha \leq 138°$ and nominal load ratio R 0.05 and 0.5.

Substituting the new value for ΔK_1 in Eq. 8.4, the control radius results $R_C = 0.568$mm. As the difference with respect to the previous value is slightly greater than 6%, the results can be considered consistent and the new control radius for ADI can be set at $R_C = \mathbf{0.53mm}$. The choice to use a critical radius equal to 0.53mm instead of 0.57mm is an engineering approximation on the safe-side, as it leads to greater values of the strain energy density.

An other attempt to calibrate and consequently verify the control radius for Austempered Ductile Iron was by the mean of the SED Approach itself. The purpose was to synthesize the ground joints under axial loading and the ground joints under four-point-bending loading in terms of the Strain Energy Density. The iterative method follows the steps:

1. By the mean of FE analyses, calculate of the SED for each joint tested under four-point-bending loading, varying the control radius R_c into a proper range of values ($0.1 < R_C < 1.1mm$);

2. Plot the ΔW_{4PB} versus the number of cycles (one curve for each R_C);

3. Compare ΔW_{4PB} at 2million cycles (PS50%) for ground joint under 4PB loading to the value of ΔW_{AX} at 2million cycles for ground joints under axial loading;

4. continue until:

$$\Delta W_{4PB} = \Delta W_{AX} \; at \; 2 \cdot 10^6 \; cycle$$

.

The convergence is reached for a control radius equal to 1mm, as shown in Figure 8.11.

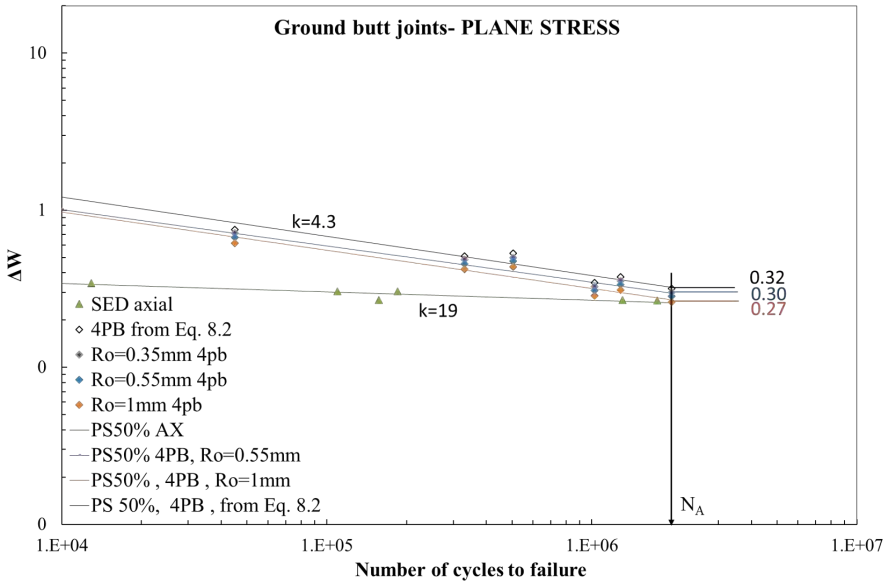

Figure 8.11: Plot of the SED of full-penetration ground butt-joints at different control radius R_C.

The control radius obtained with the iterative method is almost double the one from the analytic formula 8.4. The difference might be due to certain simplistic generalisations introduced in the FE models. In particular, the assumption made for the material fails to cater for the sizeable influence of the welding process, which alters the mechanical properties of the ADI and, consequently, its fatigue limit. On the contrary, cracks are mainly driven by the stress raising effect in notched specimens and the assumption of pure Austempered Ductile Iron for the FE models is acceptable. Thus, comparing the strain energy density between ground butt-joints and V-notched joints seems the most correct method to define the control radius Rc.

8.3.2 Design curve in terms of Notch Stress Intensity Factors for dissimilar ADI-to-steel joints

Starting from the FE models reported above, the analyses were carried out as explained in Section 7.4.2. The applied load was 1MPa on all the joints and the N-SIF K_1 for unit load was scaled to the actual ΔK_1 later on, multiplying K_1 for the nominal stress $\Delta\sigma_{nom}$. It is worth noting that all the joint were modelled considering an V-notch opening angle 2α equal to 135°, even though some series presents an averaged opening angle greater than 140°. As the unit measure of K_1 is $[MPamm^{1-\lambda_1}]$ and λ_1 is a function of 2α, the latter simplification was necessary in order to compare all the tested joints on the same ΔK_1-N curve. Thereby, some joints, e.g. cruciform full-penetration k-butt joints (series F), may not synthesize very well within the others series. Tables 8.3- 8.8 report the

obtained results for all the joints.

Specimen code	N	$\Delta\sigma_nom$ [MPa]	K_1 $[MPamm^{0.236}]$	ΔK_1 $[MPamm^{0.236}]$
B6-1	590273	291.08	1.81	527.82
B6-2	331582	293.63	1.81	532.43
B6-3	826913	330.80	1.81	599.85
B2-6*	103560	321.40	1.81	582.80
B5-1*	261184	301.37	1.81	546.47
B2-4	228112	307.85	1.81	558.23
B5-2	358504	293.42	1.81	532.06
B2-3	455291	240.34	1.81	435.82
B5-4	590166	267.56	1.81	485.16
B5-6	625883	254.98	1.81	462.36
B5-5	627827	233.33	1.81	423.09
B5-3	974888	261.11	1.81	473.47
B5-1	2000000	226.73	1.81	411.14
B2-6	2000000	227.20	1.81	411.98

*=specimen retested after run-out

Table 8.3: NSIF ΔK_1 of full-penetration butt-joints

Specimen code	N	$\Delta\sigma_{nom}$ [MPa]	K_1 $[MPamm^{0.236}]$	ΔK_1 $[MPamm^{0.236}]$
C15-2	49352	225.56	1.91	326.26
C17-4	35956	276.38	1.91	329.11
C18-2	179361	290.55	1.91	370.78
C18-3	109229	316.69	1.91	360.25
C16-3	110198	266.48	1.91	337.79
C17-1	1691834	222.75	1.91	345.06
C17-1	609664	267.30	1.91	328.88
C13-3	107812	267.07	1.91	269.39
C16-2	242797	282.99	1.91	299.89
C9-1	52884	363.51	1.91	285.80
C12-2	587809	287.80	1.91	261.53

Table 8.4: NSIF ΔK_1 of cruciform nlc fillet-welds joints (R=0.5)

Specimen code	N	$\Delta\sigma_{nom}$ [MPa]	K_1 $[MPamm^{0.236}]$	ΔK_1 $[MPamm^{0.236}]$
C11-1	782127	322.30	1.92	618.37
C12-1	153004	431.16	1.92	827.23
C7-1	175019	328.02	1.92	629.34
C8-3	175437	406.02	1.92	778.98
C7-3	226568	325.97	1.92	625.40
C5-2	299261	409.98	1.92	786.58
C5-1	327322	360.45	1.92	691.56
C9-3	104687	326.57	1.92	626.55
C10-2	104527	457.49	1.92	877.75
C8-2	54270	487.65	1.92	935.60
C11-2	90293	465.42	1.92	892.96
C8-1	82159	398.00	1.92	763.59
C8-1*	2000000	287.44	1.92	551.48
C5-2*	2000000	318.27	1.92	610.63

*=specimen retested after run-out

Table 8.5: NSIF ΔK_1 of cruciform nlc fillet-welds joints (R=0.05)

Specimen code	R	N	$\Delta\sigma_{nom}$ [MPa]	K_1 $[MPamm^{0.236}]$	ΔK_1 $[MPamm^{0.236}]$
D2-2	0.05	2000000	110.12	2.80	308.12
D2-1	0.05	2000000	149.98	2.80	419.64
D2-1*	0.05	271405	299.96	2.80	839.28
D2-3	0.05	2000000	174.95	2.80	489.52
D1-1	0.05	353034	234.57	2.80	656.32
D1-6	0.05	1990000	200.99	2.80	562.38
D1-6 *	0.05	2000000	240.69	2.80	673.46
D1-6 **	0.05	350104	285.36	2.80	798.44
D2-6	0.05	174533	306.93	2.80	858.79
D2-4	0.05	73446	325.98	2.80	912.09
D1-2	0.05	42005	336.61	2.80	941.83
D1-5	0.05	60781	343.21	2.80	960.30
D3-1	0.5	512356	236.32	2.80	661.22
D3-2	0.5	209569	226.83	2.80	634.67

*=specimen retested after run-out

Table 8.6: NSIF ΔK_1 of T nlc fillet-welds joints (R=0.05+0.5)

Specimen code	R	N	$\Delta\sigma_{nom}$ [MPa]	K_1 $[MPamm^{0.236}]$	ΔK_1 $[MPamm^{0.236}]$
E3-1	0.05	118526	208.33	3.06	636.58
E2-1	0.05	2000000	174.56	3.06	533.40
E2-1*	0.05	256157	192.02	3.06	586.74
E4-3	0.05	548082	185.46	3.06	566.70
E4-1	0.05	140969	227.84	3.06	696.20
E4-2	0.05	248030	185.06	3.06	565.47
E3-3	0.05	82736	235.98	3.06	721.05
E2-4	0.5	60672	186.57	3.06	570.07
E2-2	0.5	89887	187.50	3.06	572.93
E2-6	0.5	80167	173.70	3.06	530.75
E3-4	0.5	94490	160.09	3.06	489.17

*=specimen retested after run-out

Table 8.7: NSIF ΔK_1 of cruciform load-carrying fillet-welds joints (R=0.05+0.5)

Specimen code	R	N	$\Delta\sigma_{nom}$ [MPa]	K_1 $[MPamm^{0.236}]$	ΔK_1 $[MPamm^{0.236}]$
F1-4	0.05	544633	162.96	1.93	314.91
F1-5	0.05	122085	243.11	1.93	469.78
F1-6	0.05	300768	172.07	1.93	332.52
F4-1	0.05	186215	267.74	1.93	517.38
F4-2	0.05	111413	324.39	1.93	626.86
F4-3	0.05	2000000	168.75	1.93	326.09
F4-3*	0.05	1222986	191.25	1.93	369.57
F4-5	0.05	39973	395.25	1.93	763.78
F4-4	0.05	289979	338.59	1.93	654.30
F3-2	0.5	266386	237.89	1.93	459.70
F2-2	0.5	49658	328.73	1.93	635.24

*=specimen retested after run-out

Table 8.8: NSIF ΔK_1 of cruciform full-penetration k-butt joints (R=0.05+0.5)

Following Figures 8.12 and 8.13 plot the design curve in terms of the N-SIF K_1 against the number of cycles to failure for ADI-to-steel welded joints. In the first one, only the joints tested at nominal load ratio R=0.05 are considered. The scatter index T_σ is equal to 2.24 and the inverse slope is 6.62. As expected, the scatter of the experimental data is lower than the one in terms of the Nominal Stress approach ($T_\sigma = 3.64$).
In the same figure, the N-SIF design curve at PS97.7% for homogeneous steel joints is plotted. As it can be seen, almost all the dissimilar joints present higher fatigue strength than the one suggested in the literature for homogeneous joints, specially at very high-cycles fatigue life. ΔK_1 at 2million cycles and survival probability PS97.7% is equal to $302 MPamm^{0.236}$, that is 30% higher than the corresponding value for the steel welded joints. In the second plot, joints tested at both nominal load ratio R=0.05 and R=0.5 are taken into account. In this

case, the slope is 7.94 and the scatter index T_σ is increased up to 2.67, but still lower than the one in terms of the Nominal Stress. The value of ΔK_1 at 2million cycles (PS97.7%) is now equal to $263 MPamm^{0.236}$: the experimental results outline a slightly lower fatigue resistance for the joints tested at nominal load ratio R=0.5 and the influence of the mean stress σ_m cannot be totally excluded, particularly for cruciform joints with load-carrying fillet-welds (series E). It can therefore be concluded that generally the N-SIF design curve for homogeneus steel joints can be employed for the fatigue assessment of dissimilar ADI-to-steel welded joints, even thought care must be taken when considering nominal load ratio greater than 0.5 and fatigue life under 100 000 cycles. Indeed, dissimilar joints show lower fatigue strength under very high loads than the corresponding homogeneous steel joints.

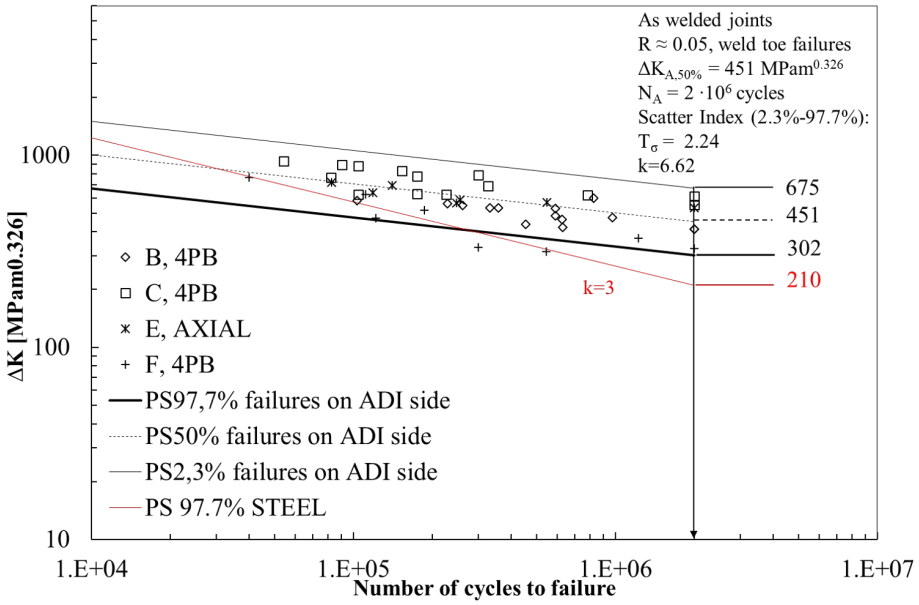

Figure 8.12: Design curve in terms of N-SIF for dissimilar ADI-to-Steel joints

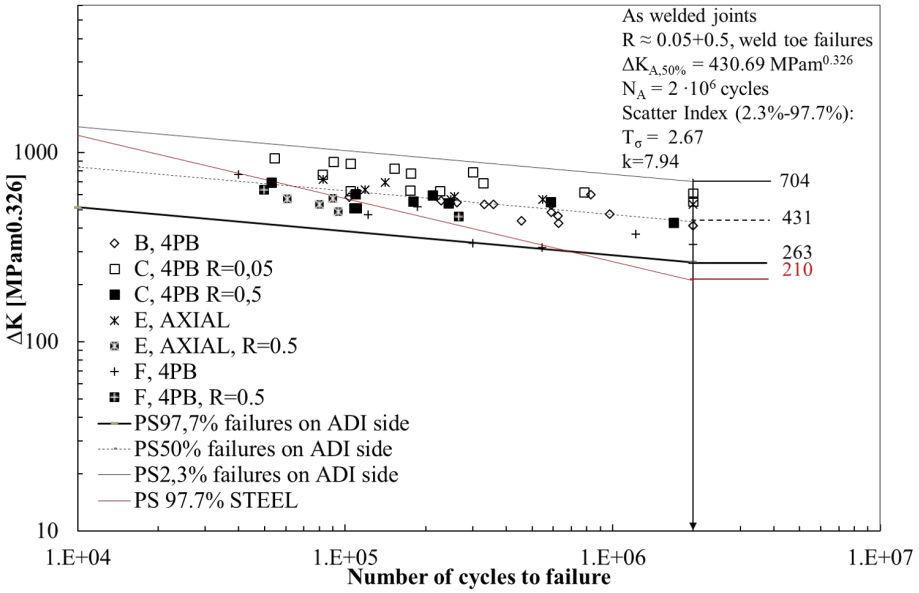

Figure 8.13: Design curve in terms of N-SIF for dissimilar ADI-to-Steel joints

8.3.3 Design curve in terms of Strain Energy Density for dissimilar ADI-to-steel joints

The analyses were carried out as explained in Section 7.4.3, considering a control volume with a critical radius equalt to 0.55mm. The applied load was 1MPa on all the joints and the energy density for unit load was scaled to the actual ΔW later on, multiplying W for the nominal stress $\Delta\sigma_{nom}^2$. All the joints were modelled considering the real geometric parameters, as the SED approach solves the problem related to the different opening angle 2α of the V-nocth (the unit measure does not depend on the William's exponent anymore). Tables 8.9- 8.14 report the obtained results for all the joints.

Specimen code	R	N	$\Delta\sigma_{nom}$ [MPa]	SED*10^6 $[Nmm/mm^3]$	ΔW $[Nmm/mm^3]$
B6-1	0.05	590273	291.08	3.66	0.310
B6-2	0.05	331582	293.63	3.66	0.315
B6-3	0.05	826913	330.80	3.66	0.400
B2-6*	0.05	103560	321.40	3.66	0.378
B5-1*	0.05	261184	301.37	3.66	0.332
B2-4	0.05	228112	307.85	3.66	0.347
B5-2	0.05	358504	293.42	3.66	0.315
B2-3	0.05	455291	240.34	3.66	0.211
B5-4	0.05	590166	267.56	3.66	0.262
B5-6	0.05	625883	254.98	3.66	0.238
B5-5	0.05	627827	233.33	3.66	0.199
B5-3	0.05	974888	261.11	3.66	0.249
B5-1	0.05	2000000	226.73	3.66	0.188
B2-6	0.05	2000000	227.20	3.66	0.189

*=specimen retested after run-out

Table 8.9: SED of full-penetration butt-joints

Specimen code	R	N	$\Delta\sigma_{nom}$ [MPa]	SED*10^6 $[Nmm/mm^3]$	ΔW $[Nmm/mm^3]$
C15-2	0.5	49352	225.56	3.067	0.156
C17-4	0.5	35956	276.38	3.067	0.234
C18-2	0.5	179361	290.55	3.067	0.259
C18-3	0.5	109229	316.69	3.067	0.308
C16-3	0.5	110198	266.48	3.067	0.218
C17-1	0.5	1691834	222.75	3.067	0.152
C17-1	0.5	609664	267.30	3.067	0.219
C13-3	0.5	107812	267.07	3.067	0.219
C16-2	0.5	242797	282.99	3.067	0.246
C9-1	0.5	52884	363.51	3.067	0.405
C12-2	0.5	587809	287.80	3.067	0.254
C9-2	0.5	212312	311.16	3.067	0.297

Table 8.10: SED of cruciform nlc fillet-welds joints (R=0.5)

Specimen code	R	N	$\Delta\sigma_{nom}$ [MPa]	SED*10^6 $[Nmm/mm^3]$	ΔW $[Nmm/mm^3]$
C11-1	0.05	782127	322.30	3.383	0.351
C12-1	0.05	153004	431.16	3.383	0.629
C7-1	0.05	175019	328.02	3.383	0.364
C8-3	0.05	175437	406.02	3.383	0.558
C7-3	0.05	226568	325.97	3.383	0.360
C5-2	0.05	299261	409.98	3.383	0.569
C5-1	0.05	327322	360.45	3.383	0.440
C9-3	0.05	104687	326.57	3.383	0.361
C10-2	0.05	104527	457.49	3.383	0.708
C8-2	0.05	54270	487.65	3.383	0.805
C11-2	0.05	90293	465.42	3.383	0.733
C8-1	0.05	82159	398.00	3.383	0.536
C8-1*	0.05	2000000	287.44	3.383	0.280
C5-2*	0.05	2000000	318.27	3.383	0.343

*=specimen retested after run-out

Table 8.11: SED of cruciform nlc fillet-welds joints (R=0.05)

Specimen code	R	N	$\Delta\sigma_{nom}$ [MPa]	SED*10^6 $[Nmm/mm^3]$	ΔW $[Nmm/mm^3]$
D2-2	0.05	2000000	110.12	6.726	0.082
D2-1	0.05	2000000	149.98	6.726	0.151
D2-1*	0.05	271405	299.96	6.726	0.605
D2-3	0.05	2000000	174.95	6.726	0.206
D1-1	0.05	353034	234.57	6.726	0.370
D1-6	0.05	1990000	200.99	6.726	0.272
D1-6*	0.05	2000000	240.69	6.726	0.390
D1-6*	0.05	350104	285.36	6.726	0.548
D2-6	0.05	174533	306.93	6.726	0.634
D2-4	0.05	73446	325.98	6.726	0.715
D1-2	0.05	42005	336.61	6.726	0.762
D1-5	0.05	60781	343.21	6.726	0.792
D3-1	0.5	512356	236.32	6.726	0.376
D3-2	0.5	209569	226.83	6.726	0.346

*=specimen retested after run-out

Table 8.12: SED of T nlc fillet-welds joints (R=0.05+0.5)

Specimen code	R	N	$\Delta\sigma_{nom}$ [MPa]	SED*10^6 $[Nmm/mm^3]$	ΔW $[Nmm/mm^3]$
E3-1	0.05	118526	208.33	7.723	0.335
E2-1*	0.05	2000000	174.56	7.723	0.235
E4-3	0.05	548082	185.46	7.723	0.266
E4-1	0.05	140969	227.84	7.723	0.401
E4-2	0.05	248030	185.06	7.723	0.264
E3-3	0.05	82736	235.98	7.723	0.430
E2-4	0.5	60672	186.57	7.723	0.269
E2-2	0.5	89887	187.50	7.723	0.272
E2-6	0.5	80167	173.70	7.723	0.233
E3-4	0.5	94490	160.09	7.723	0.198

*=specimen retested after run-out

Table 8.13: SED of cruciform load-carrying fillet-welds joints (R=0.05+0.5)

Specimen code	R	N	$\Delta\sigma_{nom}$ [MPa]	SED*10^6 $[Nmm/mm^3]$	ΔW $[Nmm/mm^3]$
F1-4	0.05	118526	544633	4.475	0.119
F1-4	0.05	544633	162.96	4.475	0.119
F1-5	0.05	122085	243.11	4.475	0.265
F1-6	0.05	300768	172.07	4.475	0.133
F4-1	0.05	186215	267.74	3.959	0.284
F4-2	0.05	111413	324.39	3.959	0.417
F4-3	0.05	2000000	168.75	3.959	0.113
F4-3*	0.05	1222986	191.25	3.959	0.145
F4-5	0.05	39973	395.25	3.959	0.618
F4-4	0.05	289979	338.59	3.959	0.454
F3-2	0.5	266386	237.89	3.959	0.224
F2-2	0.5	49658	328.73	3.959	0.428

*=specimen retested after run-out

Table 8.14: SED of cruciform full-penetration k-butt joints (R=0.05+0.5)

Following Figures 8.14 and 8.15 plot the design curve in terms of the Strain Energy Density ΔW against the number of cycles to failure for ADI-to-steel welded joints. As in the previous section, only the joints tested at nominal load ratio R=0.05 are considered in the first plot,while joints tested at both nominal load ratio R=0.05 and R=0.5 are taken into account in the second plot. In the same figure, the SED design curve at PS97.7% for homogeneous steel joints is plotted. As it can be seen, almost all the dissimilar joints present higher fatigue strength than the one suggested in the literature, specially at very high-cycles fatigue life and nominal load ratio R=0.05. ΔW at 2million cycles and at survival probability PS97.7% is equal to $0.08 Nmm/mm^3$, that is 27% higher than the corresponding value for the steel welded joints. The slope goes from 3.4 in the first plot up to 4.65 considering all the joints, while the scatter index T_σ remains equal to ≈ 2.5 in both cases. As expected, the scatter

of the experimenta data is lower than the one in terms of the Nominal Stress Approach.
The results in terms of Strain Energy Density outline a slightly lower fatigue resistance for the joints tested at nominal load ratio R=0.5 with respect to the one at R=0.05. Furthermore, dissimilar joints present a lower curve at PS97% than the one for corresponding homogeneous steel joints in terms of SED. Following this, it can be concluded that generally the SED design curve for homogeneous steel joints can be employed for the fatigue assessment of dissimilar ADI-to-steel welded joints only with respect to very long-standing fatigue life and nominal load ratio ≈ 0.

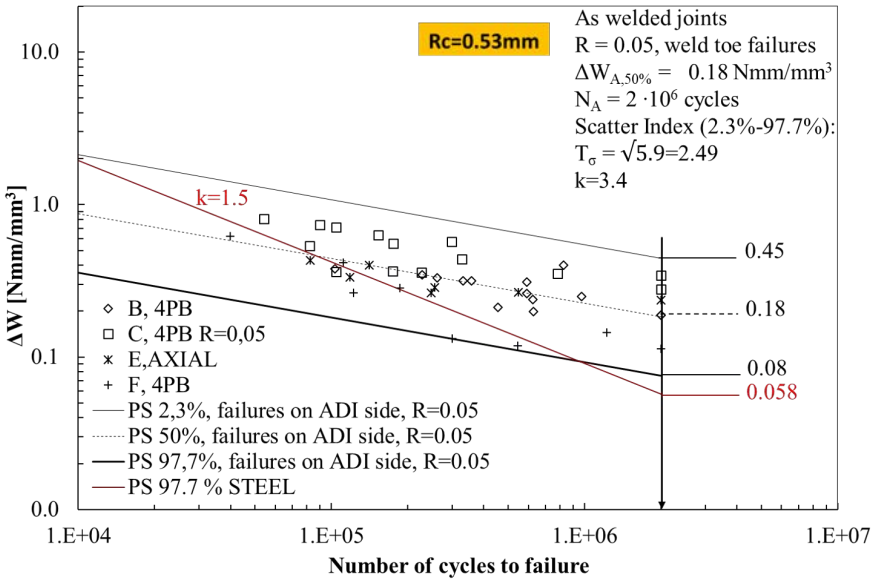

Figure 8.14: Design curve in terms of SED for dissimilar ADI-to-Steel joints

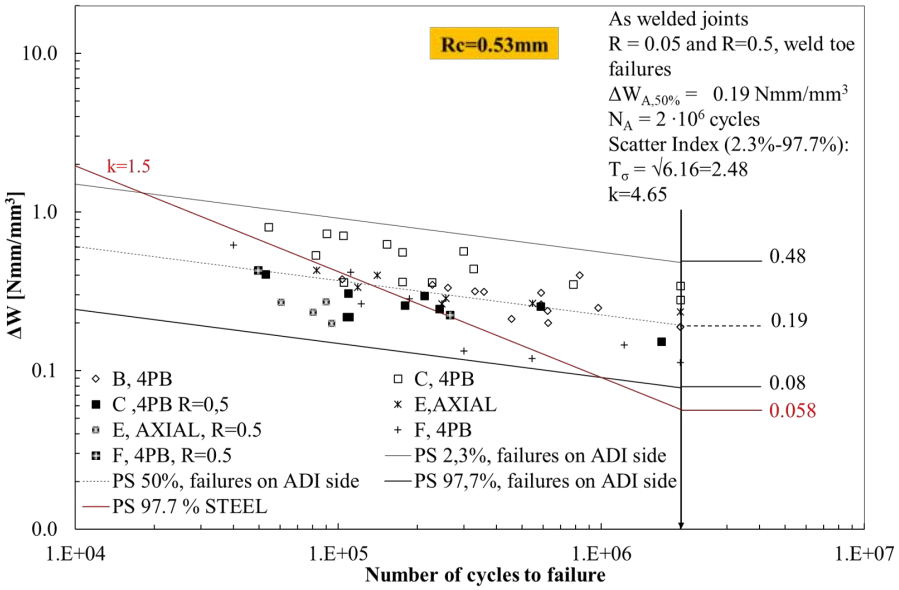

Figure 8.15: Design curve in terms of SED for dissimilar ADI-to-Steel joints

8.3.4 Design curve in terms of Equivalent Peak Stress for dissimilar ADI-to-steel joints

The analyses were carried out as explained in Section 7.4.4. The applied load was 1MPa on all the joints and the energy density for unit load was scaled to the actual $\Delta\sigma_{eq,peak}$ later on, multiplying $\sigma_{eq,peak}$ for the nominal stress $\Delta\sigma_{nom}$ and considering a radius equal to 0.55mm. All the joints were modelled considering the real geometric parameters, as the unit measure is [MPa] and it is independent from the opening angle 2α. Tables 8.15- 8.20 report the obtained results for all the joints.

Specimen code	R	N	$\Delta\sigma_{nom}$ [MPa]	$\sigma_{eq,peak}$ [MPa]	$\Delta\sigma_{eq,peak}$ [MPa]
B6-1	0.05	590273	291.08	1.504	326.26
B6-2	0.05	331582	293.63	1.504	329.11
B6-3	0.05	826913	330.80	1.504	370.78
B2-6*	0.05	103560	321.40	1.504	360.25
B5-1s*	0.05	261184	301.37	1.504	337.79
B2-4	0.05	228112	307.85	1.504	345.06
B5-2	0.05	358504	293.42	1.504	328.88
B2-3	0.05	455291	240.34	1.504	269.39
B5-4	0.05	590166	267.56	1.504	299.89
B5-6	0.05	625883	254.98	1.504	285.80
B5-5	0.05	627827	233.33	1.504	261.53
B5-3	0.05	974888	261.11	1.504	292.66
B5-1	0.05	2000000	226.73	1.504	254.14
B2-6	0.05	2000000	227.20	1.504	254.66

*=specimen retested after run-out

Table 8.15: PSM of full-penetration butt-joints

Specimen code	R	N	$\Delta\sigma_{nom}$ [MPa]	$\sigma_{eq,peak}$ [MPa]	$\Delta\sigma_{eq,peak}$ [MPa]
C15-2	0.05	49352	225.56	1.112	257.59
C17-4	0.05	35956	276.38	1.112	315.62
C18-2	0.05	179361	290.55	1.112	331.81
C18-3	0.05	109229	316.69	1.112	361.66
C16-3	0.05	110198	266.48	1.112	304.31
C17-1	0.05	1691834	222.75	1.112	254.38
C17-1	0.05	609664	267.30	1.112	305.26
C13-3	0.05	107812	267.07	1.112	304.99
C16-2	0.05	242797	282.99	1.112	323.17
C9-1	0.05	52884	363.51	1.112	415.13
C12-2	0.05	587809	287.80	1.112	328.66
C9-2	0.05	212312	311.16	1.112	355.34

Table 8.16: PSM of cruciform nlc fillet-welds joints (R=0.5)

Specimen code	R	N	$\Delta\sigma_{nom}$ [MPa]	$\sigma_{eq,peak}$ [MPa]	$\Delta\sigma_{eq,peak}$ [MPa]
C11-1	0.5	782127	322.30	1.128	375.40
C12-1	0.5	153004	431.16	1.128	502.19
C7-1	0.5	175019	328.02	1.128	382.06
C8-3	0.5	175437	406.02	1.128	472.90
C7-3	0.5	226568	325.97	1.128	379.67
C5-2	0.5	299261	409.98	1.128	477.52
C5-1	0.5	327322	360.45	1.128	419.83
C9-3	0.5	104687	326.57	1.128	380.37
C10-2	0.5	104527	457.49	1.128	532.86
C8-2	0.5	54270	487.65	1.128	567.99
C11-2	0.5	90293	465.42	1.128	542.10
C8-1	0.5	82159	398.00	1.128	463.56
C8-1*	0.5	2000000	287.44	1.128	334.80
C5-2	0.5	2000000	318.27	1.128	370.70

*=specimen retested after run-out

Table 8.17: PSM of cruciform nlc fillet-welds joints (R=0.05)

Specimen code	R	N	$\Delta\sigma_{nom}$ [MPa]	$\sigma_{eq,peak}$ [MPa]	$\Delta\sigma_{eq,peak}$ [MPa]
D2-2	0.05	2000000	110.12	1.385	240.29
D2-1	0.05	2000000	149.98	1.385	327.26
D2-1*	0.05	271405	299.96	1.385	654.53
D2-3	0.05	2000000	174.95	1.385	381.76
D1-1	0.05	353034	234.57	1.385	511.85
D1-6	0.05	1990000	200.99	1.385	438.58
D1-6*	0.05	2000000	240.69	1.385	525.21
D1-6*	0.05	350104	285.36	1.385	622.68
D2-6	0.05	174533	306.93	1.385	669.75
D2-4	0.05	73446	325.98	1.385	711.31
D1-2	0.05	42005	336.61	1.385	734.51
D1-5	0.05	60781	343.21	1.385	748.91
D3-1	0.5	512356	236.32	1.385	515.67
D3-2	0.5	209569	226.83	1.385	494.96

*=specimen retested after run-out

Table 8.18: PSM of T nlc fillet-welds joints (R=0.05+0.5)

Specimen code	R	N	$\Delta\sigma_{nom}$ [MPa]	$\sigma_{eq,peak}$ [MPa]	$\Delta\sigma_{eq,peak}$ [MPa]
E3-1	0.05	118526	208.33	1.532	327.59
E2-1	0.05	2000000	174.56	1.532	274.49
E2-1*	0.05	256157	192.02	1.532	301.94
E4-3	0.05	548082	185.46	1.532	291.63
E4-1	0.05	140969	227.84	1.532	358.27
E4-2	0.05	248030	185.06	1.532	291.00
E3-3	0.05	82736	235.98	1.532	371.06
E2-4	0.5	60672	186.57	1.532	293.37
E2-2	0.5	89887	187.50	1.532	294.83
E2-6	0.5	80167	173.70	1.532	273.13
E3-4	0.5	94490	160.09	1.532	251.73

*=specimen retested after run-out

Table 8.19: PSM of cruciform load-carrying fillet-welds joints (R=0.05+0.5)

Specimen code	R	N	$\Delta\sigma_{nom}$ [MPa]	$\sigma_{eq,peak}$ [MPa]	$\Delta\sigma_{eq,peak}$ [MPa]
F1-4	0.05	544633	162.96	1.21	205.46
F1-5	0.05	122085	243.11	1.21	306.51
F1-6	0.05	300768	172.07	1.21	216.95
F4-1	0.05	186215	267.74	1.21	337.56
F4-2	0.05	111413	324.39	1.21	408.99
F4-3	0.05	2000000	168.75	1.21	212.76
F4-3*	0.05	1222986	191.25	1.21	241.13
F4-5	0.05	39973	395.25	1.21	498.32
F4-4	0.05	289979	338.59	1.21	426.90
F3-2	0.5	266386	237.89	1.21	299.93
F2-2	0.5	49658	328.73	1.21	414.46

*=specimen retested after run-out

Table 8.20: PSM of cruciform full-penetration k-butt joints (R=0.05+0.5)

Figures 8.16 and 8.17 plot the design curve in terms of the Equivalent Peak Stress $\sigma_{eq,peak}$ against the number of cycles to failure for ADI-to-steel welded joints, tested at nominal load ratio R=0.05 and for all the joints together respectively. As the equivalent peak stress is derived straight forward from the definition of Strain Energy Density for notched details, the conclusions that can be drawn from these design curves are basically the same as the SED approach's ones. As it can be seen, the dissimilar joints present higher fatigue resistance at very high-cycles fatigue life and nominal load ratio R=0.05 in comparison to the corresponding steel joints. The slope goes from 6.5 in the first plot up to 7.9 considering all the tested joints, while the scatter index T_σ remains equal to ≈ 2.7 in both cases. As expected, the scatter of the experimental data is lower than the one in terms of the Nominal Stress.
The results in terms of PSM approach outline a slightly lower fatigue resistance

for the joints tested at nominal load ratio R=0.5 with respect to the ones at R=0.05. Furthermore, dissimilar joints generally present lower fatigue strength at PS97% than the corresponding homogeneous steel joints. It can be concluded that generally the PSM design curve for homogeneous steel joints can be employed for the fatigue assessment of dissimilar ADI-to-steel welded joints only with respect to very long-standing fatigue life and nominal load ratio R $\approx$ 0.

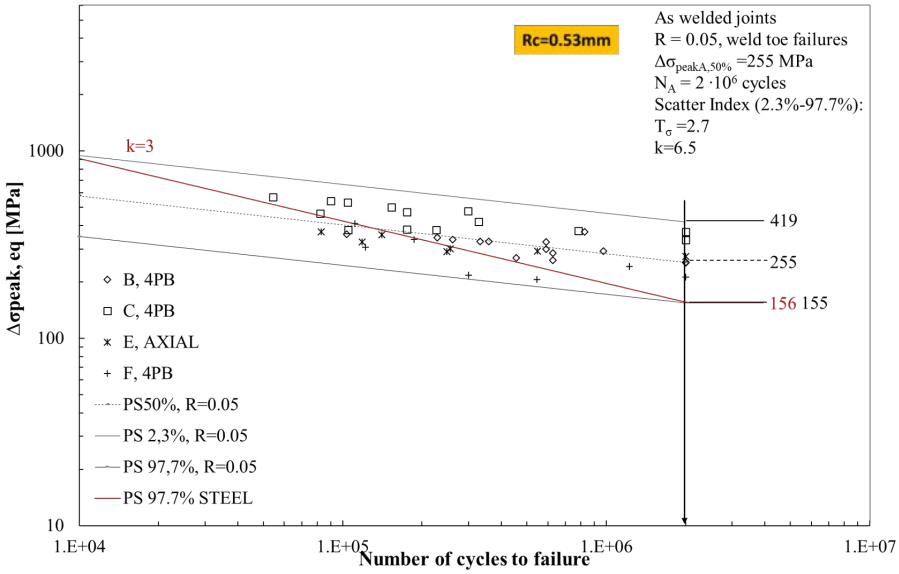

Figure 8.16: Design curve in terms of PSM for dissimilar ADI-to-Steel joints

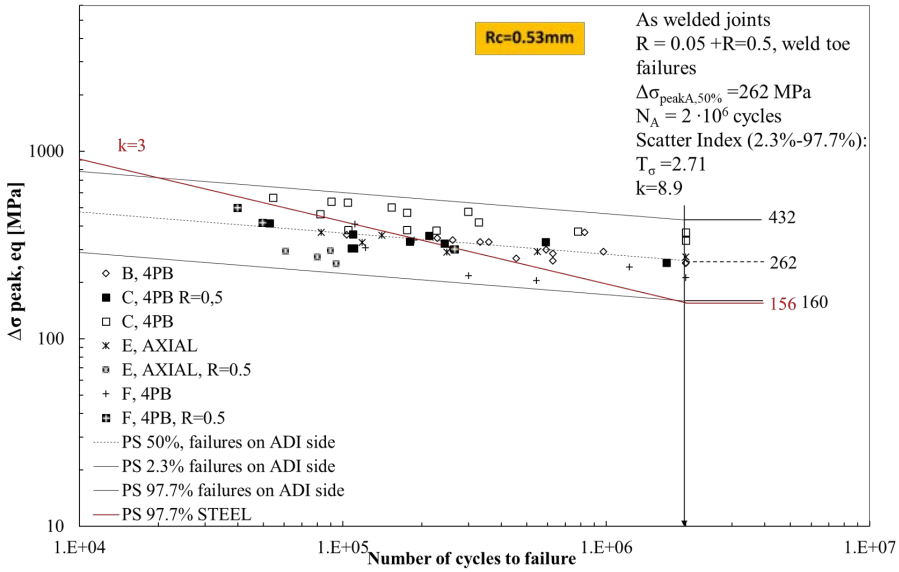

Figure 8.17: Design curve in terms of PSM for dissimilar ADI-to-Steel joints

Chapter 9

Conclusion

The present contribution delved into the mechanical properties and the fatigue behaviour of austempered ductile iron-to-steel dissimilar joints, starting from the material characterisation and experimental fatigue tests, going up to the application of latest local approaches based on fracture mechanics.
Regarding the specimens characterisation, micro-hardness profiles were obtained for one joint from each series. The ADI's hardness is generally around 300-400HV, while Steel presents 190HV hardness on average. The measurements also enlightened a peak of hardness ($\approx 700HV$) at the interface between the weld bead and the Heat Affected Zone on the ADI side. Metallographic analyses confirmed that the detected peak is due to presence of ledeburite, the brittle material caused by the metastable solidification of ADI after re-melting.
Before performing the fatigue tests, linear and angular misalignment were quantified for all the joints as the specimens are straightened by the perfectly-aligned clamps of the testing machine. As a consequence of this, secondary bending moments may superpose to the applied nominal stress and the experimental results could be biased. Thus, full-penetration butt-welded joints, cruciform non-load-carrying filled-welded joints and cruciform full-penetration K-butt-welded joints were tested under four-point-bending loading in order to avoid the effect of their pronounced misalignments. All other series, i.e. ADI plain specimens, partial-penetration butt-welded joints, full-penetration ground butt-welded joints, T non-load-carrying fillet-welded joints and cruciform load-carrying fillet-welded joints, were tested under axial loading. In particular, partial-penetration butt-welded joints and cruciform load-carrying fillet-welded joints had their extremes milled to minimize the linear misalignment.
In the first place, fatigue tests were performed at nominal load ratio R equal to 0.05 and design S-N curves in terms of nominal stress were derived for each structural detail. The categories at survival probability of 97.7% (confidence level 95%) were compared with the ones suggested in current International Standards and Recommendations for the corresponding homogeneous steel welded joints. It has been observed that the endurable stress ranges of austempered ductile iron-to-steel dissimilar arc-welded joints are higher than the FAT values suggested for the corresponding steel welded joints. Consequently, current standards can be applied on the safe side for the fatigue assessment of ADI-to-steel dissimilar joints at the medium-high cycles fatigue regime. On the contrary, dissimilar joints present lower fatigue performance with respect to homogeneous steel welded joints at low cycles fatigue regime, especially below $2 \cdot 10^5$ cy-

cles. Due to the lack of experimental data in this range of fatigue life, further investigations are needed to completely characterise the fatigue behaviour of austempered ductile iron-to-steel dissimilar arc-welded joints.
Fatigue test were also performed at nominal load ratio R equal to 0.5 to investigate the influence of the mean stress. The experimental results were generally in line with previous data at R=0.05, even though the performance was slightly lower for cruciform non-load-carrying filled-welded joints and cruciform load-carrying fillet-welded joints. Thus, the influence of the nominal load ratio cannot be totally excluded on the base of the results obtained in this work.
Having considered a variety of geometries, it was convenient to synthesise the experimental data on one design curve. As the S-N curve based on the Nominal Stress Approach led to very high scatter band, Finite Element Analyses were performed to study the local stress field in the neighbourhood of the weld toe, where cracks initiate, and to define more sensible parameters for the fatigue assessment of dissimilar ADI-to-steel joints. Then, local approaches, i.e. Notch Stress Intensity Factor approach, the Strain Energy Density Approach and the Peak Stress Method, were employed.
First, it was necessary to calibrate the control radius R_C for Austemprered Ductile Iron. To do so, the Strain Energy Density ΔW for full-penetration ground butt-welded joints was matched to the one of a selection of V-notched joints with toe opening angle 2α equal to $\approx 135°$, both of them calculated at $2 \cdot 10^6$ cycles. The calibration yielded to a control radius equal to 0.53mm.
At this point, design curves were defined in terms of NSIF K_1, SED ΔW and Equivalent Peak Stress $\Delta\sigma_{eq,peak}$. The scatter of the experimental data decreased with respect to the Nominal Stress approach, going from a scatter index of T_σ=3.7 to a value of T_σ=2.7. However, more accurate FE analysis shall be carried out considering the bi-material models as both steel and ADI are present in the joint, particularly at the cracks' nucleation site.
Nevertheless, the new curves confirmed that the fatigue limit of dissimilar welded joints is higher than the one suggested in the literature for corresponding homogenous steel welded joints, even thought their performance decreases for medium-low cycles fatigue regime.

9.1 Future works

The present work lightened some characteristics of the fatigue behaviour of Austempered Ductile Iron-to-Steel welded joints. However, some research needs have to be pointed out.
Metallographic analyses and micro-hardness profiles outlined some hallmarks of these dissimilar joint, but it is also necessary to quantify the amount of residual stress and its influence on the fatigue resistance.
Moreover, further experimental tests should be carried out at higher stress ranges and nominal load ratio $R > 0$ to completely understand the fatigue behaviour of dissimilar ADI-to-steel joints.
Regarding the application of local approaches, bi-material models shall be considered for improving the accuracy of the FE analyses.

Appendices

Appendix A

Riassunto esteso in lingua italiana

A.1 Introduzione

Negli ultimi anni, sempre più spesso si è cercato di combinare diversi materiali nella stessa struttura per aumentare le performance dei prodotti e tenere il passo con l'innovazione. Da un lato, la combinazione di diversi materiali permette di sfruttre al meglio le caratteristiche e le proprietà meccaniche degli stessi. D'altro canto però, unire insieme diverse classi di materiali può essere un sfida non facile da vincere a causa delle discrepanze in termini di proprietà chimiche, termiche o elettriche. Inoltre, la potenziale incompatibilità fra materiali può essere problematica non solo per il processo di unione stesso, ma anche per l'integrità strutturale del prodotto durante la sua vita utile. Infatti, giunzioni ibride possono presentare microstrutture più vulnerabili che, sommate alle differenze in termini di proprietà plastiche ed elastiche, possono favorire l'innesco e la propagazione di cricche all'interno del componente.
Recentemente ci sono state molte pubblicazione riguardanti i vantaggi e le problematiche derivanti dall'utilizzo di strutture ibride. Nel contesto delle saldature, in particolare della saldatura ad arco, giunzione ibride formate da acciao e ghisa sferoidale austemperata (ADI) offrono la possibilità di migliorare la risposta meccanica di componenti strutturali. Infatti, la ghisa austemperata vanta di ottime proptietà meccaniche come elevata resistenza all'usura e buona resistanza statica, a fatica e all'impatto. Inoltre, la ghisa presenta un peso specifico minore di quello dell'acciaio e permette di alleggerire notevolmete le strutture, grazie anche alla possibità di essere colata in forme complesse e spessori ridotti. L'acciao quindi può essere utilizzato solo dove strettamente necessario, con una conseguente riduzione dei costi di produzione e una maggiore flessibilità di progettazione.
Dato che le giunzioni saldate devono essere in grado di sostenere importanti carici ciclici in condizioni di servizio, lo scopo di questa tesi è quello di analizzare il comportamento a fatica di giunzioni saldate ibride in acciaio e ghisa sferoidale austemperata. In particolare, sono state confrontate le categorie proposte dagli Standands Internazionali per le giunzioni omogenee saldate in acciaio con quelle ottenute sperimentalmente per le giunzioni ibride acciao-ghisa sferoidale austemperata. Inizialmente, i giunti sono stati caratterizzati grazie ad analisi

metallografiche, misure di microdurezza e tensioni residue. Per ogni provino è stata misurata l'entità dei disallineamenti, sia angolari che lineari. In seguito, test a fatica sono stati svolti per caratterizzare la durabilità strutturale di tali giunti. Quindi, dai dati sperimentali, sono state ricavate le curve S-N di progettazione e le classi di resistenza per ogni geometria. Per definire queste curve è stato fatto riferimento all'approccio in tensione nominale, suggerito dalle normative e maggiormente diffuso nell'ambito della progettagione meccanica. Il limite maggiore di questo approccio è la non considerazione dell'intensificarsi del campo tensionale in prossimità del cordone di saldatura. Dato che la resistenza a fatica è un femomeno locale, condizionato dalla geometria e dalle dimensioni del componente, è estrememnte conveniente applicare dei metodi che tengano in considerazione la concentrazione delle tensioni. In tal modo, i dati sperimentali possono essere rappresentati in un'unica curva, riducendo la dispersione dei dati e aumentando l'accuratezza della previsione sulla vita a fatica. Per questo motivo, sono state messe a punte delle ulteriori curve di progettazione tramite l'applicazione di approcci locali basati sull'estensione non-convenzionale della mecchanica della frattura.

A.2 Sommario

I capitoli di questa tesi sono organizzati come segue.

- il Capitolo 2 riassume lo Stato dell'arte sulla saldatura ad arco e sulle proprietà meccaniche della ghisa sferoidale austeperata.
- il Capitolo 3 fornisce una breve revisione dei lavori correlati più recenti.
- il Capitolo 4 descrive la procedura utilizzata per le misure dei disallineamenti e riporta i risultati per ogni giunto.
- il Capitolo 5 riporta i risultati relativi alla caratterizzazione dei provini. In particolare, al suo interno sono riportati i profili di microdurezza e le analisi metallografiche.
- nel Capitolo 6 sono riportati i risultati sperimentali dei test a fatica e vengono definite le curve di progettazione basate sul range di tensione nominale.
- il Capitolo 7 introduce la teoria alla base degli approcci locali basati sulla meccanica della frattura e fornisce una guida per eseguire le analisi agli Elementi Finiti sul Software Ansys APDL.
- nel Capitolo 8 vengono messi a punto gli approcci locali per giunzioni saldate ibride e vengono proposte delle nuove curve di progettazione che sintetizzano i risultati sperimentali.

A.3 Risultati e conclusioni

In questa sezione vengono riassunti in breve i risultati della campagna sperimentale condotta sui giunti dissimili acciaio-ghisa sferoidale austemperata. Dal punto di vista della caratterizzazione dei giunti, i profili di microdurezza sono

stati ottenuti per ogni geometria. In particolare il materiale base ADI presenta generalmente una durezza variabile fra 300HV e 400HV, mentre la durezza dell'acciaio si aggira intorno ai 180-190HV. Tramite queste misure, è stato anche identificato un picco di elevata durezza ($\approx 700HV$) in corrispondenza dell'interfaccia tra la Zona Fusa e la Zona Termicamente Alterata dell'ADI. Analisi metallografiche hanno evidenziato che tale picco di durezza è dovuto alla presenza di ledeburite, materiale duro e fragile che si forma durante la ri-solidificazione dell'ADI a seguito della fusione indotta dal processo di saldatura.
Questa zona ledeburitica, presente lungo tutto il profilo del cordone di saldatura sul lato della ghisa, è stato anche identificato come punto preferenziale di innesco delle cricche, mentre la loro propagazione è prevalentemente guidata dallo stato tensionale prensente all'apice del piede cordone e/o della radice. Solo nel caso dei giunti testa a testa a piena penetrazione rasati, la cricca innesca e propaga nello strato ledeburitico.
Prima di eseguire i test a fatica, i disallineamenti angolari e lineari sono stati misurati per tutti i provini. Dato che le morse della macchina di prova sono perfettamente allineate,i giunti tendono ad essere raddrizzati durante l'afferraggio e disallineamenti pronunciati possono produrre tensioni parassite di bending. Queste tensioni, sommate alla tensione nominale applicata, possono falsare i risultati dei test sperimentali. Per questo motivo, le serie che presentavano disallimenti elevati sono state testate a carico di flessione a 4 punti. In particolare, sono stati testati a flessione i giunti:

- Testa a testa piena penetrazione;
- Croce doppio irrigidimento a cordone non portante;
- Croce piena penetrazione;

mentre i giunti testati a trazione sono:

- Testa a testa piena penetrazione rasati;
- Testa a testa parziale penetrazione;
- Croce a cordone portante;
- T con cordoni non portant;
- Provini lisci in ADI.

Inoltre, i giunti testa a testa parziale penetrazione e i croce a cordone portante sono stati fresati alle estremità per ottenere quattro facce perfetttamente allineate e parallele: in questo modo, l'effetto del disallineamento lineare viene minimizzato. I test a fatica sono stati condotti inizialmente a rapporto di ciclo R=0.05 e, per ogni geometria, sono state ottenute le curve di progettazione in termini di tensione nominale. Le categorie a probabilità di soppravvivenza 97.7% (livello di confidenza 95%) sono state quindi confrontante con le categorie in Normativa per i corrispondenti giunti omogenei in acciaio. E' stato osservato che il limite di fatica dei giunti dissimili acciaio-ghisa speforidale austemperata è generalmente più alto di quelli suggeriti. Di conseguenza, la progettazione a fatica di giunzioni saldate ibride può essere condotta in vantaggio di sicurezza utilizzando le curve fornite dagli attuali Standards. In particolare, questa assunzione è corretta per durabilità elevate (alto numero di cicli previsto per la

rottura), ma non è altrettanto vero quando si considerano range di tensioni più elevati e vite a fatica inferiori, in particolare sotto i $2 \cdot 10^5$ cicli: infatti le curve per le giunzioni ibride scendono al di sotto di quelle degli acciai e presantono quindi performance inferiori.
Per completare il quadro delle prove a fatica, alcuni test sono stati condotti a rapporto di ciclo R=0.5. In generale, i nuovi dati si allineano con i risutati ottenuti per R=0.05, anche se per alcune tipogie di giunto la resistenza appare leggermente inferiore, come nel caso dei croce doppio irrigidimento con cordone non portante e i croce a cordone portante. Per questo motivo, sulla base dei risultati ottenuti in questa tesi, non si può escludere totalmente l'influenza della tensione media intorno alla quale oscilla il carico applicato.
In termini di tensione nominale, i dati sperimentali non riescono ad essere sintetizzati su un'unica curva di progettazione e risulta quindi necessario definire diverse classi di resistenza per ogni dettaglio strutturale. Ciò avviene perché la fatica è un fenomeno locale, influenzato dalle dimensioni e dalla geometria del giunto stesso. Per sintetizzare le diverse serie, si deve ricorrere ai cosidetti Aprrocci Locali. Questi metodi vanno a considerare il campo tensionale all'apice dell'intaglio, dove le tensioni si intensificato e dove avviene la nucleazione della cricca. In particolare, sono stati applicati: l'approccio basato sui Fattori di intensificazione delle tensini (N-SIF), l'approccio basato sulla Densità di Energia di Deformazione (SED) e il Peak Stress Metod (PSM).
Le nuove curve di progettazione presentano una riduzione dell'indice di dispersione (T_σ=2.7 contro T_σ=3.7 in approccio nominale) e riassumono tutti i dati dentro un'unica curva, includendo al loro interno l'effetto scala e l'effetto della geometria.
Per poter applicare gli approcci SED e PSM, si è resa necessaria la calibrazione del volume di controllo all'apice dell'intaglio. La calibrazione è stata eseguita uguagliando il limite di fatica dei giunti rasati a quello dei giunti intagliati, calcolato in termini di densità di energia di deformazione ad un numero di cicli di riferimento (in questo caso il limite di fatica è stato posto a 2milioni di cicli). Il raggio del volume di controllo è risultato pari a 0.53mm. Le curve corfermano il trend già osservato in precedenza: il giunti ibridi acciao-ADI hanno resistenza maggiore a bassi carichi e per vite a fatica a medio-alto numero di cicli, mentre tendono ad aver performance inferiori rispetto ai giunti omogenei acciaio-acciaio man mano che i carichi diventano più elevati.

A.4 Sviluppi futuri

Questo lavoro ha messo in luce alcune delle caratteristiche del comportamento a fatica delle giunzioni saldate ibride acciaio-ghisa sferoidale austemperata.
Analisi metallografiche e profili di durezza hanno permesso una prima caratterizzazione dei giunti, ma ulteriori studi metallurgici sono necessari: in particolare, misurare l'entità delle tensioni residue e definire la loro influenza sulla vita a fatica potrebbe essere un buon punto di partenza per ulteriori indagini su queste giunzioni saldate.
Inoltre, ulteriori test sperimentali ad alto carico e a rapporto di ciclo $R > 0$ sarebbero utili per completare la caratterizzazione del comportamento a fatica di questi giunti.

Per quanto riguarda l'applicazione degli approcci locali, modelli bi-materiale andrebbero messi a punto al fine di aumentare l'accuratezza delle analisi agli Elementi Finiti.

Appendix B

Experimental data sheets

B.1 Joints from series A

Specimen code A3-4			
Loading condition:	Fatigue test, axial	**Material**:	ADI-S355
Date	July 2019	**Lab. operator**:	Pullin Elena

Data of fatigue tests			
$A\,[mm^2] =$	240.0	Frequency $[Hz]$	20.0
$\Delta F\,[kN] =$	65.0	$\Delta\sigma_{nom}\,[MPa]$	270.83
$F_{min}\,[kN] =$	68.4		
$F_{max}\,[kN] =$	3.4	Nominal Load Ratio R	0.05
Number of cycles to failure=	67315.0		

Notes:	Crack initiation at the weld root , then propagated through the weld bead

B.2 Joints from series B

Specimen code B6-1			
Loading condition:	Fatigue test, four-point bending	**Material**:	ADI-S355
Date	July 2019	**Lab. operator**:	Pullin Elena

Data of fatigue tests			
$W_f\,[mm^3] =$	681.8	Frequency $[Hz]$	8.0
$\Delta F\,[kN] =$	27.0	$\Delta\sigma_{nom}\,[MPa]$	291.08
$F_{min}\,[kN] =$	1.4		
$F_{max}\,[kN] =$	28.4	Nominal Load Ratio R	0.05
Number of cycles to failure=	590273.0		

Notes: Crack initiation at the weld toe on the ADI side, then propagated through the thickness of the joint

Specimen code B6-2			
Loading condition:	Fatigue test, four-point bending	**Material**:	ADI-S355
Date	July 2019	**Lab. operator**:	Pullin Elena

Data of fatigue tests			
$W_f\,[mm^3] =$	666.7	Frequency $[Hz]$	15.0
$\Delta F\,[kN] =$	29.0	$\Delta\sigma_{nom}\,[MPa]$	293.63
$F_{min}\,[kN] =$	1.5		
$F_{max}\,[kN] =$	30.5	Nominal Load Ratio R	0.05
Number of cycles to failure=	331582.0		

Notes: Crack initiation at the weld toe on the ADI side, then propagated through the thickness of the joint

Specimen code B6-3			
Loading condition:	Fatigue test, four-point bending	**Material**:	ADI-S355
Date	July 2019	**Lab. operator**:	Pullin Elena

Data of fatigue tests			
$W_f\,[mm^3] =$	687.7	Frequency $[Hz]$	15.0
$\Delta F\,[kN] =$	26.0	$\Delta\sigma_{nom}\,[MPa]$	330.8
$F_{min}\,[kN] =$	1.4		
$F_{max}\,[kN] =$	27.4	Nominal Load Ratio R	0.05
Number of cycles to failure=	826913.0		

Notes: Crack initiation at the weld toe on the steel side, then propagated through the thickness of the joint

Specimen code B8-5			
Loading condition:	Fatigue test, axial	**Material**:	ADI-S355
Date	July 2019	**Lab. operator**:	Pullin Elena

Data of fatigue tests			
$A\,[mm^2] =$	324.0	Frequency $[Hz]$	30.0
$\Delta F\,[kN] =$	97.0	$\Delta\sigma_{nom}\,[MPa]$	299.38
$F_{min}\,[kN] =$	5.1		
$F_{max}\,[kN] =$	102.1	Nominal Load Ratio R	0.05
Number of cycles to failure=	1764636.0		

Notes:	Crack initiation at the weld toe on the ADI side, then propagated at the interface between ADI and weld bead

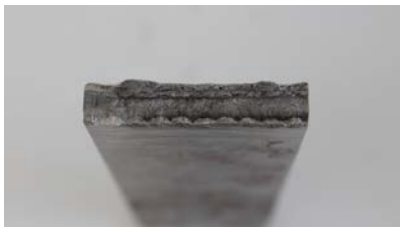

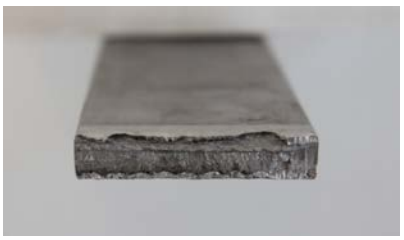

Specimen code B8-4			
Loading condition:	Fatigue test, axial	**Material**:	ADI-S355
Date	July 2019	**Lab. operator**:	Pullin Elena

Data of fatigue tests			
$A\,[mm^2] =$	336.2	Frequency $[Hz]$	25.0
$\Delta F\,[kN] =$	100.0	$\Delta\sigma_{nom}\,[MPa]$	297.49
$F_{min}\,[kN] =$	5.3		
$F_{max}\,[kN] =$	105.3	Nominal Load Ratio R	0.05
Number of cycles to failure=	286396.0		

Notes: Failure far away from the weld bead

Specimen code B8-3			
Loading condition:	Fatigue test, axial	**Material**:	ADI-S355
Date	July 2019	**Lab. operator**:	Pullin Elena

Data of fatigue tests			
$A\,[mm^2] =$	333.7	Frequency $[Hz]$	20.0
$\Delta F\,[kN] =$	105.0	$\Delta\sigma_{nom}\,[MPa]$	314.62
$F_{min}\,[kN] =$	5.5		
$F_{max}\,[kN] =$	110.5	Nominal Load Ratio R	0.05
Number of cycles to failure=	183159.0		

Notes: Failure far away from the weld bead, defect on surface

Specimen code B8-1			
Loading condition:	Fatigue test, four-point bending	**Material**:	ADI-S355
Date	July 2019	**Lab. operator**:	Pullin Elena

Data of fatigue tests			
$W_f\,[mm^3] =$	461.6	Frequency $[Hz]$	15.0
$\Delta F\,[kN] =$	21.0	$\Delta\sigma_{nom}\,[MPa]$	341.23
$F_{min}\,[kN] =$	1.1		
$F_{max}\,[kN] =$	22.1	Nominal Load Ratio R	0.05
Number of cycles to failure=	1024018.0		

Notes: Crack initiation at the weld toe on the ADI side, then propagated through the thickness of the joint

Specimen code B7-3			
Loading condition:	Fatigue test, four-point bending	**Material**:	ADI-S355
Date	July 2019	**Lab. operator**:	Pullin Elena

Data of fatigue tests			
$W_f\,[mm^3] =$	505.9	Frequency $[Hz]$	10.0
$\Delta F\,[kN] =$	24.0	$\Delta\sigma_{nom}\,[MPa]$	355.83
$F_{min}\,[kN] =$	1.3		
$F_{max}\,[kN] =$	25.3	Nominal Load Ratio R	0.05
Number of cycles to failure=	1281889.0		

Notes: Run-out under 22kN axial loading. Retest: crack initiation at the weld toe on the ADI side, then propagated at the interface between ADI and weld bead

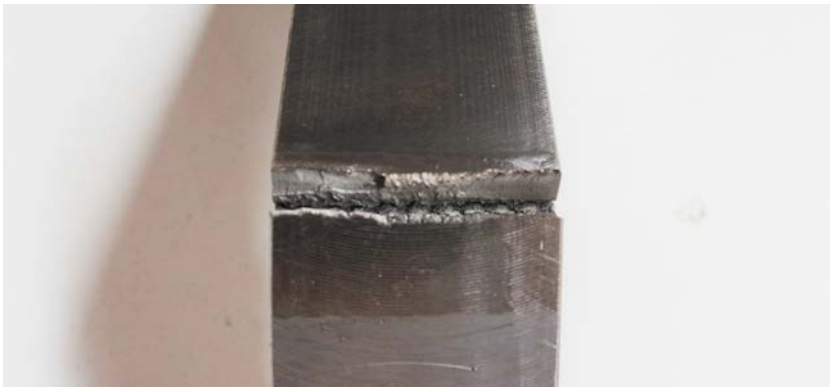

B.3 Joints from series C

Specimen code C15-2			
Loading condition:	Fatigue test, four-point bending	**Material**:	ADI-S355
Date	July 2019	**Lab. operator**:	Pullin Elena

Data of fatigue tests			
$W_f\,[mm^3] =$	665.0	Frequency $[Hz]$	20.0
$\Delta F\,[kN] =$	20.0	$\Delta\sigma_{nom}\,[MPa]$	225.56
$F_{min}\,[kN] =$	20.0		
$F_{max}\,[kN] =$	40.0	Nominal Load Ratio R	0.5
Number of cycles to failure=	49352.0		

Notes: Crack initiation at the weld toe on the ADI side, then propagated through the thickness of the joint. Defect of surface near the weld toe

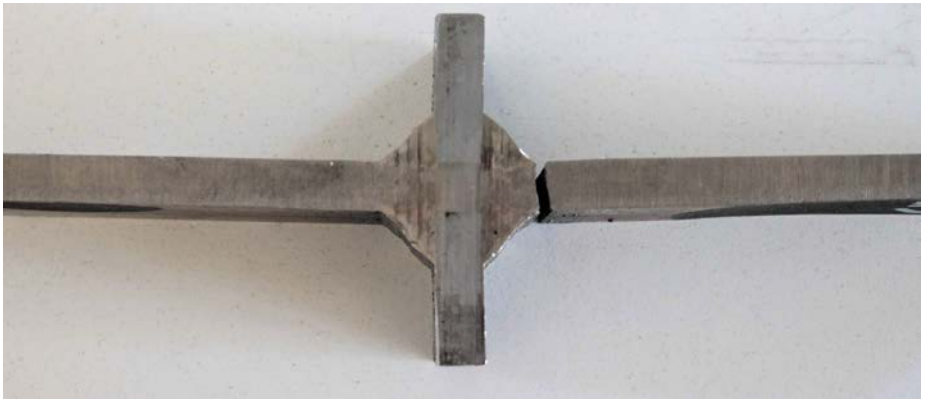

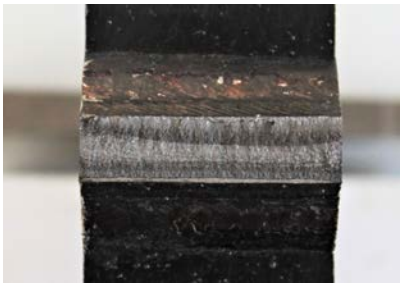

Specimen code C17-4			
Loading condition:	Fatigue test, four-point bending	**Material**:	ADI-S355
Date	July 2019	**Lab. operator**:	Pullin Elena

Data of fatigue tests			
$W_f\,[mm^3] =$	666.7	Frequency $[Hz]$	20.0
$\Delta F\,[kN] =$	22.0	$\Delta\sigma_{nom}\,[MPa]$	276.38
$F_{min}\,[kN] =$	22.0		
$F_{max}\,[kN] =$	44.0	Nominal Load Ratio R	0.5
Number of cycles to failure=	35956.0		

Notes: Crack initiation at the weld toe on the ADI side, then propagated through the thickness of the joint. Defect of surface near the weld toe

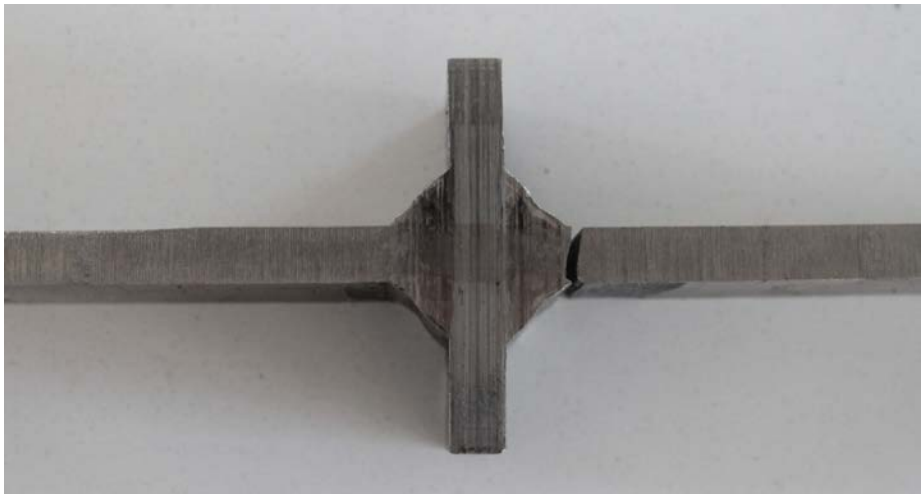

Specimen code C18-2			
Loading condition:	Fatigue test, four-point bending	**Material**:	ADI-S355
Date	July 2019	**Lab. operator**:	Pullin Elena

Data of fatigue tests			
$W_f\,[mm^3] =$	666.7	Frequency $[Hz]$	25.0
$\Delta F\,[kN] =$	26.0	$\Delta\sigma_{nom}\,[MPa]$	290.55
$F_{min}\,[kN] =$	26.0		
$F_{max}\,[kN] =$	52.0	Nominal Load Ratio R	0.5
Number of cycles to failure=	179361.0		

Notes: Crack initiation at the weld toe on the ADI side, then propagated through the thickness of the joint

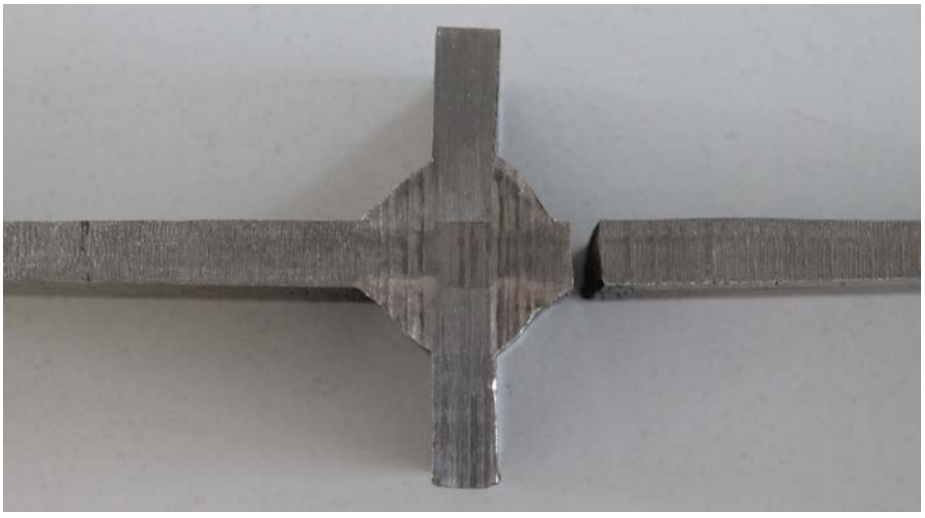

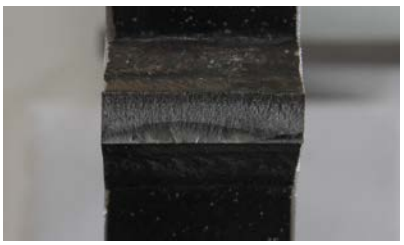

Specimen code C18-3			
Loading condition:	Fatigue test, four-point bending	**Material**:	ADI-S355
Date	July 2019	**Lab. operator**:	Pullin Elena

Data of fatigue tests			
$W_f\,[mm^3] =$	665.0	Frequency $[Hz]$	20.0
$\Delta F\,[kN] =$	26.0	$\Delta\sigma_{nom}\,[MPa]$	316.69
$F_{min}\,[kN] =$	26.0		
$F_{max}\,[kN] =$	52.0	Nominal Load Ratio R	0.5
Number of cycles to failure=	109229.0		

Notes: Crack initiation at the weld toe on the ADI side, then propagated through the thickness of the joint

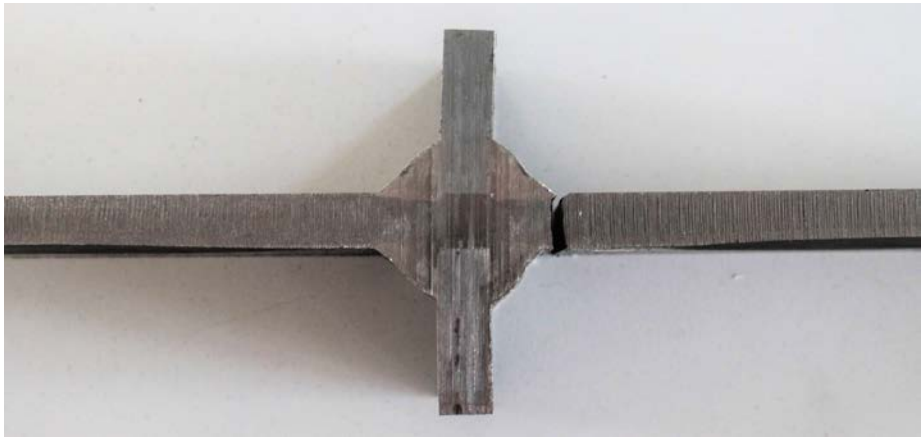

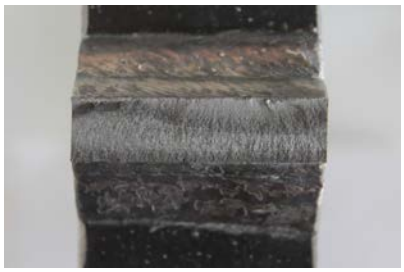

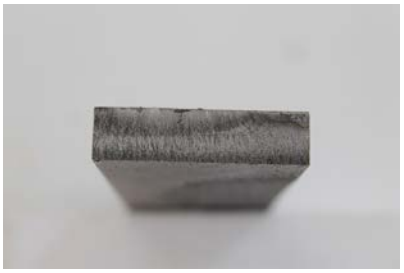

Specimen code C16-3			
Loading condition:	Fatigue test, four-point bending	**Material**:	ADI-S355
Date	July 2019	**Lab. operator**:	Pullin Elena

Data of fatigue tests			
$W_f\,[mm^3] =$	666.7	Frequency $[Hz]$	20.0
$\Delta F\,[kN] =$	22.0	$\Delta\sigma_{nom}\,[MPa]$	266.48
$F_{min}\,[kN] =$	22.0		
$F_{max}\,[kN] =$	44.0	Nominal Load Ratio R	0.5
Number of cycles to failure=	110198.0		

Notes: Crack initiation at the weld toe on the ADI side, then propagated through the thickness of the joint

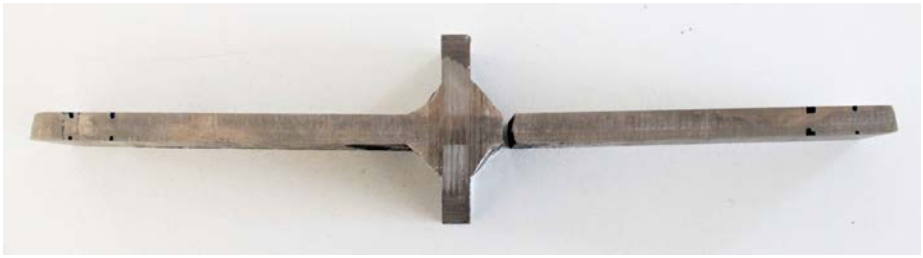

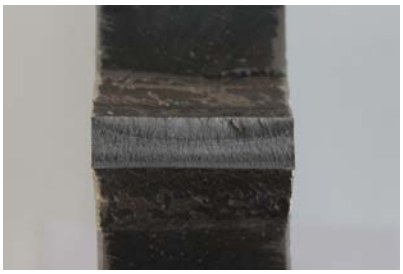

Specimen code C17-1			
Loading condition:	Fatigue test, four-point bending	**Material**:	ADI-S355
Date	July 2019	**Lab. operator**:	Pullin Elena

Data of fatigue tests			
$W_f\,[mm^3] =$	666.7	Frequency $[Hz]$	20.0
$\Delta F\,[kN] =$	24.0	$\Delta\sigma_{nom}\,[MPa]$	267.3
$F_{min}\,[kN] =$	24.0		
$F_{max}\,[kN] =$	48.0	Nominal Load Ratio R	0.5
Number of cycles to failure=	609664.0		

Notes: Run-out under 20KN bending load, retest and failure far from the weld

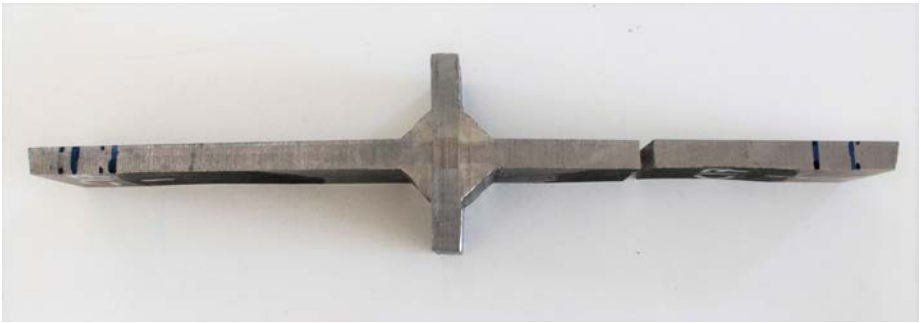

Specimen code C13-3			
Loading condition:	Fatigue test, four-point bending	**Material**:	ADI-S355
Date	July 2019	**Lab. operator**:	Pullin Elena

Data of fatigue tests			
$W_f\,[mm^3] =$	665.0	Frequency $[Hz]$	20.0
$\Delta F\,[kN] =$	24.0	$\Delta\sigma_{nom}\,[MPa]$	267.07
$F_{min}\,[kN] =$	24.0		
$F_{max}\,[kN] =$	48.0	Nominal Load Ratio R	0.5
Number of cycles to failure=	107812.0		

Notes: Crack initiation at the weld toe on the ADI side, then propagated through the thickness of the joint

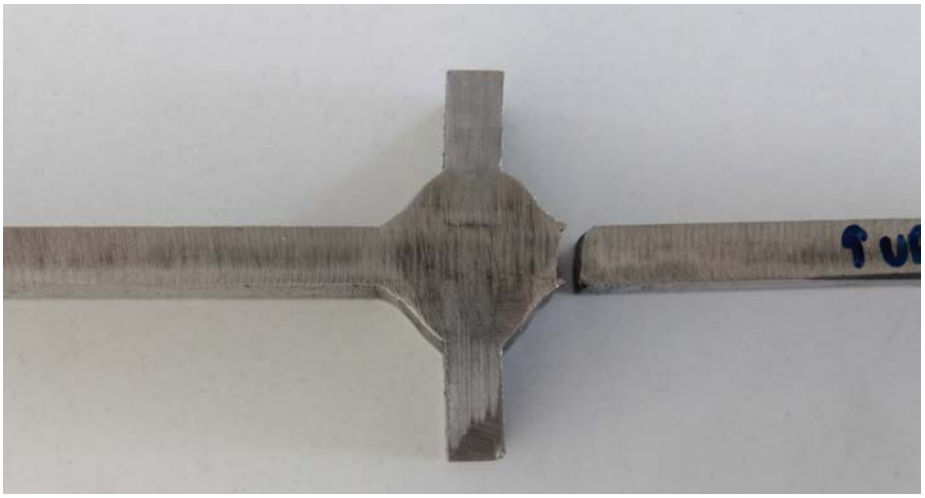

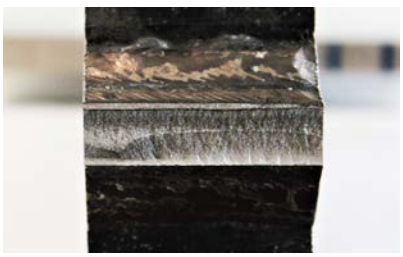

Specimen code C16-2			
Loading condition:	Fatigue test, four-point bending	**Material**:	ADI-S355
Date	July 2019	**Lab. operator**:	Pullin Elena

Data of fatigue tests			
$W_f\,[mm^3] =$	658.3	Frequency $[Hz]$	20.0
$\Delta F\,[kN] =$	27.0	$\Delta\sigma_{nom}\,[MPa]$	282.99
$F_{min}\,[kN] =$	27.0		
$F_{max}\,[kN] =$	54.0	Nominal Load Ratio R	0.5
Number of cycles to failure=	242797.0		

Notes: Crack initiation at the weld toe on the ADI side, then propagated through the thickness of the joint

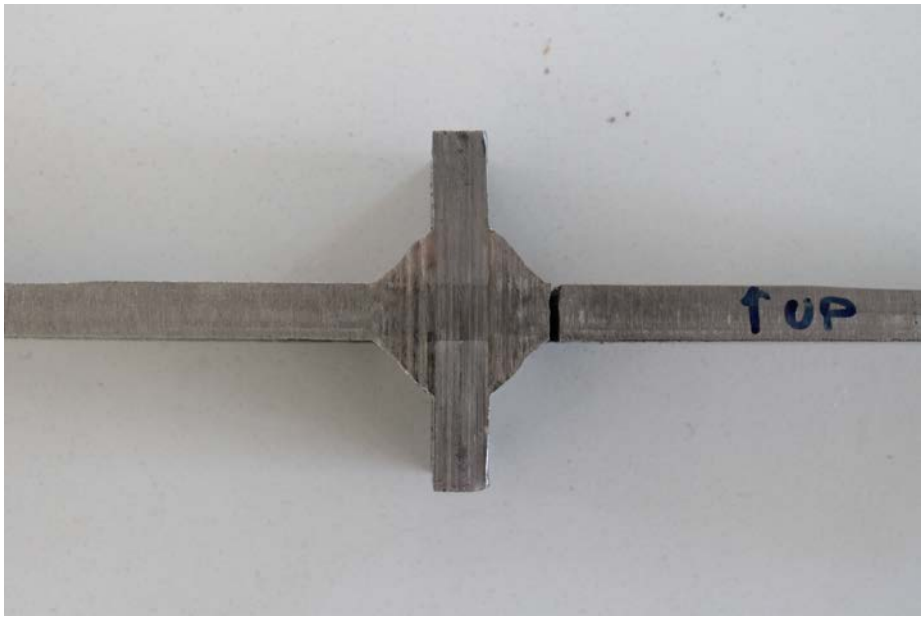

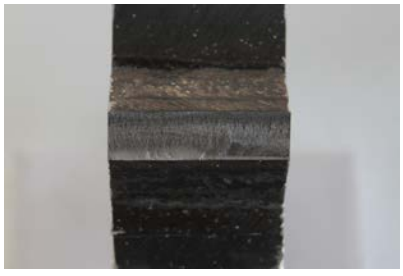

Specimen code C13-2			
Loading condition:	Fatigue test, four-point bending	**Material**:	ADI-S355
Date	July 2019	**Lab. operator**:	Pullin Elena

Data of fatigue tests			
$W_f\,[mm^3] =$	693.6	Frequency $[Hz]$	20.0
$\Delta F\,[kN] =$	30.0	$\Delta\sigma_{nom}\,[MPa]$	324.39
$F_{min}\,[kN] =$	1.6		
$F_{max}\,[kN] =$	31.6	Nominal Load Ratio R	0.05
Number of cycles to failure=	232241.0		

Notes: Failure far away from the weld bead

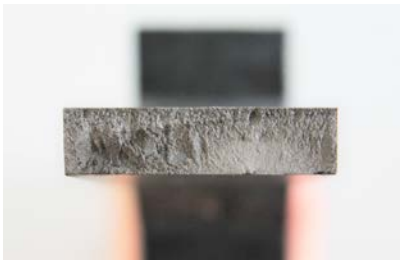

Specimen code C14-2			
Loading condition:	Fatigue test, four-point bending	**Material**:	ADI-S355
Date	July 2019	**Lab. operator**:	Pullin Elena

Data of fatigue tests			
$W_f\,[mm^3] =$	693.6	Frequency $[Hz]$	15.0
$\Delta F\,[kN] =$	30.0	$\Delta\sigma_{nom}\,[MPa]$	324.39
$F_{min}\,[kN] =$	1.6		
$F_{max}\,[kN] =$	31.6	Nominal Load Ratio R	0.05
Number of cycles to failure=	227000.0		

Notes: Failure far away from the weld bead, near the strut

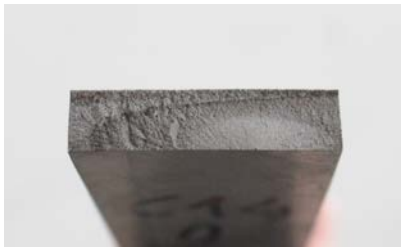

Specimen code C14-1			
Loading condition:	Fatigue test, four-point bending	**Material**:	ADI-S355
Date	July 2019	**Lab. operator**:	Pullin Elena

Data of fatigue tests			
$W_f\,[mm^3] =$	685.2	Frequency $[Hz]$	20.0
$\Delta F\,[kN] =$	30.0	$\Delta\sigma_{nom}\,[MPa]$	328.39
$F_{min}\,[kN] =$	1.6		
$F_{max}\,[kN] =$	31.6	Nominal Load Ratio R	0.05
Number of cycles to failure=	252144.0		

Notes: Failure far away from the weld bead, near the strut

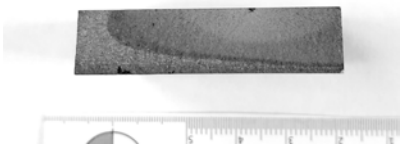

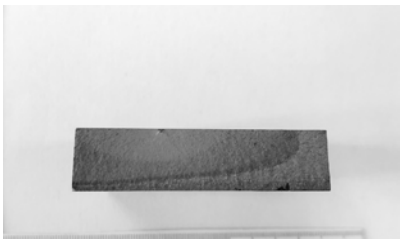

Specimen code C14-2			
Loading condition:	Fatigue test, four-point bending	**Material**:	ADI-S355
Date	July 2019	**Lab. operator**:	Pullin Elena

Data of fatigue tests			
$W_f\,[mm^3] =$	693.6	Frequency $[Hz]$	15.0
$\Delta F\,[kN] =$	30.0	$\Delta\sigma_{nom}\,[MPa]$	324.39
$F_{min}\,[kN] =$	1.6		
$F_{max}\,[kN] =$	31.6	Nominal Load Ratio R	0.05
Number of cycles to failure=	227000.0		

Notes: Failure far away from the weld bead, near the strut

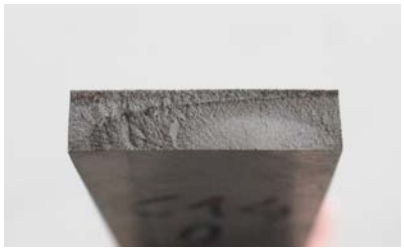

B.4 Joints from series D

Specimen code D1-1			
Loading condition:	Fatigue test, axial	**Material**:	ADI-S355
Date	July 2019	**Lab. operator**:	Pullin Elena

Data of fatigue tests			
$A\,[mm^2] =$	405.0	Frequency $[Hz]$	30.0
$\Delta F\,[kN] =$	95.0	$\Delta\sigma_{nom}\,[MPa]$	234.57
$F_{min}\,[kN] =$	5.0		
$F_{max}\,[kN] =$	100.0	Nominal Load Ratio R	0.05
Number of cycles to failure=	353034.0		

Notes: Crack initiation at the weld toe on the steel plate, then propagated through the thickness of the joint

Specimen code D1-6			
Loading condition:	Fatigue test, axial	**Material**:	ADI-S355
Date	July 2019	**Lab. operator**:	Pullin Elena

Data of fatigue tests			
$A\,[mm^2] =$	403.0	Frequency $[Hz]$	30.0
$\Delta F\,[kN] =$	115.0	$\Delta\sigma_{nom}\,[MPa]$	200.99
$F_{min}\,[kN] =$	6.0		
$F_{max}\,[kN] =$	121.0	Nominal Load Ratio R	0.05
Number of cycles to failure=	1990000.0		

Notes: Run-out under 81kN and 97kN axial loading. Retest at 115kN; crack initiation at the weld toe on the steel plate, then propagated through the thickness of the joint

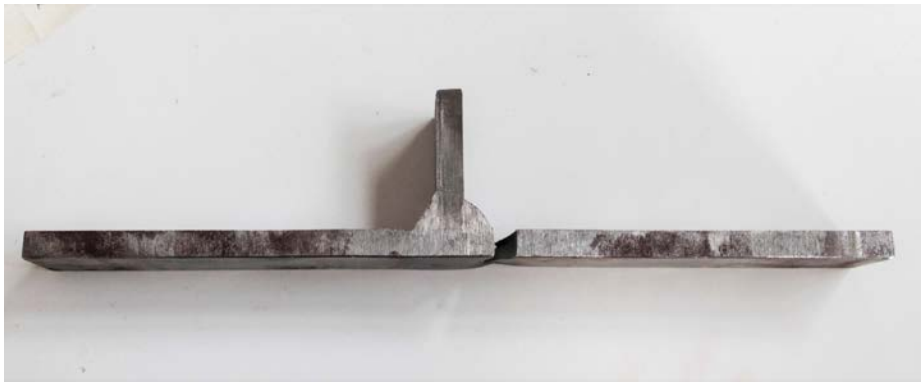

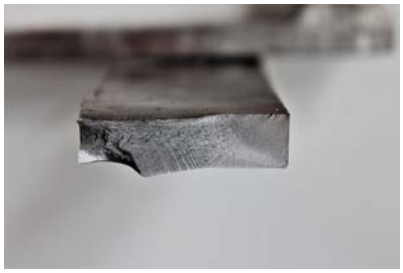

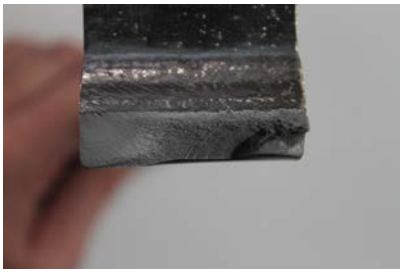

Specimen code D2-6			
Loading condition:	Fatigue test, axial	**Material**:	ADI-S355
Date	July 2019	**Lab. operator**:	Pullin Elena

Data of fatigue tests

$A\,[mm^2] =$	404.0	Frequency $[Hz]$	15.0
$\Delta F\,[kN] =$	124.0	$\Delta\sigma_{nom}\,[MPa]$	306.93
$F_{min}\,[kN] =$	6.5		
$F_{max}\,[kN] =$	130.5	Nominal Load Ratio R	0.05
Number of cycles to failure=	174533.0		

Notes: Crack initiation at the weld toe on the steel plate, then propagated through the thickness of the joint

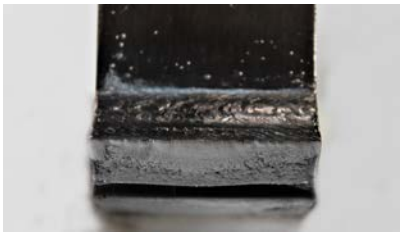

Specimen code D2-4			
Loading condition:	Fatigue test, axial	**Material**:	ADI-S355
Date	July 2019	**Lab. operator**:	Pullin Elena

Data of fatigue tests			
$A\,[mm^2] =$	408.0	Frequency $[Hz]$	15.0
$\Delta F\,[kN] =$	133.0	$\Delta\sigma_{nom}\,[MPa]$	325.98
$F_{min}\,[kN] =$	7.0		
$F_{max}\,[kN] =$	140.0	Nominal Load Ratio R	0.05
Number of cycles to failure=	73446.0		

Notes:	Crack initiation at the weld toe on the steel plate, then propagated through the thickness of the joint

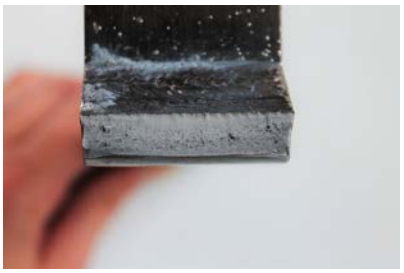

B.5 Joints from series E

Specimen code E3-1			
Loading condition:	Fatigue test, axial	**Material**:	ADI-S355
Date	July 2019	**Lab. operator**:	Pullin Elena

Data of fatigue tests			
$A\,[mm^2] =$	408.0	Frequency $[Hz]$	30.0
$\Delta F\,[kN] =$	85.0	$\Delta\sigma_{nom}\,[MPa]$	208.33
$F_{min}\,[kN] =$	4.5		
$F_{max}\,[kN] =$	89.5	Nominal Load Ratio R	0.05
Number of cycles to failure=	118526.0		

Notes: Crack initiation at the weld toe on the ADI side, then propagated through the thickness of the joint

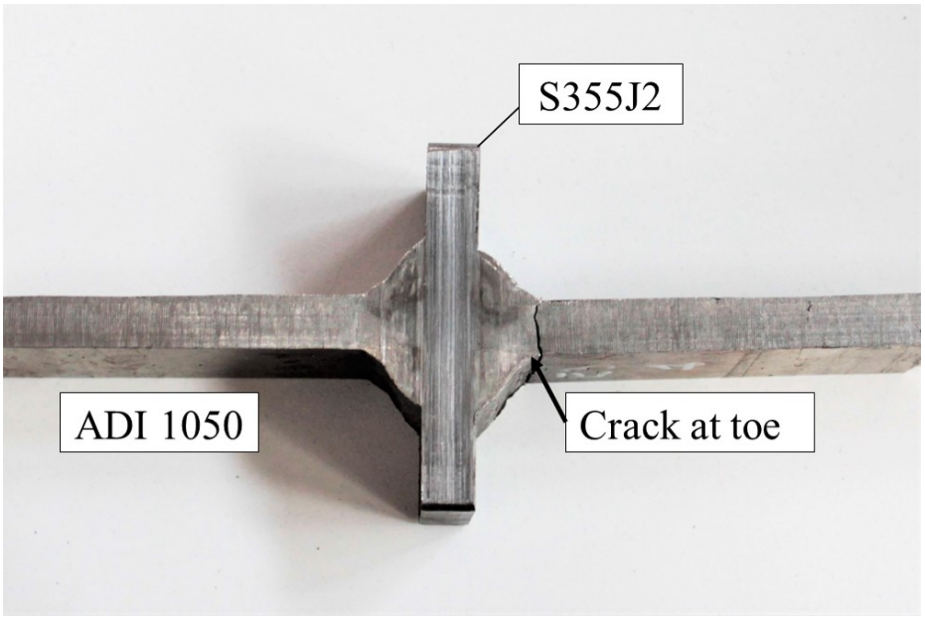

Specimen code E2-1			
Loading condition:	Fatigue test, axial	**Material**:	ADI-S355
Date	July 2019	**Lab. operator**:	Pullin Elena

Data of fatigue tests			
$A\,[mm^2] =$	401.0	Frequency $[Hz]$	30.0
$\Delta F\,[kN] =$	77.0	$\Delta\sigma_{nom}\,[MPa]$	192.02
$F_{min}\,[kN] =$	4.1		
$F_{max}\,[kN] =$	81.1	Nominal Load Ratio R	0.05
Number of cycles to failure=	256157.0		

Notes: run-out under 70kN,retest

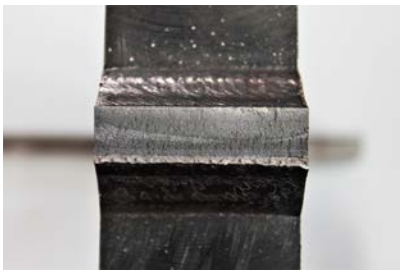

Specimen code E4-3			
Loading condition:	Fatigue test, axial	**Material**:	ADI-S355
Date	July 2019	**Lab. operator**:	Pullin Elena

Data of fatigue tests

$A\,[mm^2] =$	399.0	Frequency $[Hz]$	30.0
$\Delta F\,[kN] =$	74.0	$\Delta\sigma_{nom}\,[MPa]$	185.46
$F_{min}\,[kN] =$	3.9		
$F_{max}\,[kN] =$	77.9	Nominal Load Ratio R	0.05
Number of cycles to failure=	548082.0		

Notes: Crack initiation at the weld toe on the ADI side, then propagated through the thickness of the joint

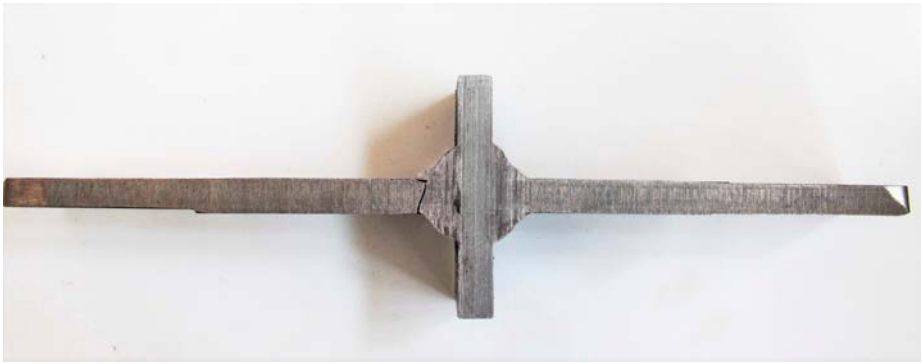

Specimen code E4-1			
Loading condition:	Fatigue test, axial	**Material**:	ADI-S355
Date	July 2019	**Lab. operator**:	Pullin Elena

Data of fatigue tests			
$A\,[mm^2] =$	395.0	Frequency $[Hz]$	30.0
$\Delta F\,[kN] =$	90.0	$\Delta\sigma_{nom}\,[MPa]$	227.84
$F_{min}\,[kN] =$	4.7		
$F_{max}\,[kN] =$	94.7	Nominal Load Ratio R	0.05
Number of cycles to failure=	140969.0		

Notes:	Crack initiation at the weld toe on the ADI side, then propagated through the thickness of the joint

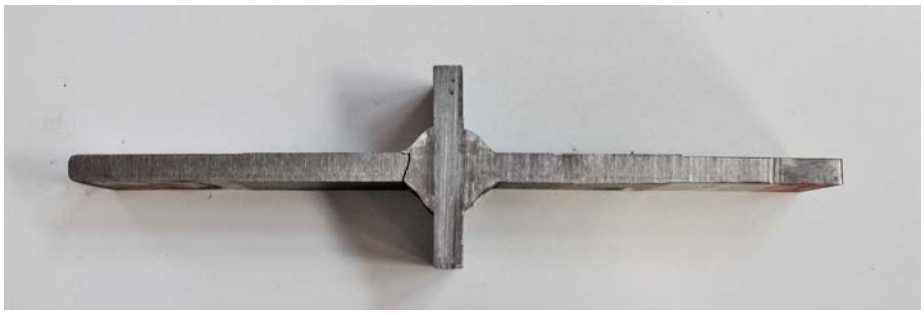

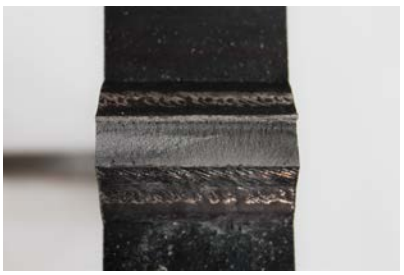

Specimen code E4-2			
Loading condition:	Fatigue test, axial	**Material**:	ADI-S355
Date	July 2019	**Lab. operator**:	Pullin Elena

Data of fatigue tests			
$A\,[mm^2] =$	389.1	Frequency $[Hz]$	30.0
$\Delta F\,[kN] =$	72.0	$\Delta\sigma_{nom}\,[MPa]$	185.06
$F_{min}\,[kN] =$	3.8		
$F_{max}\,[kN] =$	75.8	Nominal Load Ratio R	0.05
Number of cycles to failure=	248030.0		

Notes: Crack initiation at the weld toe on the ADI side, then propagated through the thickness of the joint

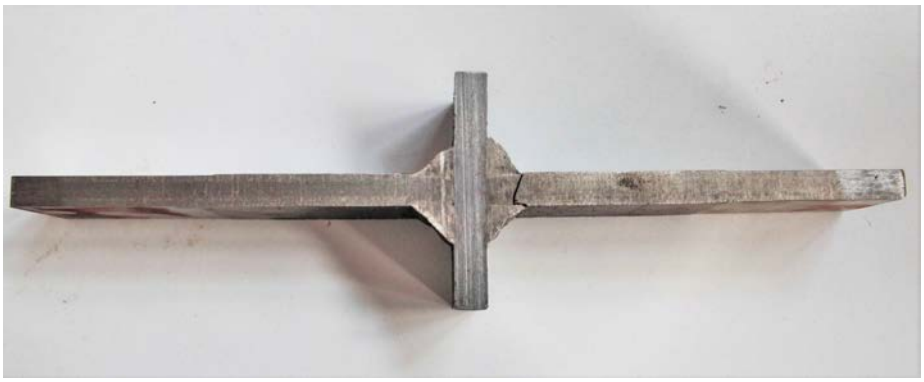

Specimen code E2-3			
Loading condition:	Fatigue test, axial	**Material**:	ADI-S355
Date	July 2019	**Lab. operator**:	Pullin Elena

Data of fatigue tests			
$A\,[mm^2] =$	404.0	Frequency $[Hz]$	30.0
$\Delta F\,[kN] =$	71.0	$\Delta\sigma_{nom}\,[MPa]$	175.74
$F_{min}\,[kN] =$	3.7		
$F_{max}\,[kN] =$	74.7	Nominal Load Ratio R	0.05
Number of cycles to failure=	1200162.0		

Notes: Failure far away from the weld bead

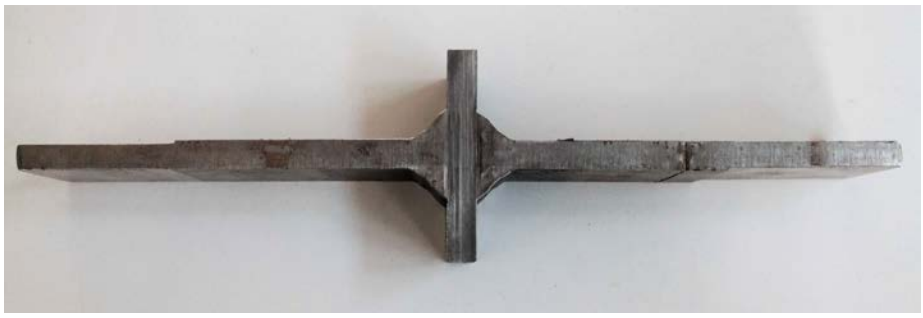

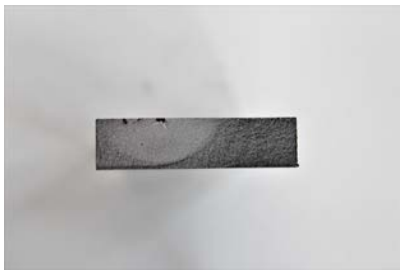

Specimen code E3-3			
Loading condition:	Fatigue test, axial	**Material**:	ADI-S355
Date	July 2019	**Lab. operator**:	Pullin Elena

Data of fatigue tests			
$A\,[mm^2] =$	411.1	Frequency $[Hz]$	30.0
$\Delta F\,[kN] =$	97.0	$\Delta\sigma_{nom}\,[MPa]$	235.98
$F_{min}\,[kN] =$	5.1		
$F_{max}\,[kN] =$	102.1	Nominal Load Ratio R	0.05
Number of cycles to failure=	82736.0		

Notes: Crack initiation at the weld toe on the ADI side, then propagated through the thickness of the joint

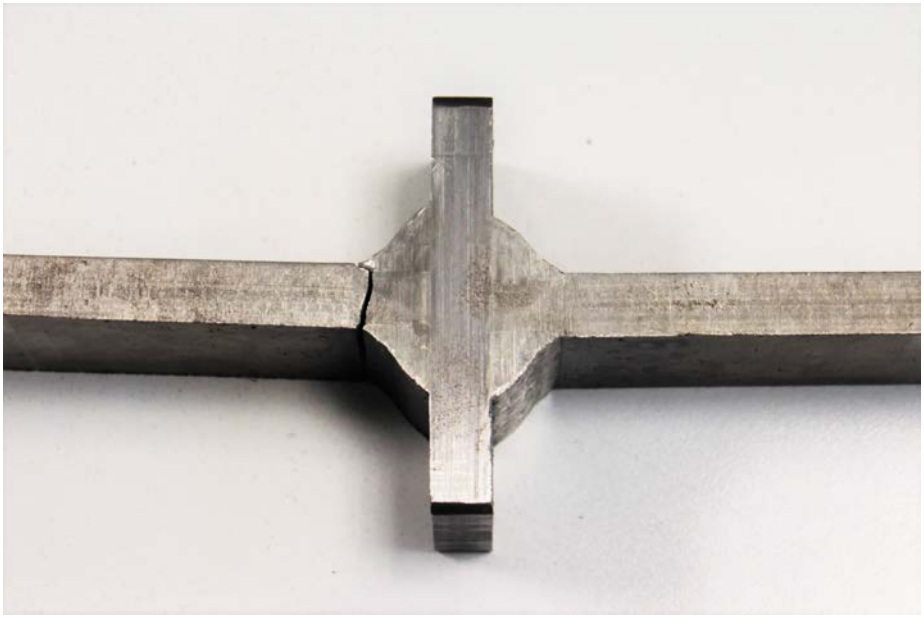

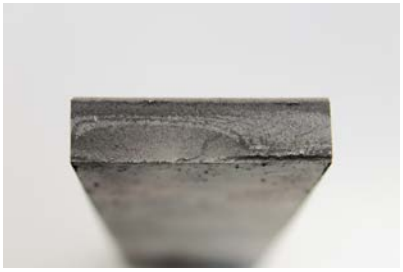

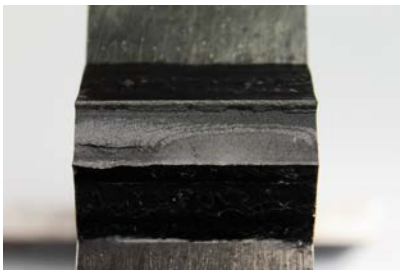

B.6 Joints from series F

Specimen code F4-1			
Loading condition:	Fatigue test, four-point bending	**Material**:	ADI-S355
Date	July 2019	**Lab. operator**:	Pullin Elena

Data of fatigue tests			
$W_f\,[mm^3] =$	663.3	Frequency $[Hz]$	15.0
$\Delta F\,[kN] =$	24.0	$\Delta\sigma_{nom}\,[MPa]$	271.36
$F_{min}\,[kN] =$	1.3		
$F_{max}\,[kN] =$	25.3	Nominal Load Ratio R	0.05
Number of cycles to failure=	186215.0		

Notes: Crack initiation at the weld toe on the ADI side, then propagated through the thickness of the joint

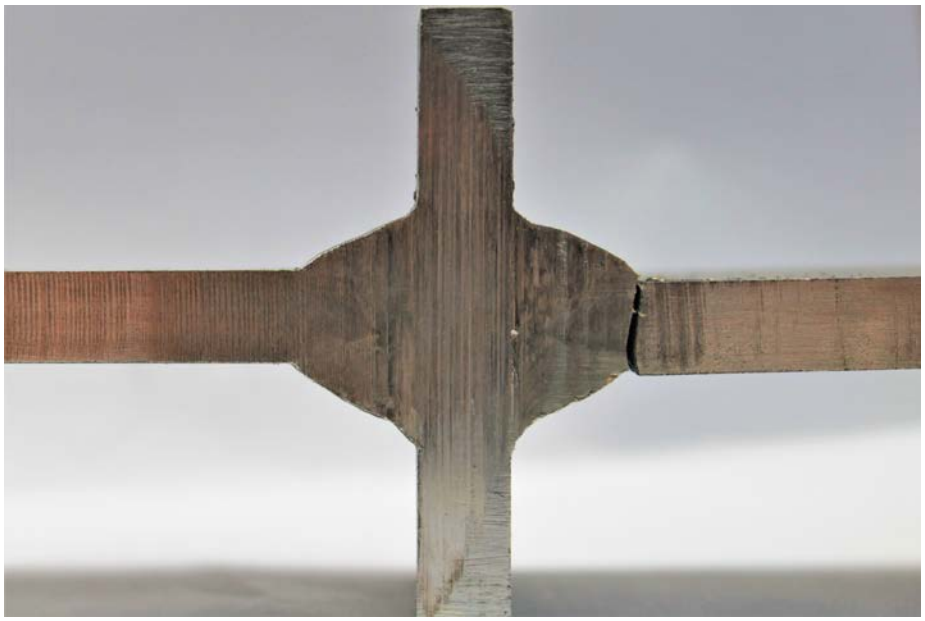

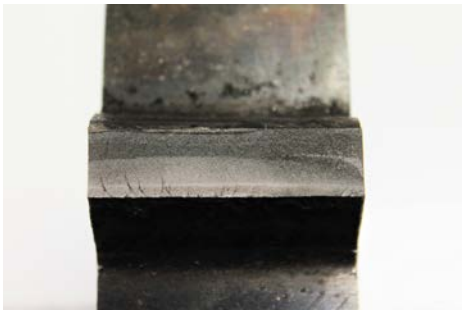

Specimen code F4-2			
Loading condition:	Fatigue test, four-point bending	**Material**:	ADI-S355
Date	July 2019	**Lab. operator**:	Pullin Elena

Data of fatigue tests			
$W_f\,[mm^3] =$	693.6	Frequency $[Hz]$	15.0
$\Delta F\,[kN] =$	30.0	$\Delta\sigma_{nom}\,[MPa]$	324.39
$F_{min}\,[kN] =$	1.6		
$F_{max}\,[kN] =$	31.6	Nominal Load Ratio R	0.05
Number of cycles to failure=	111413.0		

Notes:	Crack initiation at the weld toe on the ADI side, then propagated through the thickness of the joint

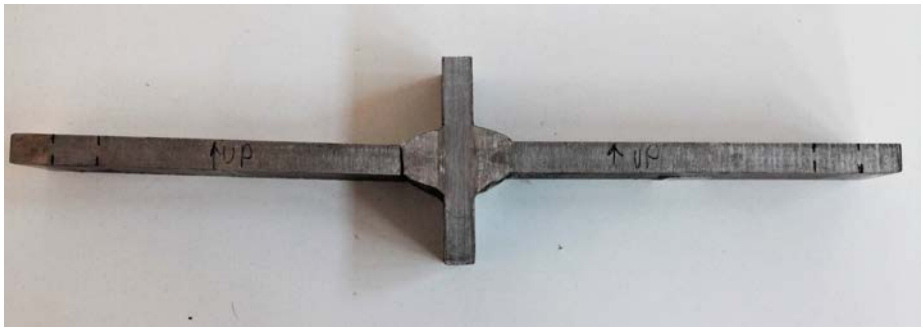

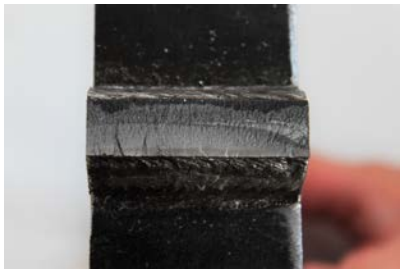

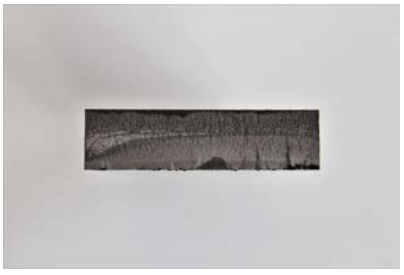

Specimen code F4-3			
Loading condition:	Fatigue test, four-point bending	**Material**:	ADI-S355
Date	July 2019	**Lab. operator**:	Pullin Elena

Data of fatigue tests			
$W_f\,[mm^3] =$	666.7	Frequency $[Hz]$	15.0
$\Delta F\,[kN] =$	17.0	$\Delta\sigma_{nom}\,[MPa]$	191.25
$F_{min}\,[kN] =$	0.9		
$F_{max}\,[kN] =$	17.9	Nominal Load Ratio R	0.05
Number of cycles to failure=	1222986.0		

Notes: Run-out under 15kN axial loading. Retest: crack initiation at the weld toe on the ADI side, then propagated through the thickness of the joint

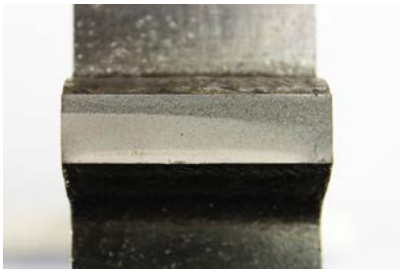

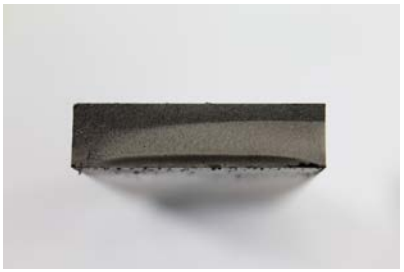

Specimen code F4-5			
Loading condition:	Fatigue test, four-point bending	**Material**:	ADI-S355
Date	July 2019	**Lab. operator**:	Pullin Elena

Data of fatigue tests			
$W_f\,[mm^3] =$	721.1	Frequency $[Hz]$	15.0
$\Delta F\,[kN] =$	38.0	$\Delta\sigma_{nom}\,[MPa]$	395.25
$F_{min}\,[kN] =$	2.0		
$F_{max}\,[kN] =$	40.0	Nominal Load Ratio R	0.05
Number of cycles to failure=	39973.0		

Notes: Crack initiation at the weld toe on the ADI side, then propagated through the thickness of the joint

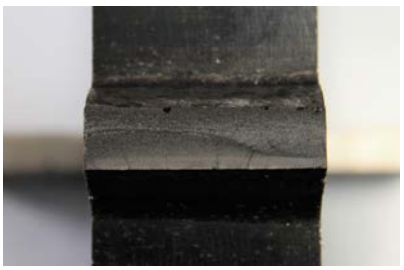

Specimen code F4-4			
Loading condition:	Fatigue test, four-point bending	**Material**:	ADI-S355
Date	July 2019	**Lab. operator**:	Pullin Elena

Data of fatigue tests			
$W_f\,[mm^3] =$	686.7	Frequency $[Hz]$	15.0
$\Delta F\,[kN] =$	31.0	$\Delta\sigma_{nom}\,[MPa]$	338.59
$F_{min}\,[kN] =$	1.6		
$F_{max}\,[kN] =$	32.6	Nominal Load Ratio R	0.05
Number of cycles to failure=	289979.0		

Notes: Failure far away from the weld bead

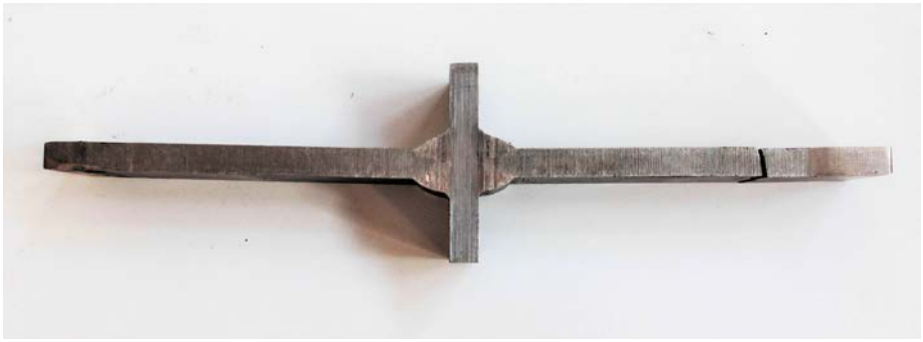

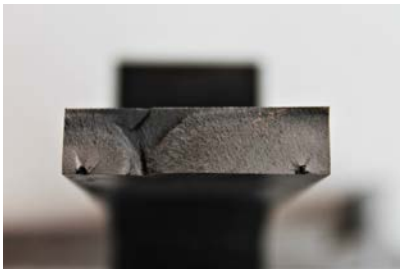

B.7 Plain specimens

Specimen code L1			
Loading condition:	Fatigue test, axial	**Material**:	ADI-S355
Date	July 2019	**Lab. operator**:	Pullin Elena

Data of fatigue tests			
$A\,[mm^2] =$	131.7	Frequency $[Hz]$	10.0
$\Delta F\,[kN] =$	57.0	$\Delta\sigma_{nom}\,[MPa]$	432.74
$F_{min}\,[kN] =$	3.0		
$F_{max}\,[kN] =$	60.0	Nominal Load Ratio R	0.05
Number of cycles to failure=	706530.0		

Notes: Run-out under 45kN and retest

Specimen code L2			
Loading condition:	Fatigue test, axial	**Material**:	ADI-S355
Date	July 2019	**Lab. operator**:	Pullin Elena

Data of fatigue tests			
$A\,[mm^2] =$	129.8	Frequency $[Hz]$	10.0
$\Delta F\,[kN] =$	66.0	$\Delta\sigma_{nom}\,[MPa]$	508.67
$F_{min}\,[kN] =$	3.5		
$F_{max}\,[kN] =$	69.5	Nominal Load Ratio R	0.05
Number of cycles to failure=	255318.0		

Notes:

Specimen code L3			
Loading condition:	Fatigue test, axial	**Material**:	ADI-S355
Date	July 2019	**Lab. operator**:	Pullin Elena

Data of fatigue tests			
$A\,[mm^2] =$	135.0	Frequency $[Hz]$	10.0
$\Delta F\,[kN] =$	76.0	$\Delta\sigma_{nom}\,[MPa]$	562.96
$F_{min}\,[kN] =$	4.0		
$F_{max}\,[kN] =$	80.0	Nominal Load Ratio R	0.05
Number of cycles to failure=	20505.0		

Notes:

Specimen code L4			
Loading condition:	Fatigue test, axial	**Material**:	ADI-S355
Date	July 2019	**Lab. operator**:	Pullin Elena

Data of fatigue tests			
$A\,[mm^2] =$	135.0	Frequency $[Hz]$	10.0
$\Delta F\,[kN] =$	72.0	$\Delta\sigma_{nom}\,[MPa]$	533.33
$F_{min}\,[kN] =$	3.8		
$F_{max}\,[kN] =$	75.8	Nominal Load Ratio R	0.05
Number of cycles to failure=	76723.0		

Notes:

Specimen code L5			
Loading condition:	Fatigue test, axial	**Material**:	ADI-S355
Date	July 2019	**Lab. operator**:	Pullin Elena
Data of fatigue tests			
$A\,[mm^2] =$	132.0	Frequency $[Hz]$	10.0
$\Delta F\,[kN] =$	55.0	$\Delta\sigma_{nom}\,[MPa]$	416.67
$F_{min}\,[kN] =$	2.9		
$F_{max}\,[kN] =$	57.9	Nominal Load Ratio R	0.05
Number of cycles to failure=	101859.0		
Notes:			

Specimen code L6			
Loading condition:	Fatigue test, axial	**Material**:	ADI-S355
Date	July 2019	**Lab. operator**:	Pullin Elena

Data of fatigue tests			
$A\,[mm^2] =$	132.0	Frequency $[Hz]$	10.0
$\Delta F\,[kN] =$	54.0	$\Delta\sigma_{nom}\,[MPa]$	409.09
$F_{min}\,[kN] =$	2.8		
$F_{max}\,[kN] =$	56.8	Nominal Load Ratio R	0.05
Number of cycles to failure=	362387.0		

Notes: Run-out under 50kN and retest

Appendix C

APDL scripts

C.1 APDL codes for series A

Codice C.1: Series A: APDL for N-SIF approach

```
/CLEAR, NOSTART

! GEOMETRICAL PARAMETERS

MATERIAL= 2   ! 1= STEEL 2=ADI
ltot= 180     ! Total length of the
    specimen
Ro_S355=0.28    ! Control radius for
    steel
Ro_ADI=0.28   ! Control radius for
    ADI
Ro_su_d= 5    ! Parameter for mesh
    refinement
load= 1     ! 1=axial loading, 2=
    four-point-bending loading

!--------------------------
!Definition of vectors

*DIM,b_value,,12    !*DIM,PAR,TYPE,
    IMAX
*DIM,h_value,,12
*DIM,t_value,,12
*DIM,l_root_value,,12
*DIM,alfaADI_value,,12    !*DIM,PAR,
    TYPE,IMAX
*DIM,alfaS355_value,,12
  b_value(1) = 14.82,8.277,7.145,...
  b_value(11) =11.69,12.771

  h_value(1) =2.136,0.909,1.128,...
  h_value(11)=2.037,2.162

  t_value(1)=10,12,11.9,12.05,...
  t_value(11)=10.1,10.1,

  alfaADI_value(1) =
    151.392,141.194,143.616,...
  alfaADI_value(11) = 141.044,137.231
       !Toe opening angle on ADI side
  alfaS355_value(1) =
    151.179,159.146,142.431,...
  alfaS355_value(11)
    =135.807,141.582,  !Toe opening
    angle on steel side

  l_root_value(1) =
    4.85,4.247,4.437,3.881,4.137,...
  l_root_value(11) = 3.15,3.933,


!-----------------------
!Setting the do-cycle

  i_ini = 1   ! Starting value for i
  i_fin = 12    ! Final value for i

  !Begin do-cycle

  *DO,i,i_ini,i_fin,1 !*DO,PAR,IVAL,
    FVAL,INC

  h = h_value(i)
  b = b_value(i)        ! Width of
    the weld bead
  alfa_ADI = alfaADI_value(i)   ! Toe
     opening angle on ADI side
  alfa_S355= alfaS355_value(i)    !
    Toe opening angle on steel side
  l_root=l_root_value(i)      ! Half-
    length of the root
  t=t_value(i)/2        ! Half-
    thickness of the specimen

  pi= 4*atan(1)
  c_S355=h/tan((180-alfa_S355)*pi
    /180)
  c_ADI=h/tan((180-alfa_ADI)*pi/180)
!-------------------------
/PREP7
!ELEMENT TYPE
ET,1,PLANE182

KEYOPT,1,1,3
KEYOPT,1,3,2
KEYOPT,1,6,0

!MATERIAL

MPTEMP,,,,,,,,
MPTEMP,1,0
```

```
MPDATA,EX,1,,206000
MPDATA,PRXY,1,,0.3

MPTEMP,,,,,,,,
MPTEMP,1,0
MPDATA,EX,2,,168000
MPDATA,PRXY,2,,0.27

CSYS,0
K,1,0,0,0,
K,2,ltot/2,0,0,
K,3,ltot/2,t,0,
K,4,b/2,t,0,
K,5,b/2-c_ADI,t+h,0,
K,6,0, t+h,0,
K,7,-b/2+c_S355,t+h,0,
K,8,-b/2,t,0,
K,9,-ltot/2,t,0
K,10,-ltot/2,0,0

LSTR,1,2
LSTR,2,3
LSTR,3,4
LSTR,4,5
LSTR,5,6
LSTR,6,7
LSTR,7,8
LSTR,8,9
LSTR,9,10
LSTR,10,1      1

!control volume ADI with radius 0.28
    mm
kwpave,4
CSYS,4
K,103,-0.28,0,0,
K,102,+0.28,0,0,
K,101,0,0.28,0,
K,100,0,-0.28,0,


LARC,103,100,4,0.28,
LARC,100,102,4,0.28,
LARC,101,103,4,0.28,

LSBL,4,13,,,KEEP
LSBL,13,14,,,KEEP
LDELE,4
LCOMB,16,11
LCOMB,11,12
LDIV,11, , ,2,0
LSBL,3,4,,,KEEP

!control volume ADI with radius
    0.0001mm

K,108,-0.0001,0,0,
K,109,0,-0.0001,0,
K,110,+0.0001,0,0,
K,111,0,+0.0001,0,

LARC,108,109,4,0.0001,
LARC,109,110,4,0.0001,
LARC,108,111,4,0.0001,

LSBL,13,16,,,KEEP
LSBL,14,17,,,KEEP
LSBL,17,13,,,KEEP
LDELE,21
LCOMB,3,16
LCOMB,3,14
LSTR,4,12
LSBL,3,14,,,KEEP
LSBL,14,16,,,KEEP
```

```
!control volume steel with radius
    0.28mm

kwpave,8
CSYS,4
K,104,-0.28,0,0,
K,105,0,-0.28,0,
K,106,+0.28,0,0,
K,107,0,+0.28,0,

LARC,104,105,8,0.28,
LARC,105,106,8,0.28,
LARC,106,107,8,0.28,

LSBL,7,23,,,KEEP
LSBL,8,14,,,KEEP
LSBL,23,25,,,KEEP
LCOMB,14,22,
LDELE,27
LCOMB,14,8
LDIV,8, , ,2,0

!control volume steel with radius
    0.0001mm

K,112,-0.0001,0,0,
K,113,0,-0.0001,0,
K,114,+0.0001,0,0,
K,115,0,+0.0001,0,

LARC,112,113,8,0.0001,
LARC,113,114,8,0.0001,
LARC,114,115,8,0.0001,

LSBL,7,22,,,KEEP
LSBL,25,27,,,KEEP
LSBL,27,7,,,KEEP
LCOMB,22,23,
LDELE,31
LCOMB,22,25
LDIV,22,,,2,0

LSTR,8,18
LSTR,18,16

!Control volume at the Root
CSYS,0
NUMSTR,line,40

K,120,0,l_root/2,0,
K,121,+0.01,0,0,
K,122,-0.01,0,0,

LSTR,      120,       121
LSTR,       120,       122
LSTR,       6,      120

LSBL,1,40,,,KEEP
LSBL,10,41,,,KEEP
LDELE,43
LDELE,45



! Generation of the AREAS

AL, 16,3,13
AL,17,18,3
AL,16,20,11,21
AL,21,4,19,17
AL,42,40,44,12,2,4,11,15,5

AL,28,25,22
AL,7,23,25
AL,22,29,8,27
```

```
AL,23,27,14,30
AL,42,41,46,9,26,8,14,24,6

NUMSTR,line,1

!Generation of the MESH


TYPE, 1
MAT, MATERIAL
REAL,
ESYS, 0
SECNUM,

KSCON,4,0.000001,0,16,2,

!ADI SIDE
LESIZE,13, , ,5,1, , , ,1
LESIZE,3, , ,5,1, , , ,1
LESIZE,18, , ,5,1, , , ,1
LESIZE,20, , ,50,1/2000, , , ,1
LESIZE,21, , ,50,1/2000, , , ,1
LESIZE,19, , ,50,1/2000, , , ,1
LESIZE,17, , ,8,1, , , ,1
LESIZE,16, , ,8,1, , , ,1
LESIZE,11, , ,8,1, , , ,1
LESIZE,4, , ,8,1, , , ,1


MSHKEY, 1
AMESH,3

MSHKEY, 1
AMESH,4

MSHKEY,0
AMESH,1

MSHKEY,0
AMESH,2

d1= 10*Ro_ADI/Ro_su_d
ESIZE,d1,0
MSHKEY, 0
AMESH,5

!STEEL SIDE

LESIZE,7, , ,5,1, , , ,1
LESIZE,25, , ,5,1, , , ,1
LESIZE,28, , ,5,1, , , ,1
LESIZE,30, , ,50,1/2000, , , ,1
LESIZE,27, , ,50,2000, , , ,1
LESIZE,29, , ,50,1/2000, , , ,1
LESIZE,22, , ,8,1, , , ,1
LESIZE,23, , ,8,1, , , ,1
LESIZE,14, , ,8,1, , , ,1
LESIZE,8, , ,8,1, , , ,1


MSHKEY, 1
AMESH,6

MSHKEY, 1
AMESH,7

MSHKEY,0
AMESH,8

MSHKEY,0
AMESH,9

d2= 10*Ro_S355/Ro_su_d
ESIZE,d2,0
MSHKEY, 0
AMESH,10

! BOUNDARY CONDITIONS AND LOADS
DL,9,,UX
DK,10,,,,0,UY

*IF, load, EQ,1,THEN
  SFL, 2,PRES, -1
  DL,46,,SYMM
  DL,44,,SYMM
*ELSE
  SFL,2,PRES, 0, -1
  DL,46,,ASYM
  DL,44,,ASYM
*ENDIF

FINISH

CSKP,11,0,4,12,11,1,1,
CSYS,11,

! SOLUTION
/SOL
SOLVE
FINISH

! POST-PROCESSING
/POST1
RSYS,11

LPLOT
LSEL,S, , ,      21
NSLL,S
NPLOT
PRNSOL,S,COMP



*VGET,sel,NODE, ,NSEL,,
*VGET,posx,NODE, ,LOC,X
*VGET,posy,NODE, ,LOC,Y
*VGET,stress,NODE, ,S,Y

*CFOPEN,'RESULTS_NSIF_BUTT_PARTIAL','
    txt ',,APPEND
*VWRITE, 'h','b','t','material','load
    ','d',
(A8' ',A8' ',A8' ',A8' ',A8' ',A8'
    ',)
*VWRITE, h,b,t,material,load,d1,
 (F8.2,' ',F8.2,' ',F8.2,' ',F8.2,'
    ',F8.2,' ',F8.2,' ',)
*VWRITE,'posx','posy','stress',
(A8' ',A8' ',A8' ',)

*VMASK,sel
*VWRITE,posx(1),posy(1), stress(1), ,
      , , , , ,
(F12.6,F12.6,F12.6,)
*CFCLOS

!DELETE ALL DATA

  /PREP7

  ALLSEL,ALL    !select everything
  ACLEAR,ALL    !Delete MESH
  ADELE,ALL   !Delete areas
  LDELE,ALL   !Delete lines
  KDELE,ALL   !Delete keypoints

!END do-cycles

*ENDDO
```

```
FINISH
```

Codice C.2: Series A: APDL for SED approach

```
/CLEAR, NOSTART

!GEOMETRICAL PARAMETERS
MATERIAL= 2   ! 1= STEEL 2=ADI
ltot= 180     ! Total length of the
    specimen
alfa_S355= 135  ! Toe opening angle
    on steel side
alfa_ADI=135  ! Toe opening angle on
    ADI side
Ro_S355=0.28  ! Control radius for
    steel
Ro_ADI=0.28   ! Control radius for
    ADI
Ro_su_d= 5    ! Parameter fo mesh
    refinement
b= 10     ! Width of the weld bead
h= 1.46     ! Height of the weld bead
t= 5.3875     ! Half-thickness of the
     specimen
l_root= 1.4   ! Half-length of the
    root
t_su_d= 8   ! Parameter for mesh
    refinement
load= 1     ! 1=axial loading, 2=
    four-point-bending loading
!-------------------------

*CFOPEN, 'RESULTS_SED_BUTT_PARTIAL','
    txt',,APPEND
*VWRITE, 'h','b','t','alfa_S355','
    alfa_ADI','material','load','
    Ro_ADI','d', 'SED_STEEL*10^6','
    SED_ADI*10^6','SED_ROOT*10^6',
(' ',A8' ',A8' ',A8' ',A8' ',A8' ',A8
    ' ',A8' ',A8' ',A8' ',A8' ',A8'
    ',A8' ')
*CFCLOS

pi= 4*atan(1)
c_S355=h/tan((180-alfa_S355)*pi/180)
c_ADI=h/tan((180-alfa_ADI)*pi/180)

!------------------
/PREP7
!ELEMENT TYPE
ET,1,PLANE182

KEYOPT,1,1,3
KEYOPT,1,3,2
KEYOPT,1,6,0

!MATERIAL

MPTEMP,,,,,,,,
MPTEMP,1,0
MPDATA,EX,1,,206000
MPDATA,PRXY,1,,0.3

MPTEMP,,,,,,,,
MPTEMP,1,0
MPDATA,EX,2,,168000
MPDATA,PRXY,2,,0.27

K,1,0,0,0,
K,2,ltot,0,0,
K,3,ltot,t,0,
K,4,ltot/2+b/2,t,0,
K,5,ltot/2+b/2-c_ADI,t+h,0,
K,6,ltot/2, t+h,0,
K,7,ltot/2-b/2+c_S355,t+h,0,
K,8,ltot/2-b/2,t,0,
K,9,0,t,0

LSTR,1,2
LSTR,2,3
LSTR,3,4
LSTR,4,5
LSTR,5,6
LSTR,6,7
LSTR,7,8
LSTR,8,9
LSTR,9,1

NUMSTR,line,11

!control volume ADI
kwpave,4
CSYS,4
K,103,-Ro_ADI,0,0,
K,102,+Ro_ADI,0,0,
K,101,0,Ro_ADI,0,
K,100,0,-Ro_ADI,0,

LARC,103,100,4,Ro_ADI,
LARC,100,102,4,Ro_ADI,
LARC,101,103,4,Ro_ADI,
LSBL,4,13,,,KEEP
LSBL,3,12,,,KEEP
LSBL,13,14,,,KEEP
LDELE,18
!control volume steel with radius
    0.28mm

kwpave,8
CSYS,4
K,104,-Ro_S355,0,0,
K,105,0,-Ro_S355,0,
K,106,+Ro_S355,0,0,
K,107,0,+Ro_S355,0,

LARC,104,105,8,Ro_S355,
LARC,105,106,8,Ro_S355,
LARC,106,107,8,Ro_S355,
LSBL,7,20,,,KEEP
LSBL,8,13,,,KEEP
LSBL,20,22,,,KEEP
LDELE,26
LCOMB,13,18,
LCOMB,13,25
LCOMB,11,12,
LCOMB,11,19

!Root

!kwpave,1
CSYS,0
NUMSTR,line,30

K,120,ltot/2,l_root/2,0,
K,121,ltot/2+0.01,0,0,
K,122,ltot/2-0.01,0,0,

LSTR,      120,       121
LSTR,       120,       122

LSBL,1,30,,,KEEP
LSBL,32,31,,,KEEP
LDELE,35

kwpave,120
CSYS,4
```

```
CIRCLE,120,Ro_S355, , ,, ,
LSBL,36,31,,,KEEP
LSBL,37,30,,,KEEP
LDELE,39
LDELE,40
LSBL,31,38,,,KEEP
LSBL,30,36,,,KEEP

AL,13,23,22
AL,11,14,17
AL,32,35,38,36,37,31
LSEL,S,,,2
LSEL,A,,,5,6
LSEL,A,,,11,
LSEL,A,,,13
LSEL,A,,,15,16
LSEL,A,,,9
LSEL,A,,,21
LSEL,A,,,24
LSEL,A,,,38,40
LSEL,A,,,32,36
AL,ALL
ALLSEL

CSYS,0
NUMSTR,line,1

!Generation of the MESH

TYPE, 1
MAT, MATERIAL
REAL,
ESYS, 0
SECNUM,
d= Ro_ADI/Ro_su_d ! globa element
     size mesh

ESIZE,d,0
MSHKEY, 0
AMESH, 1

ESIZE,d,0
MSHKEY, 0
AMESH, 2
ESIZE,d,0
MSHKEY, 0
AMESH, 3

d1= 10*Ro_ADI/Ro_su_d

ESIZE,d1,0
MSHKEY,0
AMESH,4

! BOUNDARY CONDITIONS AND LOADS
DL,9,,UX
DK,1,,,,0,UY
*IF, load, EQ,1,THEN
  SFL, 2,PRES, -1
  !
  DL,34,,SYMM
  DL,33,,SYMM
*ELSE
  SFL,2,PRES, 0, -1
  DL,33,,ASYM
  DL,34,,ASYM
*ENDIF

FINISH

! solution
/SOL
SOLVE
FINISH

! POST-PROCESSING

/POST1
ASLL,S
ASEL,S, , ,1,
ESLA,S
AVPRIN,0, ,
ETABLE, ,SENE,
AVPRIN,0, ,
ETABLE, ,VOLU,
SSUM
PRETAB,SENE,VOLU

*GET, ENERGY_S355,SSUM,0,ITEM,SENE
*GET,VOLU_S355,SSUM, 0,ITEM, VOLU

SED_S355= ENERGY_S355/VOLU_S355

ASLL,S
ASEL,S, , ,2,
ESLA,S
AVPRIN,0, ,
ETABLE, ,SENE,
AVPRIN,0, ,
ETABLE, ,VOLU,
SSUM
PRETAB,SENE,VOLU

*GET, ENERGY_ADI,SSUM,0,ITEM,SENE
*GET,VOLU_ADI,SSUM, 0,ITEM, VOLU

SED_ADI= ENERGY_ADI/VOLU_ADI

ASLL,S
ASEL,S, , ,3,
ESLA,S
AVPRIN,0, ,
ETABLE, ,SENE,
AVPRIN,0, ,
ETABLE, ,VOLU,
SSUM
PRETAB,SENE,VOLU

*GET, ENERGY_ROOT,SSUM,0,ITEM,SENE
*GET,VOLU_ROOT,SSUM, 0,ITEM, VOLU

SED_ROOT= ENERGY_ROOT/VOLU_ROOT

*CFOPEN, 'RESULTS_SED_BUTT_PARTIAL','
     txt',,APPEND
*VWRITE, h,b,t,alfa_S355,alfa_ADI,
     material,load,d,Ro_ADI,SED_S355,
     SED_ADI,SED_ROOT
(F8.2,' ',F8.2,' ',F8.2,' ',F8.2,' ',
     F8.2,' ',F8.2,' ',F8.2,' ',F8.2,'
      ',F8.2,' ',F10.4,' ',F10.4,' ',
     F10.4,)
*CFCLOS


FINISH
```

Codice C.3: Series A: APDL for PSM approach

```
/CLEAR, NOSTART

! GEOMETRICAL PARAMETES

MATERIAL= 2     ! 1= STEEL 2=ADI
ltot= 180     ! Half-length of the
     specimen
```

```
alfa_S355= 135    ! Toe opening angle
     on steel side
alfa_ADI=135    ! Toe opening angle
    on ADI side
Ro_S355=0.28    ! Control radius for
    steel
Ro_ADI=0.28   ! Control radius for
    ADI
Ro_su_d= 5    ! Parameter fo mesh
    refinement
b= 10     ! Width of the weld bead
h= 1.46     ! Height of the root
t= 5.3875     ! Half-thickness of the
     specimen
l_root= 1.4   ! Half-length of the
    root
t_su_d= 8   ! Parameter for mesh
    refinement
load= 1     ! 1=axial loading, 2=
    four-point-bending loading
!------------------------------

pi= 4*atan(1)
c_S355=h/tan((180-alfa_S355)*pi/180)
c_ADI=h/tan((180-alfa_ADI)*pi/180)


/PREP7
!ELEMENT TYPE
ET,1,PLANE182

KEYOPT,1,1,3
KEYOPT,1,3,2
KEYOPT,1,6,0
!MATERIAL

MPTEMP,,,,,,,,
MPTEMP,1,0
MPDATA,EX,1,,206000
MPDATA,PRXY,1,,0.3

MPTEMP,,,,,,,,
MPTEMP,1,0
MPDATA,EX,2,,168000
MPDATA,PRXY,2,,0.27

K,1,0,0,0,
K,2,ltot,0,0,
K,3,ltot,t,0,
K,4,ltot/2+b/2,t,0,
K,5,ltot/2+b/2-c_ADI,t+h,0,
K,6,ltot/2, t+h,0,
K,7,ltot/2-b/2+c_S355,t+h,0,
K,8,ltot/2-b/2,t,0,
K,9,0,t,0


LSTR,        1,        2
LSTR,        2,        3
LSTR,        3,        4
LSTR,        4,        5
LSTR,        5,        6
LSTR,        6,        7
LSTR,        7,        8
LSTR,        8,        9
LSTR,        9,        1


K,10,ltot/2,l_root,0,
K,11,ltot/2+0.01,0,0,
K,12,ltot/2-0.01,0,0,

LSTR,        10,        11
LSTR,        10,        12
LSBL,1,11,,,KEEP
LSBL,13,10,,,KEEP
LDELE,14


LSEL,S,,,1,12
AL,ALL
ALLSEL



!Generation of the mesh


TYPE, 1
MAT, MATERIAL
REAL,
ESYS, 0
SECNUM,

d= t/t_su_d! globa element size mesh

ESIZE,d,0
MSHKEY, 0
AMESH, 1


! BOUNDARY CONDITIONS AND LOADS
DL,9,,UX
DK,1,,,,0,UY

*IF, load, EQ,1,THEN
  SFL, 2,PRES, -1
  !
  DL,1,,SYMM
  DL,12,,SYMM
*ELSE
  SFL,2,PRES, 0, -1

  DL,1,,ASYM
  DL,12,,ASYM
*ENDIF


KWPAVE,       4
WPROTA,-(360-alfa_ADI)/2,0 , 0
CSWPLA, 11, 0, ,
CSYS,11,


FINISH

! SOLUTION
/SOL
SOLVE
FINISH


! POST-PROCESSING

/POST1
RSYS,11
PLNSOL, S,Y, 0,1.0
/AUTO,1
/REPLO
/REP,FAST
/ui, copy,save,bmp,full,color,reverse
    ,portrait, no

KSEL,S, , ,4
NSLK,R
NSORT,S,Y,0,0,1
*GET,psm,SORT,0,MAX
ALLS,ALL
```

```
*CFOPEN, 'RESULTS_PSM_BUTT_PARTIAL','
    txt',,APPEND
*VWRITE, 'h','alfa_ADI','t','b','
    material','load','d','PSM',
(' ',A8' ',A8' ',A8' ',A8' ',A8' ',A8
    ' ',A8' ',A8' ',)
*VWRITE, h,alfa_ADI,t,b,material,load
    ,d,psm
(F8.2,' ',F8.2,' ',F8.2,' ',F8.2,' ',
    F8.2,' ',F8.2,' ',F8.2,' ',F10
    .4,' ',)
 !*VWRITE, 'h','b','t','materiale','
    carico','d','PSM'
(F8.2,' ',F8.2,' ',F8.2,' ',F8.2,' ',
    F8.2,' ',F8.2,' ',F8.2,' ',)
*CFCLOS

FINISH
```

C.2 APDL codes for series B

Codice C.4: Series B: APDL for N-SIF approach

```
/CLEAR, NOSTART

!PARAMETRI DA SETTARE

MATERIAL= 2   ! 1= STEEL 2=ADI
b= 14.78    ! Width of the weld bead
h= 1.86     ! Height of the weld bead
t= 5.02     ! Half-thickness of the
    specimen
ltot= 270   ! Total length of the
    specimen
alfa_S355= 135  ! Toe opening angle
    on steel side
alfa_ADI=135  ! Toe opening angle on
    ADI side
Ro_S355=0.28  ! Control radius for
    steel
Ro_ADI=0.28   ! Control radius for
    ADI
Ro_su_d= 5    ! Parameter for mesh
    refinement
load= 1     ! 1=axial loading, 2=
    four-point-bending loading

pi= 4*atan(1) ! pi greco
c_S355=h/tan((180-alfa_S355)*pi/180)
c_ADI=h/tan((180-alfa_ADI)*pi/180)

!------------------------

/PREP7
!ELEMENT TYPE
ET,1,PLANE182

KEYOPT,1,1,3
KEYOPT,1,3,2
KEYOPT,1,6,0

!MATERIAL

MPTEMP,,,,,,,,
MPTEMP,1,0
MPDATA,EX,1,,206000
MPDATA,PRXY,1,,0.3

MPTEMP,,,,,,,,
MPTEMP,1,0
MPDATA,EX,2,,168000
MPDATA,PRXY,2,,0.27

CSYS,4
K,1,0,0,0,
K,2,ltot/2,0,0,
K,3,ltot/2,t,0,
K,4,b/2,t,0,
K,5,b/2-c_ADI,t+h,0,
K,6,0, t+h,0,
K,7,-b/2+c_S355,t+h,0,
K,8,-b/2,t,0,
K,9,-ltot/2,t,0
K,10,-ltot/2,0,0

LSTR,1,2
LSTR,2,3
LSTR,3,4
LSTR,4,5
LSTR,5,6
LSTR,6,7
LSTR,7,8
LSTR,8,9
LSTR,9,10
LSTR,10,1
!control volume ADI
kwpave,4
CSYS,4
K,103,-0.28,0,0,
K,102,+0.28,0,0,
K,101,0,0.28,0,
K,100,0,-0.28,0,

LARC,103,100,4,0.28,
LARC,100,102,4,0.28,
LARC,101,103,4,0.28,

LSBL,4,13,,,KEEP
LSBL,13,14,,,KEEP
LDELE,4
LCOMB,16,11
LCOMB,11,12
LDIV,11, , ,2,0
LSBL,3,4,,,KEEP

K,108,-0.0001,0,0,
K,109,0,-0.0001,0,
K,110,+0.0001,0,0,
K,111,0,+0.0001,0,

LARC,108,109,4,0.0001,
LARC,109,110,4,0.0001,
LARC,108,111,4,0.0001,

LSBL,13,16,,,KEEP
LSBL,14,17,,,KEEP
LSBL,17,13,,,KEEP
LDELE,21
LCOMB,3,16
LCOMB,3,14
LSTR,4,12
LSBL,3,14,,,KEEP
LSBL,14,16,,,KEEP

!control volume steel with radius
    0.28mm

kwpave,8
CSYS,4
K,104,-0.28,0,0,
K,105,0,-0.28,0,
K,106,+0.28,0,0,
```

```
K,107,0,+0.28,0,

LARC,104,105,8,0.28,
LARC,105,106,8,0.28,
LARC,106,107,8,0.28,

LSBL,7,23,,,KEEP
LSBL,8,14,,,KEEP
LSBL,23,25,,,KEEP
LCOMB,14,22,
LDELE,27
LCOMB,14,8
LDIV,8, , ,2,0


K,112,-0.0001,0,0,
K,113,0,-0.0001,0,
K,114,+0.0001,0,0,
K,115,0,+0.0001,0,

LARC,112,113,8,0.0001,
LARC,113,114,8,0.0001,
LARC,114,115,8,0.0001,

LSBL,7,22,,,KEEP
LSBL,25,27,,,KEEP
LSBL,27,7,,,KEEP
LCOMB,22,23,
LDELE,31
LCOMB,22,25
LDIV,22,,,2,0

LSTR,8,18
LSTR,18,16
LSTR,6,1

AL, 16,3,13
AL,17,18,3
AL,16,20,11,21
AL,21,4,19,17
AL,11,4,12,2,1,31,5,15

AL,28,25,22
AL,7,23,25
AL,22,29,8,27
AL,23,27,14,30
AL,8,14,26,9,10,31,6,24

!Generation of the MESH

TYPE, 1
MAT, MATERIALE
REAL,
ESYS, 0
SECNUM,

KSCON,4,0.000001,0,8,2,

LESIZE,13, , ,5,1, , , ,0
LESIZE,3, , ,5,1, , , ,0
LESIZE,18, , ,5,1, , , ,0
LESIZE,20, , ,50,1/2000, , , ,0
LESIZE,21, , ,50,1/2000, , , ,0
LESIZE,19, , ,50,1/2000, , , ,0
LESIZE,17, , ,8,1, , , ,0
LESIZE,16, , ,8,1, , , ,0
LESIZE,11, , ,8,1, , , ,0
LESIZE,4, , ,8,1, , , ,0

MSHKEY,0
AMESH,1

MSHKEY,0
AMESH,2

MSHKEY, 1
AMESH,3

MSHKEY, 1
AMESH,4

d1= 10*Ro_ADI/Ro_su_d
ESIZE,d1,0
MSHKEY, 0
AMESH,5

LESIZE,7, , ,5,1, , , ,1
LESIZE,25, , ,5,1, , , ,1
LESIZE,28, , ,5,1, , , ,1
LESIZE,30, , ,50,1/2000, , , ,1
LESIZE,27, , ,50,2000, , , ,1
LESIZE,29, , ,50,1/2000, , , ,1
LESIZE,22, , ,8,1, , , ,1
LESIZE,23, , ,8,1, , , ,1
LESIZE,14, , ,8,1, , , ,1
LESIZE,8, , ,8,1, , , ,1

MSHKEY, 1
AMESH,6

MSHKEY, 1
AMESH,7

MSHKEY,0
AMESH,8

MSHKEY,0
AMESH,9

d2= 10*Ro_S355/Ro_su_d
ESIZE,d2,0
MSHKEY, 0
AMESH,10

! BOUNDARY CONDITIONS AND LOADS
DL,9,,UX
DK,10,,,,0,UY
*IF, carico, EQ,1,THEN
  SFL, 2,PRES, -1
  DL,1,,SYMM
  DL,10,,SYMM
*ELSE
  SFL,2,PRES, 0, -1
  DL,1,,ASYM
  DL,10,,ASYM
*ENDIF

FINISH

CSKP,11,0,4,12,11,1,1,
CSYS,11,

!SOLUTION
/SOL
SOLVE
FINISH

!POST-PROCESSING
/POST1
RSYS,11

LPLOT
LSEL,S, , ,      21
NSLL,S
NPLOT
PRNSOL,S,COMP

*VGET,sel,NODE, ,NSEL,,
*VGET,posx,NODE, ,LOC,X
*VGET,posy,NODE, ,LOC,Y
```

```
*VGET,stress,NODE, ,S,Y
*CFOPEN,'RESULTS_NSIF_BUTT','txt ',,
    APPEND
*VWRITE, 'h','b','t','material','LOAD
    ','d',
(A8' ',A8' ',A8' ',A8' ',A8' ',A8'
    ',)
*VWRITE, h,b,t,material,load,d1,
 (F8.2,' ',F8.2,' ',F8.2,' ',F8.2,'
    ',F8.2,' ',F8.2,' ',)
 *VWRITE,'posx','posy','stress',
(A8' ',A8' ',A8' ',)
*VMASK,sel
*VWRITE,posx(1),posy(1), stress(1), ,
     , , , , ,
(F12.6,F12.6,F12.6,)
*CFCLOS

FINISH
```

Codice C.5: Series B: APDL for SED approach

```
/CLEAR, NOSTART

! GEOMETRICAL PARAMETERS

MATERIAL= 2   ! 1= STEEL 2=ADI
b= 14.78    ! Width of the weld bead
h= 1.86     ! Height of the weld bead
t= 5.02     ! Half-thickness of the
    specimen
ltot= 270   ! total length of the
    specimen
alfa_S355= 135  ! Toe opening angle
    on steel side
alfa_ADI=135  ! Toe opening angle on
    ADI side
Ro_S355=0.28  ! Control radius for
    steel
Ro_ADI=0.55   ! Control radius for
    ADI
Ro_su_d= 5    ! Parameter for mesh
    refinement
load= 1     ! 1=axial loading, 2=
    four-point-bending loading

*CFOPEN, 'RESULTS_SED_BUTT_FULL','csv
    ',,APPEND
*VWRITE, 'h','b','t','alfa_S355','
    alfa_ADI','materiale','carico','d
    ','SED_toe1*10^6', 'SED_ADI*10^6
%c,%c,%c,%c,%c,%c,%c,%c,%c,%c,%c,
*CFCLOS

pi= 4*atan(1) ! pi greco
c_S355=h/tan((180-alfa_S355)*pi/180)
c_ADI=h/tan((180-alfa_ADI)*pi/180)

!---------------------
/PREP7
!ELEMENT TYPE
ET,1,PLANE182

KEYOPT,1,1,3
KEYOPT,1,3,2
KEYOPT,1,6,0

!MATERIAL

MPTEMP,,,,,,,,
MPTEMP,1,0
MPDATA,EX,1,,206000
MPDATA,PRXY,1,,0.3

MPTEMP,,,,,,,,
MPTEMP,1,0
MPDATA,EX,2,,168000
MPDATA,PRXY,2,,0.27

K,1,0,0,0,
K,2,ltot,0,0,
K,3,ltot,t,0,
K,4,ltot/2+b/2,t,0,
K,5,ltot/2+b/2-c_ADI,t+h,0,
K,6,ltot/2, t+h,0,
K,7,ltot/2-b/2+c_S355,t+h,0,
K,8,ltot/2-b/2,t,0,
K,9,0,t,0

LSTR,1,2
LSTR,2,3
LSTR,3,4
LSTR,4,5
LSTR,5,6
LSTR,6,7
LSTR,7,8
LSTR,8,9
LSTR,9,1

NUMSTR,line,11

!control volume ADI with radius
kwpave,4
CSYS,4
K,103,-Ro_ADI,0,0,
K,102,+Ro_ADI,0,0,
K,101,0,Ro_ADI,0,
K,100,0,-Ro_ADI,0,

LARC,103,100,4,Ro_ADI,
LARC,100,102,4,Ro_ADI,
LARC,101,103,4,Ro_ADI,
LSBL,4,13,,,KEEP
LSBL,3,12,,,KEEP
LSBL,13,14,,,KEEP
LDELE,18
!control volume steel with radius
    0.28mm

kwpave,8
CSYS,4
K,104,-Ro_S355,0,0,
K,105,0,-Ro_S355,0,
K,106,+Ro_S355,0,0,
K,107,0,+Ro_S355,0,

LARC,104,105,8,Ro_S355,
LARC,105,106,8,Ro_S355,
LARC,106,107,8,Ro_S355,
LSBL,7,20,,,KEEP
LSBL,8,13,,,KEEP
LSBL,20,22,,,KEEP
LDELE,26
LCOMB,13,18,
LCOMB,13,25
LCOMB,11,12,
LCOMB,11,19

AL,13,23,22
AL,11,14,17
LSEL,S,,,1,2
LSEL,A,,,5,6
LSEL,A,,,11,
LSEL,A,,,13
LSEL,A,,,15,16
LSEL,A,,,9
LSEL,A,,,21
LSEL,A,,,24
```

```
AL,ALL
ALLSEL
NUMSTR,line,1

!Generation of the MESH

TYPE, 1
MAT, MATERIALE
REAL,
ESYS, 0
SECNUM,
d= Ro_ADI/Ro_su_d ! globa element
     size mesh

ESIZE,d,0
MSHKEY, 0
AMESH, 1

ESIZE,d,0
MSHKEY, 0
AMESH, 2

d1= 10*Ro_ADI/Ro_su_d


ESIZE,d1,0
MSHKEY,0
AMESH,3
! BOUNDARY CONDITIONS AND LOADS
DL,9,,UX
DK,1,,,,0,UY

*IF, carico, EQ,1,THEN
  SFL, 2,PRES, -1
  DL,1,,SYMM
*ELSE
  SFL,2,PRES, 0, -1
  DL,1,,ASYM
*ENDIF

FINISH
! SOLUTION
/SOL
SOLVE
FINISH

! POST-PROCESSING

/POST1
ASLL,S
ASEL,S, , ,1,
ESLA,S
AVPRIN,0, ,
ETABLE, ,SENE,
AVPRIN,0, ,
ETABLE, ,VOLU,
SSUM
PRETAB,SENE,VOLU


*GET, ENERGY_S355,SSUM,0,ITEM,SENE
*GET,VOLU_S355,SSUM, 0,ITEM, VOLU

SED_S355= ENERGY_S355/VOLU_S355

ASLL,S
ASEL,S, , ,2,
ESLA,S
AVPRIN,0, ,
ETABLE, ,SENE,
AVPRIN,0, ,
ETABLE, ,VOLU,
SSUM
PRETAB,SENE,VOLU


*GET, ENERGY_ADI,SSUM,0,ITEM,SENE
*GET,VOLU_ADI,SSUM, 0,ITEM, VOLU

SED_ADI= ENERGY_ADI/VOLU_ADI

*CFOPEN, 'RESULTS_SED_BUTT_FULL','txt
     ',,APPEND
*VWRITE, 'h','b','t','alfa_S355','
     alfa_ADI','material','load','d','
     Ro','SED_ADI*10^6'
(' ',A8' ',A8' ',A8' ',A8' ',A8' ',A8
     ' ',A8' ',A8' ',A8' ',A8' ',A8'
     ')
*VWRITE, h,b,t,alfa_S355,alfa_ADI,
     material,load,d,Ro_ADI,SED_ADI
     *10**6
(F8.2,' ',F8.2,' ',F8.2,' ',F8.2,' ',
     F8.2,' ',F8.2,' ',F8.2,' ',F8.2,'
      ',F8.2,' ',F10.4,' ',F10.4,' ',)
*CFCLOS
FINISH
```

Codice C.6: Series B: APDL for PSM approach

```
/CLEAR, NOSTART

!Geometrical parameters
MATERIAL= 2   ! 1= STEEL 2=ADI
b= 14.78    ! Width of the weld bead
h= 1.86     ! Height of the weld bead
t= 5.02     ! Half-thickness of the
     specimen
ltot= 270   ! Total lenght of the
     specimen
alfa_S355=135 ! Toe opening angle on
     steel side
alfa_ADI=140.34 !  Toe opening angle
     on ADI side
t_su_d= 8   ! Parameter for mesh
     refinement
load= 1     ! 1=axial loading, 2=
     four-point-bending loading

pi= 4*atan(1)
c_S355=h/tan((180-alfa_S355)*pi/180)
c_ADI=h/tan((180-alfa_ADI)*pi/180)

/PREP7
!ELEMENT TYPE

ET,1,PLANE182

KEYOPT,1,1,3
KEYOPT,1,3,2
KEYOPT,1,6,0

!MATERIAL

MPTEMP,,,,,,,,
MPTEMP,1,0
MPDATA,EX,1,,206000
MPDATA,PRXY,1,,0.3

MPTEMP,,,,,,,,
MPTEMP,1,0
MPDATA,EX,2,,168000
MPDATA,PRXY,2,,0.27

K,1,0,0,0,
K,2,ltot,0,0,
K,3,ltot,t,0,
K,4,ltot/2+b/2,t,0,
```

```
K,5,ltot/2+b/2-c_ADI,t+h,0,
K,6,ltot/2, t+h,0,
K,7,ltot/2-b/2+c_S355,t+h,0,
K,8,ltot/2-b/2,t,0,
K,9,0,t,0


LSTR,1,2
LSTR,2,3
LSTR,3,4
LSTR,4,5
LSTR,5,6
LSTR,6,7
LSTR,7,8
LSTR,8,9
LSTR,9,1

AL,1,2,3,4,5,6,7,8,9,

CIRCLE,4, , , ,360,1,
LCOMB,11,12
LSBL,11,4,KEEP
LDELE,10
LDELE,13
LDIV,12, , ,2,0
LSTR,4,13
LDELE,10,
LDELE,12
CSKP,11,0,4,13,10,1,1

!Generation of the MESH

TYPE, 1
MAT, MATERIAL
REAL,
ESYS, 0
SECNUM,

d= t/t_su_d! globa element size mesh

ESIZE,d,0
MSHKEY, 0
AMESH, 1

! BOUNDARY CONDITIONS AND LOADS
DL,9,,UX
DK,1,,,,0,UY

*IF, carico, EQ,1,THEN
  SFL, 2,PRES, -1
  DL,1,,SYMM
*ELSE
  SFL,2,PRES, 0, -1
  DL,1,,ASYM
*ENDIF

FINISH

KWPAVE,       4
WPROTA,-(360-alfa_ADI)/2,0 , 0
CSWPLA, 11, 0, ,
CSYS,11,

! solution
/SOL
SOLVE
FINISH

! POST-PROCESSING

/POST1

RSYS,11
PLNSOL, S,Y, 0,1.0
/AUTO,1
/REPLOT
/REP,FAST
/ui, copy,save,bmp,full,color,reverse
     ,portrait, no

KSEL,S, , ,4
NSLK,R
NSORT,S,Y,0,0,1
*GET,psm,SORT,0,MAX
ALLS,ALL


*CFOPEN, 'RESULTS_PSM_BUTT_FULL','txt
     ',,APPEND
*VWRITE, 'h','alfa_ADI','t','b','
     material','load','d','PSM',
(' ',A8' ',A8' ',A8' ',A8' ',A8' ',A8
     ' ',A8' ',A8' ',)
*VWRITE, h,alfa_ADI,t,b,material,load
     ,d,psm
(F8.2,' ',F8.2,' ',F8.2,' ',F8.2,' ',
     F8.2,' ',F8.2,' ',F8.2,' ',F10
     .4,' ',)
*CFCLOS

FINISH
```

C.3 APDL codes for series C

Codice C.7: Series C: APDL for N-SIF approach

```
/CLEAR, NOSTART

!GEOMETRICAL PARAMETERS

MATERIAL= 2     ! 1= STEEL 2=ADI
R_CICLO=2       ! NOMINAL LOAD RATIO
      1=0.05 2=0.5
*IF, R_CICLO, EQ,1,THEN
  R=0.05
  h=9.707       ! Height of the weld
     bead R=0,05
  t= 5.09       ! Half-thickness of
     the specimen R=0,05
  alfa_ADI=136.788  ! Toe opening
     angle on ADI side ADI R=0,05
*ELSE
  R=0.5
  h= 11.267   ! Height of the weld
     bead R=0,5
  t= 5.009    ! Half-thickness of the
      specimen R=0,5
  alfa_ADI=136.53   ! Toe opening
     angle on ADI side R=0,5
*ENDIF

ltot= 300     ! Total length of the
     specimen
h_irr= 40
t_irr= 5    ! Half-thickness of the
     steel plate
Ro_S355=0.28  ! Control radius for
     steel
Ro_ADI=0.28   ! Control radius for
     ADI
Ro_su_d= 5    ! Parameter fo mesh
     refinement
```

```
load= 1     ! 1=axial loading, 2=
     four-point-bending loading

pi= 4*atan(1) ! pi greco
c_S355=h/tan((180-alfa_S355)*pi/180)
c_ADI=h/tan((180-alfa_ADI)*pi/180)

!---------------------------

/PREP7
!ELEMENT TYPE
ET,1,PLANE182

KEYOPT,1,1,3
KEYOPT,1,3,2
KEYOPT,1,6,0

!MATERIAL

MPTEMP,,,,,,,,
MPTEMP,1,0
MPDATA,EX,1,,206000
MPDATA,PRXY,1,,0.3

MPTEMP,,,,,,,,
MPTEMP,1,0
MPDATA,EX,2,,168000
MPDATA,PRXY,2,,0.27

CSYS,4
K,1,0,0,0,
K,2,ltot/2,0,0,
K,3,ltot/2,t,0,
K,4,t_irr+C_ADI,t,0,
K,5,t_irr,t+h,0,
K,6,t_irr,h_irr,0,
K,7,0,h_irr,0,

LSTR,1,2
LSTR,2,3
LSTR,3,4
LSTR,4,5
LSTR,5,6
LSTR,6,7
LSTR,7,1

!control volume ADI with radius 0.28
     mm
kwpave,4
CSYS,4
K,103,-0.28,0,0,
K,102,+0.28,0,0,
K,101,0,0.28,0,
K,100,0,-0.28,0,



LARC,103,100,4,0.28,
LARC,100,102,4,0.28,
LARC,101,103,4,0.28,
LSBL,3,9,,,KEEP
LSBL,4,10,,,KEEP
LSBL,10,3,,,KEEP
LDELE,4
LCOMB,14,8,
LCOMB,8,9
LDIV,8, , ,2,0
LSTR,4,9
!control volume ADI with radius
     0,0001
kwpave,4
CSYS,4
K,104,-0.0001,0,0,
K,105,0,-0.0001,0,
K,106,+0.0001,0,0,
K,107,0,0.0001,0,

LARC,104,105,4,0.0001,
LARC,105,106,4,0.0001,
LARC,104,107,4,0.0001,
LSBL,10,9,,,KEEP
LCOMB,14,17,
LCOMB,15,16
LSBL,12,14,,,KEEP
LSBL,3,15,,,KEEP
LSBL,15,12,,,KEEP
LDELE,18
LSBL,9,3,,,KEEP

!root
kwpave,1
CSYS,4
K,20,0,t,0
K,21,t_irr,t,0
K,22,0,t-0.01,0
LSTR,20,21
LSTR,21,22
LSBL,7,9,,,KEEP
LSBL,20,19,,,KEEP
LDELE,22


AL,3,15,12
AL,14,15,10
AL,3,17,8,18
AL,14,18,4,16

LSEL,S,,,1,2,
LSEL,A,,,4,
LSEL,A,,,8,9
LSEL,A,,,5,7,
LSEL,A,,,11,
LSEL,A,,,13,
LSEL,A,,,19,
LSEL,A,,,21,
AL,ALL
ALLSEL

!Generation of the mesh

TYPE, 1
MAT, MATERIAL
REAL,
ESYS, 0
SECNUM,

KSCON,4,0.000001,0,16,2,

LESIZE,12, , ,5,1, , , ,1
LESIZE,15, , ,5,1, , , ,1
LESIZE,10, , ,5,1, , , ,1
LESIZE,17, , ,50,1/2000, , , ,1
LESIZE,18, , ,50,1/2000, , , ,1
LESIZE,16, , ,50,1/2000, , , ,1
LESIZE,8, , ,8,1, , , ,1
LESIZE,4, , ,8,1, , , ,1
LESIZE,3, , ,8,1, , , ,1
LESIZE,14, , ,8,1, , , ,1

MSHKEY, 1
AMESH,3

MSHKEY, 1
AMESH,4

MSHKEY,0
AMESH,1

MSHKEY,0
AMESH,2
```

```
d1= 10*Ro_ADI/Ro_su_d
ESIZE,d1,0
MSHKEY, 0
AMESH,5

! BOUNDARY CONDITIONS AND LOADS
DL,2,,UY
DK,1,,,,0,UX
*IF, load, EQ,1,THEN
  SFL, 2,PRES, -1
  DL,1,,SYMM
  DL,7,,SYMM
  DL,21,,SYMM
*ELSE
  SFL,2,PRES, 0, -1
  DL,1,,ASYM
  DL,7,,SYMM
  DL,21,,SYMM
*ENDIF

FINISH

CSKP,11,0,4,10,106,1,1,
CSYS,11,

!SOLUTION
/SOL
SOLVE
FINISH
! POST-PROCESSING

/POST1
RSYS,11
LPLOT
LSEL,S, , ,       18
NSLL,S
NPLOT
PRNSOL,S,COMP

*VGET,sel,NODE, ,NSEL,,
*VGET,posx,NODE, ,LOC,X
*VGET,posy,NODE, ,LOC,Y
*VGET,stress,NODE, ,S,Y
*CFOPEN,'RESULTS_NSIF_NLC_CRUCIFURM
    ','txt ',,APPEND
*VWRITE, 'h','t','alfa_ADI','material
    ','load','d1',
(' ',A8' ',A8' ',A8' ',A9' ',A8' ')
*VWRITE, h,b,t,alfa_ADI,material,load
    ,d1,
 (F8.2,' ',F8.2,' ',F8.2,' ',F8.2,'
    ',F8.2,' ',F8.2,' ',F8.2,' ',F8
    .2,' ',)
 *VWRITE,'posx','posy','stress',
(A8' ',A8' ',A8' ',)
*VMASK,sel
*VWRITE,posx(1),posy(1),stress(1) , ,
    , , , , ,
(F12.6,F12.6,F12.6)
*CFCLOS

FINISH
```

Codice C.8: Series C: APDL for SED approach

```
/CLEAR, NOSTART

!GEOMETRICAL PARAMETERS

MATERIAL= 2   ! 1= STEEL 2=ADI
R_CICLO=2 !  NOMINAL LOAD RATIO
    1=0.05 2=0.5
*IF, R_CICLO, EQ,1,THEN
  R=0.05
  h=9.707       ! Height of the weld
    bead R=0,05
  t= 5.09       ! Half-thickness of
    the specimen R=0,05
  alfa_ADI=136.788  ! Toe opening
    angle on ADI side ADI R=0,05
*ELSE
  R=0.5
  h= 11.267     ! Height of the weld
    bead R=0,5
  t= 5.009      ! Half-thickness of
    the specimen R=0,5
  alfa_ADI=136.53   ! Toe opening
    angle on ADI side R=0,5
*ENDIF

ltot= 300   ! Total length of the
    specimen
h_irr= 40
t_irr= 5  ! Total length of the
    specimen

Ro_S355=0.28  ! Control radius for
    steel
Ro_ADI=0.55   ! Control radius for
    ADI
Ro_su_d= 5    ! Parameter for mesh
    refinement
load= 1     ! 1=axial loading, 2=
    four-point-bending loading

pi= 4*atan(1) ! pi greco
c_ADI=h/tan((180-alfa_ADI)*pi/180)

!-----------------------------
/PREP7
!ELEMENT TYPE
ET,1,PLANE182

KEYOPT,1,1,3
KEYOPT,1,3,2
KEYOPT,1,6,0

!MATERIAL

MPTEMP,,,,,,,,
MPTEMP,1,0
MPDATA,EX,1,,206000
MPDATA,PRXY,1,,0.3

MPTEMP,,,,,,,,
MPTEMP,1,0
MPDATA,EX,2,,168000
MPDATA,PRXY,2,,0.27

K,1,0,0,0,
K,2,ltot/2,0,0,
K,3,ltot/2,t,0,
K,4,t_irr+C_ADI,t,0,
K,5,t_irr,t+h,0,
K,6,t_irr,h_irr,0,
K,7,0,h_irr,0,

LSTR,1,2
LSTR,2,3
LSTR,3,4
LSTR,4,5
LSTR,5,6
LSTR,6,7
LSTR,7,1

!control volume ADI with radius 0.28
    mm
```

```
kwpave,4
CSYS,4
K,103,-Ro_ADI,0,0,
K,102,+Ro_ADI,0,0,
K,101,0,Ro_ADI,0,
K,100,0,-Ro_ADI,0,

LARC,103,100,4,Ro_ADI,
LARC,100,102,4,Ro_ADI,
LARC,101,103,4,Ro_ADI,
LSBL,3,9,,,KEEP
LSBL,4,10,,,KEEP
LSBL,10,3,,,KEEP
LDELE,4
LCOMB,14,8,
LCOMB,8,9
LDIV,8, , ,2,0
LSTR,4,9

kwpave,1
CSYS,4
K,20,0,t,0
K,21,t_irr,t,0
K,22,0,t-0.01,0
LSTR,20,21
LSTR,21,22
LSBL,7,14,,,KEEP
LSBL,16,10,,,KEEP
LDELE,17

AL,3,8,9
AL,9,4,12
LSEL,S,,,1,2
LSEL,A,,,4,8
LSEL,A,,,10,11
LSEL,A,,,13,15
AL,ALL
ALLSEL

!Generation of the mesh

TYPE, 1
MAT, MATERIAL
REAL,
ESYS, 0
SECNUM,

d= Ro_ADI/Ro_su_d ! globa element
     size mesh

ESIZE,d,0
MSHKEY,0
AMESH,1
ESIZE,d,0
MSHKEY,0
AMESH,2

d1= 10*Ro_ADI/Ro_su_d ! globa element
      size mesh
ESIZE,d1,0
MSHKEY, 0
AMESH,3

! BOUNDARY CONDITIONS AND LOADS
DL,2,,UY
DK,1,,,,0,UX
*IF, load, EQ,1,THEN
  SFL, 2,PRES, -1
  DL,1,,SYMM
  DL,7,,SYMM
  DL,15,,SYMM
*ELSE
  SFL,2,PRES, 0, -1
  DL,1,,ASYM
  DL,7,,SYMM
  DL,15,,SYMM
*ENDIF

FINISH

!solution
/SOL
SOLVE
FINISH

! POST-PROCESSING

/POST1
ASLL,S
ASEL,S, , ,1,2
ESLA,S
AVPRIN,0, ,
ETABLE, ,SENE,
AVPRIN,0, ,
ETABLE, ,VOLU,
SSUM
PRETAB,SENE,VOLU

*GET,ENERGY_ADI,SSUM,0,ITEM,SENE
*GET,VOLU_ADI,SSUM, 0,ITEM, VOLU

SED_ADI=ENERGY_ADI/VOLU_ADI

*CFOPEN, 'RESULTS_SED_CRUCIFURM','txt
     ',,APPEND
*VWRITE, 'h','alfa_ADI','t','R','
     material','load','d','Ro_ADI','
     SED_ADI',
(' ',A8' ',A8' ',A8' ',A8' ',A8
     ' ',A8' ',A8' ',)
*VWRITE, h,alfa_ADI,t,material,R,load
     ,d,Ro_ADI,SED_ADI*10**6,
(F8.2,' ',F8.2,' ',F8.2,' ',F8.2,' ',
     F8.2,' ',F8.2,' ',F10.4,' ',F10
     .4,' ',F10.8,' ',)
*CFCLOS
FINISH
```

Codice C.9: Series C: APDL for PSM approach

```
/CLEAR, NOSTART

!GEOMETRICAL PARAMETERS

MATERIAL= 2   ! 1= STEEL 2=ADI
R_CICLO=2 !  NOMINAL LOAD RATIO
     1=0.05 2=0.5

*IF, R_CICLO, EQ,1,THEN
  R=0.05
  h=9.707       ! Height of the weld
     bead R=0,05
  t= 5.09       ! Half-thickness of
     the specimen R=0,05
  alfa_ADI=136.788  ! Toe opening
     angle on ADI side ADI R=0,05
*ELSE
  R=0.5
  h= 11.267     ! Height of the weld
     bead R=0,5
  t= 5.009      ! Half-thickness of
     the specimen R=0,5
  alfa_ADI=136.53   ! Toe opening
     angle on ADI side R=0,5
*ENDIF
```

```
ltot= 300     ! Total length of the
    specimen
h_irr= 40   ! Height of the steel
    plate
t_irr= 5    ! Half-thickness of the
    steel plate

t_su_d= 3   ! Parameter for mesh
    refinement
load= 1     ! 1=axial loading, 2=
    four-point-bending loading

pi= 4*atan(1) ! pi greco
c_S355=h/tan((180-alfa_S355)*pi/180)
c_ADI=h/tan((180-alfa_ADI)*pi/180)

!------------------------
/PREP7
!ELEMENT TYPE
ET,1,PLANE182

KEYOPT,1,1,3
KEYOPT,1,3,2
KEYOPT,1,6,0

!MATERIAL

MPTEMP,,,,,,,,
MPTEMP,1,0
MPDATA,EX,1,,206000
MPDATA,PRXY,1,,0.3

MPTEMP,,,,,,,,
MPTEMP,1,0
MPDATA,EX,2,,168000
MPDATA,PRXY,2,,0.27

K,1,0,0,0,
K,2,ltot/2,0,0,
K,3,ltot/2,t,0,
K,4,t_irr+C_ADI,t,0,
K,5,t_irr,t+h,0,
K,6,t_irr,h_irr,0,
K,7,0,h_irr,0,


LSTR,1,2
LSTR,2,3
LSTR,3,4
LSTR,4,5
LSTR,5,6
LSTR,6,7
LSTR,7,1

kwpave,1
CSYS,4
K,20,0,t,0
K,21,t_irr,t,0
K,22,0,t-0.01,0
LSTR,20,21
LSTR,21,22
LSBL,7,8,,,KEEP
LSBL,10,9,,,KEEP
LDELE,12

!generazione delle aree
LSEL,S,,,1,11
AL,ALL
ALLSEL

CIRCLE,4, , , ,360,1,
LCOMB,12,13
LSBL,12,4,KEEP
LDELE,10
LDELE,14
LDIV,13, , ,2,0
LSTR,4,11
LDELE,10,
LDELE,13,
CSKP,11,0,4,11,8,1,1

!GENERATION OF THE MESH

TYPE, 1
MAT, MATERIAL
REAL,
ESYS, 0
SECNUM,

d= t/t_su_d! globa element size mesh

ESIZE,d,0
MSHKEY,0
AMESH,1

! BOUNDARY CONDITIONS AND LOADS

DL,2,,UY
DK,1,,,,0,UX
*IF, load, EQ,1,THEN
  SFL, 2,PRES, -1
  DL,1,,SYMM
  DL,7,,SYMM
  DL,11,,SYMM
*ELSE
  SFL,2,PRES, 0, -1
  DL,1,,ASYM
  DL,7,,SYMM
  DL,11,,SYMM
*ENDIF

FINISH

KWPAVE,       4
WPROTA,-(360-alfa_ADI)/2,0 , 0
CSWPLA, 11, 0, ,
CSYS,11,

! SOLUTION
/SOL
SOLVE
FINISH

! POST-PROCESSING

/POST1

RSYS,11
PLNSOL, S,Y, 0,1.0

KSEL,S, , ,4
NSLK,R
NSORT,S,Y,0,0,1
*GET,psm,SORT,0,MAX
ALLS,ALL

*CFOPEN, 'RESULTS_PSM_CRUCIFURM','txt
     ',,APPEND
*VWRITE, 'h','alfa_ADI','t','material
     ','R','LOAD','d','PSM',
(' ',A8' ',A8' ',A8' ',A8' ',A8' ',A8
     ' ',A8' ',A8' ',)
*VWRITE, h,alfa_ADI,t,material,R,load
     ,d,psm
(F8.2,' ',F8.2,' ',F8.2,' ',F8.2,' ',
     F8.2,' ',F8.2,' ',F8.2,' ',F10
     .4,' ',)
*CFCLOS
```

```
FINISH
```

C.4 APDL codes for series D

Codice C.10: Series D: APDL for N-SIF approach

```
/CLEAR, NOSTART

!Geometrical parameters

MATERIAL= 2   ! 1= STEEL 2=ADI
h= 10     ! Height of the weld bead
ltot= 300   ! Total length of the
     specimen
h_irr= 40   ! Total height of the
     specimen
t= 10       !Thickness of the
     specimen
t_irr= 5    ! Total length of the
     specimen
alfa_S355= 135  ! Toe opening angle
     on steel side
alfa_ADI=135  ! Toe opening angle on
     ADI side
Ro_S355=0.28  ! Control radius for
     steel
Ro_ADI=0.55   ! Control radius for
     ADI
Ro_su_d= 5    ! Parameter for mesh
     refinement
load= 1     ! 1=axial loading, 2=
     four-point-bending loading

pi= 4*atan(1) ! pi greco
c_S355=h/tan((180-alfa_S355)*pi/180)
c_ADI=h/tan((180-alfa_ADI)*pi/180)

!------------------------
/PREP7
!ELEMENT TYPE
ET,1,PLANE182

KEYOPT,1,1,3
KEYOPT,1,3,2
KEYOPT,1,6,0
!material
MPTEMP,,,,,,,,
MPTEMP,1,0
MPDATA,EX,1,,206000
MPDATA,PRXY,1,,0.3

MPTEMP,,,,,,,,
MPTEMP,1,0
MPDATA,EX,2,,168000
MPDATA,PRXY,2,,0.27

CSYS,4
K,1,0,0,0,
K,2,ltot/2,0,0,
K,3,ltot/2,t,0,
K,4,t_irr+C_S355,t,0,
K,5,t_irr,t+h,0,
K,6,t_irr,h_irr,0,
K,7,0,h_irr,0,


LSTR,1,2
LSTR,2,3
LSTR,3,4
LSTR,4,5
LSTR,5,6
LSTR,6,7
LSTR,7,1

!control volume ADI
kwpave,4
CSYS,4
K,103,-0.28,0,0,
K,102,+0.28,0,0,
K,101,0,0.28,0,
K,100,0,-0.28,0,

 LARC,103,100,4,0.28,
LARC,100,102,4,0.28,
LARC,101,103,4,0.28,
LSBL,3,9,,,KEEP
LSBL,4,10,,,KEEP
LSBL,10,3,,,KEEP
LDELE,4
LCOMB,14,8,
LCOMB,8,9
LDIV,8, , ,2,0
LSTR,4,9

!control volume ADI
kwpave,4
CSYS,4
K,104,-0.0001,0,0,
K,105,0,-0.0001,0,
K,106,+0.0001,0,0,
K,107,0,0.0001,0,

LARC,104,105,4,0.0001,
LARC,105,106,4,0.0001,
LARC,104,107,4,0.0001,
LSBL,10,9,,,KEEP
LCOMB,14,17,
LCOMB,15,16
LSBL,12,14,,,KEEP
LSBL,3,15,,,KEEP
LSBL,15,12,,,KEEP
LDELE,18
LSBL,9,3,,,KEEP

!root
kwpave,1
CSYS,4
K,20,0,t,0
K,21,t_irr,t,0
K,22,0,t-0.01,0
LSTR,20,21
LSTR,21,22
LSBL,7,9,,,KEEP
LSBL,20,19,,,KEEP
LDELE,22

AL,3,15,12
AL,14,15,10
AL,3,17,8,18
AL,14,18,4,16

LSEL,S,,,1,2,
LSEL,A,,,4,
LSEL,A,,,8,9
LSEL,A,,,5,7,
LSEL,A,,,11,
LSEL,A,,,13,
LSEL,A,,,19,
LSEL,A,,,21,
AL,ALL
ALLSEL
!Generation of the mesh
TYPE, 1
MAT, MATERIAL
```

```
REAL,
ESYS, 0
SECNUM,


KSCON,4,,0,16,

LESIZE,12, , ,5,1, , , ,1
LESIZE,15, , ,5,1, , , ,1
LESIZE,10, , ,5,1, , , ,1
LESIZE,17, , ,50,1/2000, , , ,1
LESIZE,18, , ,50,1/2000, , , ,1
LESIZE,16, , ,50,1/2000, , , ,1
LESIZE,8, , ,8,1, , , ,1
LESIZE,4, , ,8,1, , , ,1
LESIZE,3, , ,8,1, , , ,1
LESIZE,14, , ,8,1, , , ,1

MSHKEY, 1
AMESH,3

MSHKEY, 1
AMESH,4

MSHKEY,0
AMESH,1

MSHKEY,0
AMESH,2

d1= 10*Ro_S355/Ro_su_d
ESIZE,d1,0
MSHKEY, 0
AMESH,5

! BOUNDARY CONDITIONS AND LOADS
DL,1,,UY
DK,2,,,,0,UY
*IF, load, EQ,1,THEN
  SFL, 2,PRES, -1
  DL,7,,SYMM
  DL,21,,SYMM
*ELSE
  SFL,2,PRES, 1, -1
  DL,7,,SYMM
  DL,21,,SYMM
*ENDIF

FINISH

CSKP,11,0,4,10,106,1,1,
CSYS,11,

!SOLUTION

/SOL
SOLVE
FINISH

! POST-PROCESSING

/POST1
RSYS,11

LPLOT
LSEL,S, , ,      18
NSLL,S
NPLOT

PRNSOL,S,COMP

*VGET,sel,NODE, ,NSEL,,
*VGET,posx,NODE, ,LOC,X
*VGET,posy,NODE, ,LOC,Y
*VGET,stress,NODE, ,S,Y
*CFOPEN,'RESULTS_NSIF_D','csv',,
    APPEND
*VWRITE, 'h','t','alfa_S355','
    material','load','d1',
(' ',A8' ',A8' ',A8' ',A9' ',A8' ')
*VWRITE, h,b,t,alfa_S355,material,
    load,d1,
 (F8.2,' ',F8.2,' ',F8.2,' ',F8.2,'
    ',F8.2,' ',F8.2,' ',F8.2,' ',F8
    .2,' ',)
*VMASK,sel
*VWRITE,'posx','posy','stress',
(A8' ',A8' ',A8' ',)
*VMASK,sel
*VWRITE,posx(1),
%G
*VMASK,sel
*VWRITE,stress(1)
%G
*CFCLOS

FINISH
```

Codice C.11: Series D: APDL for SED approach

```
/CLEAR, NOSTART

!Geometrical parameters

MATERIAL= 2   ! 1= STEEL 2=ADI
h= 10     ! Height of the weld bead
ltot= 300   ! Total length of the
    specimen
h_irr= 40   ! Total height of the
    specimen
t= 10       !Thickness of the
    specimen
t_irr= 5    ! Total length of the
    specimen
alfa_S355= 135  ! Toe opening angle
    on steel side
alfa_ADI=135  ! Toe opening angle on
    ADI side
Ro_S355=0.28  ! Control radius for
    steel
Ro_ADI=0.55   ! Control radius for
    ADI
Ro_su_d= 5    ! Parameter for mesh
    refinement
load= 1     ! 1=axial loading, 2=
    four-point-bending loading
!------------------------------
*CFOPEN, 'RESULTS_SED_CRUCIFURM','txt
    ',,APPEND
*VWRITE, 'h','alfa_ADI','t','material
    ','load','Ro_ADI','d','SED_toe1
    *10^6',
(' ',A8' ',A8' ',A8' ',A8' ',A8' ',A8
    ' ',A8' ',A8' ',)
*CFCLOS
!------------------------------

pi= 4*atan(1) ! pi greco
c_S355=h/tan((180-alfa_S355)*pi/180)
c_ADI=h/tan((180-alfa_ADI)*pi/180)

/PREP7
!ELEMENT TYPE
ET,1,PLANE182

KEYOPT,1,1,3
KEYOPT,1,3,2
KEYOPT,1,6,0
```

```
!material

MPTEMP,,,,,,,,
MPTEMP,1,0
MPDATA,EX,1,,206000
MPDATA,PRXY,1,,0.3

MPTEMP,,,,,,,,
MPTEMP,1,0
MPDATA,EX,2,,168000
MPDATA,PRXY,2,,0.27

K,1,0,0,0,
K,2,ltot/2,0,0,
K,3,ltot/2,t,0,
K,4,t_irr+C_ADI,t,0,
K,5,t_irr,t+h,0,
K,6,t_irr,h_irr,0,
K,7,0,h_irr,0,

LSTR,1,2
LSTR,2,3
LSTR,3,4
LSTR,4,5
LSTR,5,6
LSTR,6,7
LSTR,7,1

!control volume steel
kwpave,4
CSYS,4
K,103,-Ro_S355,0,0,
K,102,+Ro_S355,0,0,
K,101,0,Ro_S355,0,
K,100,0,-Ro_S355,0,

LARC,103,100,4,Ro_S355,
LARC,100,102,4,Ro_S355,
LARC,101,103,4,Ro_S355,
LSBL,3,9,,,KEEP
LSBL,4,10,,,KEEP
LSBL,10,3,,,KEEP
LDELE,4
LCOMB,14,8,
LCOMB,8,9
LDIV,8, , ,2,0
LSTR,4,9

kwpave,1
CSYS,4
K,20,0,t,0
K,21,t_irr,t,0
K,22,0,t-0.01,0
LSTR,20,21
LSTR,21,22
LSBL,7,14,,,KEEP
LSBL,16,10,,,KEEP
LDELE,17

AL,3,8,9
AL,9,4,12
LSEL,S,,,1,2
LSEL,A,,,4,8
LSEL,A,,,10,11
LSEL,A,,,13,15
AL,ALL
ALLSEL

CSYS,0
!Generation of the mesh
TYPE, 1
MAT, MATERIAL
REAL,
ESYS, 0
SECNUM,

d= Ro_ADI/Ro_su_d ! globa element
    size mesh

ESIZE,d,0
MSHKEY,0
AMESH,1
ESIZE,d,0
MSHKEY,0
AMESH,2

d1= 10*Ro_ADI/Ro_su_d ! globa element
     size mesh
ESIZE,d1,0
MSHKEY, 0
AMESH,3

! BOUNDARY CONDITIONS AND LOADS

DK,2,,,,0,UY
*IF, load, EQ,1,THEN
  SFL, 2,PRES, -1
  DL,7,,SYMM
  DL,15,,SYMM
*ELSE
  SFL,2,PRES, 1, -1
  DL,7,,SYMM
  DL,15,,SYMM
*ENDIF

FINISH

!SOLUTION
/SOL
SOLVE
FINISH

! POST-PROCESSING

/POST1
ASLL,S
ASEL,S, , ,1,2
ESLA,S
AVPRIN,0, ,
ETABLE, ,SENE,
AVPRIN,0, ,
ETABLE, ,VOLU,
SSUM
PRETAB,SENE,VOLU

*GET,ENERGY_ADI,SSUM,0,ITEM,SENE
*GET,VOLU_ADI,SSUM, 0,ITEM, VOLU

SED_ADI=ENERGY_ADI/VOLU_ADI

*CFOPEN, 'RESULTS_SED_D','txt',,
    APPEND
*VWRITE, h,alfa_ADI,t,material,load,
    Ro_ADI,d,SED_ADI*10**6
(F8.2,' ',F8.2,' ',F8.2,' ',F8.2,' ',
    F8.2,' ',F8.2,' ',F8.2,' ',F10
    .4,' ',)
*CFCLOS
FINISH
```

Codice C.12: Series D: APDL for PSM approach

```
/CLEAR, NOSTART

!Geometrical parameters

MATERIAL= 2   ! 1= STEEL 2=ADI
```

```
h= 10     ! Height of the weld bead
ltot= 300   ! Total length of the
     specimen
h_irr= 40   ! Total height of the
     specimen
t= 10       !Thickness of the
     specimen
t_irr= 5    ! Total length of the
     specimen
alfa_S355= 135  ! Toe opening angle
     on steel side
alfa_ADI=135  ! Toe opening angle on
     ADI side
t_su_d= 3   ! Parameter for mesh
     refinement
load= 1     ! 1=axial loading, 2=
     four-point-bending loading

pi= 4*atan(1)
c_S355=h/tan((180-alfa_S355)*pi/180)
c_ADI=h/tan((180-alfa_ADI)*pi/180)
!------------------------------
/PREP7
!ELEMENT TYPE
ET,1,PLANE182
KEYOPT,1,1,3
KEYOPT,1,3,2
KEYOPT,1,6,0

!MATERIAL

MPTEMP,,,,,,,,
MPTEMP,1,0
MPDATA,EX,1,,206000
MPDATA,PRXY,1,,0.3

MPTEMP,,,,,,,,
MPTEMP,1,0
MPDATA,EX,2,,168000
MPDATA,PRXY,2,,0.27

K,1,0,0,0,
K,2,ltot/2,0,0,
K,3,ltot/2,t,0,
K,4,t_irr+C_ADI,t,0,
K,5,t_irr,t+h,0,
K,6,t_irr,h_irr,0,
K,7,0,h_irr,0,

LSTR,1,2
LSTR,2,3
LSTR,3,4
LSTR,4,5
LSTR,5,6
LSTR,6,7
LSTR,7,1

kwpave,1
CSYS,4
K,20,0,t,0
K,21,t_irr,t,0
K,22,0,t-0.01,0
LSTR,20,21
LSTR,21,22
LSBL,7,8,,,KEEP
LSBL,10,9,,,KEEP
LDELE,12

LSEL,S,,,1,11
AL,ALL
ALLSEL

!Generation of the mesh

TYPE, 1
MAT, MATERIAL
REAL,
ESYS, 0
SECNUM,

d= t/t_su_d! globa element size mesh

ESIZE,d,0
MSHKEY,0
AMESH,1

! BOUNDARY CONDITIONS AND LOADS
DL,1,,UY
DK,2,,,,0,UY
*IF, load, EQ,1,THEN
  SFL, 2,PRES, -1
  DL,7,,SYMM
  DL,11,,SYMM
*ELSE
  SFL,2,PRES, 1, -1
  DL,7,,SYMM
  DL,11,,SYMM
*ENDIF

FINISH

KWPAVE,       4
WPROTA,-(360-alfa_ADI)/2,0 , 0
CSWPLA, 11, 0, ,
CSYS,11,

! Solution
/SOL
SOLVE
FINISH

! POST-PROCESSING

/POST1

RSYS,11

KSEL,S, , ,4
NSLK,R
NSORT,S,Y,0,0,1
*GET,psm,SORT,0,MAX
ALLS,ALL

*CFOPEN, 'RESULTS_PSM_D','txt',,
     APPEND
*VWRITE, 'h','alfa_ADI','t','material
     ','load','d','PSM',
(' ',A8' ',A8' ',A8' ',A8' ',A8' ',A8
     ' ',A8' ',)
*VWRITE, h,alfa_ADI,t,material,load,d
     ,psm
(F8.2,' ',F8.2,' ',F8.2,' ',F8.2,' ',
     F8.2,' ',F8.2,' ',F10.4,' ',)
*CFCLOS

FINISH
```

C.5 APDL codes for series E

Codice C.13: Series E: APDL for N-SIF approach

```
/CLEAR, NOSTART

!Geometrical parameters
```

```
MATERIAL= 2   ! 1= STEEL 2=ADI
h= 10     ! Height of the weld bead
ltot= 300   ! Total length of the
    specimen
h_irr= 40   ! Total height of the
    specimen
t= 5.008    !Thickness of the
    specimen
t_irr= 5    ! Total length of the
    specimen
alfa_S355= 141.7 ! Toe opening angle
    on steel side
alfa_ADI=135  ! Toe opening angle on
    ADI side
Ro_S355=0.28  ! Control radius for
    steel
Ro_ADI=0.55   ! Control radius for
    ADI
Ro_su_d= 5    ! Parameter for mesh
    refinement
load= 1     ! 1=axial loading, 2=
    four-point-bending loading

pi= 4*atan(1) ! pi greco
c_S355=h/tan((180-alfa_S355)*pi/180)
c_ADI=h/tan((180-alfa_ADI)*pi/180)

!------------------------------
/PREP7
!ELEMENT TYPE
ET,1,PLANE182

KEYOPT,1,1,3
KEYOPT,1,3,2
KEYOPT,1,6,0

!material

MPTEMP,,,,,,,,
MPTEMP,1,0
MPDATA,EX,1,,206000
MPDATA,PRXY,1,,0.3

MPTEMP,,,,,,,,
MPTEMP,1,0
MPDATA,EX,2,,168000
MPDATA,PRXY,2,,0.27

CSYS,4
K,1,0,0,0,
K,2,ltot/2,0,0,
K,3,ltot/2,t,0,
K,4,t_irr+C_ADI,t,0,
K,5,t_irr,t+h,0,
K,6,t_irr,h_irr,0,
K,7,0,h_irr,0,


LSTR,1,2
LSTR,2,3
LSTR,3,4
LSTR,4,5
LSTR,5,6
LSTR,6,7
LSTR,7,1

!control volume ADI
kwpave,4
CSYS,4
K,103,-0.28,0,0,
K,102,+0.28,0,0,
K,101,0,0.28,0,
K,100,0,-0.28,0,
LARC,103,100,4,0.28,
LARC,100,102,4,0.28,
LARC,101,103,4,0.28,
LSBL,3,9,,,KEEP
LSBL,4,10,,,KEEP
LSBL,10,3,,,KEEP
LDELE,4
LCOMB,14,8,
LCOMB,8,9
LDIV,8, , ,2,0
LSTR,4,9

kwpave,4
CSYS,4
K,104,-0.0001,0,0,
K,105,0,-0.0001,0,
K,106,+0.0001,0,0,
K,107,0,0.0001,0,

LARC,104,105,4,0.0001,
LARC,105,106,4,0.0001,
LARC,104,107,4,0.0001,
LSBL,10,9,,,KEEP
LCOMB,14,17,
LCOMB,15,16
LSBL,12,14,,,KEEP
LSBL,3,15,,,KEEP
LSBL,15,12,,,KEEP
LDELE,18
LSBL,9,3,,,KEEP

!root
kwpave,1
CSYS,4
K,20,t_irr,,0
K,21,t_irr,t,0
K,22,t_irr-0.01,0,0
LSTR,20,21
LSTR,21,22
LSBL,1,9,,,KEEP
LSBL,20,19,,,KEEP
LDELE,22

AL,3,15,12
AL,14,15,10
AL,3,17,8,18
AL,14,18,4,16

LSEL,S,,,1,2,
LSEL,A,,,4,
LSEL,A,,,8,9
LSEL,A,,,5,7,
LSEL,A,,,11,
LSEL,A,,,13,
LSEL,A,,,19,
LSEL,A,,,21,
AL,ALL
ALLSEL


!Generation of the mesh

TYPE, 1
MAT, MATERIAL
REAL,
ESYS, 0
SECNUM,

KSCON,4,0.000001,0,16,2,

LESIZE,12, , ,5,1, , , ,1
LESIZE,15, , ,5,1, , , ,1
LESIZE,10, , ,5,1, , , ,1
LESIZE,17, , ,50,1/2000, , , ,1
LESIZE,18, , ,50,1/2000, , , ,1
```

```
LESIZE,16, , ,50,1/2000, , , ,1
LESIZE,8, , ,8,1, , , ,1
LESIZE,4, , ,8,1, , , ,1
LESIZE,3, , ,8,1, , , ,1
LESIZE,14, , ,8,1, , , ,1


MSHKEY, 1
AMESH,3

MSHKEY, 1
AMESH,4

MSHKEY,0
AMESH,1

MSHKEY,0
AMESH,2

d1= 10*Ro_ADI/Ro_su_d
ESIZE,d1,0
MSHKEY, 0
AMESH,5

! BOUNDARY CONDITIONS AND LOADS
DL,2,,UY
DK,1,,,,0,UX
*IF, load, EQ,1,THEN
  SFL, 2,PRES, -1
  DL,1,,SYMM
  DL,21,,SYMM
  DL,7,,SYMM
*ELSE
  SFL,2,PRES, 0, -1
  DL,1,,ASYM
  DL,21,,ASYM
  DL,7,,SYMM
*ENDIF

FINISH

CSKP,11,0,4,10,106,1,1,
CSYS,11,

!Solution

/SOL
SOLVE
FINISH

! POST-PROCESSING

/POST1
RSYS,11

LPLOT
LSEL,S, , ,      18
NSLL,S
NPLOT
PRNSOL,S,COMP

*VGET,sel,NODE, ,NSEL,,
*VGET,posx,NODE, ,LOC,X
*VGET,posy,NODE, ,LOC,Y
*VGET,stress,NODE, ,S,Y

*CFOPEN,'RESULTS_NSIF_E_CRUCIFURM','
    csv',,APPEND
*VWRITE, 'h','t','alfa_ADI','material
    ','load','d1',
%C,%C,%C,%C,%C,%C,
*VWRITE, h,t,alfa_ADI,material,load,
    d1,
 %G,%G,%G,%G,%G,%G,
*VWRITE,'posx','stress',
%C,%C,%C
*VMASK,sel
*VWRITE,posx(1),stress(1)
%G,%G
*CFCLOS

FINISH
```

Codice C.14: Series E: APDL for SED approach

```
/CLEAR, NOSTART

!Geometrical parameters

MATERIAL= 2   ! 1= STEEL 2=ADI
h= 10   ! Height of the weld bead
ltot= 300 ! Total length of the
    specimen
h_irr= 40 ! Total height of the
    specimen
t= 5.008  !Thickness of the specimen
t_irr= 5  ! Total length of the
    specimen
alfa_S355= 141.7! Toe opening angle
    on steel side
alfa_ADI=135  ! Toe opening angle on
    ADI side
Ro_S355=0.28  ! Control radius for
    steel
Ro_ADI=0.55 ! Control radius for ADI
Ro_su_d= 5  ! Parameter for mesh
    refinement
load= 1   ! 1=axial loading, 2= four-
    point-bending loading

pi= 4*atan(1) ! pi greco
c_S355=h/tan((180-alfa_S355)*pi/180)
c_ADI=h/tan((180-alfa_ADI)*pi/180)

!--------------------------------

/PREP7
!ELEMENT TYPE
ET,1,PLANE182

KEYOPT,1,1,3
KEYOPT,1,3,2
KEYOPT,1,6,0

!material

MPTEMP,,,,,,,,
MPTEMP,1,0
MPDATA,EX,1,,206000
MPDATA,PRXY,1,,0.3

MPTEMP,,,,,,,,
MPTEMP,1,0
MPDATA,EX,2,,168000
MPDATA,PRXY,2,,0.27

K,1,0,0,0,
K,2,ltot/2,0,0,
K,3,ltot/2,t,0,
K,4,t_irr+C_ADI,t,0,
K,5,t_irr,t+h,0,
K,6,t_irr,h_irr,0,
K,7,0,h_irr,0,

LSTR,1,2
LSTR,2,3
LSTR,3,4
LSTR,4,5
```

```
LSTR,5,6
LSTR,6,7
LSTR,7,1

!control volume ADI
kwpave,4
CSYS,4
K,103,-Ro_ADI,0,0,
K,102,+Ro_ADI,0,0,
K,101,0,Ro_ADI,0,
K,100,0,-Ro_ADI,0,

LARC,103,100,4,Ro_ADI,
LARC,100,102,4,Ro_ADI,
LARC,101,103,4,Ro_ADI,
LSBL,3,9,,,KEEP
LSBL,4,10,,,KEEP
LSBL,10,3,,,KEEP
LDELE,4
LCOMB,14,8,
LCOMB,8,9
LDIV,8, , ,2,0
LSTR,4,9

!root

kwpave,1
CSYS,4
K,20,t_irr,,0
K,21,t_irr,t,0
K,22,t_irr-0.01,0,0
LSTR,20,21
LSTR,21,22
LSBL,1,14,,,KEEP
LSBL,16,10,,,KEEP
LDELE,17

AL,3,8,9
AL,9,4,12
LSEL,S,,,1,2
LSEL,A,,,4,8
LSEL,A,,,10,11
LSEL,A,,,13,15
AL,ALL
ALLSEL

CSYS,0

!MESH
TYPE, 1
MAT, MATERIAL
REAL,
ESYS, 0
SECNUM,

d= Ro_ADI/Ro_su_d ! globa element
     size mesh

ESIZE,d,0
MSHKEY,0
AMESH,1

ESIZE,d,0
MSHKEY,0
AMESH,2

d1=t/t_su_d !globa element size mesh
ESIZE,d1,0
MSHKEY, 0
AMESH,3

! BOUNDARY CONDITIONS AND LOADS
DL,2,,UY
DK,1,,,,0,UX
*IF, load, EQ,1,THEN
  SFL, 2,PRES, -1
  DL,1,,SYMM
  DL,15,,SYMM
  DL,7,,SYMM
*ELSE
  SFL,2,PRES, 0, -1
  DL,1,,ASYM
  DL,15,,ASYM
  DL,7,,SYMM
*ENDIF

FINISH

!Solution
/SOL
SOLVE
FINISH

! POST-PROCESSING

/POST1

ASLL,S
ASEL,S, , ,1,2
ESLA,S
AVPRIN,0, ,
ETABLE, ,SENE,
AVPRIN,0, ,
ETABLE, ,VOLU,
SSUM
PRETAB,SENE,VOLU

*GET,ENERGY_ADI,SSUM,0,ITEM,SENE
*GET,VOLU_ADI,SSUM, 0,ITEM, VOLU

SED_ADI=ENERGY_ADI/VOLU_ADI

*CFOPEN, 'RESULTS_SED_CRUCIFURM_E','
     txt',,APPEND
*VWRITE, 'h','alfa_ADI','t','material
     ','load','d','SED_toe1*10^6',
(' ',A8' ',A8' ',A8' ',A8' ',A8' ',A8
     ' ',A8' ',)
*VWRITE, h,alfa_ADI,t,material,load,d
     ,Ro_ADI,SED_ADI*10**6
(F8.2,' ',F8.2,' ',F8.2,' ',F8.2,' ',
     F8.2,' ',F8.2,' ',F8.2,' ',F10
     .4,' ',)

FINISH
```

Codice C.15: Series E: APDL for PSM approach

```
/CLEAR, NOSTART

!Geometrical parameters

MATERIAL= 2   ! 1= STEEL 2=ADI
h= 10     ! Height of the weld bead
ltot= 300   ! Total length of the
     specimen
h_irr= 40   ! Total height of the
     specimen
t= 5.008    !Thickness of the
     specimen
t_irr= 5    ! Total length of the
     specimen
alfa_S355= 141.7! Toe opening angle
     on steel side
alfa_ADI=135  ! Toe opening angle on
     ADI side
t_su_d= 3   ! Parameter for mesh
     refinement
```

```
load= 1     ! 1=axial loading, 2=
    four-point-bending loading

pi= 4*atan(1) ! pi greco
c_S355=h/tan((180-alfa_S355)*pi/180)
c_ADI=h/tan((180-alfa_ADI)*pi/180)

!---------------------------
/PREP7
!ELEMENT TYPE
ET,1,PLANE182

KEYOPT,1,1,3
KEYOPT,1,3,2
KEYOPT,1,6,0

!material
MPTEMP,,,,,,,,
MPTEMP,1,0
MPDATA,EX,1,,206000
MPDATA,PRXY,1,,0.3

MPTEMP,,,,,,,,
MPTEMP,1,0
MPDATA,EX,2,,168000
MPDATA,PRXY,2,,0.27

K,1,0,0,0,
K,2,ltot/2,0,0,
K,3,ltot/2,t,0,
K,4,t_irr+C_ADI,t,0,
K,5,t_irr,t+h,0,
K,6,t_irr,h_irr,0,
K,7,0,h_irr,0,


LSTR,1,2
LSTR,2,3
LSTR,3,4
LSTR,4,5
LSTR,5,6
LSTR,6,7
LSTR,7,1

kwpave,1
CSYS,4
K,20,t_irr,,0
K,21,t_irr,t,0
K,22,t_irr-0.01,0,0
LSTR,20,21
LSTR,21,22
LSBL,1,8,,,KEEP
LSBL,10,9,,,KEEP
LDELE,12

LSEL,S,,,1,11
AL,ALL
ALLSEL
!MESH
TYPE, 1
MAT, MATERIAL
REAL,
ESYS, 0
SECNUM,

d= t/t_su_d! globa element size mesh

ESIZE,d,0
MSHKEY,0
AMESH,1


/COLOR, ELEM, BLAC
EPLOT
/AUTO,1
/DIST, 1, 0.05,1
/FOCUS,,1,b/2,t,0,0
/REP, FAST
/REPLOT
/ui, copy,save,bmp,full,color,reverse
    ,portrait, no
! BOUNDARY CONDITIONS AND LOADS

DL,2,,UY
DK,1,,,,0,UX
*IF, load, EQ,1,THEN
  SFL, 2,PRES, -1
  DL,1,,SYMM
  DL,11,,SYMM
  DL,7,,SYMM

*ELSE
  SFL,2,PRES, 0, -1
  DL,1,,ASYM
  DL,11,,ASYM
  DL,7,,SYMM
*ENDIF

FINISH

KWPAVE,       4
WPROTA,-(360-alfa_ADI)/2,0 , 0
CSWPLA, 11, 0, ,
CSYS,11,

! Solution
/SOL
SOLVE
FINISH

! POST-PROCESSING

/POST1
RSYS,11
PLNSOL, S,Y, 0,1.0

KSEL,S, , ,4
NSLK,R
NSORT,S,Y,0,0,1
*GET,psm,SORT,0,MAX
ALLS,ALL

*CFOPEN, 'RESULTS_PSM_CRUCIFURM_E','
    txt',,APPEND
*VWRITE, 'h','alfa_ADI','t','material
    ','load','d','PSM',
(' ',A8' ',A8' ',A8' ',A8' ',A8' ',A8
    ' ',A8' ',)
*VWRITE, h,alfa_ADI,t,material,load,d
    ,psm
(F8.2,' ',F8.2,' ',F8.2,' ',F8.2,' ',
    F8.2,' ',F8.2,' ',F10.4,' ',)
*CFCLOS

FINISH
```

C.6 APDL codes for series F

Codice C.16: Series F: APDL for N-SIF approach

```
/CLEAR, NOSTART

!Geometrical parameters
MATERIAL= 2   ! 1= STEEL 2=ADI
```

```
h= 10   ! Height of the weld bead
ltot= 300 ! Total length of the
     specimen
h_irr= 40 ! Total height of the
     specimen
t= 5.2654   !Thickness of the
     specimen
t_irr= 5  ! Total length of the
     specimen
alfa_S355= 146.5! Toe opening angle
     on steel side
alfa_ADI=135  ! Toe opening angle on
     ADI side
Ro_S355=0.28  ! Control radius for
     steel
Ro_ADI=0.55 ! Control radius for ADI
Ro_su_d= 5  ! Parameter for mesh
     refinement
load= 2   ! 1=axial loading, 2= four-
     point-bending loading


pi= 4*atan(1) ! pi greco
c_S355=h/tan((180-alfa_S355)*pi/180)
c_ADI=h/tan((180-alfa_ADI)*pi/180)

/PREP7
!ELEMENT TYPE
ET,1,PLANE182

KEYOPT,1,1,3
KEYOPT,1,3,2
KEYOPT,1,6,0

!MATERIAL

MPTEMP,,,,,,,,
MPTEMP,1,0
MPDATA,EX,1,,206000
MPDATA,PRXY,1,,0.3

MPTEMP,,,,,,,,
MPTEMP,1,0
MPDATA,EX,2,,168000
MPDATA,PRXY,2,,0.27

CSYS,4
K,1,0,0,0,
K,2,ltot/2,0,0,
K,3,ltot/2,t,0,
K,4,t_irr+C_ADI,t,0,
K,5,t_irr,t+h,0,
K,6,t_irr,h_irr,0,
K,7,0,h_irr,0,


LSTR,1,2
LSTR,2,3
LSTR,3,4
LSTR,4,5
LSTR,5,6
LSTR,6,7
LSTR,7,1

!control volume ADI 8
kwpave,4
CSYS,4
K,103,-0.28,0,0,
K,102,+0.28,0,0,
K,101,0,0.28,0,
K,100,0,-0.28,0,


LARC,103,100,4,0.28,
LARC,100,102,4,0.28,
LARC,101,103,4,0.28,
LSBL,3,9,,,KEEP
LSBL,4,10,,,KEEP
LSBL,10,3,,,KEEP
LDELE,4
LCOMB,14,8,
LCOMB,8,9
LDIV,8, , ,2,0
LSTR,4,9

!control volume ADI  0,0001
kwpave,4
CSYS,4
K,104,-0.0001,0,0,
K,105,0,-0.0001,0,
K,106,+0.0001,0,0,
K,107,0,0.0001,0,

LARC,104,105,4,0.0001,
LARC,105,106,4,0.0001,
LARC,104,107,4,0.0001,
LSBL,10,9,,,KEEP
LCOMB,14,17,
LCOMB,15,16
LSBL,12,14,,,KEEP
LSBL,3,15,,,KEEP
LSBL,15,12,,,KEEP
LDELE,18
LSBL,9,3,,,KEEP

AL,3,15,12
AL,14,15,10
AL,3,17,8,18
AL,14,18,4,16

LSEL,S,,,1,2,
LSEL,A,,,4,
LSEL,A,,,8,9
LSEL,A,,,5,7,
LSEL,A,,,11,
LSEL,A,,,13,
AL,ALL
ALLSEL



!MESH

TYPE, 1
MAT, MATERIAL
REAL,
ESYS, 0
SECNUM,

KSCON,4,,0,16,
LESIZE,12, , ,5,, , , ,1
LESIZE,15, , ,5,, , , ,1
LESIZE,10, , ,5,, , , ,1
LESIZE,17, , ,50,1/2000, , , ,1
LESIZE,18, , ,50,1/2000, , , ,1
LESIZE,16, , ,50,1/2000, , , ,1
LESIZE,8, , ,8,1, , , ,1
LESIZE,4, , ,8,1, , , ,1
LESIZE,3, , ,8,1, , , ,1
LESIZE,14, , ,8,1, , , ,1


MSHKEY, 1
AMESH,3

MSHKEY, 1
AMESH,4

MSHKEY,0
AMESH,1
```

```
MSHKEY,0
AMESH,2

d1= 10*Ro_ADI/Ro_su_d
ESIZE,d1,0
MSHKEY, 0
AMESH,5
! BOUNDARY CONDITIONS AND LOADS
DL,2,,UY

*IF, load, EQ,1,THEN
  SFL, 2,PRES, -1
  DL,1,,SYMM
  DL,7,,SYMM

*ELSE
  SFL,2,PRES, 0, -1
  DL,1,,ASYM
  DL,7,,SYMM
*ENDIF

FINISH

CSKP,11,0,4,10,106,1,1,
CSYS,11,

!solution

/SOL
SOLVE
FINISH

! POST-PROCESSING

/POST1
RSYS,11

LPLOT
LSEL,S, , ,      18
NSLL,S
NPLOT

PRNSOL,S,COMP

*VGET,sel,NODE, ,NSEL,,
*VGET,posx,NODE, ,LOC,X
*VGET,posy,NODE, ,LOC,Y
*VGET,stress,NODE, ,S,Y

*CFOPEN,'RESULTS_NSIF_F_CRUCIFURM','
     csv',,APPEND
*VWRITE, 'h','t','alfa_ADI','material
     ','load','d1',
%C,%C,%C,%C,%C,%C,
*VWRITE, h,t,alfa_ADI,material,load,
     d1,
 %G,%G,%G,%G,%G,%G,
*VWRITE,'posx','stress',
%C,%C,%C
*VMASK,sel
*VWRITE,posx(1),stress(1)
%G,%G
*CFCLOS

FINISH
```

Codice C.17: Series F: APDL for SED approach

```
/CLEAR, NOSTART

!Geometrical parameters
MATERIAL= 2   ! 1= STEEL 2=ADI
h= 10   ! Height of the weld bead
ltot= 300 ! Total length of the
     specimen
h_irr= 40 ! Total height of the
     specimen
t= 5.2654   !Thickness of the
     specimen
t_irr= 5  ! Total length of the
     specimen
alfa_S355= 146.5! Toe opening angle
     on steel side
alfa_ADI=135  ! Toe opening angle on
     ADI side
Ro_S355=0.28  ! Control radius for
     steel
Ro_ADI=0.55 ! Control radius for ADI
Ro_su_d= 5  ! Parameter for mesh
     refinement
load= 2   ! 1=axial loading, 2= four-
     point-bending loading

*CFOPEN, 'RESULTS_SED_CRUCIFURM','txt
     ',,APPEND
*VWRITE, 'h','alfa_ADI','t','
     materiale','carico','Ro_ADI','d
     ','SED_ADI*10^6',
(' ',A8' ',A8' ',A8' ',A8' ',A8' ',A8
     ' ',A8' ',A8' ',)
*CFCLOS

pi= 4*atan(1)! pi greco
c_ADI=h/tan((180-alfa_ADI)*pi/180)

!---------------------------

/PREP7
!ELEMENT TYPE
ET,1,PLANE182

KEYOPT,1,1,3
KEYOPT,1,3,2
KEYOPT,1,6,0

!material

MPTEMP,,,,,,,,
MPTEMP,1,0
MPDATA,EX,1,,206000
MPDATA,PRXY,1,,0.3

MPTEMP,,,,,,,,
MPTEMP,1,0
MPDATA,EX,2,,168000
MPDATA,PRXY,2,,0.27



K,1,0,0,0,
K,2,ltot/2,0,0,
K,3,ltot/2,t,0,
K,4,t_irr+C_ADI,t,0,
K,5,t_irr,t+h,0,
K,6,t_irr,h_irr,0,
K,7,0,h_irr,0,


LSTR,1,2
LSTR,2,3
LSTR,3,4
LSTR,4,5
LSTR,5,6
LSTR,6,7
LSTR,7,1

!control volume ADI
```

```
kwpave,4
CSYS,4
K,103,-Ro_ADI,0,0,
K,102,+Ro_ADI,0,0,
K,101,0,Ro_ADI,0,
K,100,0,-Ro_ADI,0,


LARC,103,100,4,Ro_ADI,
LARC,100,102,4,Ro_ADI,
LARC,101,103,4,Ro_ADI,
LSBL,3,9,,,KEEP
LSBL,4,10,,,KEEP
LSBL,10,3,,,KEEP
LDELE,4
LCOMB,14,8,
LCOMB,8,9
LDIV,8, , ,2,0
LSTR,4,9

AL,3,8,9
AL,9,4,12
LSEL,S,,,1,2
LSEL,A,,,4,8
LSEL,A,,,10,11
LSEL,A,,,13
AL,ALL
ALLSEL

CSYS,0

!MESH

TYPE, 1
MAT, MATERIAL
REAL,
ESYS, 0
SECNUM,

d= Ro_ADI/Ro_su_d !globa element size
      mesh

ESIZE,d,0
MSHKEY,0
AMESH,1
ESIZE,d,0
MSHKEY,0
AMESH,2

d1= 10*Ro_ADI/Ro_su_d !globa element
     size mesh
ESIZE,d1,0
MSHKEY, 0
AMESH,3

! BOUNDARY CONDITIONS AND LOADS

DL,2,,UY
DK,1,,,,0,UX
*IF, load, EQ,1,THEN
  SFL, 2,PRES, -1
  DL,1,,SYMM
  DL,7,,SYMM
*ELSE
  SFL,2,PRES, 0, -1
  DL,1,,ASYM
  DL,7,,SYMM
*ENDIF

FINISH

!SOLUTION
/SOL
SOLVE
FINISH

! POST-PROCESSING
/POST1
ASLL,S
ASEL,S, , ,1,2
ESLA,S
AVPRIN,0, ,
ETABLE, ,SENE,
AVPRIN,0, ,
ETABLE, ,VOLU,
SSUM
PRETAB,SENE,VOLU

*GET,ENERGY_ADI,SSUM,0,ITEM,SENE
*GET,VOLU_ADI,SSUM, 0,ITEM, VOLU

SED_ADI=ENERGY_ADI/VOLU_ADI

*CFOPEN, 'RESULTS_SED_CRUCIFURM_F','
     txt',,APPEND
*VWRITE, 'h','alfa_ADI','t','material
     ','carico','d','Ro','SED_ADI
     *10^6',
(' ',A8' ',A8' ',A8' ',A8' ',A8' ',A8
     ' ',A8' ',A8' ',)
*VWRITE, h,alfa_ADI,t,material,carico
     ,d,Ro_ADI,SED_ADI*10**6
(F8.2,' ',F8.2,' ',F8.2,' ',F8.2,' ',
     F8.2,' ',F8.2,' ',F8.2,' ',F10
     .4,' ',F10.4,' ',)
*CFCLOS
FINISH
```

Codice C.18: Series F: APDL for PSM approach

```
/CLEAR, NOSTART

!Geometrical parameters
MATERIAL= 2   ! 1= STEEL 2=ADI
h= 10   ! Height of the weld bead
ltot= 300 ! Total length of the
     specimen
h_irr= 40 ! Total height of the
     specimen
t= 5.2654   !Thickness of the
     specimen
t_irr= 5  ! Total length of the
     specimen
alfa_S355= 146.5! Toe opening angle
     on steel side
alfa_ADI=135  ! Toe opening angle on
     ADI side
t_su_d= 3 ! Parameter for mesh
     refinement
load= 2   ! 1=axial loading, 2= four-
     point-bending loading

pi= 4*atan(1) ! pi greco
c_S355=h/tan((180-alfa_S355)*pi/180)
c_ADI=h/tan((180-alfa_ADI)*pi/180)
!------------------------

/PREP7
!ELEMENT TYPE
ET,1,PLANE182

KEYOPT,1,1,3
KEYOPT,1,3,2
KEYOPT,1,6,0

!material

MPTEMP,,,,,,,,
```

```
MPTEMP,1,0
MPDATA,EX,1,,206000
MPDATA,PRXY,1,,0.3

MPTEMP,,,,,,,,
MPTEMP,1,0
MPDATA,EX,2,,168000
MPDATA,PRXY,2,,0.27

K,1,0,0,0,
K,2,ltot/2,0,0,
K,3,ltot/2,t,0,
K,4,t_irr+C_ADI,t,0,
K,5,t_irr,t+h,0,
K,6,t_irr,h_irr,0,
K,7,0,h_irr,0,


LSTR,1,2
LSTR,2,3
LSTR,3,4
LSTR,4,5
LSTR,5,6
LSTR,6,7
LSTR,7,1


LSEL,S,,,1,11
AL,ALL
ALLSEL


!MESH

TYPE, 1
MAT, MATERIAL
REAL,
ESYS, 0
SECNUM,

d= t/t_su_d! globa element size mesh

ESIZE,d,0
MSHKEY,0
AMESH,1
! BOUNDARY CONDITIONS AND LOADS
DL,2,,UY
DK,1,,,,0,UX
```

```
*IF, load, EQ,1,THEN
  SFL, 2,PRES, -1
  DL,1,,SYMM
  DL,7,,SYMM

*ELSE
  SFL,2,PRES, 0, -1
  DL,1,,ASYM
  DL,7,,SYMM
*ENDIF
FINISH

KWPAVE,       4
WPROTA,-(360-alfa_ADI)/2,0 , 0
CSWPLA, 11, 0, ,
CSYS,11,

! SOLUTION
/SOL
SOLVE
FINISH

! POST-PROCESSING

/POST1

RSYS,11
PLNSOL, S,Y, 0,1.0

KSEL,S, , ,4
NSLK,R
NSORT,S,Y,0,0,1
*GET,psm,SORT,0,MAX
ALLS,ALL
*CFOPEN, 'RESULTS_PSM_CRUCIFURM_F','
    txt',,APPEND
*VWRITE, 'h','alfa_ADI','t','material
    ','load','d','PSM',
(' ',A8' ',A8' ',A8' ',A8' ',A8' ',A8
    ' ',A8' ',)
*VWRITE, h,alfa_ADI,t,material,load,d
    ,psm
(F8.2,' ',F8.2,' ',F8.2,' ',F8.2,' ',
    F8.2,' ',F8.2,' ',F10.4,' ',)
*CFCLOS

FINISH
```

Bibliography

[1] Daniele Berto. "Definizione di metodi per la durabilità di giunzioni saldate ibride acciaio-ghisa sferoiadale austemperata". MA thesis. Università degli Studi di Padova, 2019.

[2] *Eurocode 3: Design of steel structures – part 1–9: Fatigue*. 2005.

[3] *Eurocode 9: Design of aluminium structures - Part 1-3: Structures susceptible to fatigue*. 2011.

[4] R. Gross and A. Mendelson. "Plane elastostatic analysis of V-notched plates." In: *Int. J. Fracture Mech.* 8 (1972), pp. 267–327.

[5] A. F. Hobbacher. *Recommendations for Fatigue Design of Welded Joints and Components*. IIW Collection. IIW Collection. Springer International Publishing, 2016. ISBN: 978-3-319-23756-5. DOI: 10.1007/978-3-319-23757-2.

[6] S Katayama. "Laser welding of aluminium alloys and dissimilar metals". In: *Welding International* 18.8 (2004), pp. 618–625.

[7] Suranjit Kumar et al. "Experimental investigation of local tensile and fracture resistance behaviour of dissimilar metal weld joint: SA508 Gr.3 Cl.1 and SA312 Type 304LN: Experimental Investigation of Local Tensile and Fracture Resistance Behaviour of Dissimilar Metal Weld Joint". In: *Fatigue & Fracture of Engineering Materials & Structures* 40 (Jan. 2016).

[8] P. LAZZARIN, T. LASSEN, and P. LIVIERI. "A notch stress intensity approach applied to fatigue life predictions of welded joints with different local toe geometry". In: *Fatigue & Fracture of Engineering Materials & Structures* 26.1 (2003), pp. 49–58.

[9] P. Lazzarin and P. Livieri. "Notch stress intensity factors and fatigue strength of aluminium and steel welded joints". In: *International Journal of Fatigue* 23.3 (2001), pp. 225 –232.

[10] P. Lazzarin and R. Tovo. "A notch intensity factor approach to the stress analysis of welds". In: *Fatigue Fracture of Engineering Materials Structures* 21 (1998), pp. 1089–1103.

[11] P. Lazzarin and R. Zambardi. "A finite-volume-energy based approach to predict the static and fatigue behavior of components with sharp V-shaped notches". In: *Int. J. Fract.* 112 (2001), pp. 275–298.

[12] P. Livieri and P. Lazzarin. "Fatigue strength of steel and aluminium welded joints based on generalised stress intensity factors and local strain energy values". In: *International Journal of Fracture* 133 (2005), pp. 247–276.

[13] K. Martinsen, S.J. Hu, and B.E. Carlson. "Joining of dissimilar materials". In: *CIRP Annals* 64.2 (2015), pp. 679 –699.

[14] G Meneghetti and P Lazzarin. "Significance of the elastic peak stress evaluated by FE analyses at the point of singularity of sharp V-notched components". In: *Fatigue & Fracture of Engineering Materials & Structures* 30.2 (2007), pp. 95–106.

[15] G. Meneghetti and S. Masaggia. *Ricerca tra dipartimento di ingegneria Indutraile e Zanardi Fonderie S.p.A.* Tech. rep. Dii. 2012, p. 20.

[16] G. Meneghetti et al. "Rapid evaluation of notch stress intensity factors using the peak stress method: Comparison of commercial finite element codes for a range of mesh patterns". In: *Fatigue and Fracture of Engineering Materials and Structures* 41.5 (2018), pp. 1044–1063.

[17] "Microstructure and fatigue properties of fiber laser welded dissimilar joints between high strength low alloy and dual-phase steels". In: *Materials & Design* 51 (2013), pp. 665 –675.

[18] H Okamura and K Aota. "Joining of dissimilar materials with friction stir welding". In: *Welding International* 18.11 (2004), pp. 852–860. DOI: 10.1533/wint.2004.3344.

[19] Rajangam Paventhan, P R. Lakshminarayanan, and V Balasubramanian. "Fatigue behavior of friction welded medium carbon steel, Fatigue behaviour of friction welded medium carbon steel and austenitic stainless steel dissimilar joints". In: *Materials & Design - MATER DESIGN* 32 (Apr. 2011), pp. 1888–1894.

[20] D. I. Roberts, R. H. Ryder, and R. Viswanathan. "Performance of Dissimilar Welds in Service". In: *Journal of Pressure Vessel Technology* 107.3 (Aug. 1985), pp. 247–254.

[21] Weiya Zhang et al. "Fatigue life of a dissimilar welded joint considering the weld residual stress: Experimental and finite element simulation". In: *International Journal of Fatigue* 109 (2018), pp. 182 –190.